Volcanology of the Troodos Ophiolite (Cyprus) and mechanisms of accretion of the upper oceanic crust

Ella C. Young

Submitted in partial fulfilment of the requirements for the degree of PhD.

September 2014

Abstract

Seafloor spreading at mid-ocean ridges is accommodated by a combination of magmatic accretion and tectonic stretching of the lithosphere. Recent investigations of mid-ocean ridges show evidence for large-offset normal faults or detachments that accommodate a significant portion of the plate separation. Once thought of as rarities along the global spreading system, detachment faults are now considered to play an integral role in seafloor spreading at slow- and ultra-slow-spreading ridges. Estimates of the proportion and extent of tectonic spreading however vary widely; some authors suggest as much as 50% of the Mid Atlantic Ridge is underlain by active detachment faults. The lack of consensus is in part a consequence of the difficulty in documenting the extent of tectonic stretching and detachment faulting, especially from surface morphology alone. On the modern seafloor tectonic activity may potentially be greatly under-estimated if lava flows blanket and obscure the faulting below.

This thesis addresses the question of whether and how such 'hidden tectonics' may be accommodated beneath the seafloor by means of a field-based study of the Troodos ophiolite, Cyprus, which is believed to be a slow-spreading ridge analogue. My interdisciplinary approach utilises structural mapping, palaeomagnetism and geochemistry to investigate the spreading structure and mechanism of accretion of the Troodos upper crust. I document significant extensional faulting and rotation within the crust above a detachment fault at the level of the sheeted dyke complex, yet show that the lavas at the surface are sub-horizontal and unaffected by the deformation beneath. Unconformities in the lava section demonstrate progressively greater rotations deeper in the extrusive pile, controlled by tectonic stretching and tilting of the underlying dykes, rather than rotation by loading and/or subsidence within the lava pile as previously proposed. Ponding of late, primitive, low viscosity lava flows against normal faults on the seafloor thickens the extrusive sequence substantially and obscures the faulting below.

The study shows that syn-tectonic volcanism is an effective mechanism for filling active half-grabens at slow-spreading ridges. Tens of percent tectonic stretching at depth may be completely masked at the surface by syn-tectonic lava extrusion. Such 'hidden tectonics' may be far more common at modern mid-ocean ridges than commonly supposed.

Acknowledgements

The first and biggest thanks goes to Chris MacLeod for all the help and wisdom in the field, during discussions, and particularly with writing this thesis. Thanks also to Johan Lissenberg, Tony Morris and Julian Pearce for the helpful insights in their respective fields of expertise. It has been a pleasure working with all of you, and I look forward to publishing together soon.

Thanks goes to Stelios Nicolaides at the Geological Survey Department in Cyprus for loaning maps and field guides during my field seasons, and for discussions on Cyprus geology which I always enjoyed.

Thank you to all the people I met during my stay in CAARI, especially to Vathoulla Moustoukki for being the embodiment of Cypriot hospitality.

Thanks goes to Iain McDonald for analysing my geochemistry data. And thanks to Matt Meyer for much help in the Plymouth palaeomag lab and help with the analytical software.

Thanks also to the all inhabitants of the postgrad office, past and present. You have all been lovely company these last four years- best of luck to all of you for the future.

For putting a roof over my head this last month, I would like to thank Sabrina and Elaine. I owe them both a drink. And thanks to Hannah for help with printing this thesis in my hour of need.

Finally, heartfelt thanks to all the family and friends who have encouraged or supported me during the PhD. Mum, Dad, Hayley, Jess, and Ben, you have each made a big impression on me and for that I am grateful.

1 Introduction

1.1 Mid-ocean ridges

Seafloor spreading at mid-ocean ridges (MOR) is the key to the theory of plate tectonics. Ridges are the site of the most voluminous volcanic and magmatic activity on the planet, forming the oceanic crust which covers 60% of the surface of the Earth. The interconnected, 60,000 km-long global mid-ocean ridge system makes the single largest morphological feature on the planet, forming a range of abyssal hills that dominates the ocean floor. Plate separation at MOR is accommodated by a combination of magmatic accretion of new crust and tectonic extension, at rates ranging from <10 mm/yr to 160 mm/yr (Teagle et al., 2012). The crust in the oceans is generated by volcanism, dyking and plutonism at, or very near, the ridge axis. Usually the newly formed crust is deformed by faults that accommodate tectonic strain and flexure of the newly formed ocean lithosphere. The relative importance of magmatic accretion versus tectonic extension during spreading is closely linked to the rate of spreading.

Surveys of the modern oceans, by remote sensing, dredging and geophysical surveys, only build a picture of the tectonics and volcanism at the surface of the seafloor. Sub-surface exploration, through techniques such as seismic surveying, and direct sampling by drilling, is very difficult, and significant questions remain about the subsurface architecture of the oceanic crust.

1.1.1 Oceanic crust

Fast spreading rate MOR such as the East Pacific Rise (EPR) have high magma supply rates, such that magmatic accretion can keep pace with plate separation, such that little or no contribution from tectonic extension is necessary (~2% estimated for the East Pacific Rise: Escartin et al., 2007). At fast spreading ridges the structure of the crust has a Penrose-type pseudostratigraphy- the classic ‘layer-cake’ structure

(Penrose conference, 1972). Crust like this exhibits very uniform structure, and the consistency of the seismic P-wave velocity surveys is taken to show that fast spreading crust has a very regular architecture. The seismic layers have been correlated to the geology of most ophiolites: layer 2a represents the volcanics, layer 2b = sheeted dyke complex, layer 3 = gabbro lower crust (Christensen and Salisbury, 1972).

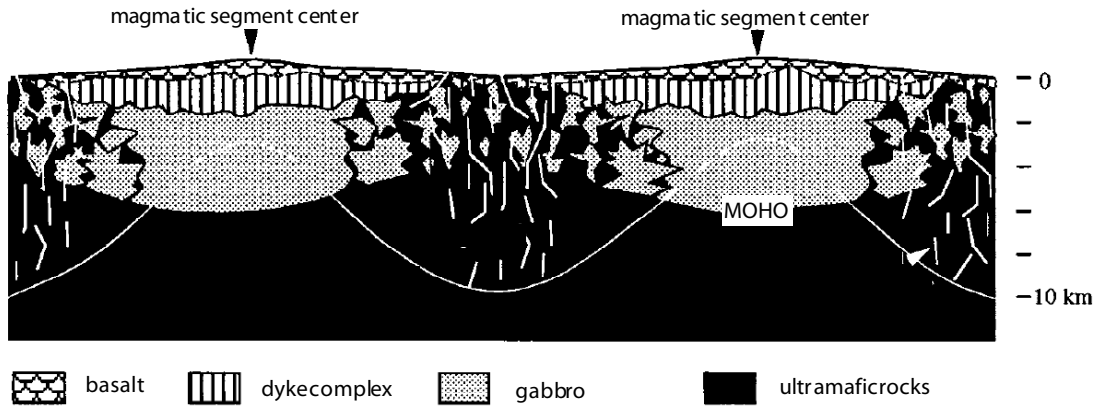

Figure 1.1 Cartoon of along-strike variability of lithospheric structure at a slow-spreading ridge. Typical 'layer-cake' crustal structure is likely at magma-rich segment centres, contrasting with the thin, discontinuous igneous crust at segment ends and/or magma-poor segments. Taken from Cannat et al. (1995).

However, slow spreading rate MOR such as the northern Mid-Atlantic Ridge (MAR) are believed to have lower magma supply rates, or intermittent supply of magma, so the tectonic element of spreading has to become more important. As a result the crust is accreted slowly during period of temporarily increased magma supply, the rest of the time faulting extends and thins the crust (e.g., Tucholke and Lin, 1994). Dredging has revealed serpentinised mantle peridotites and gabbros on the seafloor (Cannat, 1993), so clearly the Penrose-type crust is not applicable everywhere. At slow-spreading ridges oceanic magmatic crust is commonly discontinuous and segmented. The diagram in figure 1.1 below, from Cannat et al. (1995), shows an idealised discontinuous crust that is segmented along axis, with magma delivery from the mantle concentrated at segment centres. Away from the segment centres the magmatic crust is much thinner or even absent, giving rise to a heterogeneous crustal and lithospheric structure vastly different from the Penrose 'layer-cake'. Where there ought to be a gabbro sequence followed by dykes and lavas

instead there are gabbro intrusions and (partially serpentinised) mantle ultramafic rock that has been tectonically uplifted during spreading.

1.1.2 Detachment faulting

Areas of low magma supply are favourable for the development of detachment faults which can have large off-sets of many kilometres. Detachments usually occur at the ends of ridge segments when a normal valley-wall fault continues to slip for hundreds of thousands or millions of years (Cann et al., 1997). The initially steep normal faults bend due to flexure of the thin lithosphere causing the footwall to rotate to become a curved antilistric structure (Morris et al, 2009). Where the domes detachment surface is exposed on the seafloor it is called an oceanic core complex (or OCC). Corrugations on the surface of OCC are usually parallel to spreading direction, and it is thought the corrugated slip surfaces which form on the emerging footwall are equivalent to fault striations on a larger scale (Cann et al., 1997). At OCC the spreading is extremely asymmetrical and locally accommodates up to 100% of the spreading on a single structure (e.g., Searle et al., 2003; Baines et al., 2008; Grimes et al., 2008). A common feature of these core complexes is the exposure of deep crustal and mantle rocks on the seafloor, where the magmatic crust is completely absent (e.g., Cann et al., 1997; MacLeod et al., 2002). Along the MAR, OCC are frequently exposed near the ends of segments where magma supply is low (e.g., Tucholke et al., 1998).

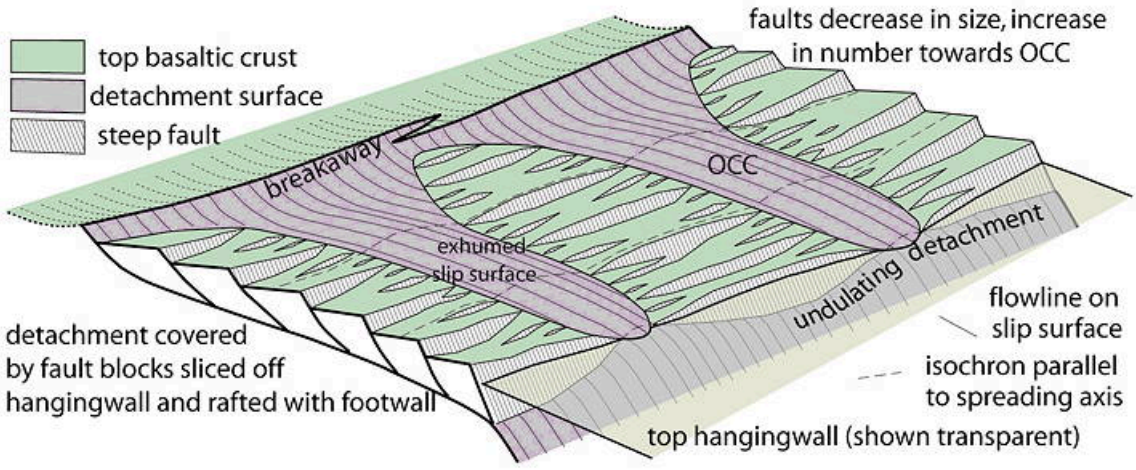

Figure 1.2 Undulating detachment surface is exposed at OCC and persists beneath crustal rider blocks where it is not exposed (Reston and Ranero, 2011).

It is unclear whether the detachments extend laterally at depth beyond the exposed OCC surface. Escartin et al. (2008) noted that up to 50% of the MAR is spreading asymmetrically and suggested that regions are underlain by detachment faults. What are the structures beneath these regions of asymmetrical spreading where detachments are not directly observed? Or perhaps detachment faults persist beneath rotated blocks of sliced off hanging wall (as in figure 1.2)? so the detachment fault could remain active at depth even though it is unseen on the seafloor surface.

1.1.3 Tectonic strain estimates

To address the outstanding questions of the subsurface tectonics, attempts have been made to estimate tectonic extension from the surface morphology of the seafloor. Tectonic strain in areas where detachments are not directly observed has been estimated from summing the heaves of exposed normal faults identified from high-resolution deep-towed side-scan sonar data of the seafloor. Escartin et al. (1999) followed this approach for the MAR 29°N region and concluded an average ~10% tectonic strain is uniform along the segment. This is in marked contrast to the MAR 13°N region which shows large variation in tectonic strain (MacLeod et al., 2009). At the areas of active OCCs the tectonic strain was up to 100%, and accommodated on to the single structure, contrasting with adjacent areas between the OCCs that exhibited only approximately 20% tectonic strain (figure 1.3).

Tectonic strain estimates go a long way to understand better the relative roles of tectonic strain and magmatic extension, but also leads to more questions. Is there really such a big difference in strain between OCCs and the adjacent areas? And are these estimates based on surface morphology alone reliable?

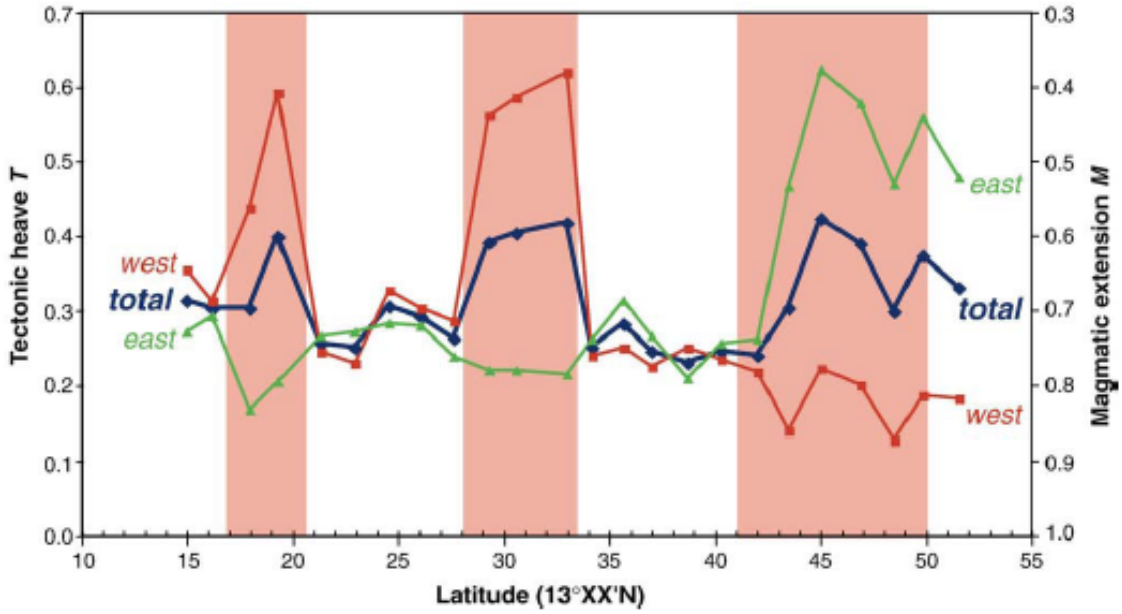

Figure 1.3. From MacLeod et al., (2009). Along axis profile of tectonic heave at MAR 13°N. Tectonic heave (T) on left y-axis, magmatic extension (M) on right y-axis. T + M = 1. Pink shading = areas on OCC, no shading = areas between.

1.2 Outline and aim

Studies of modern MOR and ophiolites have given insights into ocean crust construction through observation of surface processes. Less however is understood about the mechanisms of accretion of the upper oceanic crust, particularly at slow-spreading ridges, because the subsurface structure of the crust cannot be observed or imaged with great enough resolution. Seismic methods are of very low resolution and particularly problematical at slow-spreading ridges in particular, because of the rough seafloor. Drilling is expensive, limited and technically difficult in most ocean crustal settings. Ophiolites have therefore long been used as ocean crust analogues to allow us to examine the internal structure of the crust.

The Troodos ophiolite is an ideal choice for studying the upper crust because its extrusive sequence is arguably the most extensive and best preserved- original spreading features have been left undeformed by uplift and emplacement of the ophiolite. The field relations can be directly observed on ophiolites and then we can relate these observations to the geophysical data from modern MOR to develop robust observation based models for the upper ocean crust. The Troodos complex has long

been recognised as a suprasubduction zone ophiolite (Miyashiro, 1973; Pearce, 1975; 1980) because the lava geochemistry is different from mid-ocean ridges proper (see section 2.4 for more details). Clearly the petrogenesis of the Troodos crust is different from typical mid-ocean ridge basalts (MORB) because it is formed at a spreading centre above a subduction zone and the geochemistry is influenced by water present in the system. It would be inappropriate to make a direct comparison between the petrogenetic models of the Troodos ophiolite and mid-ocean ridges. However, the crustal architecture, tectonic deformation and volcanological styles of crustal accretion observed at Troodos are not influenced by the subduction processes. It is, therefore, appropriate to apply models based on observations from the Troodos ophiolite to other spreading centres such as those at mid-ocean ridges.

This thesis aims to address the questions mentioned above by assessing extent of sub-surface versus surface estimates of extension in the Troodos ophiolite. On Troodos we are able to look below the seafloor to see the internal structure of the upper oceanic crust and examine the original sub-seafloor architecture in 2 or even 3 dimensions, at a resolution that is unlikely ever to be possible at modern mid-ocean ridges. It will be shown here that tilting of dykes and lavas in Troodos occurs above a detachment fault, and the mechanisms by which this occurs provide insights into how tectonic stretching of the crust and simultaneous magmatic accretion can occur at a slow to intermediate spreading centre. The interaction of faulting and volcanism can be understood by constraining the relative timing of tectonic tilting and eruption, and by constraining the geometries of the upper crust units (i.e., lava flows thickening against half graben).

Six months of fieldwork were conducted in the northern flank of the ophiolite documenting the sub-seafloor tectonic extension. The approach to this is to quantify rotations in the sheeted dykes *and* the lavas by structural mapping and to applying palaeomagnetic net tectonic rotation analysis (Allerton & Vine, 1987). Spatial variations in thickness of the lavas were identified by geochemical sampling in conjunction with the compilation of all available geochemical data. This was achieved by first identifying the geochemical stratigraphy for N-S transects through the upper crust, and then by correlating the adjacent transects.

The stratigraphic framework and structural data have been interpreted together to develop a model for the spreading structure and spreading history of the Troodos

ophiolite. The observation of significant syn-volcanic extensional faulting and rotation within the crust above a detachment fault observed in the Troodos massif may be directly analogous to the process occurring along much of the Mid-Atlantic Ridge.

2 Geology of the Troodos ophiolite

The Troodos Complex on the island of Cyprus is one of the best preserved and most extensively studied ophiolites in the world. The Troodos ophiolite has played an important role in the development of the theory of plate tectonics, which had not been formulated at the time the Cyprus Geological Survey Department (GSD) began detailed mapping in the late 1950s.

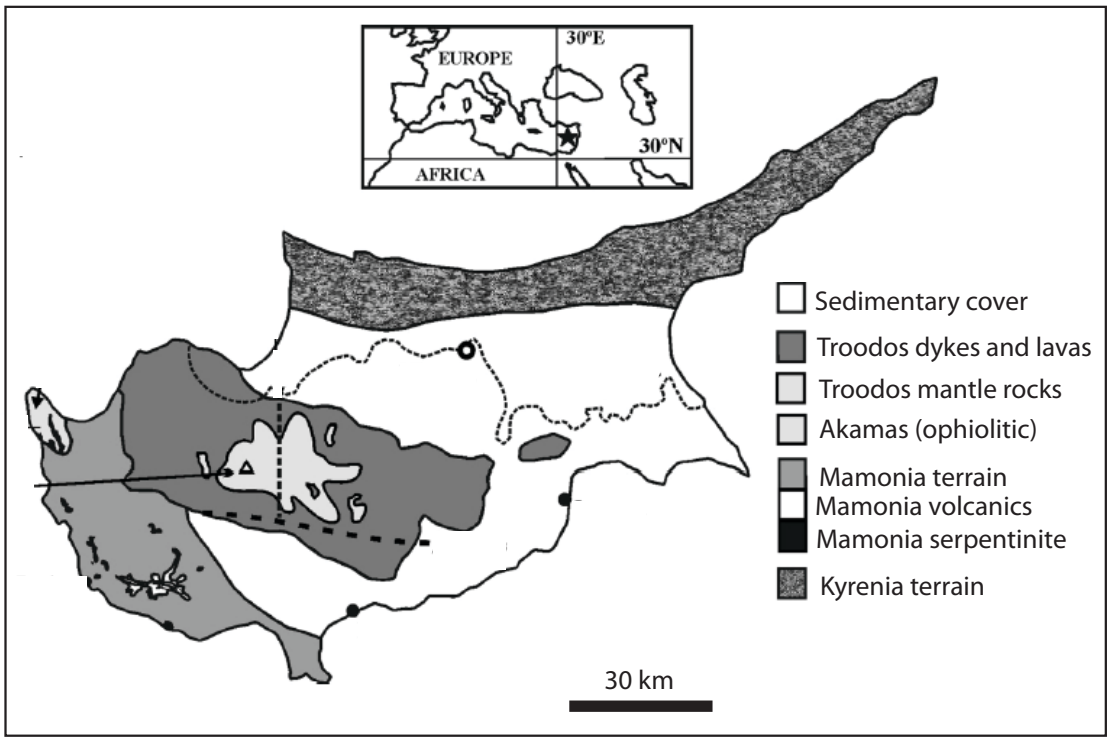

Figure 2.1 Main lithological units of Cyprus, taken from Borradaile, (2003).

2.1 Regional setting of Cyprus

The age of the ophiolite based on biostratigraphy of the oldest sediments of the ophiolite is approximately mid-late Cretaceous Turonian to Maastrictian (Urquhart & Banner, 1994). This is in close agreement with the U-Pb dates of 91.5±1.5Ma from zircons in the plagiogranites (Mukasa & Ludden, 1987), placing the igneous complex within the Turonian. During the mid-late Cretaceous, the Neo-Tethyan Ocean was

closing and there was probably a subduction zone to the south of Cyprus (dipping north) due to the northward movement of Africa (Robertson & Xenophontos, 1993). Original ocean-floor structures within the ophiolite remain intact despite a 90° anticlockwise rotation of the Troodos microplate in the late Cretaceous (e.g., Moores & Vine, 1971; Clube & Robertson, 1986), which is documented by the consistent westward magnetisation vector of the extrusive rocks and overlying sediments (Clube et al., 1985).

A long period of stability in a deep water environment lasted until the Miocene when instability and uplift began, probably a result of renewed convergence between Africa and Eurasia (Robertson & Woodcock, 1986). Uplift of Troodos accelerated in the Pleistocene when the doming of the ophiolite was caused by serpentinite diapirism, and uplift continues to the present-day. Today the highest point of the ophiolite is Mt. Olympus elevated ~1950m above sealevel where mantle serpentinite is exposed, and surrounded by lower crustal cumulates, the sheeted dyke complex, the extrusive rocks and overlying sediments in an annular fashion at successively lower elevations (Figure 2.1). Because the ophiolite is folded into an east-west trending domal anticline the entire crustal sequence is exposed in oblique section, essentially showing an across-axis slice of oceanic lithosphere.

2.2 Troodos crustal sequence

The Troodos Complex is made up of the ophiolite and the original sedimentary cover, providing a near complete section through ocean lithosphere. The structural base of the ophiolite includes ultramafic rocks from the mantle, gabbros form the lower most part of the crust, then there are the sheeted dykes, above the dykes volcanic extrusive rocks, and finally umbers and chalks are deposited on top. As well as the excellent completeness, the Troodos Complex has experienced relatively little deformation during its uplift and emplacement; this has led to very good preservation of the original spreading structures.

2.2.1 Early subdivisions of the Troodos extrusive rocks

The Geological Survey Department (or GSD) of Cyprus categorised the upper crust of Troodos into the Upper Pillow Lavas (UPL), Lower Pillow Lavas (LPL), Basal Group (BG), and the Sheeted Dyke Complex (SDC). The distinctions were based on field criteria that the early Survey mappers found to be consistent across the ophiolite, the GSD produced detailed geological maps and descriptions which were published as a series of Memoirs (Wilson and Ingham, 1959; Carr and Bear, 1960; Bear, 1960; Gass, 1960; Bagnall, 1960).

This early phase of work on the ophiolite described the UPL as dominantly olivine-phyric basalts and basaltic andesites, occurring as small pillows, with dykes forming less than 10%; the LPL, by contrast, were described as 'often intensely silicified', commonly aphyric oversaturated basalts and andesites, and sills and dykes were more frequent (Wilson, 1960).

2.2.1.1 Upper pillow lavas

The upper most unit often shows pinkish staining due to seafloor weathering of the lavas to zeolite facies, they commonly have various zeolites filling voids, spaces and vesicles. Fresh surfaces of basaltic-basaltic andesite are blue-grey. Olivine phenocrysts are commonly <1-3mm and are argilitised to orange-brown clay, only rarely are fresh glassy phenocrysts of clinopyroxene found (Gass, 1960). The most common morphology of the upper lavas is small (<1m) pillowed flows, with some thin (<1m) sheet flows (figure 2.2 A), lava breccia flows are common (clasts of lava, probably pillowed flows, which fragment during eruption and flow). Dykes in the unit are relatively rare, and they are often sinuous rather than planar. The orientation of these high-level dykes are less uniform than the dykes of deeper levels within the same domain, and less likely to be vertical (Carr & Bear, 1960).

2.2.1.2 Lower pillow lavas

The lower lavas are generally darker in colour, being predominantly green-grey partially on account of the greater alteration as seen by the presence of the alteration minerals celadonite, chalcedony and jasper are also common (Gass, 1960). The lower

lava can also be a rusty-brown colour and/or silicified, in the latter case making the rock very hard. There are no phenocrysts and the vesicles are not filled or, more rarely, filled by chalcedony. Lava morphology is different for the lower lava unit: sheet flows can be up to 3m thick (figure 2.2 C), pillows are generally larger than 1.5m, and hyaloclastite is much more common than the upper unit. Lower in the crustal section the dykes become more abundant, as dykes intrude more frequently than the upper lava group. However, at this level the dykes are often vertical and parallel but sometimes not.

2.2.1.3 Basal Group – lava-dyke transition unit

The Survey also recognised another unit, the Basal Group (BG), i.e., the transition unit from dominantly extrusive rocks above to the sheeted dyke complex (or SDC) below, which is composed of 100% dykes. The BG is considered to be a unit in its own right since it is at least as thick as either of the overlying extrusive units, and represents a different mode of emplacement/accretion (Gass, 1960). The upper boundary of the BG is a gradational and arbitrary one where the abundance of dykes at the outcrop is ~50%, and the degree of alteration increases further. Many BG outcrops in the upper half of the unit are rusty-brown in appearance, much like the lower lava group. Whereas BG outcrops in the bottom half of the unit show greenschist facies mineral assemblages of epidote-quartz-chlorite-pyrite, giving the whole outcrop an aqua-green tinge (e.g., Ayia Koroni). The abundance of lavas at BG outcrops rapidly reduces through the unit until there are only narrow screens of lava (5-10m) between dyke swarms and may account for <10% of the outcrop, and can be easily overlooked when mapping. Therefore, the lower boundary of the BG and the SDC is defined at the last appearance of lava screens (i.e., where there are 100% dykes), such as seen in figure 2.2 E. However, the lava screens may persist to even lower depths if they are present though not exposed (-or not observed). Dykes of the BG show very little difference to the SDC proper, apart from the occasional lava screens, like the SDC, the dykes of the BG have similar attitudes within the structural domains.

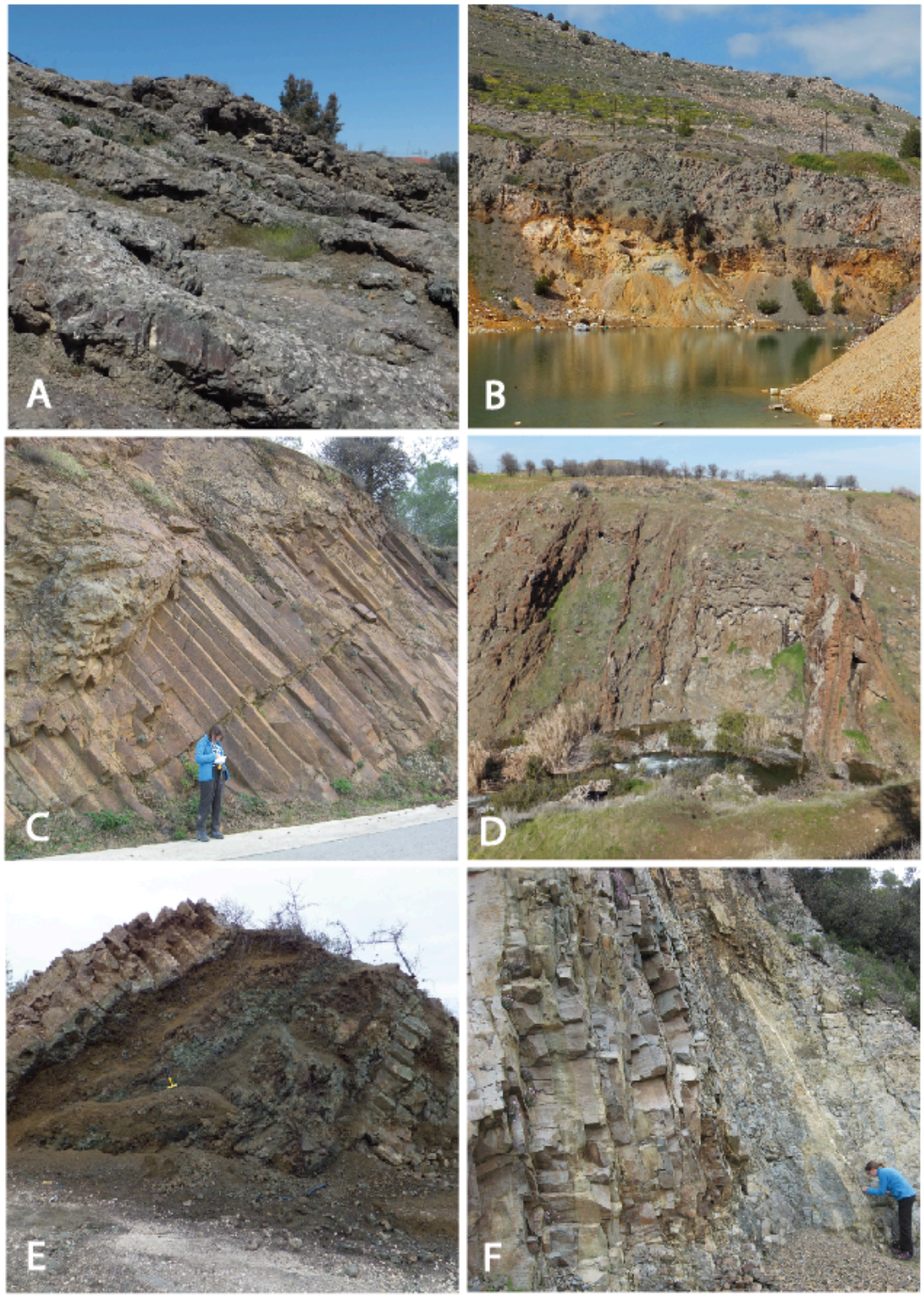

Figure 2.2 Field photographs of lavas and dykes from the northern flank of the Troodos ophiolite. A: Upper Pillow Lavas (UPL), both thin sheet flows ~50cm thick and pillowed flows are moderately tilted. B: Agrokipia pit (massive sulphide deposit) - mineralised pillow lavas covered in orange ochre are overlain by unmineralised UPL. C: Lavas from the Lower Pillow Lavas (LPL) are weathered brown, thick sheet flow with columnar cooling joints perpendicular to base of flow. D: Klirou Bridge outcrop (figure 2.3) in the LPL of the Akaki river gorge. Dykes (orange-brown) are cutting pillowed lavas, hyaloclastites, and thin sheet flows. E: Typical appearance of a Basal Group outcrop – dyke on far left (~1m thick) and on far right, between is a narrow screen of dark weathered pillows. F: Sheeted dyke complex (SDC) outcrop of parallel, steep dykes with chilled margins at their contacts.

2.2.1.4 Sheeted dyke complex

The sheeted dyke complex is easily the most widely exposed unit of the whole ophiolite, covering an area of ~80 km^2, with its distinctive high relief and carpeted in a forest of pine and carob trees. Topographiy of the SDC is characterised by high relief and takes the form of dramatic triangular hills with narrow ridges and pointed peaks. The transition from BG to the SDC is a gradational one. Four different type of contact with the underlying gabbros are observed at the upper-to-lower crust boundary in Troodos: gradational, faulted, dykes intruding gabbro, and gabbro intruding dykes. Away from the boundaries, the vast majority of SDC outcrops are remarkably similar: nothing but dykes intruded into dykes for tens of kilometres (figure 2.2 F). The dykes are fine-medium grained in the centre, and grain size reduces rapidly to a (now altered) glassy contact margin over a distance of <5cm. Cooling joints form normal to the dyke margin, and joint surfaces have commonly been weathered to a rusty-orange colour. Where there are fresh, or broken, surfaces the colour of the dolerite is blue-grey, which gives rise to the typical appearance of huge swathes of the landscape in the SDC. Although the whole complex has been altered to greenschist facies, replacement of the original mineral assemblage does not destroy the original doleritic igneous texture. The fine grained chilled margin is always preserved, as are the (steeply pitching) slickenlines that are often observed on the margins. However, in some instances very intense epidotisation has occurred, where striking bands of apple-green epidosite (quartz-epidote assemblages) have completely overgrown the original doleritic mineralogy. These result from hydrothermal fluids flowing through the dykes in channels parallel to the dyke margin (e.g., Schiffman et al., 1987). Most of the dykes of the sheeted complex are aphyric, although plagioclase, pyroxene or olivine phyric dykes have been reported. Dykes are observed intruding into the centre of older dykes, and also along the margins between two existing dykes, both of which can be determined by studying the direction of chilled margins (Kidd and Cann, 1974; Baragar, 1990).

2.2.2 Extrusive rocks subdivided by metamorphic or alteration discontinuity

Gass and Smewing (1973) noted that the Upper Pillow Lavas were probably extruded slightly later than the Lower Pillow Lavas, and probably were erupted in a slightly off-axis setting. They based their distinction on the presence of unconformities in a few places and an apparent metamorphic stratification (fig.2.3). Gass and Smewing (1973) documented a transitional metamorphic boundary in the Troodos extrusives by carefully identifying the distribution of 18 different alteration minerals in the upper crust (figure 2.3). They noticed that the zeolite assemblage for the upper and lower pillow lavas were different. The boundary between the two was defined by the disappearance of natrolite and gmelinite, and the appearance of mordenite and chalcedony. And they also noted that some other minerals appeared/disappeared very close to the boundary, such as celadonite, which gives the lower lavas their characteristic turquoise-green hue. Similarly, the lower lavas and sheeted dyke contact coincides with a change in assemblage of the alteration minerals. This contact sees the change from zeolite facies to greenschist facies by the disappearance of chalcedony and smectite (a zeolite present in all the extrusive rocks), and the appearance of quartz and chlorite, which are closely followed by pyrite and epidote a short distance below the actual boundary. Gass and Smewing noted that the metamorphic boundary does not coincide with any change in intrusive/extrusive ratio, nor with any other type of primary structure evident at the metamorphic boundary.

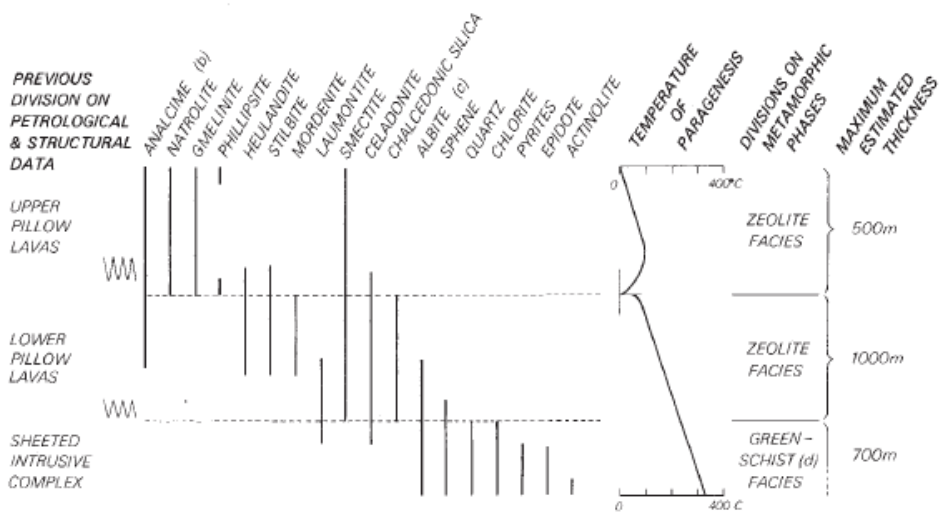

Figure 2.3 Metamorphic phases and their distribution within the Troodos extrusive rocks, the change of alteration mineral was used by Gass & Smewing (1973) to subdivide the extrusive rock sequence into Upper pillow lavas and Lower pillow lavas.

2.2.3 Geochemical subdivision of the lavas

Detailed geochemical investigations of the Akaki River section redefined the subdivision of the extrusive rocks based on TiO_2 content of fresh glass samples (e.g., Robinson et al., 1983; Schmincke et al., 1983). In the 1980s the new subdivision of the extrusive suite was made based on the observation of a general trend of decreasing TiO_2 up the section (Schmincke et al., 1983), which could be interpreted as suggesting a progressive depletion of the mantle source. On the division between the traditional low-TiO_2 'upper' lavas and the high-TiO_2 'lower' lavas Schmincke found they were not geochemically continuous (cogenetic). Robinson et al. also interpreted the geochemical trend as "two major magma suites corresponding to distinct stratigraphic intervals", and proposed the lower lavas was an evolved arc-tholeiite suite and the upper lavas were similar to boninitic lavas. Moreover, these workers failed to identify a metamorphic discontinuity within the extrusive section which Gass & Smewing (1973) found (figure 2.3), nor did the geochemical distinction correspond consistently with the 'Upper Pillow Lavas' and 'Lower Pillow Lavas' divisions defined by Wilson (1959) and Bear (1960).

2.2.4 Sulphide deposits of the extrusive sequence

Many large sulphide ore deposits have been mined for copper ore since about 4000BC, Cu-rich ore deposits in Cyprus contain 10-50% pyrite and <5% of chalcopyrite (Bear, 1963). There is extensive mineralisation within the all parts of the UPL and LPL across the ophiolite, it has been noted there are particularly large deposits at the boundary between LPL-UPL (Constantinou, 1980), for example at the Mathiatis mine. Many large massive sulphide deposits are completely within the UPL, such as the deposits at Skouriotissa and Mitsero.

A typical orebody is composed of a lenticular massive sulphide zone, beneath that the stockwork zone is made up of highly altered pillow lavas which are mineralised along a network of veinlets (Constantinou, 1972; Hutchinson & Searle, 1971). The massive sulphide deposits are often directly overlain by ochre, which when weathered become gossans of brightly coloured yellow, orange or red sediment.

Most of these Cu-rich deposits are volcanological massive sulphide (VMS) deposits and are interpreted to be seafloor exhalative deposits (Adamides, 1980). This style of mineralisation is common on the Mid-Atlantic Ridge where high temperature hydrothermal fluids are released from black smoker vents. Massive sulphide builds up in mounds on the seafloor around the vents. Deposits are preserved by burial under umber, as at Skouriotissa, or burial under lava flows (figure 2.2 B) such as the Agrokipia deposit (Adamides, 2010; Robinson & Malpas, 1990).

VMS deposits of Troodos are associated with steeply dipping normal faults or small-scale graben structures. It has been suggested by Adamides (1980) that faults are the conduits for hydrothermal fluids. In the Solea graben the largest copper mine, Skouriotissa, is still in operation. It is situated at the uppermost part of the UPL, about 500m East of the Solea fossil axis. Two deposits at Skouriotissa are located on N-S faults structures which are related to spreading at ridge (Adamides, 2010).

2.3 Early tectonic interpretations

The SDC played the most important role in conceptual advances in understanding the origin and significance of the Troodos ophiolite. Indeed, prior to the seafloor spreading hypothesis of Hess (1962) the dolerite outcrop was thought to be a folded sequence of lava flows by Bishopp in 1952. Only in 1959 did Wilson realise the dolerite outcrop was a vast swarm of parallel dykes: a sheeted dyke complex, in which the host rock to the dykes was similar existing dykes. Wilson's conclusion came before the plate tectonic theory was widely accepted and before Vine & Matthews (1963) recognised that the symmetrical magnetic anomaly 'stripes' on the seafloor were the 'smoking gun' evidence for active seafloor spreading in the oceans.

These revolutionary discoveries in the modern oceans soon after the detailed mapping of Troodos by GSD geologists led one of them, Ian Gass, to make the key conceptual advance of identifying ophiolites as having formed by seafloor spreading, and hence that the Troodos complex represented a slice of oceanic lithosphere (Gass, 1968). The presence of the extensive and uniformly North-South striking sheeted dyke complex in Troodos is evidence of high degrees of extension in a constant East-West extensional stress field, interpreted to be a direct result of spreading in the context of the plate tectonic theory (Gass, 1968; Moores and Vine, 1971). The sheeted dyke

complex outcrops for over 80km and most of this is made up of 100% parallel dykes intruding into each other, with only minor outcrops of host lava or gabbro screens at the top and base of the SDC (Gass, 1968). Gass in 1968 related the geology of the Troodos Mountains to the geophysical data of the modern ocean floors. The ophiolite exposes the complete pseudostratigraphy that is comparable with the seismic velocity layers observed in the modern oceans, where the plutonic rocks represent layer 3, sheeted dykes is layer 2B, Layer 2A being the lavas, and the sediments are layer 1.

2.4 Subduction zone debate

In the middle 1970's the tectonic setting and MOR spreading environment of the Troodos ophiolite was questioned by Miyashiro (1973) based on inconsistencies of the lava geochemistry with modern ocean lava geochemistry. The chemistry of lavas from mid-ocean ridges are extremely consistent and show very limited variability giving them a characteristic MORB (mid-ocean ridge basalt) signature quite different from basalts erupted on continents or island arcs (Pearce & Cann, 1973). Analysis of the Sheeted Dyke Complex and the Lower Pillow Lavas by Miyashiro in 1973 found they were distinctly different from MORB: some were found to be tholeiitic while others were calc-alkaline, similar to island arcs.

This led Miyashiro to suggest an island arc setting for Troodos and sparked a debate with those who believed the Troodos Complex formed at a mid-ocean ridge as supported by the field evidence (Gass, 1968; Moores & Vine, 1971). Counter-arguments were immediately put forward by Gass et al. (1975) and other authors, dismissing the island arc hypothesis because the differences in composition between the Troodos lavas and MORB could have been a result of hydrothermal alteration and weathering of the Troodos lavas. Later studies on the immobile trace elements of the Troodos lavas (Pearce, 1975; 1980) and analysis of fresh volcanic glasses (Robinson et al., 1983; Schmincke et al., 1983; Rautenschlein et al., 1985), however provided much more reliable geochemical evidence in support of Miyashiro's subduction zone hypothesis for Troodos and other ophiolites.

The broad consensus now is that the crust of Troodos must have formed in an extensional environment, because the SDC demonstrates 100km of extension over 100km of outcrop (Moores & Vine, 1971); however, this probably occurred at a

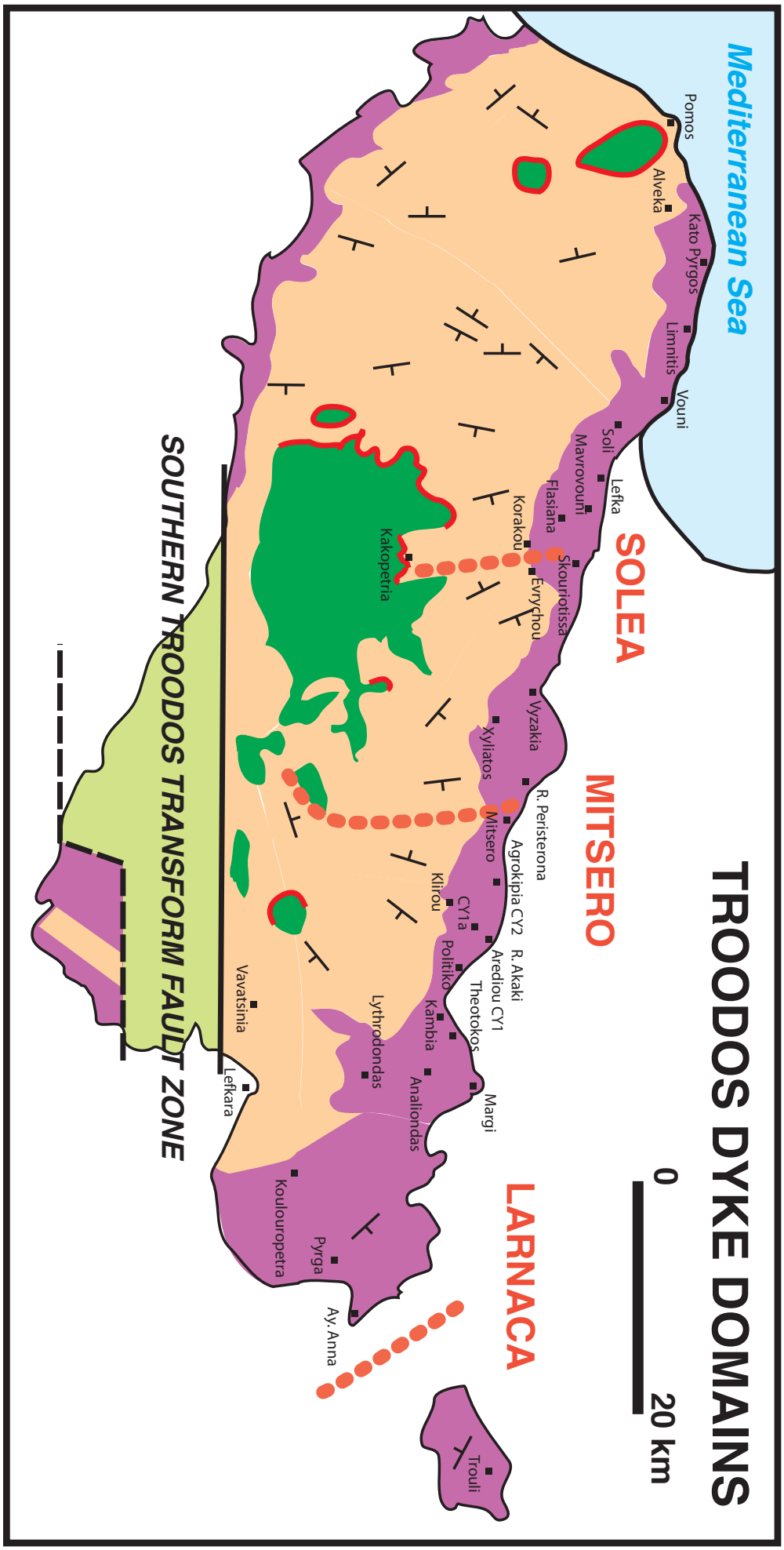
Mediterranean Sea
TROODOS DYKE DOMAINS
0
20 km
SOLEA
MITSERO
LARNACA
SOUTHERN TROODOS TRANSFORM FAULT ZONE
Pomos
Alveka
Kato Pyrgos
Limnitis
Vouni
Soli
Lefka
Mavrovouni
Flasiana
Korakou
Skouriotissa
Evrychou
Kakopetria
Vyzakia
Xyliatos
R. Peristerona
Mitsero
Agrokipia CY2
R. Akaki
Klirou
CY1a
Arediou CY1
Politiko
Theotokos
Margi
Kambia
Lythrodondas
Analiondas
Vavatsinia
Lefkara
Kouloupetra
Pyrga
Ay. Anna
Trouli

Figure 2.4 Locality map of Troodos complex. Purple = extrusive sequence; peach = sheeted dyke complex; green = gabbroic and ultramafic rocks. Red dashed lines are graben axes.

spreading axis above a subduction zone (Pearce et al., 1984). The Nd-Sr isotopes of the primitive lavas in Troodos are consistent with an arc-related setting where fluids derived from a subducting slab induce further melting in an overlying lherzolite source (McCulloch and Cameron, 1983). The proximity to a subduction zone, also known as a supra-subduction zone, can account for the island arc affinity of the lava geochemistry. Absence of any geological evidence for an island arc anywhere in the vicinity of Troodos at the time of its formation have led to the concept of the ophiolite having been formed in a 'pre-arc' setting at the initiation of subduction (e.g., Pearce et al., 1984).

2.5 Magma plumbing and pertrogenesis models

Early models of Gass (1968) and Moores & Vine (1971) envisage the LPL and BG lavas as an on-axis sequence (collectively termed Axial Sequence) host to dykes that intruded at or near to the spreading ridge, and are genetically related to the SDC (Moores and Vine, 1971). The UPL represented off-axis volcanism occurring after the Axial Sequence had been metamorphosed, to account for the alteration discontinuity which Gass & Smewing (1973) used to define the lava subdivision (see section 2.2.2 above). Smewing (1975) demonstrated the Troodos extrusive rocks had "no significant geochemical trace element break between the two divisions and that the metamorphic event divided an essentially continuous upward geochemical variation".

Many of the developments of conceptual and petrogenetic models for Troodos have been based on data from the Akaki River section of northern Troodos at Arediou (figure 2.4). They have focused on this section because it is a well exposed river canyon transecting the extrusive rocks from the top of the crust down to the SDC. It was chosen as the optimum location for drilling by the Cyprus Drilling Project which was initiated in 1981 to address questions about the structure and composition of the crust by drilling a transect of holes to construct a single composite section through the entire extrusive sequence. The aim of the project was to better understand the nature of the lava-dyke transition and to reconcile the different ways of defining the lava subdivisions. Two staggered, offset holes were drilled. The first, CY-1, was sited near

Arediou at the sediment-lava contact. It penetrated 485m into the lavas and was abandoned due to poor hole conditions. The second hole, CY-1A, was located ~1.5km south of the first hole, with the aim of continuing the drilling transect mid-way through the extrusive rocks at the point the previous hole had reached. CY-1A penetrated 700m before being terminated; this hole penetrated the lower lavas and top of the dykes (Gibson et al., 1991). The two cores have been correlated to form a composite section through 1200m of upper crust.

Detailed volcanological work was carried out on the north flank of the ophiolite along the Akaki Canyon by Schmincke et al. (1983) to accompany the drilling project. Twelve different lithological units were identified along the Akaki River section, interpreted by Schmincke et al. as erupted from individual volcanoes from discrete volcano-tectonic events which overlapped in time and space. This work went a long way to understanding how the upper crust was accreted, and they interpreted the variation of lava lithologies as being a result of episodic accretion, and related different facies within the volcanoes. Three different types of volcanic centres were distinguished from each other by the assemblage of volcanic facies and flow morphology by Schmincke & Bednarz (1990): termed by them sheet-flow volcano, breccia-flow volcano and pillow-flow volcano.

The conclusions from geochemical studies of the drill core and fresh glass samples from the Akaki River and other areas (e.g., Robinson et al., 1983; Rautenschlein et al., 1985) indicated that fractionation alone cannot explain all of the geochemical differences between the two lava groups. For example, Schmincke et al. (1983) concluded from a set of fresh glass samples that there was a major compositional break within the extrusive section. Cameron (1985) and Taylor (1990) explored further the nature of the geochemical difference and deduced that the upper lavas were more depleted than the lower lavas, suggesting that the upper lavas originated either from a more depleted mantle source and/or higher degrees of partial melting. The implication of this model for the upper lavas is that they must have been erupted some time later than the more evolved and less depleted lower lavas, probably, by anhydrous second stage melting of a previously melted peridotites source (Duncan & Green, 1980).

Taylor (1990) built a framework for the geochemical stratigraphy of the lavas covering a 20km wide part of the eastern Troodos extrusive sequence. This he did by

constructing detailed geochemical stratigraphic transects in an E-W, across-strike direction to identify petrologically and geochemically distinct horizons within the lavas. By assessing the transects across a wide area he documented the progressive thickening of packages of lavas, apparently structurally controlled.

2.6 Troodos spreading structure

Dykes of the sheeted dyke complex were intruded vertically at the fossil ridge, they exploited planes in the direction of least stress – in the case of a spreading centre this is oriented parallel with the ridge. The N-S dyke strikes within much of the Troodos sheeted dyke complex indicates the spreading direction was E-W (in present coordinates). Three structural grabens were identified by Varga & Moores (1985) on the northern flank of the ophiolite by normal faults and rotated dykes dipping symmetrically towards the graben axis. In map view there are domains of dykes and faults with similar dip and strike which define the grabens (figure 2.5) simplified map of domains, after Varga, 1991). From west to east they are named Stavros domain, Solea graben (west and east domains), Mitsero graben (west and east domains), Makhaeras domain, and the Larnaca graben (west and east domains). These grabens are widely considered to be original seafloor structures because faulting only effects the SDC and lavas, while the overlying sediments are relatively undisturbed because they post-date the stretching.

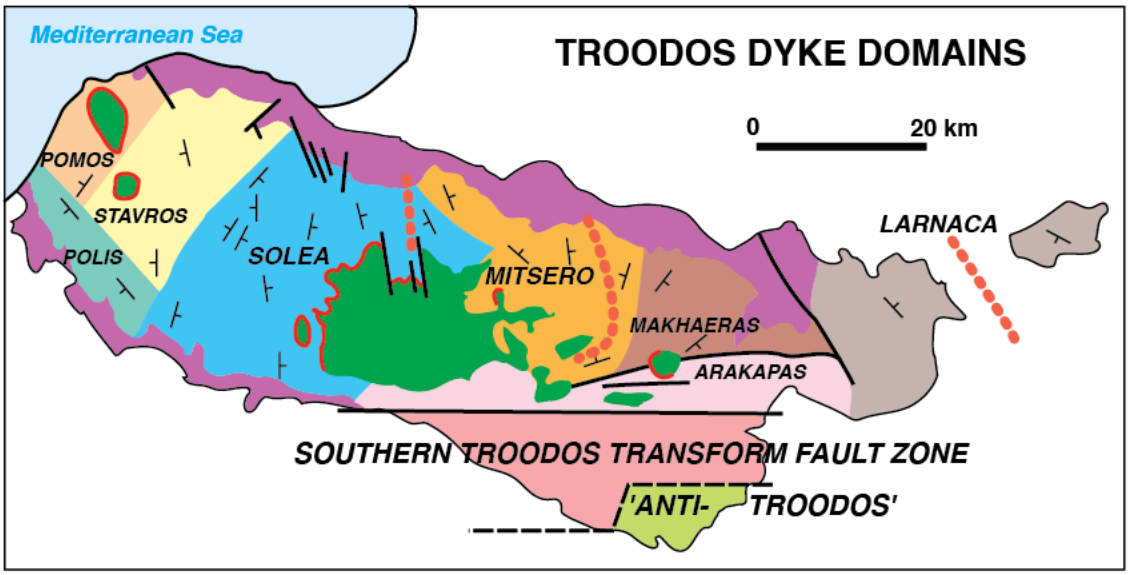

Figure 2.5 Map of dykes divided into domains of similar orientation, dyke orientations define three grabens- Solea Graben, Mitsero Graben, and Larnaca Graben (after Varga & Moores, 1990).

Varga & Moores (1985) interpreted the grabens as fossil ridge axes formed at the active ridge by extension during spreading. They realised the graben formed during magmatic accretion because there are several outcrops of steeper dykes cross-cutting shallower dipping dykes and related normal faults. The fossil ridge axes were preserved when the ridges migrated by successive eastward jumps of 8-13km. The Solea Graben is thought, by Varga & Moores, to be older than the Mitsero Graben because cross-cutting dykes at the boundary between the two grabens indicate the west-dipping dykes of the Solea Graben are cut by younger dykes of the Mitsero Graben. Varga & Moores (1985) also noted several large sulphide deposits occur in association with faulting of the grabens, namely Mavrovouni, Apliki, Skouriotissa, Agrokipia, Kambia, Mathiati and Sha.

The Solea graben is frequently cited as the best candidate for a fossil ridge axis- the tilting in the SDC fault blocks is more extreme; there are three large volcanic massive sulphide (VMS) deposits in the Solea graben (Skouriotissa, Apliki, & Mavrovouni); intense hydrothermal activity and epidotisation; and a low-angle normal fault exposed at Kakopetria (figure 2.6) bounding the SDC and the gabbros (Hurst et al., 1992; 1994). Normal faults in the SDC root onto the sub-horizontal detachment surface causing fault blocks of SDC to rotate above the detachment, which is active at depth.

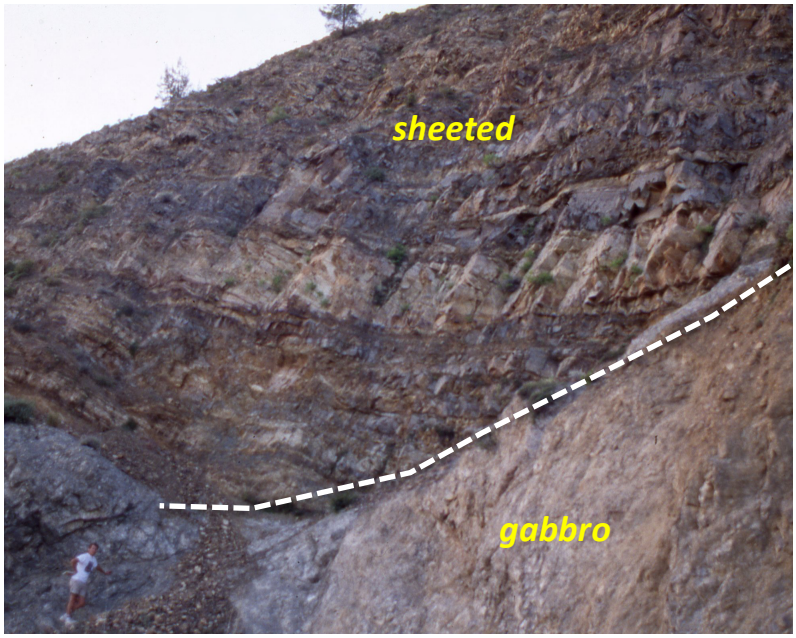

Figure 2.6 Field photo from (taken by Chris MacLeod) showing the Kakopetria detachment fault bounding the rotated sheeted dykes in the hanging wall and the gabbroic rocks of the footwall.

An alternative spreading structure of off-axis grabens was proposed by Allerton & Vine (1987) who recognised the existence of the three grabens but re-interpreted them as off-axis stretching features on the flank of a ridge (figure 2.7). They carried out a palaeomagnetic investigation of the SDC and concluded rotations were consistent with axial tectonics but suggest the original spreading structures were reactivated off-axis during a phase of antithetic faulting of renewed extension. In this model accounted for the asymmetry of the Solea and Mitsero grabens, both are wider on the west side than the right (Solea graben is about 20km wide on the west side and <5km wide on the east side). Asymmetrical grabens are expected to develop as antithetic structures to the main ridge axis to accommodate tectonic strain during extension. An off-axis setting for the formation of the Solea graben is also proposed by Schiffman et al. (1987) because fluid circulation, ore formation and an epidosite zone overprint the graben structure and therefore post-date the stretching. The Mitsero Graben was interpreted by Van Everdingen & Cawood (1995) as probably an off-axis structure, or else it formed on-axis during a time of amagmatic spreading. They calculated the horizontal extension from the present dyke dips for the Mitsero Graben and found there to be 30% extension in the west side and <10% in the east side.

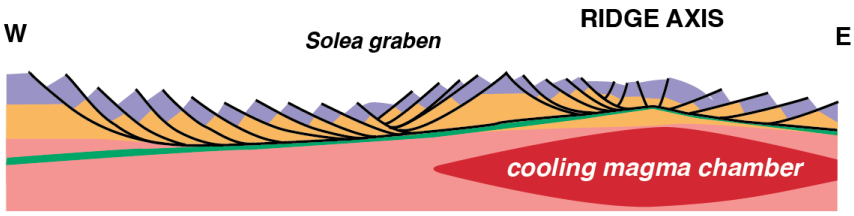

Figure 2.7 Interpretation of the Solea Graben as an antithetic structure off-axis from the main ridge axis which this model predicts would be to the east of the Solea Graben. From Allerton & Vine (1987).

The spreading rate for the Troodos spreading centres is unclear because there are no quantitative estimates due to not enough high-precision age dating. Allerton & Vine (1987) suggest the Troodos ophiolite formed at an intermediate- to fast-spreading centre because the subdued topography does not show signs of faulting as expected at slow-spreading centres. But a slow-spreading ridge is suggested by Varga & Moores (1991) who proposed that separation was accommodated by episodes of

amagmatic extension alternating with episodes of magmatic accretion (figure 2.9), similar to the slow-spreading north Mid-Atlantic Ridge.

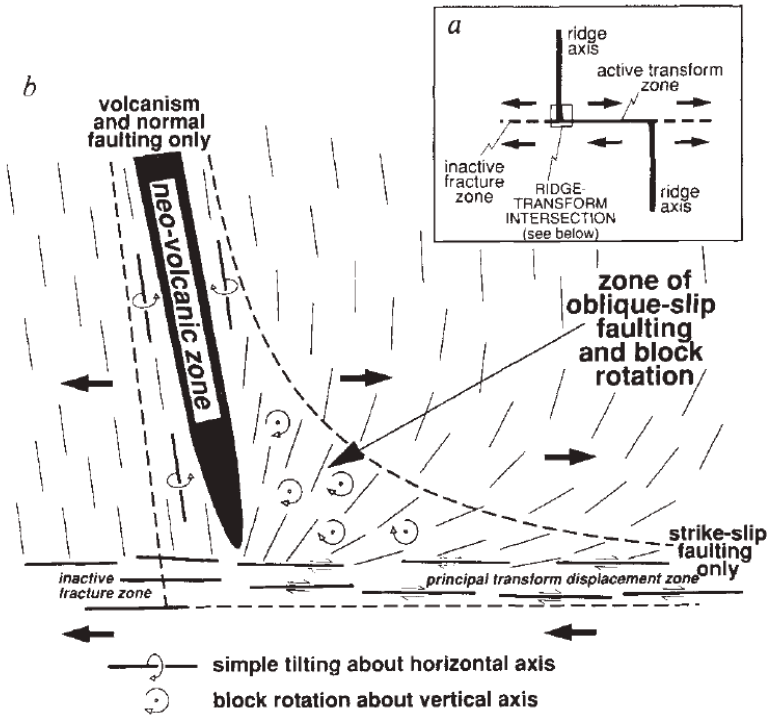

Figure 2.8 Dyke strike change from N-S to NE-SW to E-W with increasing proximity to the active transform zone, but all were initially intruded at a N-S orientation and have been subsequently block rotated by strike-slip faulting about vertical axes. Ridge axis and neo-volcanic zone of this model represent the Solea Graben axis. From MacLeod et al. (1990).

In the region immediately north of the Arakapas fault belt (figure 2.8) the strike of the dykes has progressively swung from the typical N-S trend to NE-SW through to ENE-WSW dyke strikes (MacLeod et al., 1990). Palaeomagnetic analysis of these dykes revealed the dyke swing was a result of post-emplacement clockwise block rotation of the SDC about sub-vertical rotation axes (e.g., Bonhommet et al., 1988; Morris et al., 1990; Allerton & Vine, 1987). This would require a dextral strike slip transform sense, and the field kinematic data support a dominantly dextral sense of slip (MacLeod & Murton, 1993).

2.7 Crustal accretion models

Many comparisons have been drawn between the spreading structure, inferred magma supply and plumbing, and inferred spreading rate of the Troodos ophiolite with that of

the modern oceans from OPD/IODP drilling and from other ophiolites such as Oman. One of the main outcomes of research in the modern oceans was the difficulty in imaging axial melt lenses (AML) beneath the Mid-Atlantic Ridge. By attempting to link new findings from elsewhere, new accretion models have been suggested for Troodos which go beyond the simple Penrose-type crustal accretion to account for the accumulated evidence of more complex interaction of tectonics and magmatism and hydrothermal processes.

A model for intermittent magmatic spreading and tectonic extension was proposed by Varga & Moores (1990), which they note is a common accretion style on the Mid-Atlantic Ridge particularly near large-offset transform faults. In this model the Solea graben goes through several stages in its evolution starting from a magmatically robust spreading centre when extension is accommodated by plutonism and dyking (figure 2.9). This phase is followed by a period of increased tectonic stretching and the cessation of magmatism, the grabens are formed by block rotation of numerous normal faults probably rooting into a low-angle detachment at the base of the SDC. This was followed by a phase of renewed magmatism and hydrothermal alteration and ore deposition to account for the cross-cutting epidosite zones reported by Schiffman et al. (1987). The final step for the Solea graben was the cessation of spreading altogether, allowing the graben to be preserved and the original spreading fabrics in the mantle rocks to be frozen.

Schouten & Denham (2000) advocated a model for the accretion of the upper crust based on the steepening of lavas down section as documented by magnetic inclinations of the CY-1A drill core. This model attributes the progressive unconformity to flexural subsidence caused by lava loading on the crust, resulting in lava flows dipping towards the ridge axis. However, the potential effects of tectonic stretching by block rotation along faults are not considered; and, furthermore, the underlying palaeomagnetic evidence for the lava steepening is in itself weak, as there is no declination information to accompany the inclination data.

Another model for upper crustal accretion of Troodos proposed by Schouten and Kelemen (2002) is that the Upper and Lower Pillow Lavas were segregated on the ridge

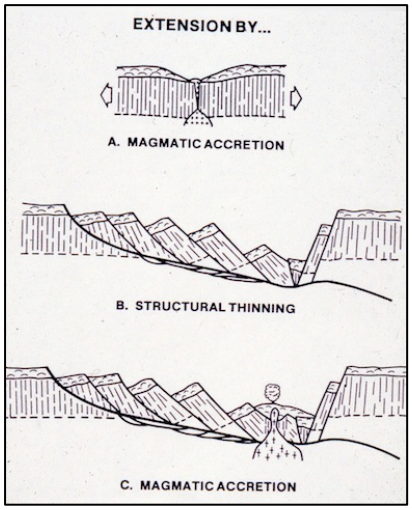

Figure 2.9 Non-steady state model for intermittent magmatic extension and tectonic extension (Varga & Moores, 1990).

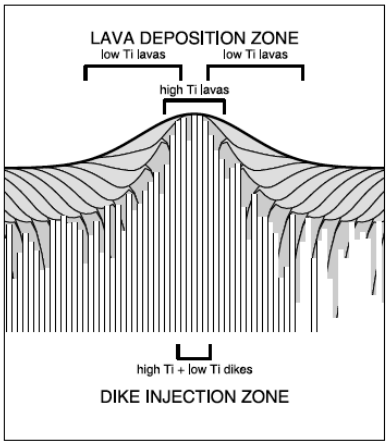

Figure 2.10 Conceptual model for build up of the lava pile, the more viscous high-Ti lavas are short flows limited to the zone of dyke injection, the less viscous low-Ti lavas erupted on-axis but flow further down slope and are deposited off-axis (Schouten & Kelemen, 2002).

slope by viscosity variations. The viscosity of the UPL with the lower TiO_2 was calculated to be lower than the high TiO_2 LPL by 2-3 orders of magnitude. Therefore, when the different compositions of lava were erupted at the ridge the lower TiO_2 lava would flow further and faster down the same slope. A cartoon of this model is shown in figure 2.10, demonstrating how the UPL flow further than the LPL.

One of the more recent models for Troodos to be published has suggested an oceanic core complex (OCC) is preserved at the outside corner of the fossil ridge-transform intersection (Nuriel et al., 2009). In the OCC model (figure 2.11) the Amiandos Fault which bounds the Mt. Olympos serpentinites and the plutonic sequence is envisaged to link with the Troodos Forest Fault (a major normal fault on the west side of the Solea graben). Previous models for asymmetric spreading at the Solea graben require the Kakopetria low-angle detachment to persist at depth beneath the tilted SDC and the block faulting to root onto the detachment surface. The OCC model goes one step further by suggesting the up-domed mantle rocks were exhumed on the seafloor and the detachment fault surface was exposed to the seawater. Oxygen isotope analyses from the serpentinite at the Amiandos Fault indicate the mantle rock was serpentinised by reaction with cold seawater, supporting the OCC model.

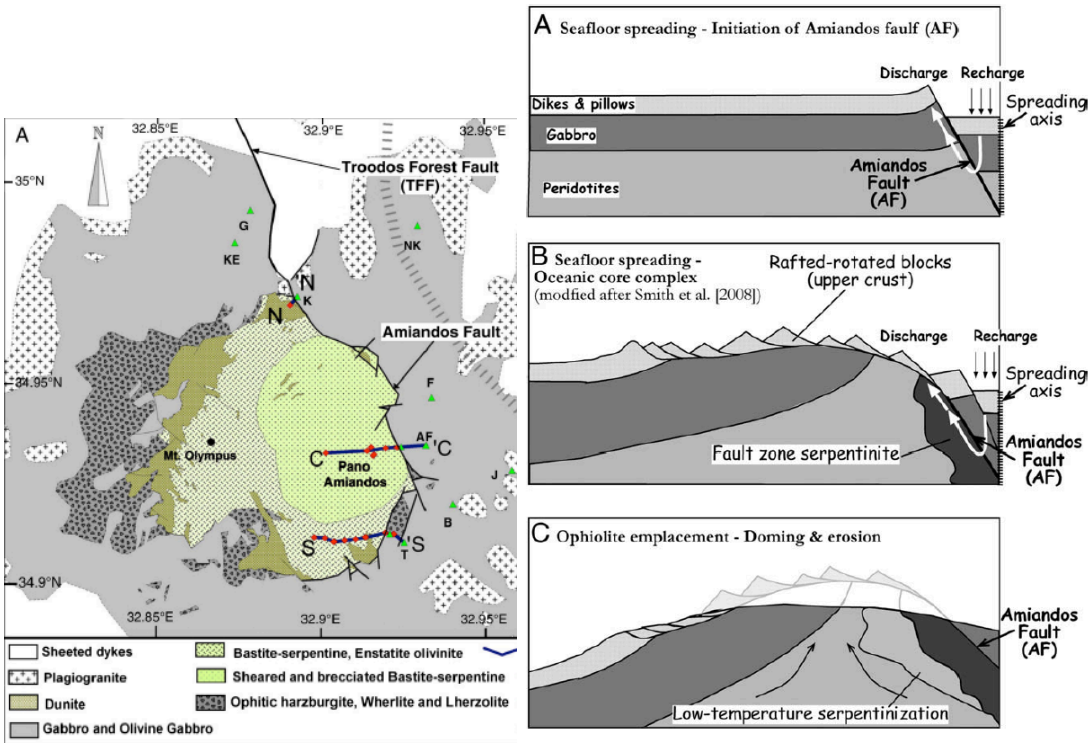

Figure 2.11 The Amiandos Fault bounding serpentinite and gabbros is re-interpreted as a detachment fault from an OCC which exposed serpentinite on the seafloor during spreading. From Nuriel et al., 2009.

2.8 Outstanding questions

This is the first study to look at the extrusive rocks systematically with view to testing existing Troodos crustal accretion models (Varga and Moores, 1985, 1990; Allerton and Vine, 1987, 1991; Hurst et al., 1992, 1994; Nuriel et al., 2009), which are either based only on the sheeted dyke complex or else are almost completely conceptual, and to link Troodos processes explicitly to ocean-floor processes.

The Varga & Moores (1990) model for intermittent stretching and magmatism seems very robust with regard to many of the observed features such as the structure of the SDC into three grabens, the position of the Kakopetria Detachment fault, overprinting of hydrothermal alteration and epidosite zone after the graben was formed, and late plutonism being evident in some areas (e.g., Eddy et al., 1998). But unanswered questions remain regarding the lava stratigraphy, the tilting of the lavas, thickness changes, and magma plumbing. In this thesis these questions are addressed by creating a robust framework for lava stratigraphy across the ophiolite to identify

areas of thickness changes, major faults, and understand how the graben structures affect the lava flows (following the approach of Taylor, 1990).

Schouten & Kelemen (2002) propose a magma plumbing model for the two lava suites of the CY-1/1A drill core, each being tapped from different parts of the lower crust. This model implies that the compositional variations are a result of fractional crystallisation, and hence the entire extrusive suite is cogenetic. It does not, however, explain the upward depletions documented in so many sections (see section 2.5 above). To test Schouten & Kelemen's model a geochemical investigation of many stratigraphic sections through the extrusive sequence has been undertaken to identify which sections are characterised by changes in magma source up-section and which sections are cogenetic throughout.

Schouten & Denham (2000) document a steepening in magnetic inclination down the CY-1/1A drill core, but their lava loading/subsidence model entirely neglects the possibility that the extensive faulting observed throughout the SDC could play a role in accommodating the inclination changes. This was tackled by conducting structural mapping across most of the northern flank of the Troodos extrusives, documenting tectonic tilting by measuring orientations of lava flows and dykes and identifying faults.

There still remains disagreement on the division of the lavas into two or more suites and the definition of those divisions. The depth of Gass & Smewing's alteration front is sometimes, but not always, consistent with the GSD's Upper and Lower pillow lava sequences. The high-Ti and low-Ti lavas generally correspond with the UPL-LPL distinctions but not everywhere do they match. Clearly the lava stratigraphy needed readdressing, which has been assessed by detailed field mapping and a more comprehensive geochemical investigation, also taking into account all available geochemical data.

3 Structural architecture

3.1 Rationale

The Troodos ophiolite is thought to have formed at a slow-intermediate rate spreading centre (as discussed in Chapter 2) based on the high degrees of tectonic extension previously recognised across the sheeted dyke complex, particularly in the Solea graben where the Kakopetria detachment fault is exposed (e.g., Hurst et al., 1992; 1994). To understand how slow to intermediate rate spreading ridges operate and how the upper oceanic crust is accreted it is essential to look at the internal structure of oceanic crust in two or, ideally, three dimensions. The Troodos ophiolite is a very well preserved across-axis slice of subduction influenced oceanic crust with original spreading structures preserved and the entire crustal sequence exposed by the uplift of Mt Olympus (see Chapter 2). The main aim of the current study is to create an accretion model based on field-relationships to better understand the spreading structure of the Troodos crust, which can then be applied to mid-ocean ridges in general.

To date there have been many field studies of the Troodos ophiolite, including detailed mapping by the Cyprus Geological Survey Department, a number of structural and palaeomagnetic studies of the sheeted dyke complex (e.g., Hurst et al., 1992; Varga et al., 1999; Allerton & Vine, 1987), and detailed volcanological studies of portions of the extrusive sequence (e.g., Schmincke et al., 1983). Although the Survey maps contain a great deal of information about the orientation of dykes and inferred faults within the sheeted dyke complex (SDC), this is not the case on the maps for the extrusive units. Where detailed volcanological studies and facies mapping of volcanic units have been carried out, there have been few attempts to relate the studies to the immediate structures or larger-scale tectonic context. Existing models for crustal accretion of Troodos are either entirely based on the SDC or else are largely conceptual (see Chapter 2 for an overview of the Troodos geology and descriptions of the models).

To address how the upper crust was accreted, detailed field investigations have been undertaken in the Troodos ophiolite, focusing on the extrusive units, dyke-lava transition ('Basal Group') and the SDC. Systematic collection of dips and strikes from dykes, lava flows, sediments and faults have been made with the aim of documenting the tilting history of the upper crust across the northern half of the ophiolite. In addition, a parallel geochemical investigation of the Troodos lavas has been undertaken, from which a systematic geochemical division within the extrusive sequence has been identified. This has been used this to help erect a stratigraphic framework which is considered to be more robust than the previous subdivisions of the lavas (as outlined in Chapter 2). This new stratigraphic framework has enabled assessment of the thickness of the lava stratigraphy in a way that has not previously been possible. This new stratigraphy is of great value in helping guide our understanding of how the volcanic pile was accreted.

One of the fundamental tools of any structural study of the extrusive section is the identification of marker flows. To a first order, lavas may be regarded as palaeo-horizontal markers, just as dykes are generally a reasonable approximation to a palaeovertical (i.e. perpendicular to the minimum compressional stress direction); however, the extent to which the assumption is valid for oceanic volcanics is questionable. Pillow lavas on the modern ocean floor in particular are observed to form predominantly on slopes (e.g., Gregg & Fink, 1995), as opposed to sheet flows in flat regions (e.g., Tominaga & Umino, 2010) so it could be argued that pillowed lava flows are inherently unreliable as tectonic markers.

In the course of this project, however, the orientation of numerous lava flows has been measured in the field to assess the amount of tectonic rotation, making the inherent assumption by so doing that the lava flow tops indeed represent a reasonable approximation (at least) to the palaeo-horizontal. This is regarded to be a justifiable assumption for the Troodos lavas for the following reasons:

1. the topmost lavas are sub-parallel to the dip of the Lefkara Formation chalks;
2. those topmost lavas are restored to the horizontal when the bedding tilt is removed;

3. in many 3D outcrops of pillows they are observed to have flattened tops which are found to be sub-planar, consistent and sub-parallel when enough are measured;
4. planar orientations of pillowed flows in 3D outcrops are similar to those of planar sheet flow tops;
5. lava flow dips are similar to the interbedded sediments that occasionally occur within the lavas;
6. dykes, which are assumed to be vertically emplaced, are often orthogonal to the lava orientations at outcrop;
7. palaeomagnetic results support these assertions because the rotations derived from the SDC immediately below the lavas can be applied to the lavas and result in coherent and consistent tectonic rotations, both in axis and magnitude (see Chapter 4).

These data have been synthesised into a structural cross-section spanning the width of the northern flank of the ophiolite from the western coast near Kokkina to Ayia Anna in the east (Figure 2.4) In effect it is a composite 2D across-axis profile, at 90° to the spreading axis as defined by the mean orientation of the dykes, which are assumed to be emplaced parallel with the axis. The Troodos mean spreading direction is here defined from the orientation of 2727 dyke measurements, here plotted on a contoured stereonet (figure 3.1). The spreading direction is considered to be the plane that fits through the centre of the best fit great circle (Bingham axis 1) and the pole to the best fit great circle (Bingham axis3). In current coordinates (i.e. neglecting the late Cretaceous 90° anticlockwise rotation of the Troodos ophiolite, Clube & Robertson, 1986) the mean Troodos spreading direction is 105.5°, and mean ridge trend 016°. The profile was drawn with the field measurements projected onto the vertical plane trending 105.5°, so the dip bars on the 2D profile are apparent dips projected onto an ESE plane.

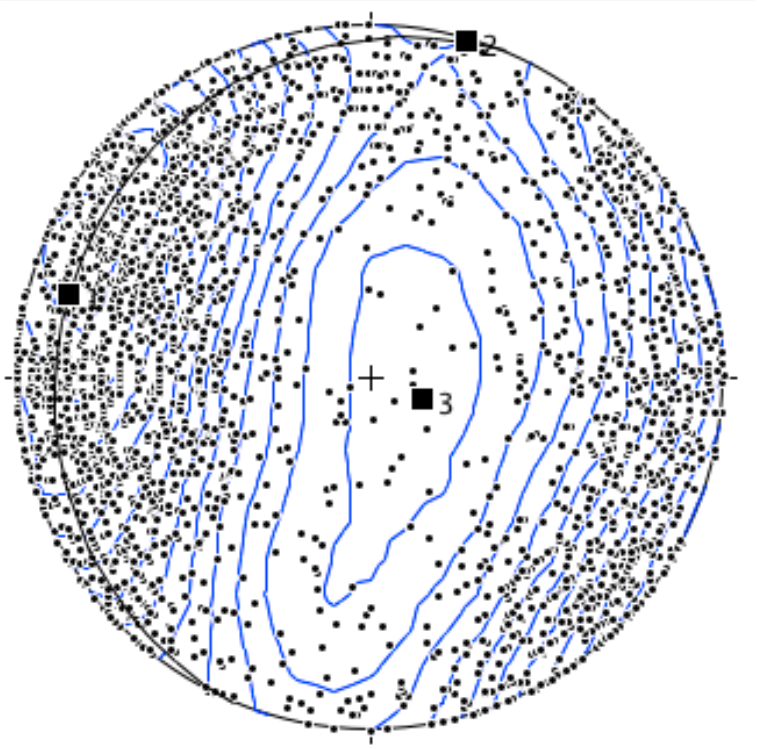

Figure 3.1 Stereonet of all dyke data plotted as poles to plane (small dots), which are statistically contoured (blue lines). Best-fit great circle is black, Bingham axes 1-3 are bold squares, axis 1 is at the mean direction for the dyke pole to plane, axis 3 is the pole-to-plane of the best-fit circle.

The top of the 2D profile (i.e., -0m) is at the lava-sediment contact, which is considered to be horizontal, and the underlying stratigraphy is 'hung' from that contact as a reference point. Because the relief of the lava-sediment contact only varies on the order of several tens of metres – which indicates the seafloor topography was rather flat – this approach is a reasonable approximation. It is supported by the similarity in tilt of the chalk beds and the topmost lava flows (see sections 3.6.1 and 3.6.3). Depths of all the structural data and geochemical samples were calculated using the true depth equation below, which also accounts for changes in present-day elevation across the outcrop (figure 3.2).

$$\text{True depth} = (\text{outcrop width} \times \sin \text{dip}) - (\Delta \text{ elevation across outcrop} \times \cos \text{dip})$$

The dip bars of the 2D profile (figure 3.4) are coloured black for lavas and pink for dykes. All the strike/dip data have been corrected for uplift tilt, and the dip has been adjusted for the orientation of the profile line.

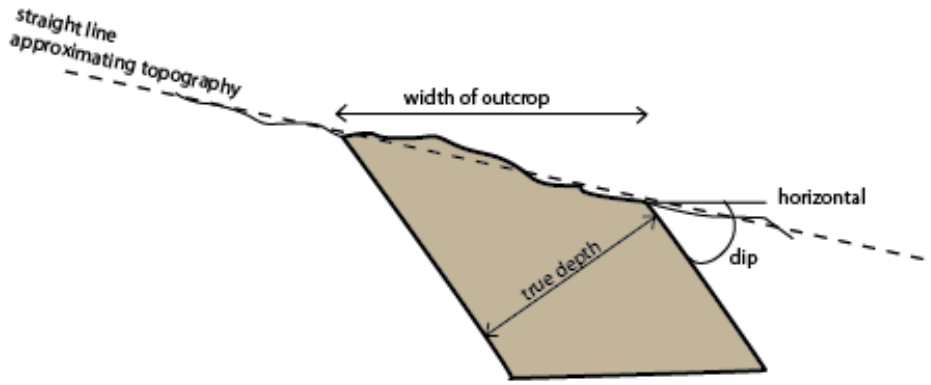

Figure 3.2 Diagram to illustrate to true depth is calculated.

3.2 Field stratigraphy of the extrusive sequence

3.2.1 Basic structure

In map view there are domains of dykes and faults with similar dip and strike which define the grabens (figure 3.1 simplified map of domains, after Varga, 1991). From west to east they are named Stavros domain, Solea graben (west and east domains), Mitsero graben (west and east domains), Makhaeras domain, and the Larnaca graben (west and east domains). More details on the history of the dyke domains can be found in Chapter two. Generally the dykes dip toward the graben centres.

The field measurements (lavas=1491; dykes=591; sediments=94; faults=180) combined with orientation data extracted from the Cyprus Survey maps and published sources and summarised for the 2D profile (figure 3.3). The structural data is described in more detail in sections 3.5 and 3.6 below. The position of geochemical samples are shown by red, blue and yellow dots, of the 627 analyses 115 are new from this study. Stratigraphic element plots (figs 3.14-3.20) have been plotted where there are enough samples along a N-S transect. The transects cover an area 25km wide have been chosen on the basis of sample density and avoiding transects which intersect large faults.

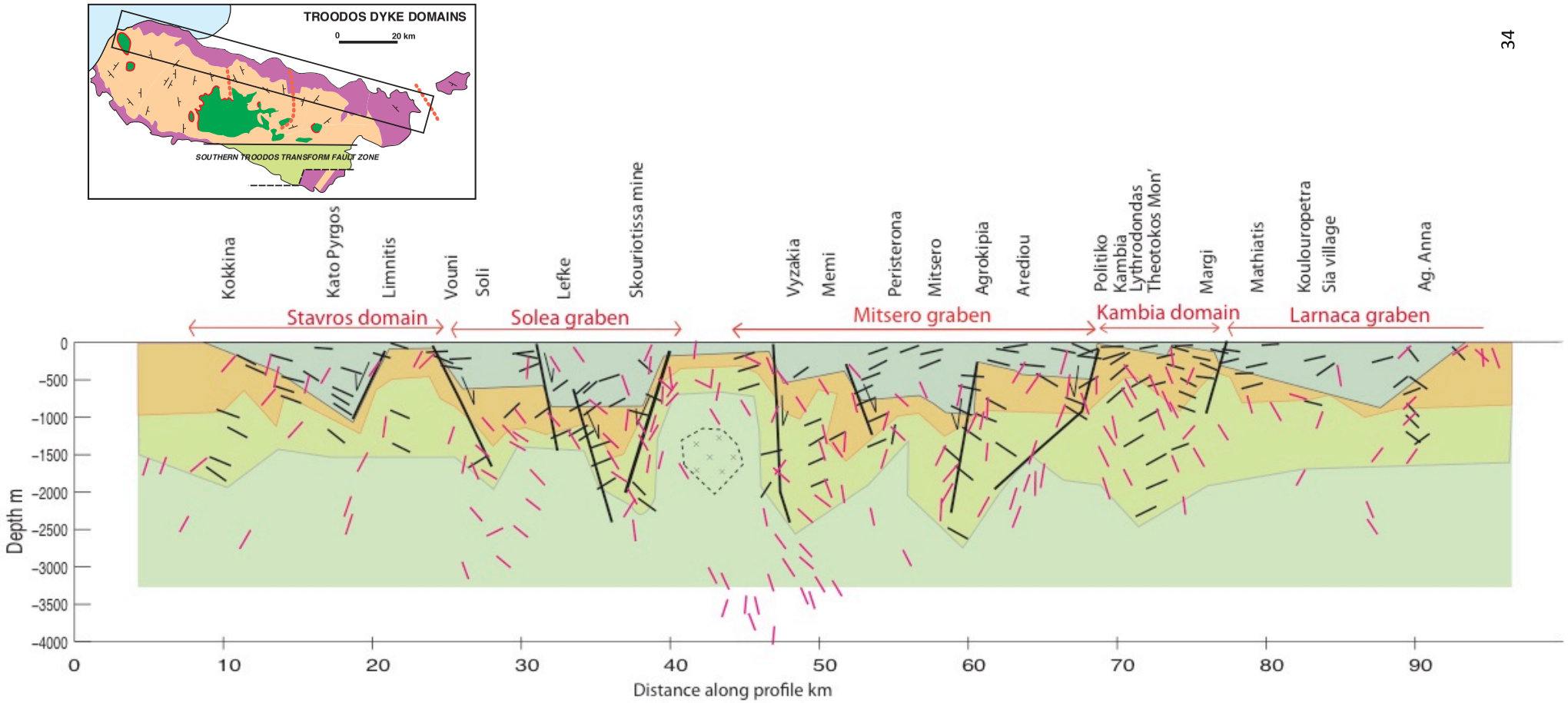

Figure 3.3 Cross-section of the upper crust across the north flank of the Troodos ophiolite (see inset map for study area). Stratigraphic units are: low-Ti lavas (blue), high-Ti lavas of the extrusive sequence (orange), high-Ti lavas of the basal group (peach), sheeted dyke complex (green). Black bars = true dip of lavas, pink bars = true dip of dykes (both projected onto plane of profile, after tilt correction).

3.3 Geochemical stratigraphy

The field observations of the extrusive rocks can only provide a very broad stratigraphy. For this thesis, therefore a geochemical study of the Troodos lavas has been carried out with the aim of better understanding whether and how the 'upper' and 'lower' lavas differ. In the course of this study, as demonstrated below, it became obvious that a systematic, stratigraphically controlled geochemical division does indeed exist in the Troodos extrusive section as seen in figure 3.4. The nature and implications of the geochemical differences for the petrogenesis of the Troodos magmas and for geodynamics are explored in Chapters 5 and 6.

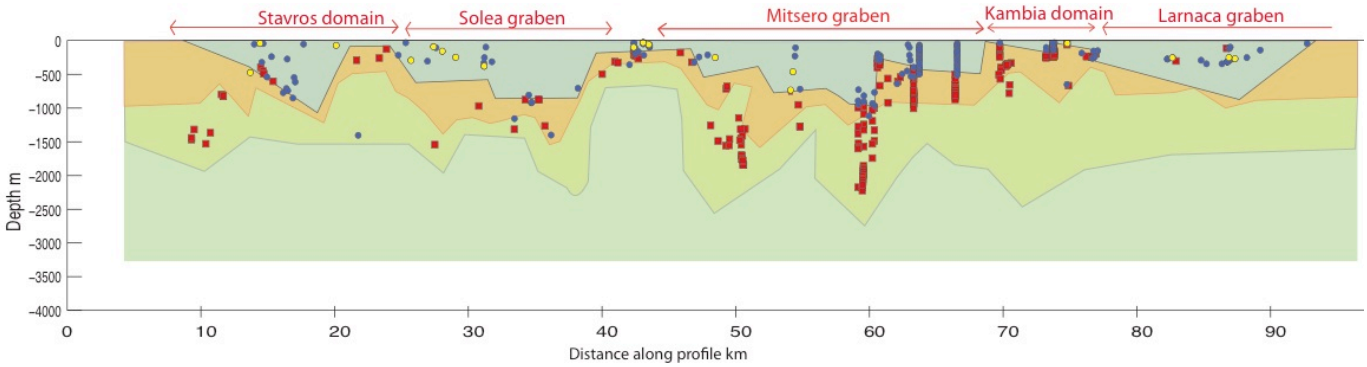

Figure 3.4 Geochemical stratigraphy of the Troodos extrusive sequence. Blue dots = low-TiO_2 lavas, red dots = high-TiO_2 lavas. The boundary between the low- TiO_2 lavas and high-TiO_2 lavas is defined by the change in TiO_2 content. Stratigraphic units are: low-Ti lavas (blue), high-Ti lavas of the extrusive sequence (orange), high-Ti lavas of the basal group (peach), sheeted dyke complex (green).

In the following sections the basic results that demonstrate this sub-division are presented. Where the geochemical data are dense enough along a north-south transect, the elements TiO_2, Zr, Y and Cr are plotted against depth. In each transect presented here systematic variations in all four elements have been found, with a step-wise decrease in incompatible elements in each individual stratigraphic section. This is most usefully expressed in practice by sub-dividing the lavas into 'high-Ti' (below) and 'low-Ti' groups (above), though the step could equally well be defined by step decreases in Zr or Y, and (usually) an increase in Cr. Accordingly, each individual geochemical analysis has been classified into either the low-Ti lava or the high-Ti lava category by demonstrating for each stratigraphic section that there is a significant and consistent difference between the geochemistry of the two groups.

The geochemical data and field evidence presented here are exclusively from the northern flank of the ophiolite. Data from each individual stratigraphic section through the ophiolite, from west to east, are presented and discussed to demonstrate the rigorous way in which the lavas were subdivided into two stratigraphic units. The density of the data is not uniform across the ophiolite, unfortunately, but this has been greatly improved by the addition of new geochemical data collected during this study. The areas of sparse geochemical data or field evidence are either in militarised areas, or have poor exposure due to farmland and/or thick vegetation cover.

3.3.1 Geochemical stratigraphy plots

The Xyliatos section (fig 3.5) through the West Mitsero domain shows a marked difference in the element abundance of the lavas: there are two clearly distinct groups. From the bottom up there is a step-decrease in TiO_2 wt.%, Zr ppm, Y ppm and a step-increase in Cr ppm. There is a gap in the analyses between -400m and -600m so the boundary can be inferred somewhere between. A second section (fig 3.6), the Peristerona section, transects through this domain 5km further east. This transect had evenly spaced analyses from very near the top down to -1300m depth. Here the same stepped-change is seen, the difference between the lower group and the upper group is even more marked. And the position of the step-change itself can be confidently identified at -720m, below which all sample are TiO_2-rich and above it all samples are TiO_2-poor.

In the East Mitsero domain, at the Mitsero transect (Figure 3.7), there are many analyses from Taylor (1990) and some new data; from -600m to -2500m there is continuous sampling. The step-changes in TiO_2, Zr and Y are well defined; although there are fewer analyses for Cr, the step-change occurs at -950m which is confidently positioned. Two kilometres further east the Agrokipia section (fig 3.8) includes data from CY2/2a drill cores as well as other samples in the area. However, this transect crosses a fault which is likely offsetting the lava stratigraphy on either side, so it is not considered to be a typical crustal section nor is it not useful for identifying the stratigraphic units. Another 3km to the east is the well-studied Akaki section (fig 3.10) with data from Rautenschlein et al. (1985) and intersected by the CY1 and CY1a drill cores. In this transect TiO_2 wt.% shows the greatest step-decrease up section, and

only a subtle decrease for the Y ppm data, step-changes in the Zr and Cr data also occur at -510m. The most easterly transect of the East Mitsero domain is located between Arediou and Politiko (figure 3.10), most of the data here is from Taylor (thesis 1988). This section demonstrates marked step-wise variations in all four elements, in each case this is found at -600m.

The Kambia transect (figure 3.11) is also mostly composed of data from Taylor (thesis, 1987), and as with the previous transect this clearly shows there are two distinct geochemical groups within the lavas which are divided by an abrupt change in TiO_2 wt.%, Zr ppm, Y ppm amd Cr ppm. There is no overlap between the two groups with depth, and point of chemical change happens at very shallow depths here- at -40m.

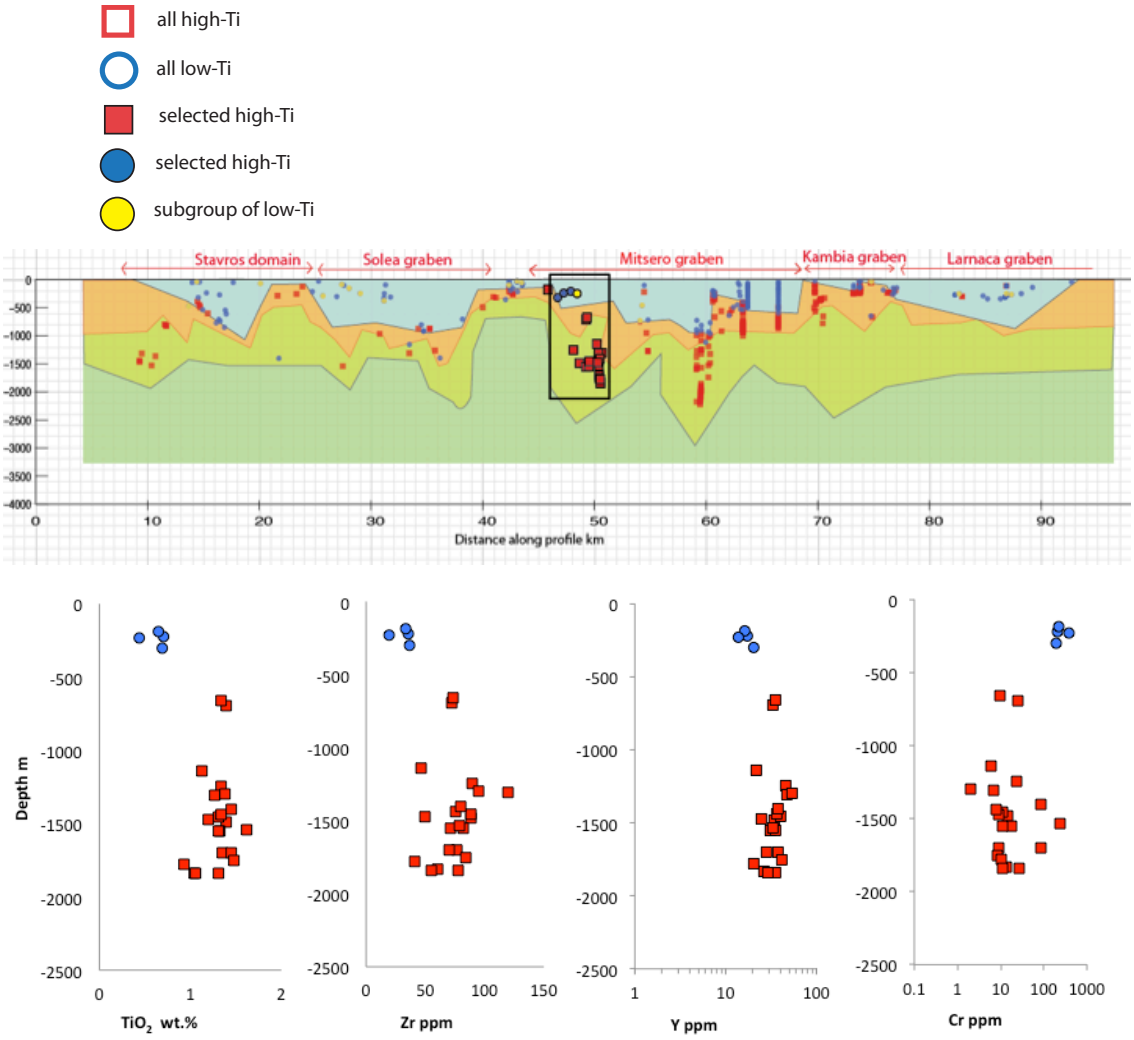

Figure 3.5 West Mitsero (west) – Xyliatos section

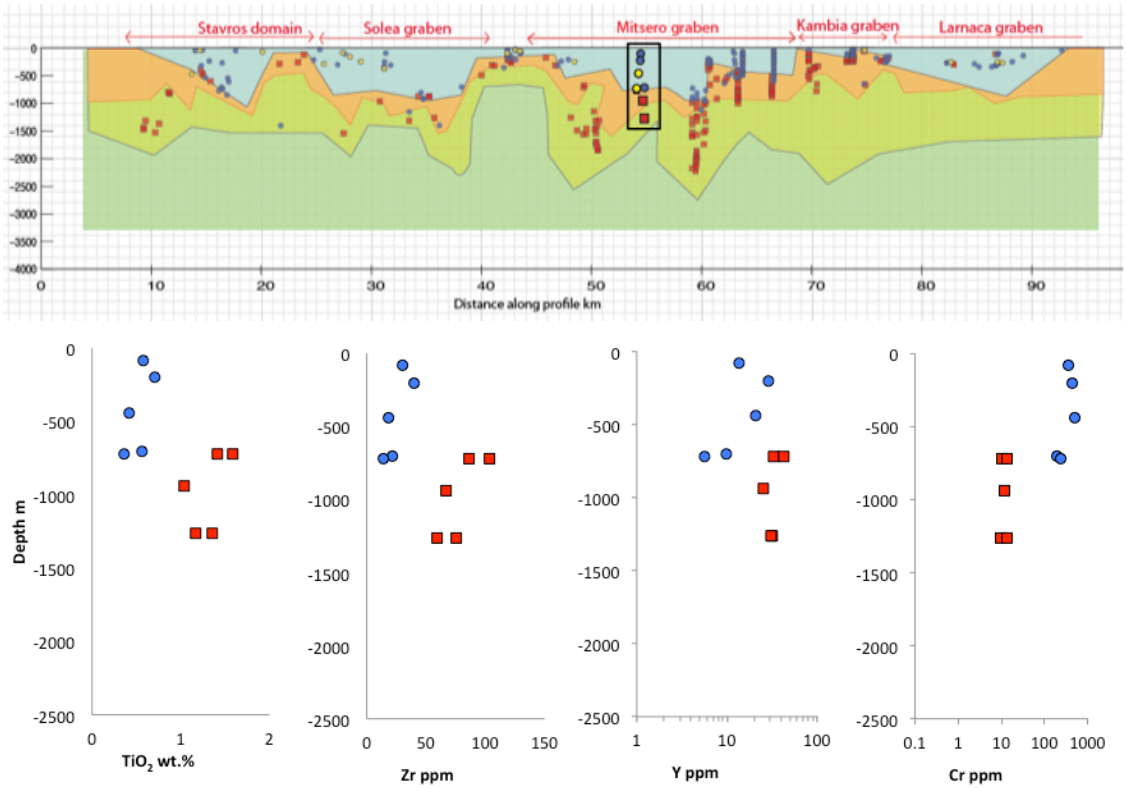

Figure 3.6 West Mitsero – Peristerona river section

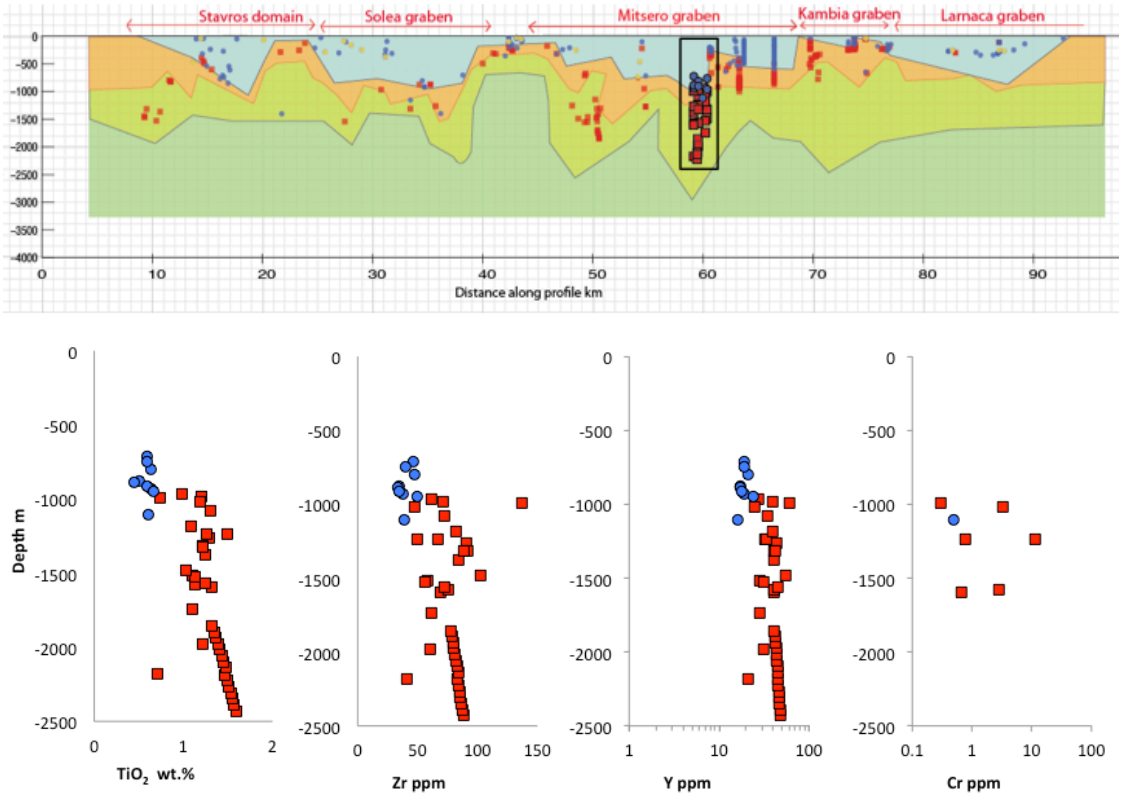

Figure 3.7 East Mitsero (near axis) – Mitsero section

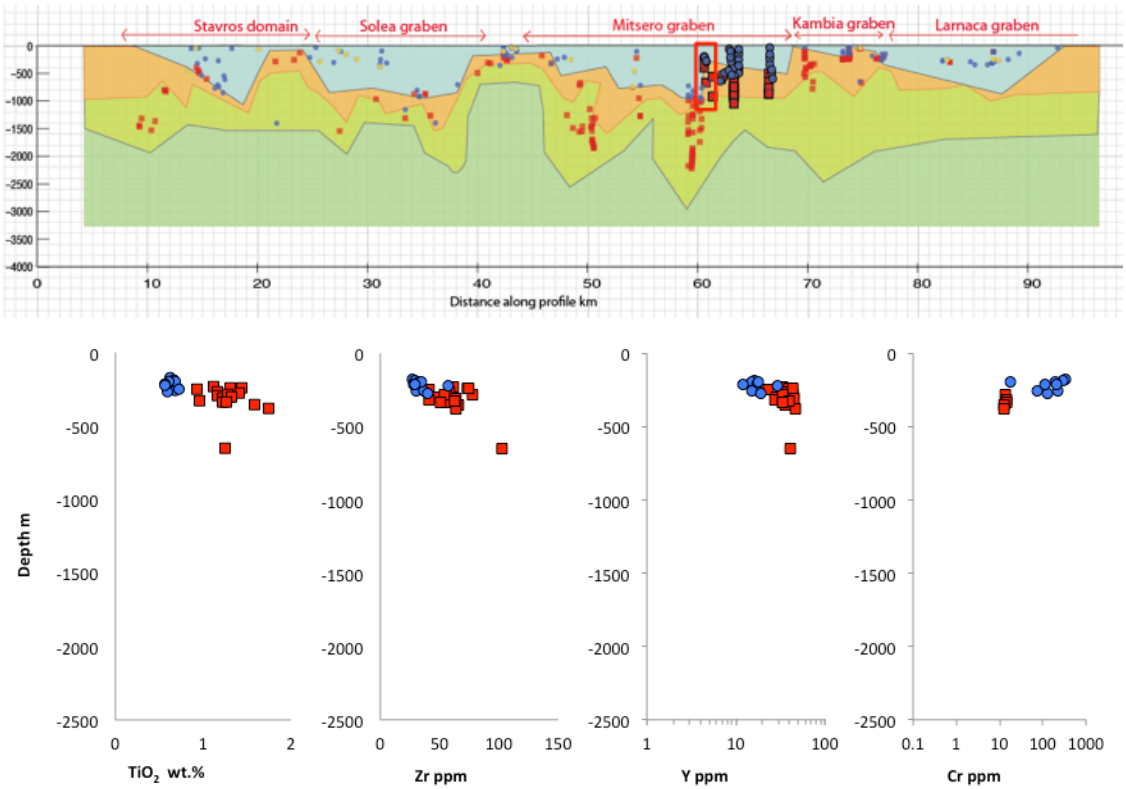

Figure 3.8 East Mitsero (east) – CY-2/2A Agrokipia section

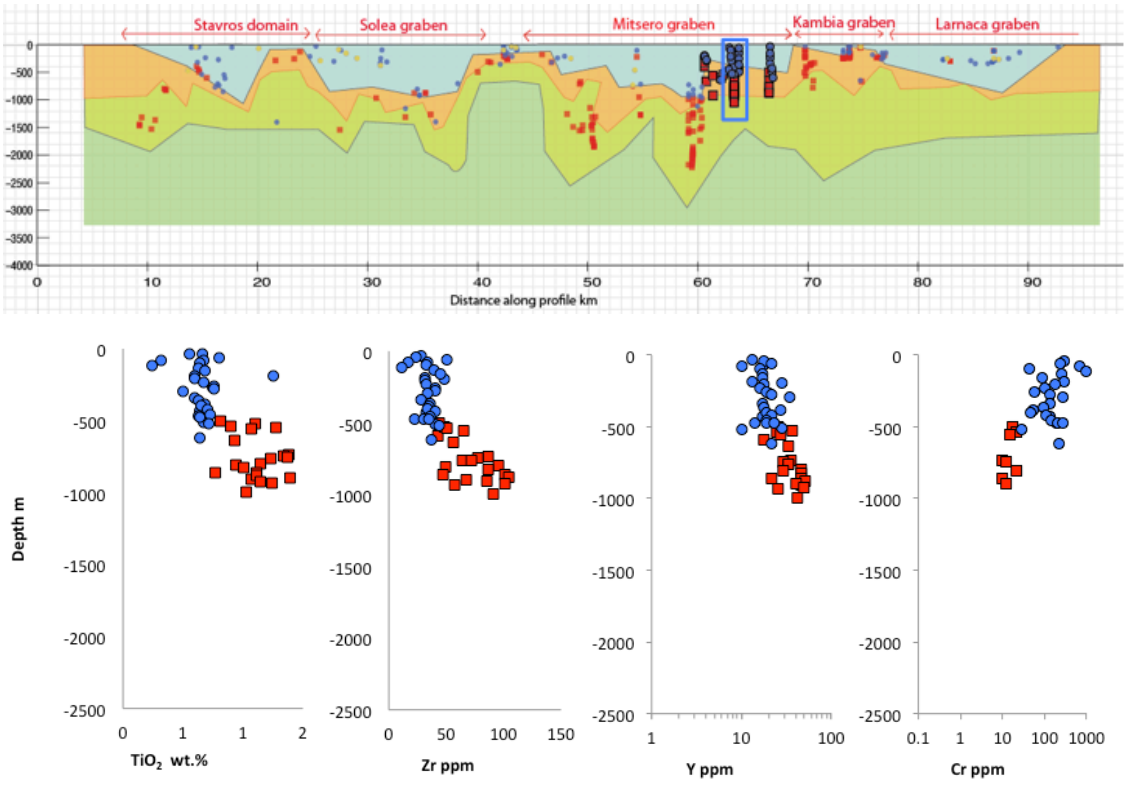

Figure 3.9 East Mitsero (east) – CY1/1A Arediou

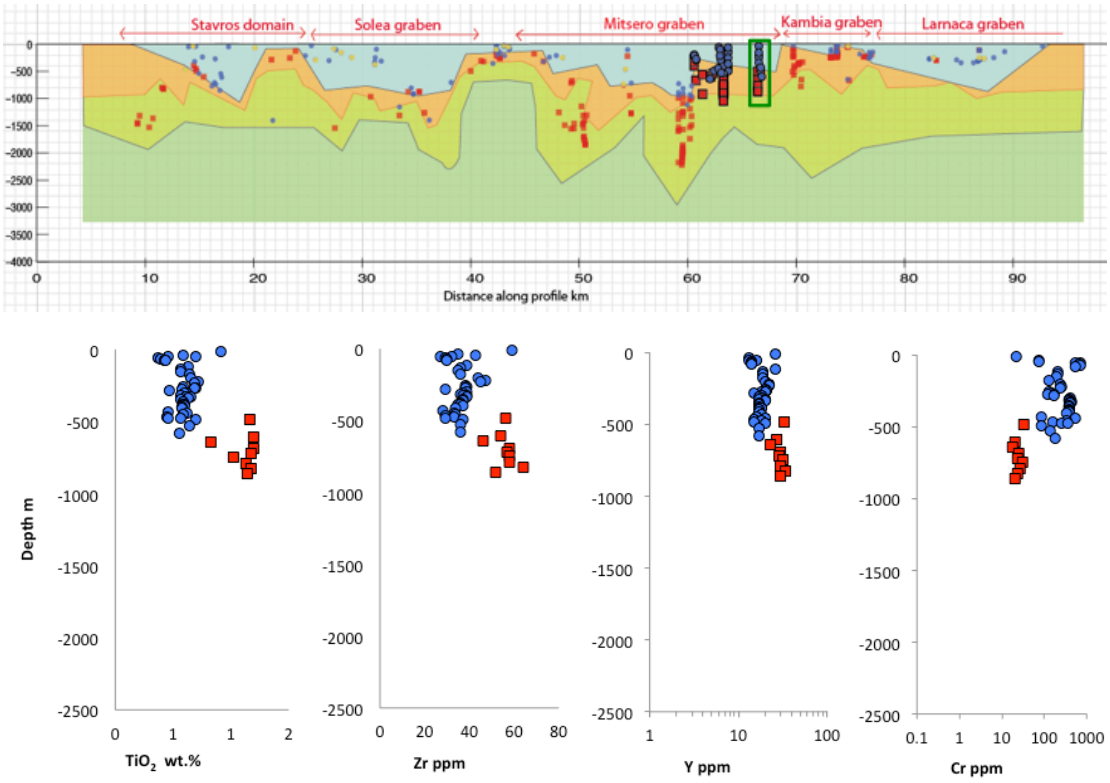

Figure 3.10 East Mitsero (east) – Politiko

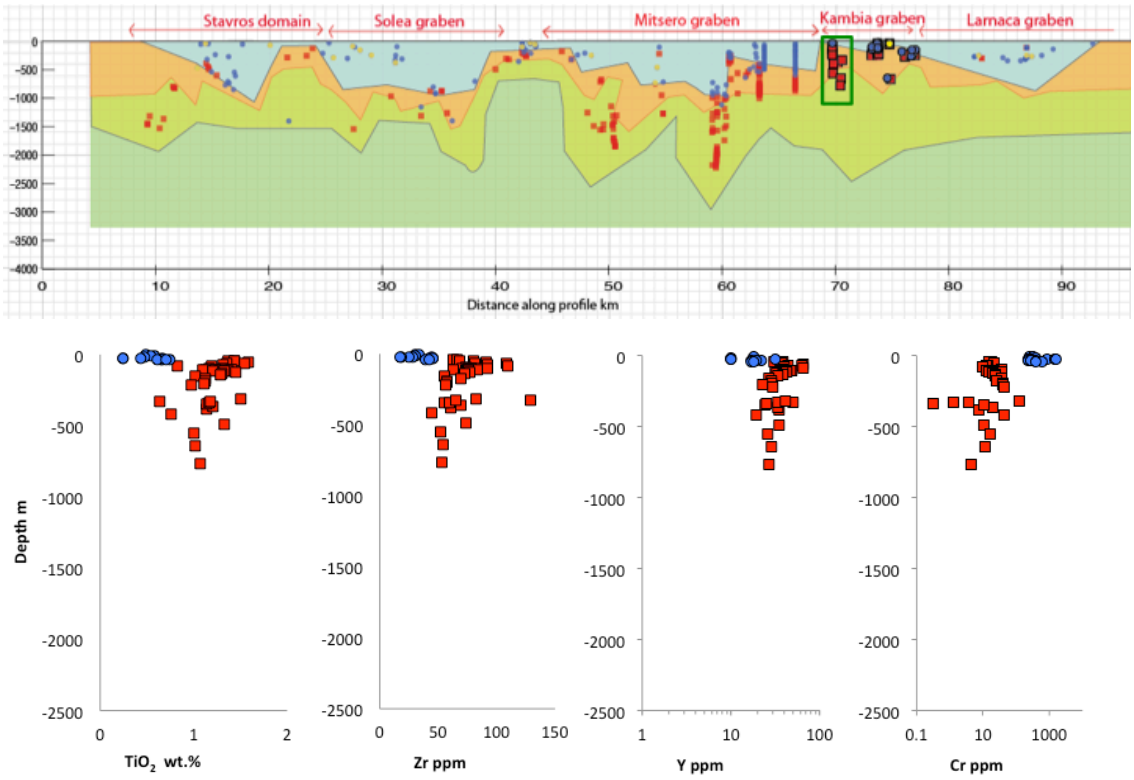

Figure 3.11 West Kambia domain – Kambia

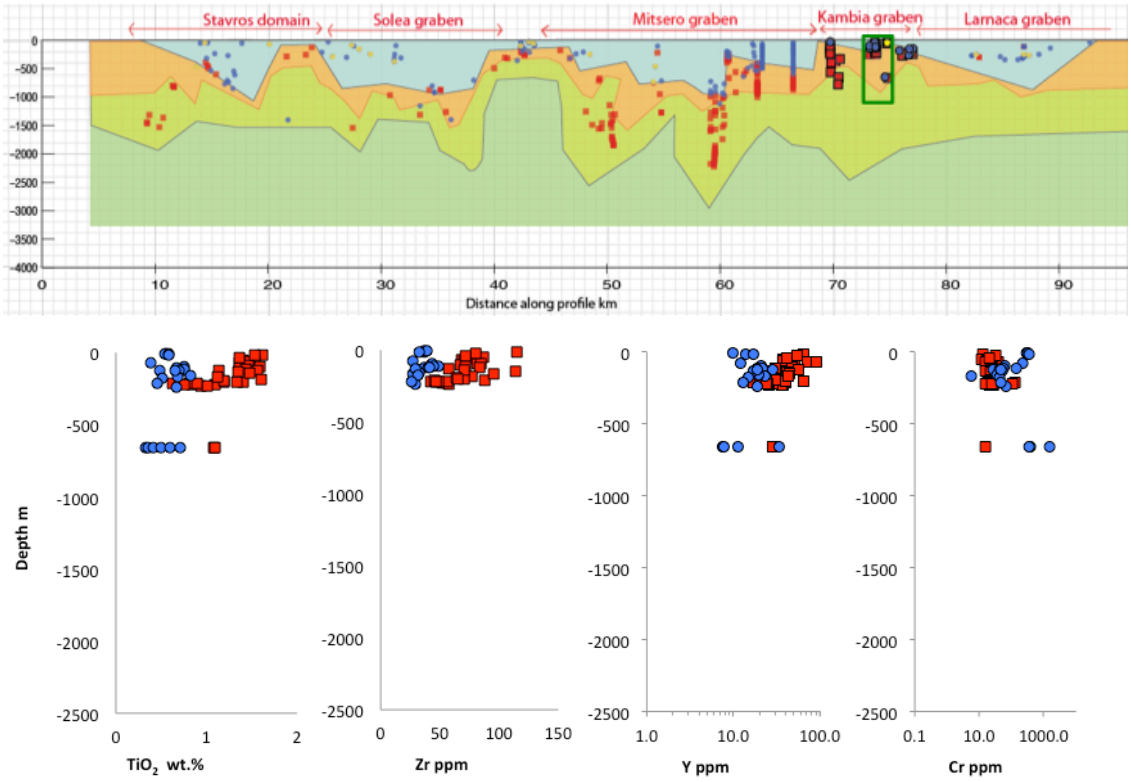

Figure 3.12 East Kambia domain – Analiondas

The only exception to this is at the domain boundary between the Mitsero and Larnaca grabens where Portnyagin et al. (1997) and Pearce (pers. com.) reported depleted low TiO_2 Basal Group lavas at depths of -650m beneath the high TiO_2 lavas. Here the stratigraphy is more complex due to the nature of the domain boundary, which is interpreted by Allerton (1988) as an intrusive contact of the younger Larnaca graben cross-cutting the older Mitsero terrane. Initial U-Pb dates of the plagiogranites at Vavatsinia (MacLeod, pers. com.) indicate that the Mitsero graben is indeed the oldest part of the ophiolite. The model suggested here, discussed further in Chapter 6, is that the 'basement' lavas are the LPL and UPL of the Mitsero graben to the west, which were (both) blanketed unconformably by 'infill' lavas (LPL and UPL) originating from the Larnaca graben to the east.

The geochemical stratigraphy always shows a stepped decrease in TiO_2 wt.%, Zr ppm, Y ppm and a stepped increase in Cr ppm, and this step-wise change occurs at the same stratigraphic depth for each of the four elements within all of the transects. Those with high Cr but low in TiO_2, Zr and Y are generally more depleted, those high in TiO_2, Zr, Y and low in Cr are relatively more evolved and generally non-depleted

(more details in section 3.5, and Chapter 5). Nowhere is there a gradual transition in either of these elements. Similarly, the typical stratigraphy does not show interbedding between the lavas with high TiO_2 and those with low TiO_2.

Based on the consistency of the geochemical stratigraphy as seen in the above transects it can be deduced that there is a systematic geochemical boundary within the extrusive sequence. This boundary divides the lower unit which are always richer in TiO_2, Zr and Y, while poorer in Cr and the upper unit, and the terms 'high-Ti lavas' and 'low-Ti lavas' will refer to the lower and upper lava groups. Because of the consistency seen in the detailed transects, the same classifications (high-Ti or low-Ti) lavas is applicable to the remaining geochemical analyses even where the samples are spatially spread out. These geochemical subdivisions are explored in more detail in section 3.4 (lava geochemistry, and still further in Chapter 5). The pattern of TiO_2 rich lavas at depth and TiO_2 poor lavas near the top is persistent across the entire ophiolite (figure 3.4).

3.4 Stratigraphy by area

Each individual geochemical analysis has been classified into either the low-Ti lava or the high-Ti lava category by demonstrating for each stratigraphic section that there is a significant and consistent difference between the geochemistry of the two groups. Where geochemical data are not available, the field descriptions have been used (e.g., colour, phenocrysts, proportion of dykes) to supplement the classification.

3.4.1 West Stavros

On the far west of the ophiolite the West Stavros domain lavas dominantly dip towards E or NE, and the dykes dip to the W (figure 3.3 & 3.14). Lava flows at the very top of the section are very gently tilted, in fact here they dip towards the north by <10°. Deeper lavas are more steeply tilted, the basal group lavas are steeply dipping between 42°-59°. The lavas have been classified into high-Ti and low-Ti lavas and their spatial distribution can be seen in figure 3.14. The two lava groups clearly have

distinctive geochemistry, as demonstrated by the Zr, Y, Cr and TiO_2 data. Here the boundary between the two lava suites is diagonal, dipping to the east at a similar attitude as the lava flow dips, forming a triangular wedge of low-Ti lavas thickening towards the east. The cluster of four high-Ti lavas at -1500m are from outcrops of the lava-dyke transition zone, these outcrops are ~30% lava screen and the remaining 70% is made up of dykes. It is noteworthy that these localities lie approximately 1km within the SDC on the 1995 Cyprus Survey 1:250,000 map; therefore, the new lava-dyke transition boundary should rightfully be placed beneath these outcrops. Directly south of Kato Pyrgos where the wedge of low-Ti lavas is almost at its thickest there are many samples occurring at depths of up to -835m, yet according to the Cyprus Survey maps the LPL-UPL contact is ~600m above this chemical boundary at -200m.

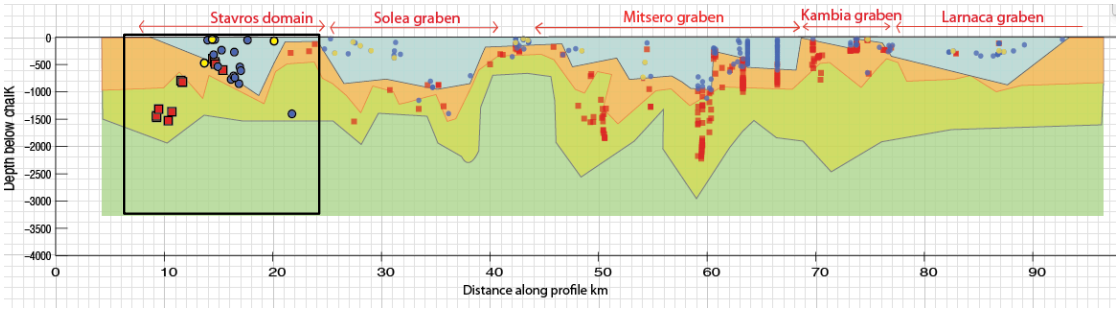

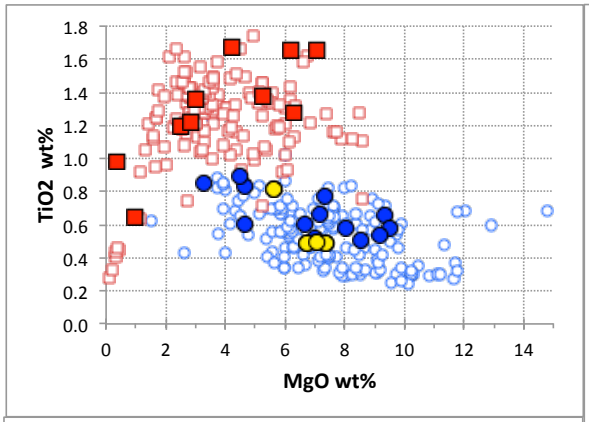

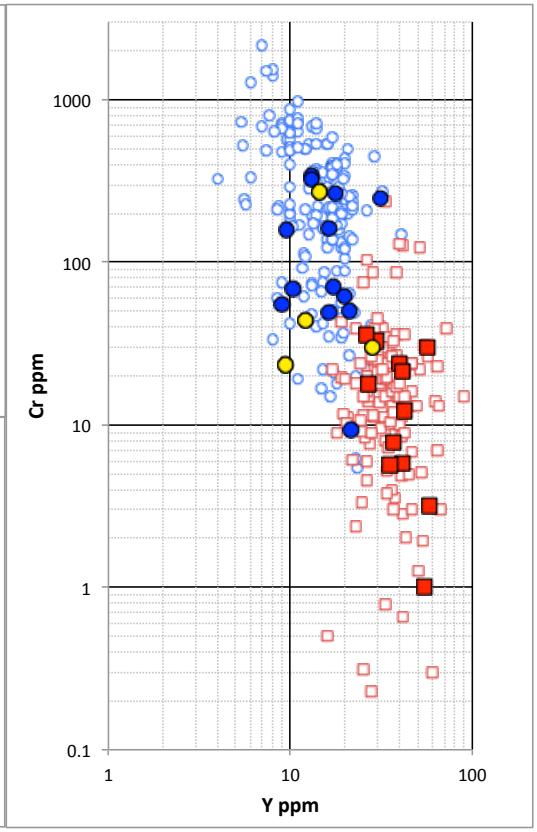

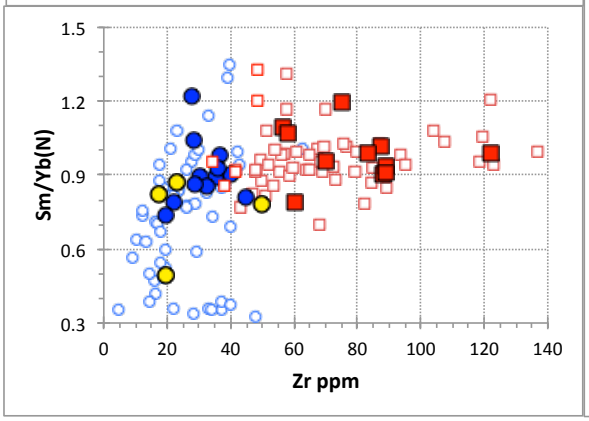

Figure 3.14 West Stavros.

3.4.2 East Stavros

This region straddles the boundary between the Stavros domain and the West Solea domain, which in map view is a diagonal boundary trending NE (Figure 3.2). The three high-Ti lavas (figure 3.14) are from an area where the dykes dip to the west and lavas to the east. Immediately east of those samples there are low-Ti lavas in abundance, and they dip towards the west so are considered to be part of the West Solea domain. The boundary between high- and low-Ti lavas appears to have steeply dipping geometry, but it cannot be traced far because all the geochemical analyses are from the upper 400m. The contact between the high-Ti and low-Ti lavas is at very shallow depths above the high-Ti lavas at -230m. The position of the geochemical boundary between low- and high-Ti lavas is approximately the same at the contact between the UPL and LPL as delineated on the 1995 Geological Survey Department map.

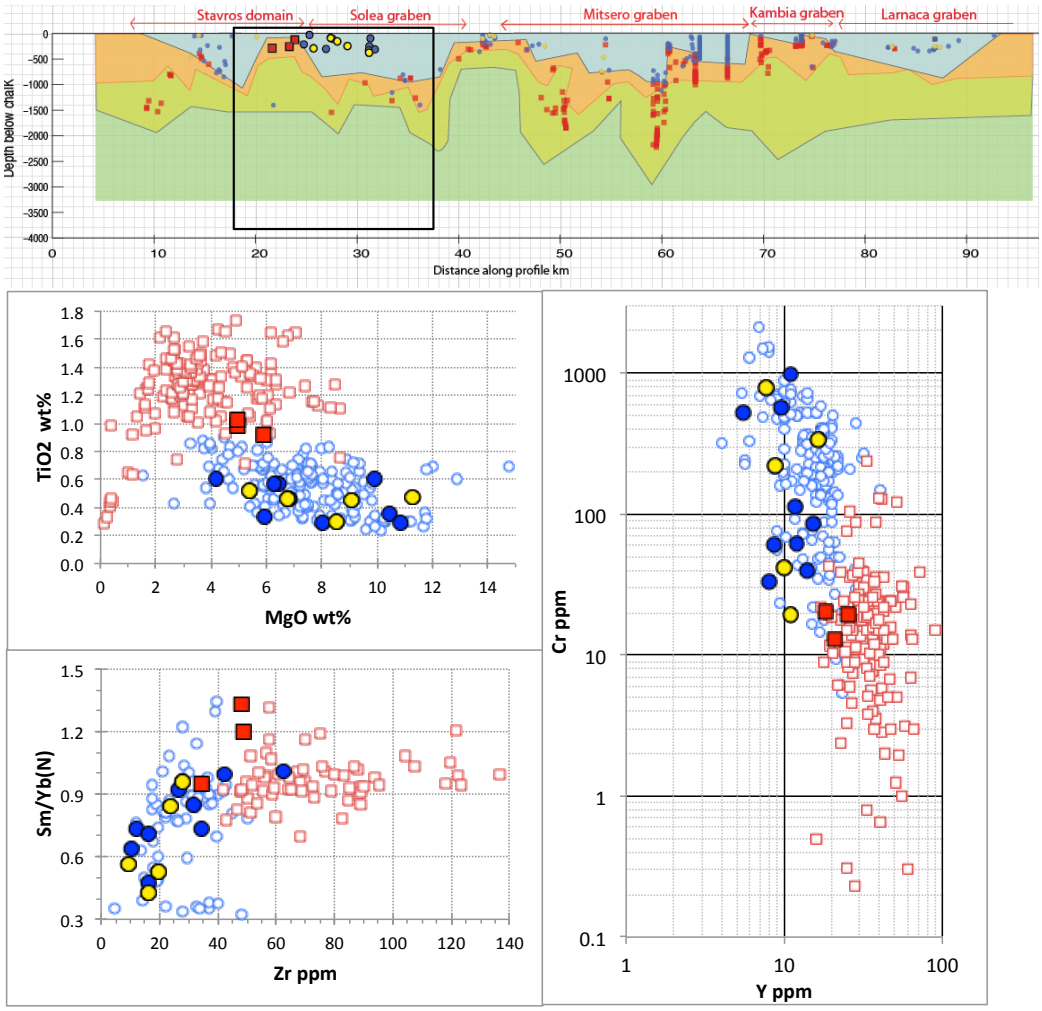

Figure 3.14 East Stavros.

Lava flows from the upper 250m are flat lying to gently dipping, but in the middle and lower part of the low-Ti unit the lavas are much more steeply tilted (several with dips 42-48° in the lower most part of the high-Ti unit, and reaching up to 58-62° in some places).

The high-Ti lavas from the East Stavros domain are lower in TiO_2 wt.% than typical high-Ti lavas, but TiO_2 content is still higher than the low-Ti lavas from this region, and the Cr and Y data also reflect the difference between the two lava groups here.

3.4.3 West Solea graben

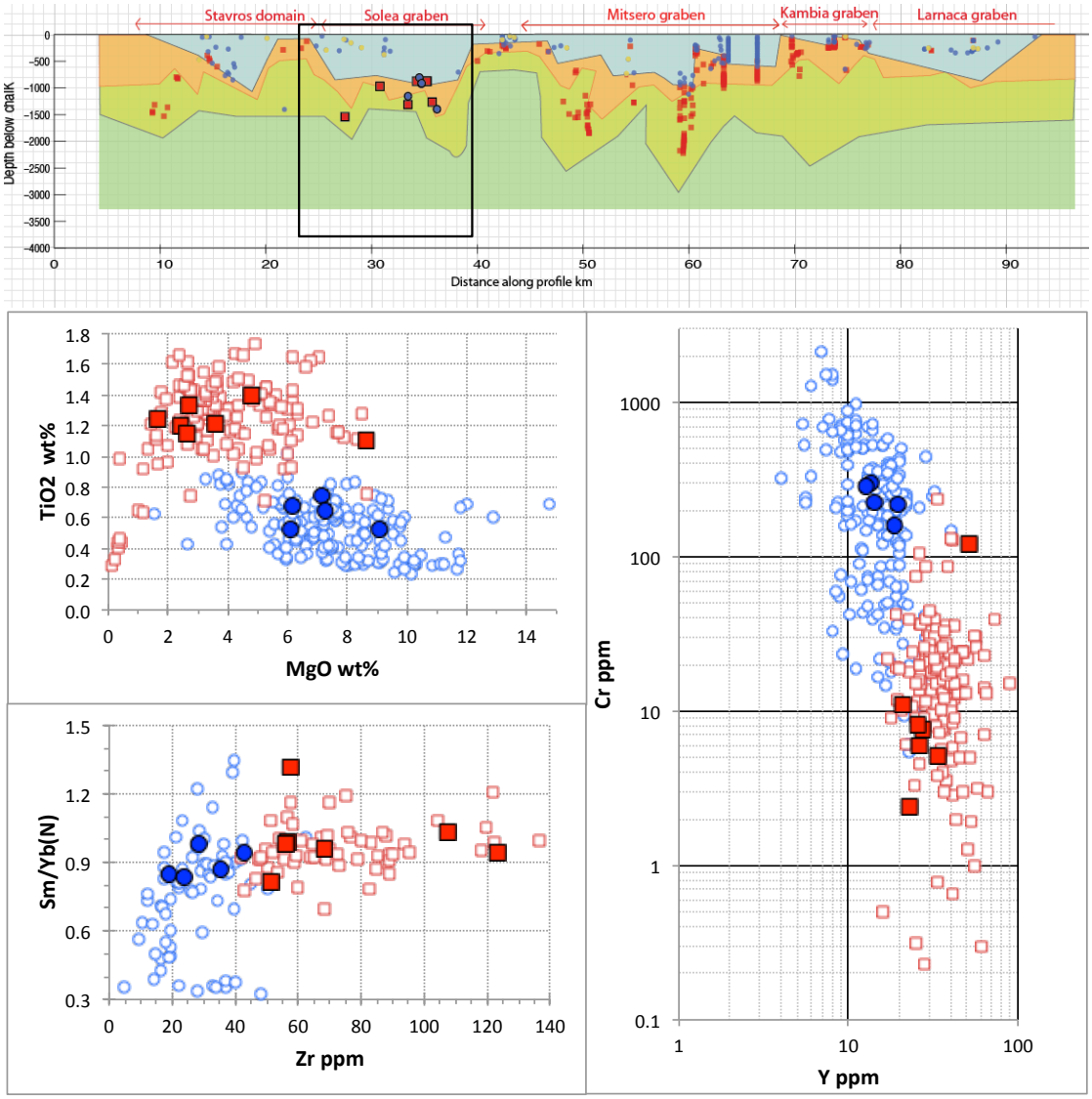

Figure 3.15 West Solea.

The Solea graben is thought to be a fossilised ridge axis (see Chapter 2), its western side being broader than the eastern side at about 12km. On the west side of the graben (figure 3.15) the dykes are often greatly tilted to the east towards the graben centre (to as little as 20° dip), and the lavas are tilted to the west away from the graben centre. The maximum dip to the extrusive section, of 43°, is seen in the high-Ti lavas at deepest levels, within the lava-dyke transition zone. Unfortunately there is a large sampling gap in both field data and geochemical data at the top of the extrusive section because this area, in the vicinity of the Skouriotissa Mine, is a militarised zone and hence inaccessible. All the geochemical plots show there to be clear differences

between the two lava groups. However, the spatial distribution of those lava groups does not form a layered stratigraphic relationship, consequently the high-Ti/low-Ti contact is poorly constrained and is mostly dependent on the field characteristics of the outcrops. The present distribution may be related to highly rotated and deformed crust in the Solea graben due to stretching during spreading.

3.4.4 East Solea graben

On the eastern side of the Solea graben (figure 3.16) the dykes tend to dip to the west, and the lavas to the east, like a mirror of the West Solea domain. This is a narrow region (5km) which has a very thin extrusive section, around 600m total thickness. The underlying SDC outcrops at very shallow depths across a distance of ~8km. The lavas conform to the TiO_2, Cr, Y and Zr sub-division criteria.

In the easternmost part of the East Solea domain the low-Ti lavas are <200m thick and sit stratigraphically on top of the high-Ti lavas. To the west of this domain the low-Ti lavas thicken dramatically, possibly against a large normal fault downthrown to the west. The precise location of the boundary at this western point is however not known, because no high-Ti lavas were encountered here. There is good agreement with the new boundary and the Geological Survey Department's LPL-UPL contact in this region.

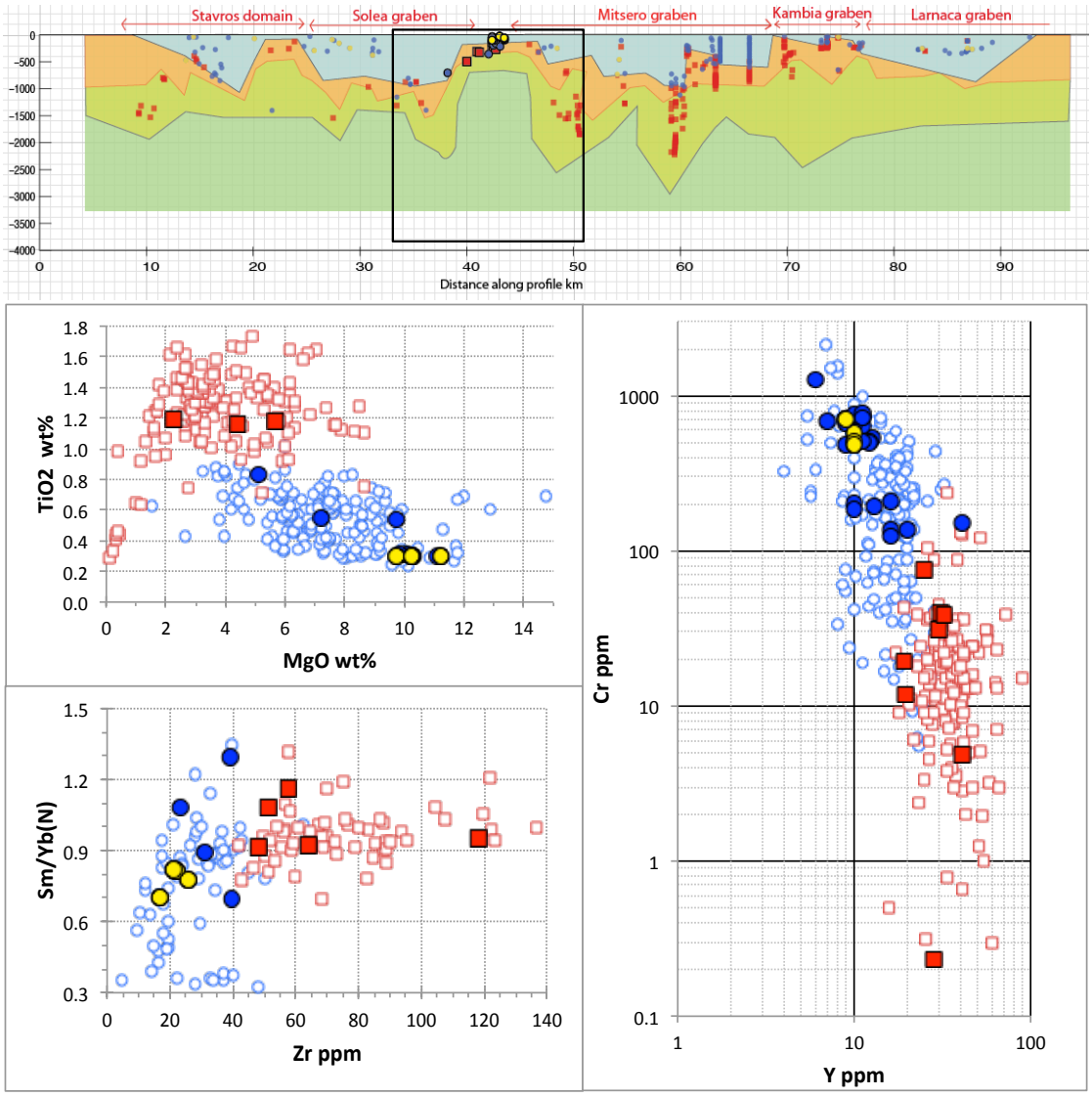

Figure 3.16 East Solea

3.4.5 West Mistero graben (west)

The Mitsero graben totals ~20km in width, and 13 km that makes up the western side where the lavas are tilted west and the dykes tilted east (figure 3.17). The western side of the graben will be discussed here as two parts since it is likely made up of two fault blocks, hence the zig-zag repetition of high-Ti and low-Ti lavas units. Firstly, the West Mitsero (west) section here, followed by the West Mitsero (near axis) section in 3.3.6.

Throughout the whole of the West Mitsero domain the lavas dip relatively consistently, with an average orientation of 179°/24° W. Unlike many other sections they do not appear to be flat-lying at the top of the extrusive series, nor do they steepen obviously with depth. Tilting of this particular section therefore appears to postdate lava extrusion here. The significance of this for the broader-scale history and evolution of the Troodos upper crust will be discussed at the end of this chapter and further in Chapter 6.

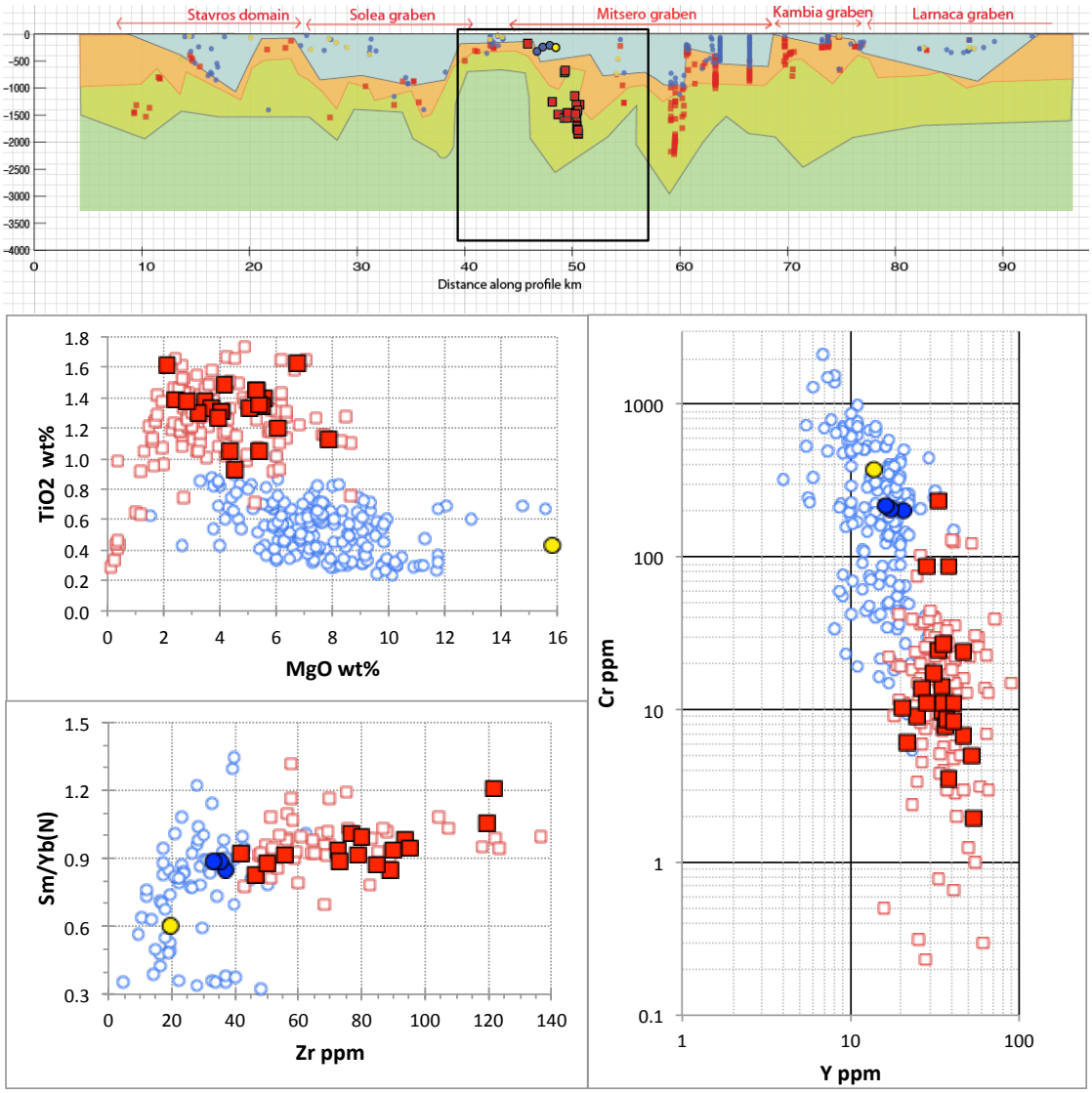

Figure 3.17 West Mitsero graben (west).

All the geochemical analyses from this area fit readily into either the high-Ti lava or low-Ti classification. There is a very shallow high-Ti lava sample at –220 m which is at the same stratigraphic level at the high-Ti lavas from the East Solea graben just ~5

km west of it (section 3.4.4)., yet immediately east of it there are four low-Ti lavas; at this point, therefore, the boundary between the two groups must be steeply dipping and must lie between the high-Ti lava sample and the low-Ti lavas. Three hundred metres directly beneath these low-Ti lavas are many more high-Ti lavas. The boundary between high- and low-Ti lavas is probably dipping parallel to the attitude of the lava flows (gently-moderately dipping to the west), and the depth of the boundary is inferred between the 300m gap (also see figure 3.6). The boundary between high-Ti and low-Ti lavas is in agreement with the traditional LPL-UPL boundary

3.4.6 West Mitsero (near axis)

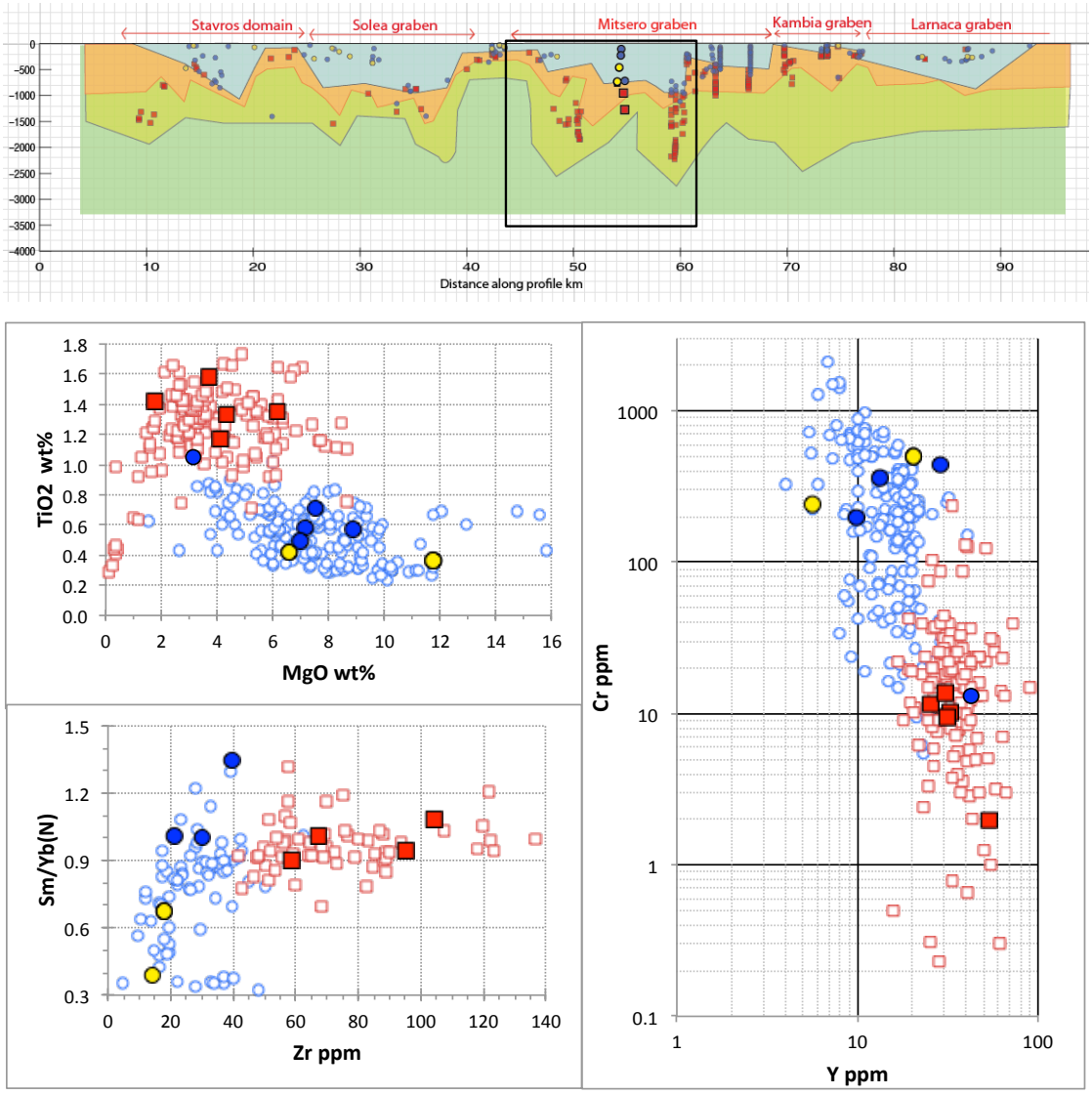

Figure 3.18 West Mitsero graben (near axis)

This transect of geochemical samples and field data taken 3km west of the Mitsero graben axis, the structural attitude here is the same as the previous section (dykes dip east, lavas dip west). Just as with the previous section, here also the lava flows are consistently dipping to the west by 24°, with no change down the section. A clear geochemical distinction between the lower high-Ti and upper low-Ti units is again evident (figure 3.18).

The boundary between low-Ti lavas and high-Ti lavas occurs at depth of -720m as seen in the Peristerona transect (figure 3.6). At the boundary both high-Ti and low-Ti lavas occur because they are in faulted contact by a down to the east large normal fault. The fault is beautifully exposed (see photo in figure 3.19) and clearly demonstrates the 'Lower Pillow Lavas' on the left are dark green with numerous sheet flows in contrast to the pale pillowed flows of the 'Upper Pillow Lavas' on the right, the fault bounding the two units here. Geochemical samples confirm the foot wall rock lavas are high-Ti and the hanging wall lavas are low-Ti lavas. This is correlated very well with the thickening of the low-Ti lavas in this section, and the relatively thinner low-Ti unit just to the west, indicating the low-Ti lavas infilling this half graben and ponded against the normal fault.

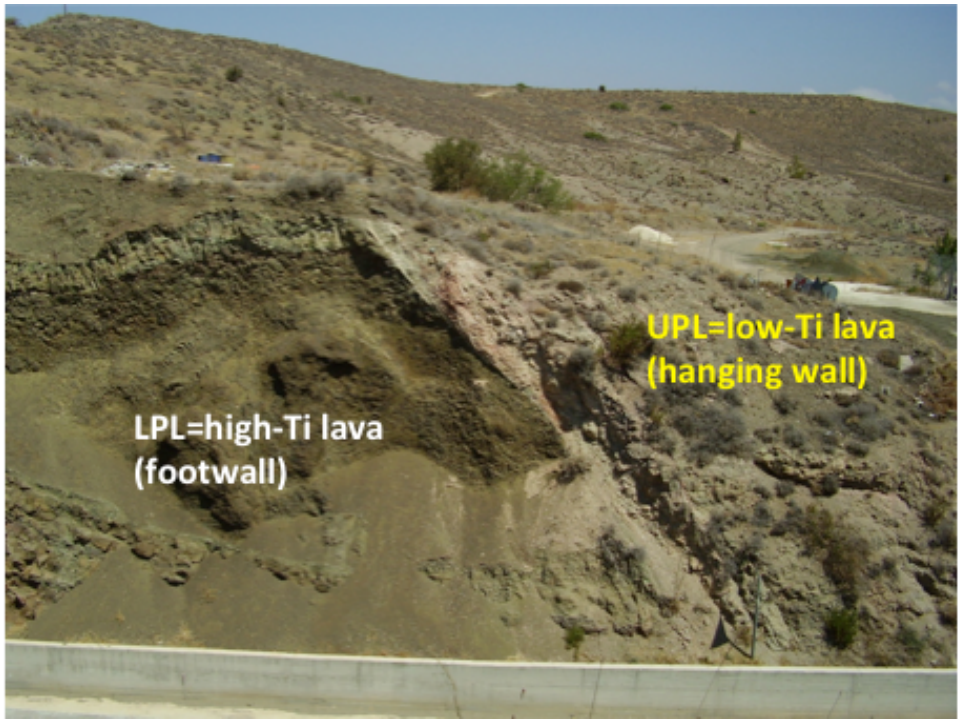

Figure 3.19 Faulted contact between high-Ti lavas and low-Ti lavas. The hanging wall block of low-Ti lavas is downthrown to the east. Photo taken facing north, near village of Kato Moni.

Depth to the boundary is well constrained here, and the attitude is probably the same or similar to the westward dipping lava flows in the region; however, the lateral continuation of this boundary is not well constrained because there are no geochemical data either side of this transect for 3.5km, and it appears to be at the same depth as the LPL-UPL boundary.

3.4.7 East Mitsero (near axis)

Crossing the axis of the Mitsero graben into the East Mitsero domain the lavas are tilted to the east and dykes to the west towards the graben centre. Orientation of the topmost lavas are sub-parallel to the overlying chalks, but at deeper levels the dips become steeper, mean orientation of 353°/43° E in the basal group in Ayia Koroni.

For the nine geochemical samples of the low-Ti lavas only one has a full geochemical analysis; the rest were not analysed for MgO, Cr, Sm or Yb so cannot be plotted on either of the three classification plots (Figure 3.20). Fortunately the TiO_2, Zr and Y were analysed in all the samples, making it possible to classify all of them into high- or low-Ti lavas (figure 3.7).

As with the boundary at the West Mitsero (near axis) section, the boundary here is conformable with the lava dips, i.e. dipping moderately to the east. Notably, this boundary lies at a depth of -950m, within what is marked as the Basal Group on the Cyprus Geological Survey maps, and significantly below what is marked as the LPL-UPL boundary, which is placed at -200m. This is a good example of where the traditional field criteria for distinguishing lava units does not correspond to the geochemical transition, the reason being because of the great thickness (almost a kilometre) of low-Ti lavas that infilled the half graben that was active during extrusion and buried the high-Ti sequence.

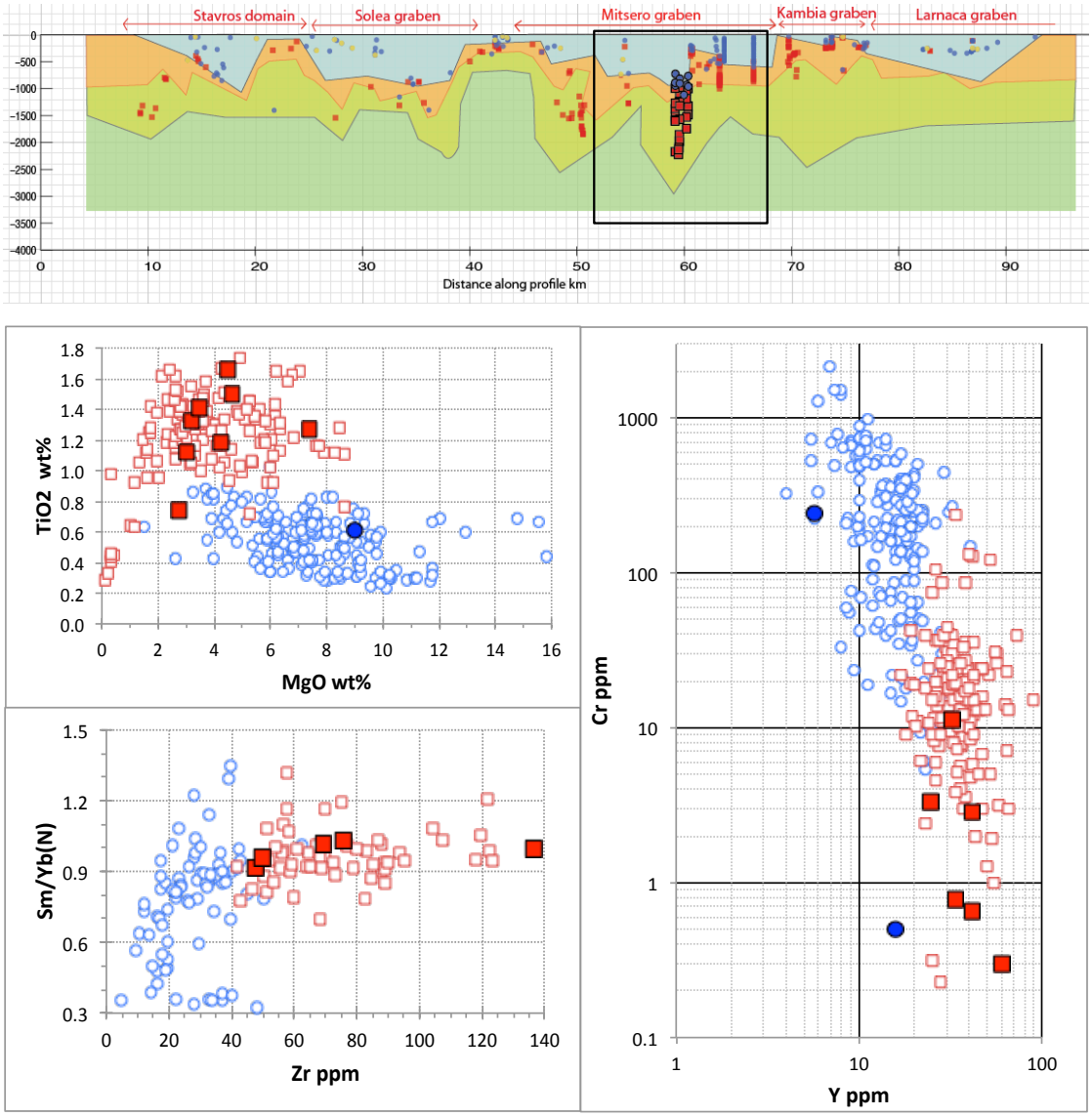

Figure 3.20 East Mitsero graben (near axis).

3.4.8 East Mitsero (east)

This domain has excellent geochemical constraint because it includes the CY2/2a drill cores at Agrokipia (figure 3.8), the data from Rautenschlein (1985) from the well-known Akaki river at Arediou (fig 3.9), CY1/1a drill cores (fig 3.10) also from the Akaki river, and a detailed transect by Taylor (1987; figure 3.10). The transects when examined together show remarkable consistency, with the boundary between the three transects getting gradually deeper from west to east, and clearly demonstrating that the contact between the two units is conformable (Figure 3.21).

The gently inclined boundary is at a depth -220m at the CY2/2a core, then at -510m for the CY1/1a core, and at -600m in the transect between Arediou and Politiko. This geometry creates a triangular wedge-shape of low-Ti lavas thickening to the east, which is similar to the West Stavros domain.

The depth of the boundary at these three transects is significantly shallower than at the transect previous section (3.4.7), where the boundary is suddenly ~440m deeper. This is most easily explained with the presence of a large normal fault that is downthrown to the west. The position of the fault is very close to the CY2/2a drill cores, this is further supported by evidence of faulting at the Agrokipia mine (Malpas, 1990). Across the three transects of the eastern East Mitsero domain the LPL-UPL contact is in close agreement with the newly defined high-Ti/low-Ti boundary.

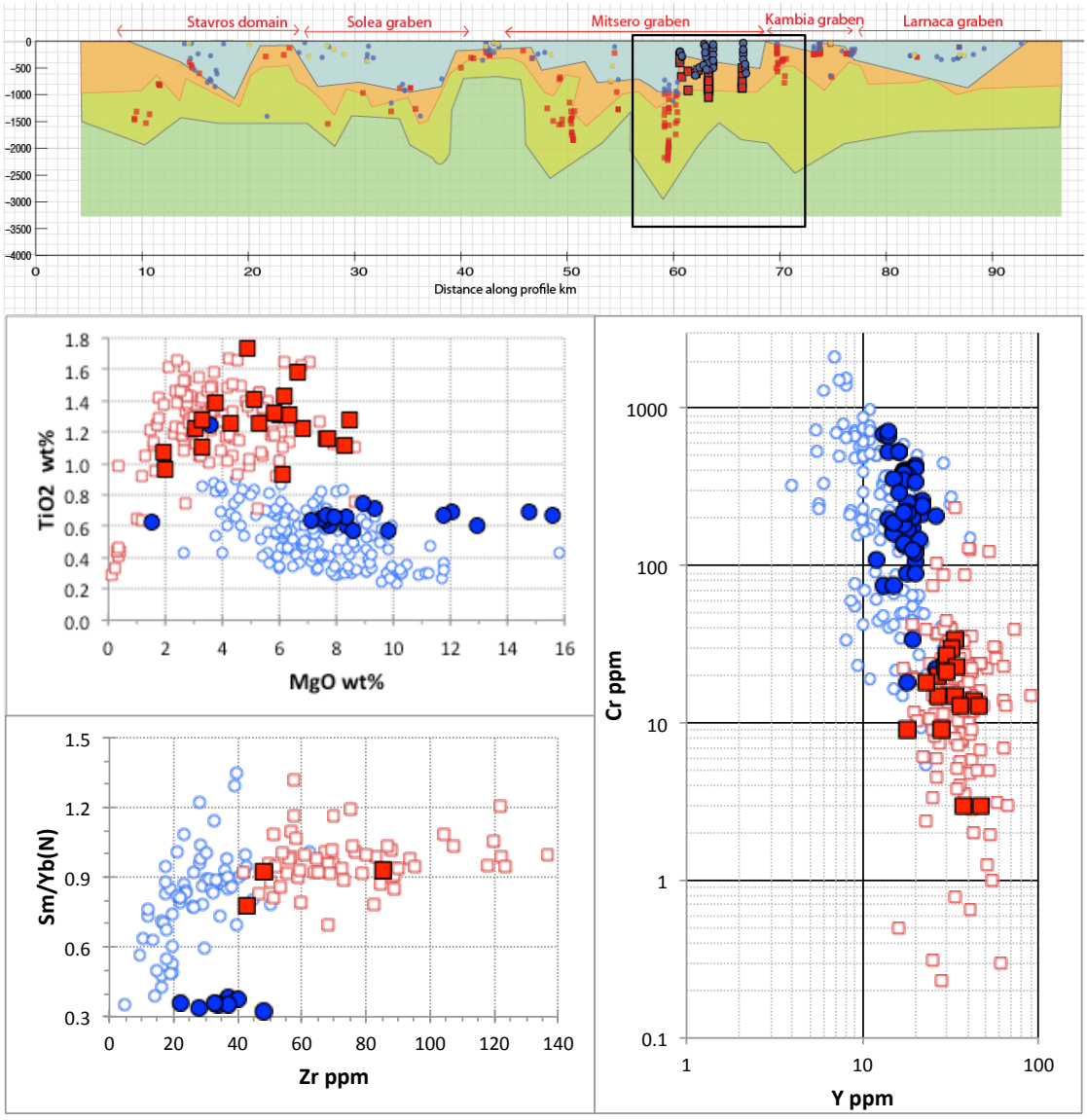

Figure 3.21 East Mitsero graben (east).

3.4.9 *Kambia Graben (Makhaeras domain)*

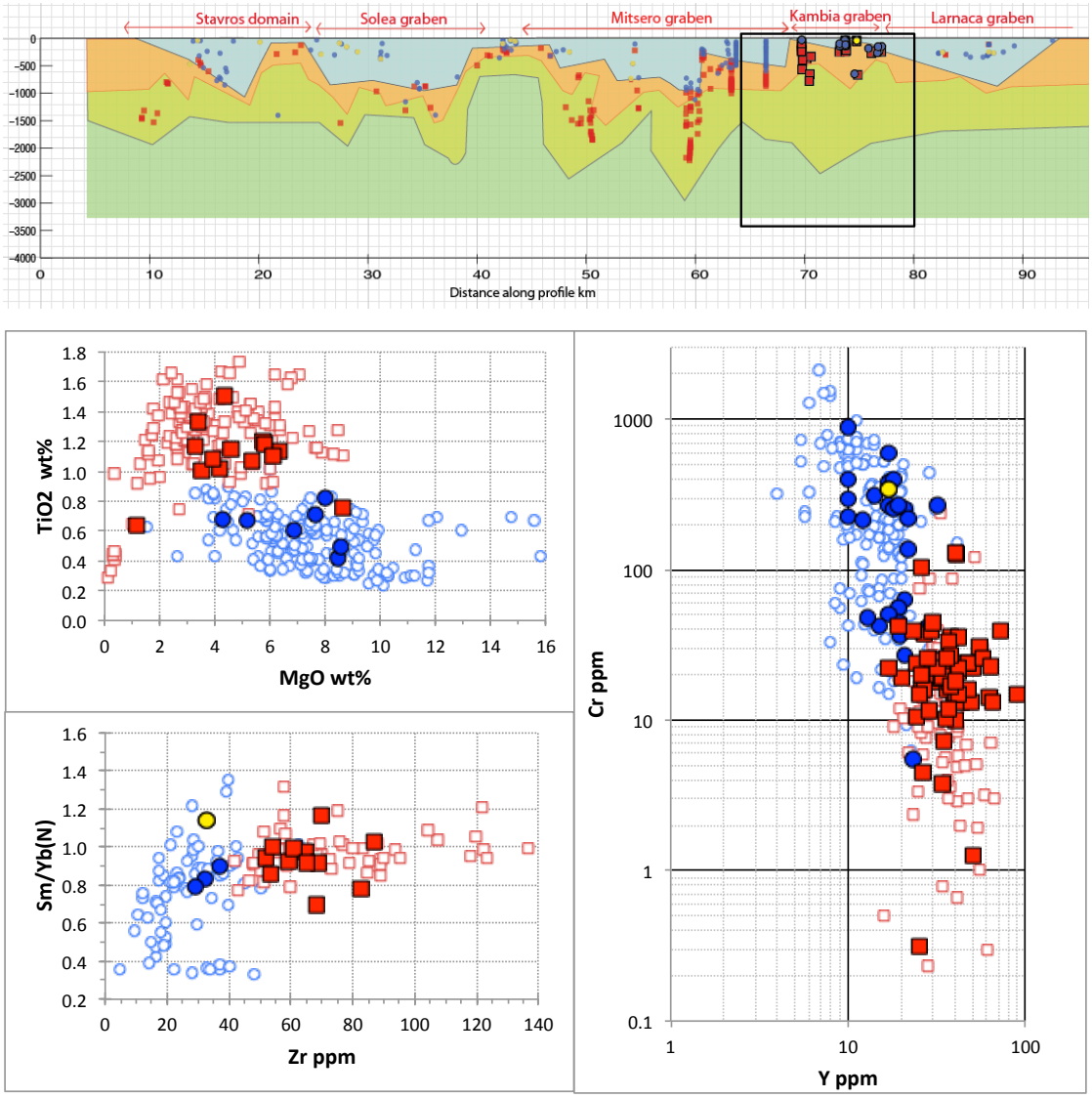

Figure 3.22 Kambia graben (Makhaeras domain).

This section is a narrow domain <10km wide with the form of a small graben, lying at the boundary of the larger scale Mitsero and Larnaca grabens. The lava flows in the western portion of this mini-graben are dipping to the west, as at Ayios Theotokos Monastery. The lava flows are flat-lying just beneath the lava-sediment contact and become steeper over the upper 500m, below which the flows remain consistent and no further steepening is observed. In the narrow eastern half (~3km wide) the lavas have the opposite sense, but it should be noted that at some outcrops there are west dipping dykes cross-cut by younger east-dipping dykes. Here again, the topmost flows are flat-lying and the lava flows beneath the surface demonstrate tectonic tilting to the east.

The West Kambia transect of figure 3.11 shows there is a clear geochemical distinction between lava groups as elsewhere, with the high-Ti lavas at the base and the low-Ti lavas overlying them. Here however the boundary occurs at only -40m below the sediment contact (which is within 100m of the Geological Survey Department LPL/UPL boundary). However the East Kambia transect (fig 3.12) shows there is no such spatial organisation of the two lava groups, yet the geochemical plots of figure 3.22 show there are two clearly distinct geochemical groups.

The boundary between the high- and low-Ti lavas is unclear because at -600m there two lava samples- one is low-Ti the other high-T, from Portnyagin et al. (1997). A petrogenetic explanation is given by Portnyagin et al. (1997) suggests there is a separate depleted low-Ti group within the high-Ti lavas. However, an alternative explanation proposed here is that these samples straddle the boundary between the Kambia graben and the Larnaca graben immediately to the east since the graben boundary is diagonal in map view.

3.4.10 West Larnaca

The region of the West Larnaca graben has very flat terrain and the effect of the uplift tilting of the ophiolite is less pronounced. The sediments that cap the volcanics are shallowly dipping ~5° to the north. As a result the depth estimates are less well constrained for this domain, and has implications for the inference of boundaries and unit thickness.

The vast majority of the lavas sampled in this domain are low-Ti lavas, each of them meeting all the chemical requirements. Only two of the samples from the West Larnaca area have been classified as high-Ti lavas, but it is clear from the three geochemical plots given that they are not typical high-Ti lavas (figure 3.23). For each of the geochemical criteria these two samples are intermediate between the low-Ti and high-Ti groups. It would appear from the 2D profile that the high-Ti and low-Ti lavas are found in very close proximity, and in the case of the most easterly high-Ti lava sample, it is apparently overlying the low-Ti samples. It is unclear whether this reflects a real distribution of the lava groups and the stratigraphy in this area could be more complex. Alternatively the uncertainty of the depth estimates may be the cause.

The most likely position of the boundary in this domain is just below the low-Ti lavas because these have been interpreted by Allerton (thesis, 1988) as an infill sequence which is lying on top of older basement lavas (probably the underlying high-Ti lavas).

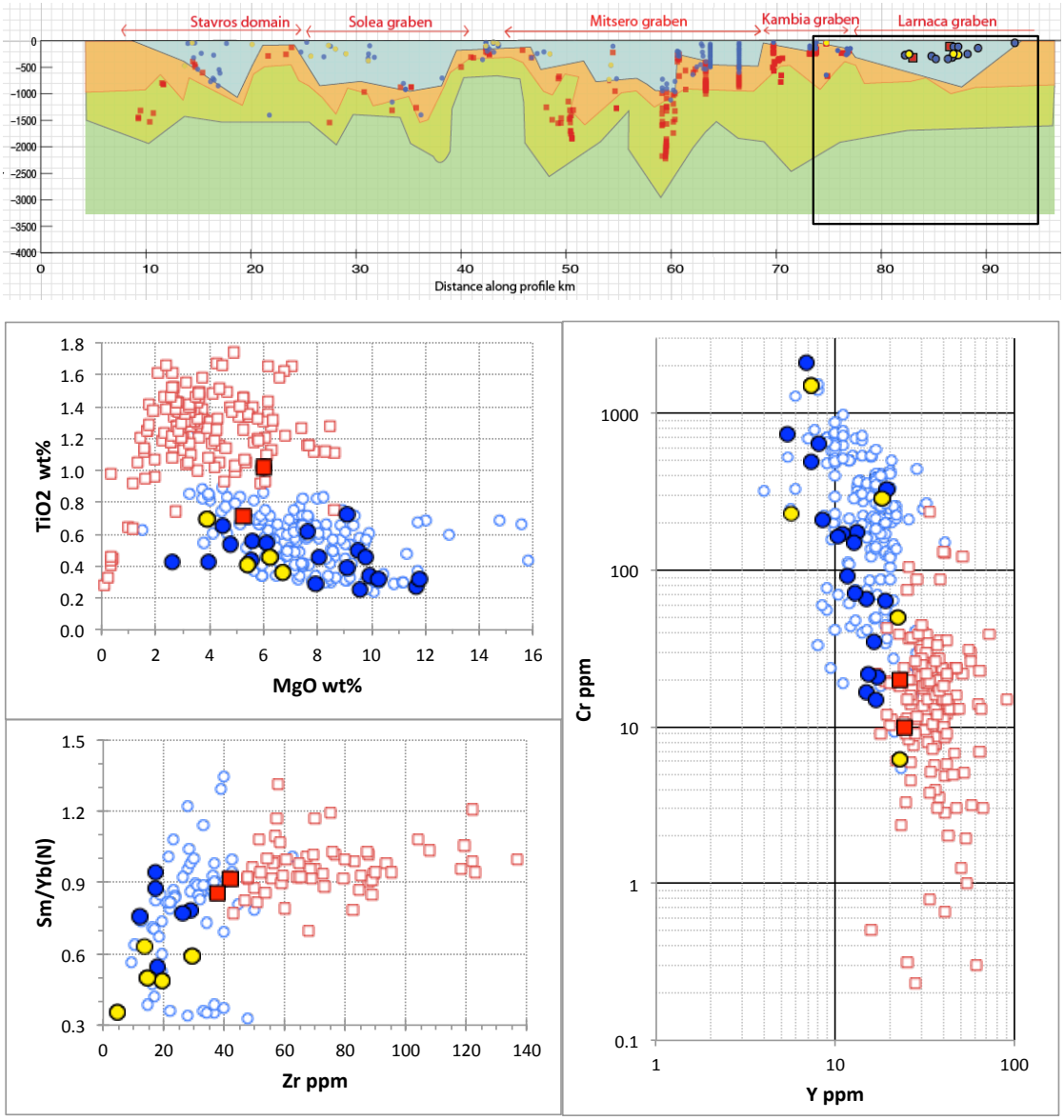

Figure 3.23 West Larnaca graben.

3.5 Basis for geochemical stratigraphy

In section 3.4 above it has been demonstrated that a systematic geochemical sub-division exists within the Troodos extrusive section. My revised, geochemical subdivision of the lava groups is largely based upon whole-rock TiO_2 wt.% contents. The majority of the analyses can be split into either a high-Ti group of >0.90 wt.% or

a low-Ti group of < 0.90 wt.%, with virtually no overlap between the two clusters of lava on the TiO_2 vs MgO plots (figure 3.24). As explored further in Chapter 5, these groupings cannot readily be related by fractional crystallisation. Only a small portion of the dataset cannot be subdivided on the basis of this criterion alone; in these instances samples can be readily discriminated using one or more other geochemical parameters. Three samples in the East Stavros domain, and two in the West Larnaca domain have intermediate TiO_2 values, but all of these can be classified as part of the 'high-Ti' suite based on their (high) Zr, Y and (low) Cr contents. Additionally, a small subset of the lavas and glasses cannot be divided purely on TiO_2 alone: these are samples which have <0.70 wt.% TiO_2 at very low MgO (<1 wt.%). These extremely evolved lavas actually belong to the high-Ti group but have low TiO_2 contents as a result of oxide saturation and fractionation. Modelled fractionation curves generated using MELTS software are presented in section 5.2.1, which shows that these very low TiO_2 lavas are part of the 'high-Ti' group. These specific samples meet the other chemical requirements for the high-Ti group.

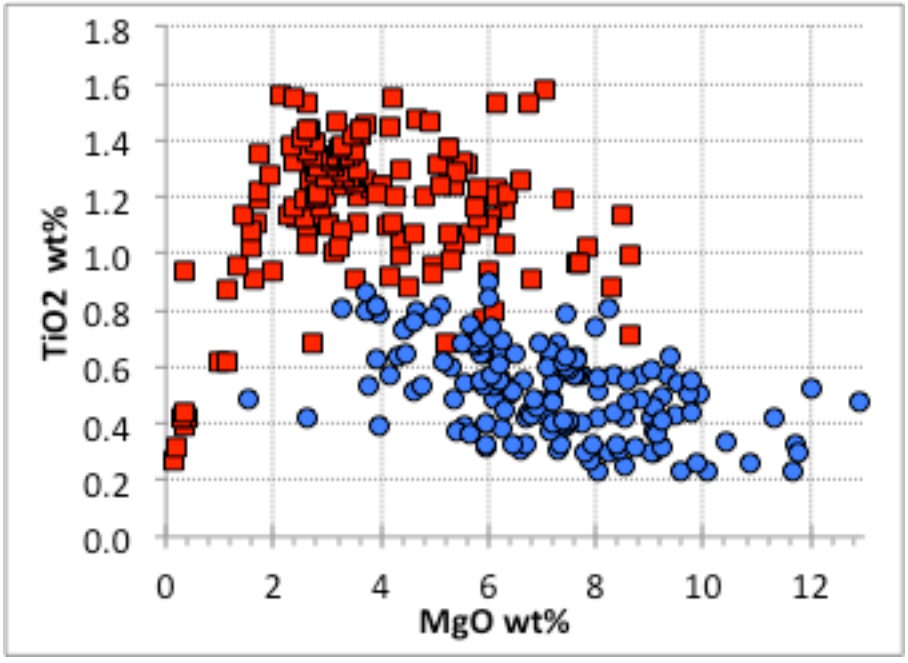

Figure 3.24. TiO_2 wt.% versus MgO wt.%, all available sample data has been plotted.

The subdivision can also be made using further immobile elements; the low-Ti group are defined as having low Y (5-20ppm), high Cr (>40ppm), and low Zr (8-48ppm), whereas the high-Ti lavas have high Y (21-64ppm), low Cr (<40ppm), and high Zr (49-95 ppm). Between them the four geochemical criteria make up a robust

basis for subdividing the extrusive suite that is applicable across the entire northern flank of the ophiolite.

The upper lava unit, the low-Ti lavas, contain a subgroup of LREE-enriched lavas that are identical to the rest of the low-Ti lavas on the basis of the four criteria outlined here. These LREE-enriched lavas are not considered to represent a separate stratigraphic unit because they do not occur as a continuous unit systematically overlying the low-Ti lavas; rather they are found within the low-Ti lavas at varying depth, sometimes overlain by low-Ti lavas. They are therefore considered to be part of the low-Ti upper lava unit. In general the high-Ti group are non-depleted and more evolved, the low-Ti group are depleted and usually more primitive, and the LREE-enriched lavas have the most marked depletion. The geochemical characteristics of all the lava groups are discussed in greater depth in Chapter 5.

As shown in the previous sections, there is a systematic geochemical boundary within the extrusive sequence occurring where there is a step-decrease in the TiO_2, Y etc. This boundary may, or may not, correspond to the Cyprus Survey's LPL-UPL division.

The low-Ti volcanics in the upper part of the extrusive section broadly coincide with the 'upper pillow lavas' as defined by Cyprus Geological Survey mapping. These lavas tend to form flows with relatively small pillows (~1m) and are commonly olivine phyric. In the lower parts of the extrusive section the high-Ti lavas occur within the 'lower pillow lavas' and 'Basal Group' units; these are almost always aphyric. It should be noted that the geochemistry of the Basal Group lavas are identical to the 'lower pillow lavas', and are classed here as a single group – the high-Ti series - the only difference being the proportion of dykes present and the grade of metamorphism.

The new subdivisions of the lavas are broadly comparable to the original subdivisions by the Survey, however, the boundaries frequently occur at different positions for each of the different subdividing systems e.g., Akaki section. The system for subdividing the lavas outlined here is unaffected by the effects of alteration because the elements selected are known to be immobile up to greenschist facies metamorphism (e.g., Pearce, 1975); therefore it reflects an original magmatic difference between the two lava groups. These magmatic differences will be discussed

in more detail in Chapter 5, along with a discussion on the petrogenesis of the volcanics.

To summarise:

Low-Ti lavas	*High-Ti lavas*
low TiO_2 <0.90%	high TiO_2 >0.90%
low Y 5-20 ppm	high Y 21-644 ppm
high Cr most >40 ppm	low Cr most <40 ppm
low Zr 4-48 ppm	high Zr 49-95+ ppm

3.6 Structural observations from the Troodos upper crust

3.6.1 Premise

Because of the Plio-Pleistocene uplift of Mount Olympus the sub-seafloor internal architecture of the Troodos ophiolite crust can be examined. This allows us an unparalleled opportunity to assess the mechanisms of accretion of the upper oceanic crust and the links between tectonic and volcanic processes in a way that surveys of the modern spreading centres cannot do because of lack of access. At an outcrop scale in the Troodos massif the original seafloor spreading structures are visible in three dimensions, and have been preserved with minor deformation.

A field survey was conducted to systematically collect orientation measurements of lava flows, dykes and faults of the Troodos ophiolite across its northern flank, and to record the field relationships (unconformities, cross-cutting relationships etc.) between the units. Ideally field measurements were collected in N-S transects from the sedimentary cover down through the lavas and into the SDC. The new dataset has been combined with the pre-existing data from the Cyprus Survey geological maps and published sources.

The planar nature of the sedimentary beds, sheeted lava flows, and dykes were easy to measure accurately. In contrast, the pillowed lava flows tend to form lobate tubes and bun-shaped bodies whose original orientations are much harder to decipher. However, on the scale of an outcrop they often display sub-planar flattened flow tops which, by comparison with the planar upper surfaces of nearby inter-lava sediments and sheet flows, can be shown to have been sub-horizontal and thereby used as a reasonable estimate of the orientation of the flow. Great care was taken at every outcrop of pillowed flows to get a meaningful estimate of flow orientation by first choosing outcrops with good 3D exposure to assess the orientations from different angles to be confident of the general attitude of the outcrop as a whole, and to avoid measuring apparent dip or feeder tubes and pipes. By collecting multiple dip measurements for each locality the mean dip can be calculated from the cluster of poles to planes when plotted on a stereonet.

3.6.2 Sedimentary cover sequence

The sediments immediately overlying the lavas are the metalliferous umbers and the radiolarite cherts of the Perapedhi Formation, the Kannaviou Formation (bentonitic clays) (all late Cretaceous: Turonian to Maastrichtian; Urquhart & Banner, 1994), the Lefkara Formation (chalk), and the Miocene Koronia Member (reef limestone) of the Pakhna Formation (Lord et al., 2000). This complete sequence is rarely preserved: commonly lavas are directly overlain by chalks or reef limestone. The Lefkara Formation covers just the eastern half of the ophiolite from Ayia Anna to Mitsero where it is extremely thin and eventually tapers out and disappears. West of the Mitsero graben the lavas are overlain by the Koronia Member reef limestone, which has abundant outcrops as far as Nikitari and beyond that only small outliers occur.

Orientations of the circum Troodos cover sequence are displayed in figure 3.25, where bedding planes have been plotted on stereonets along with the poles to plane, (red = Perapedi umbers and radiolarites; green = Lefkara chalks; blue = Koroni reef limestone).

Figure 3.25 Circum Troodos sedimentary cover sequence. Red=Perapedhi Fm; green=Lefkara Fm, Blue=Pakhna

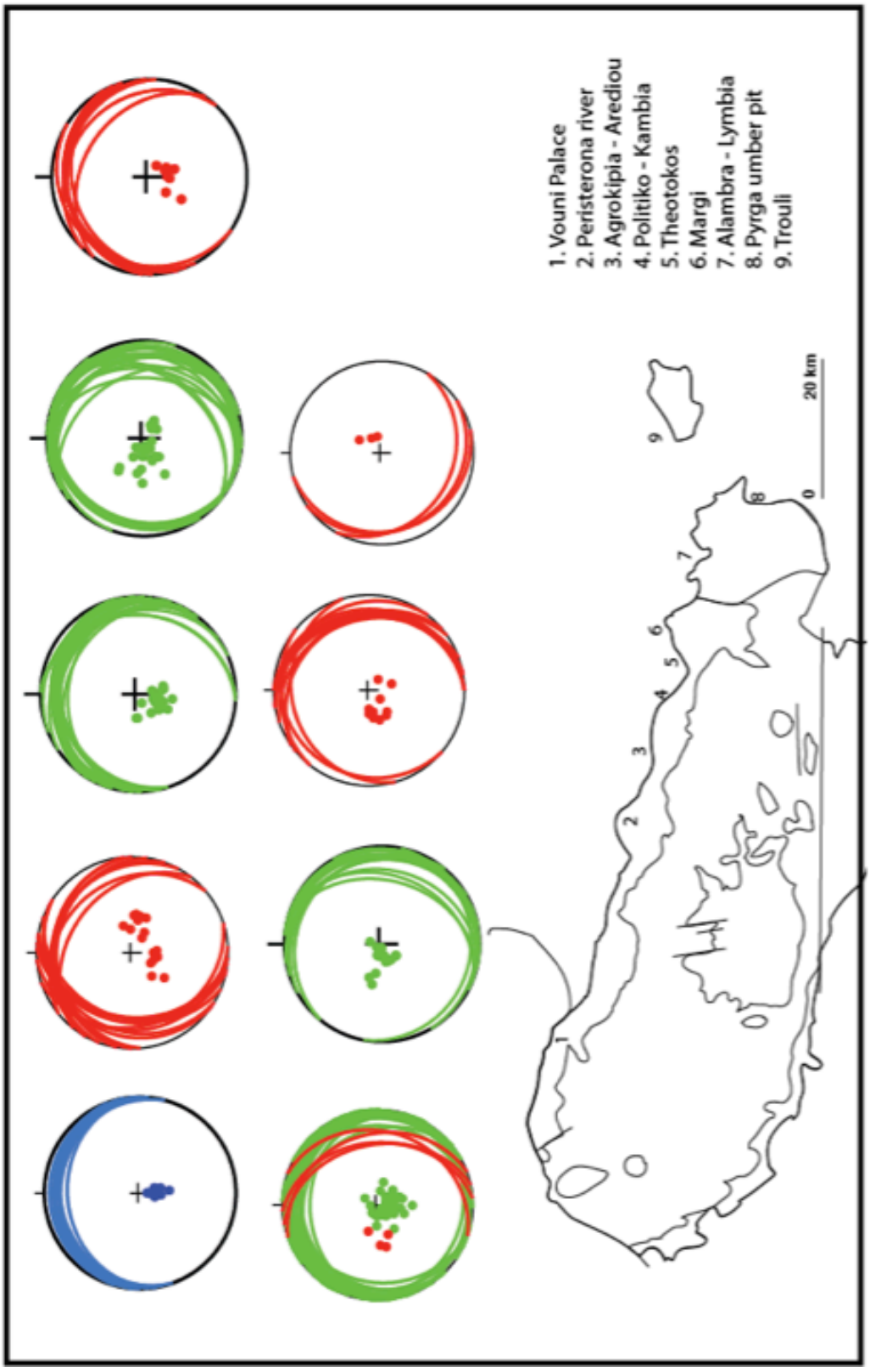

Uplift of Mt Olympus can be constrained to have occurred mostly between the Pliocene and the Pleistocene, as documented by the oldest marine terrace exposed on the south coast at 300m above present sea level (Poole and Robertson, 1991). Some of the tilts are the result of compound rotations for the pre-uplift faulting, and then the uplift tilting itself. The two rotations occurred within ~40ka, for example at Margi the umber bedding is tilted towards the East (as are the lavas immediately underlying them), yet the chalks above are tilted to the North. In the majority of cases the bedding has been tilted away from the ophiolite (figure 3.25), predominantly the outcrops along the northern flank dipping gently to the North by ~15° due to post-chalk tilting. The localities on the eastern end of the ophiolite, Alambra, Lymbia and Pyrga, show north-easterly to easterly dips because the uplift is radial away from Mt Olympus.

3.6.3 Uplift tilt correction

All the orientation measurements for the lavas and dykes have been restored to their pre-uplift orientation by removing the tectonic tilt of the sediments. The average chalk orientation is 279°/12°N, so an anti-clockwise rotation of 12° about a horizontally inclined axis trending 279° was removed from the lavas and dykes to strip off the uplift tilt.

The contact between the lavas and the sedimentary cover sequence represents the late Cretaceous to (in many places) Eocene palaeo-seafloor, and original topography of this surface is still visible by the small offsets of the lava-sediment contact. Umbers and the radiolarites commonly occur where (usually fault-bounded half graben) depressions were present in the palaeo-seafloor. The sediment has probably been swept in by currents and has accumulated in small these hollows. This is very well exhibited at Ayios Theotokos Monastery near Kambia and also in the Margi area. Faulting is also evident at the Pyrga umber pit and controlling many umber deposits on the southern flank of the ophiolite (MacLeod, 1990). In all these cases the orientation of the umbers is obviously affected greatly by the proximity to what appear to have been active faults, apparently draping over the fault scarps and probably deposited onto the actively tilting hanging wall and have been affected by compaction. At Ayios Theotokos Monastery there is well preserved slump-folding

caused from deposition on a slope at unstable angles and sliding due to gravity. Because of this umber dips do not always make the most reliable palaeohorizontal markers, but the orientation may still indicate the location and sense of faulting, and the umber orientations generally approximate to the lava dips at nearby outcrops. Radiolarite outcrops are often intensely weathered, but the original bedding can normally be revealed by excavation. In some places the radiolarite bedding has also been distorted with increasing proximity to a fault, suggesting that this lithology was sometimes draped over fault scarps and/or reactivated close to the time of radiolarite deposition in the Campanian (MacLeod, 1990). In all cases interpretation of the umber and radiolarite orientations took into careful consideration the structures present and overall disposition of the outcrop.

The apparent age of a fault – whether it was an original seafloor spreading structure or a late structure (perhaps reactivated) related to either the emplacement or uplift of the ophiolite – was determined wherever possible by considering its relationship to the overlying sediments.

3.6.4 Lava-sediment contact

In the field the uppermost lavas are often sub-parallel with the overlying sediments, and this proves to be the case along the whole northern flank of the ophiolite. In figure 3.26 the in situ orientations (poles to plane) of the Lefkara chalks and the uppermost lavas immediately below, the mean directions are indicated with an α_{95} cone of confidence. Similarity between the dip of chalks and lavas is consistent everywhere that we have orientation data and are particularly close at Vouni, Agrokipia, Kambia and Margi, while the other cases are still within 10° of each other. This demonstrates the conformable nature of the overlying chalks to the lavas and indicates these topmost lavas were originally (sub-)horizontal at the time of eruption; furthermore, it provides additional justification that the planar surfaces of pillow lava flow tops where visible in 3-D outcrops can provide reliable palaeohorizontal markers.

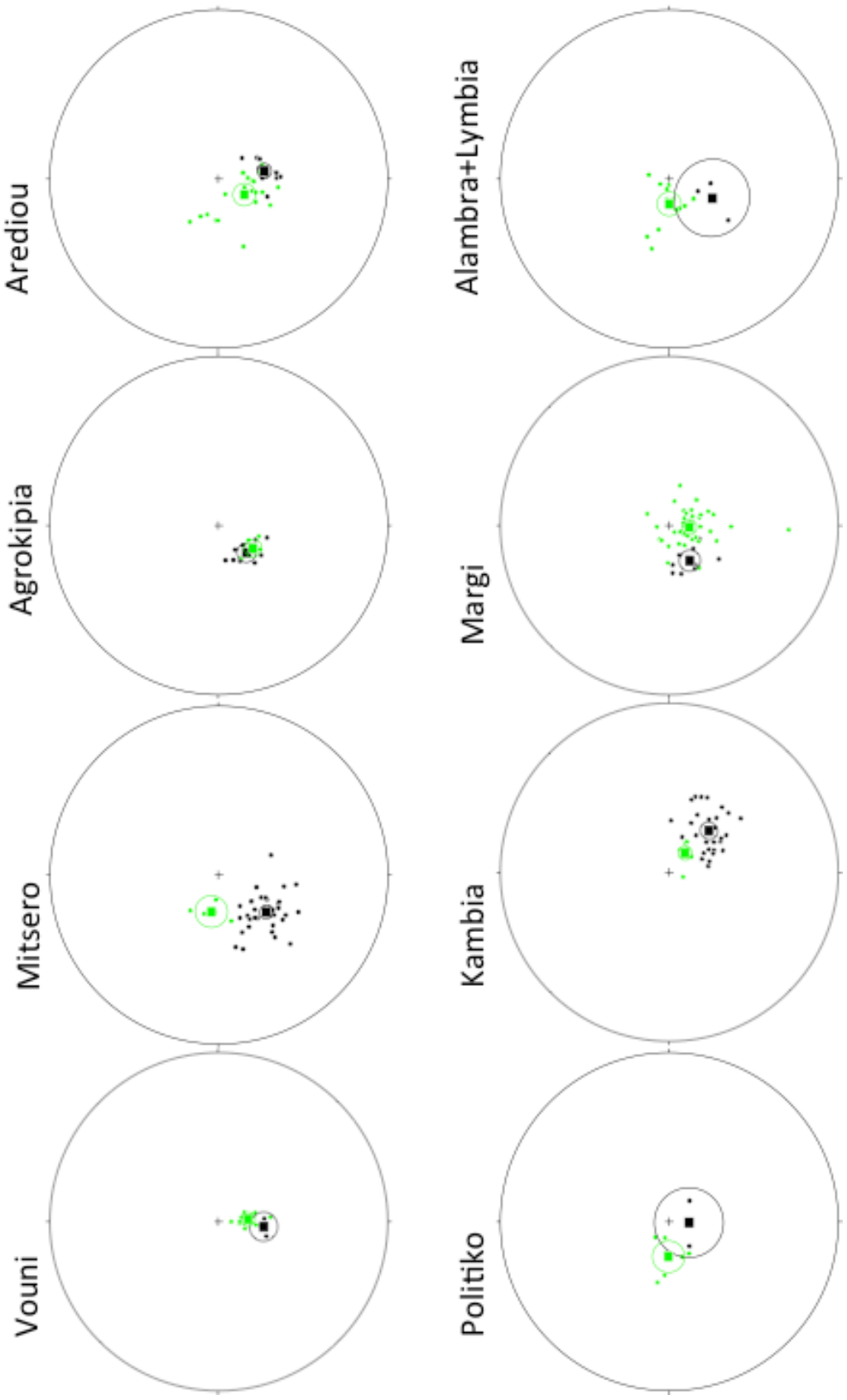

Figure 3.26 Poles to plane for topmost lavas (black) and Lefkara chalk (green). Vouni sediments are Pakhna Fm.

The nature of the lava-sediment contact is notably subdued, as can be seen in the photo in figure 3.27. The contact is easily traceable along strike, and where there are offsets (apparently due to minor faulting) in the boundary they are limited to a few 10s of metres. Palaeo-seafloor topography is represented by the relief of this contact which, as shown in figure 3.28, varies in the order of 10-50 m only. The field evidence is consistent with a contact that has experienced minimal disturbance. The synthesis chapter (Chapter 6) will explore the implications of this for ocean-floor studies that attempt to make estimates of tectonic stretching based on the sum of exposed fault heaves (e.g., Escartín et al., 1999, MacLeod et al., 2009). It may however be reliably stated that the Troodos palaeo-seafloor was much flatter, more subdued and less faulted than the sub-seafloor, giving little clue as to the tectonic processes going on at depth.

Figure 3.27 Top photo show the subdued topography of the lava-sediment contact (dark rocks are lavas, white rocks are Lefkara Fm chalks). Bottom photo shows lavas are overlain by umber and radiolarite.

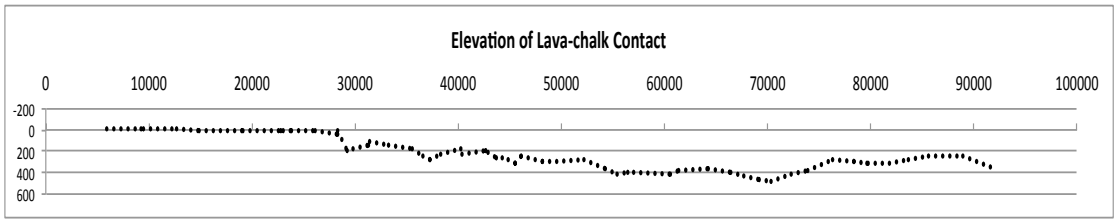

Figure 3.28 Elevation profile of the lava-sediment contact shows only small changes in the relief of the contact. This is approximate to the palaeoseafloor topography.

3.7 Orientation of the lavas down section

3.7.1 Arediou section (East Mitsero graben)

This section starts in the village of Arediou at the site of the CY-1 drill hole, and follows the Akaki river upstream to the well-known Kamaropotamos gorge (the site of the traditional LPL-UPL boundary), and continues south for a further 5km before passing into the sheeted dyke complex.

The first localities at AK02 and AK04 are the uppermost lavas of the Akaki River section, at the site of the CY-1 drill hole (figure 3.29). They are directly overlain by chalks of the Eocene Middle Lefkara formation. The orientation of these first lavas is slightly steeper than the Lefkara chalks, so the removal of the bedding tilt brings the lava dips closer to horizontal (corrected mean lava dips at AK02 and AK04 = 236°/14°NW), see figure 3.26. The lava here is dominantly pillowed flows, and they have the typical 'upper pillow lava' appearance, i.e., olivine and clinopyroxene phenocrysts are present, vesicles are filled with zeolite, and the outcrop is stained pink in colour due to seafloor weathering. Less than a kilometre upstream (lower down the section), near the village of Malounda, there is an outcrop with a sheet flow at locality FK07, however only one orientation measurement was taken at this locality.

Still further down the section are the localities of AK12 and AK14 at Kamaropotamos gorge (the site of drill core CY-1a). This locality is almost -300m deep in the crust and it is where the first occurrence of the traditional 'lower pillow lavas' are encountered along this transect (Gass, 1960). The appearance of the Kamaropotamos outcrop is typical of the LPL since there are more dykes present than at higher level localities, celadonite is abundant, sheet flows are more common, and phenocrysts are absent. Interestingly, although this outcrop at -292m fits the

description of LPL, these lavas are classified geochemically as part of the low-Ti upper unit, and are geochemically indistinct from the overlying lavas (figure 3.9). High-Ti lavas are first encountered along this transect only at -524m, more than 200m deeper than the Geological Survey Department's UPL-LPL boundary.

A little over 100m lower down the crust at FK06 (-411m) the orientation of the lavas has become steeper, now a mean direction of 356°/33°E. Dykes and sheet flows are more common at this level within the crust. Finally, at LP08 and LP10 the dykes form about 60% of the outcrop and the lava screens are silicified. From the previous locality (FK06) to this locality there has been no change in orientation of the lava flows, their mean direction is identical. Geochemical analyses of the CY-1a drill core from the equivalent depth are still low-Ti lavas, identical to the lavas above them in TiO_2, Zr, Y and Cr.

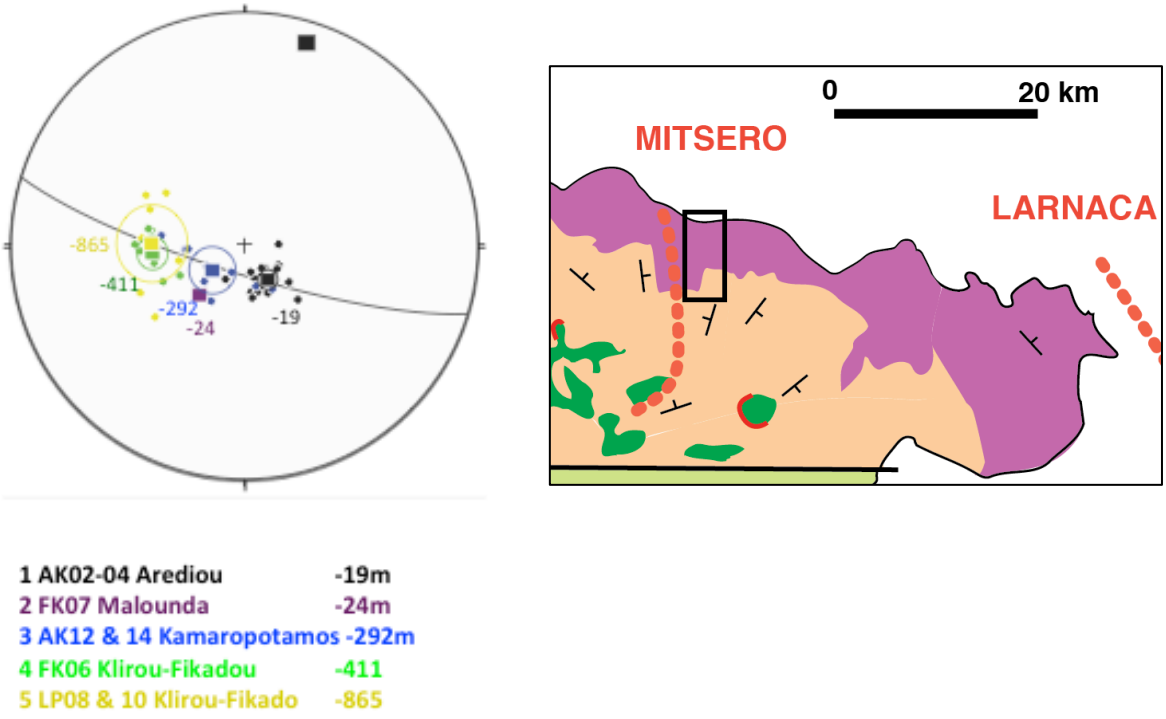

Figure 3.29 Progressive unconformity down the Arediou section. Numbers on map show the locality of the field stations. The topmost lavas are least tilted.

In summary: the tilt corrected lava poles to planes from the top of the lava section at Arediou can be restored to a near-horizontal orientation, and are very similar to the chalk pole to plane (the α_{95} cones of confidence overlap slightly). The lava poles from successively deeper parts of the crustal section show greater and greater tilts (figure 3.29). The dips increase systematically from top (236°/14°NW) to

bottom (002°/33°E) such that all the poles from this section fit along a best fit girdle which itself dips 107°/80°S. The pole-to-plane to the best-fit girdle (017°;10°) can be considered to represent the orientation if the axis of rotation. In this case the axis of rotation is sub-horizontal and with a NNE azimuth, which is consistent with a rotation on normal faults parallel to the SDC. The angle between the topmost lava flows at AK02-04 and the lowermost basal group pillows at LP08 and LP10 is 43°, which approximates the minimum (eastward) tilting of the upper crust.

3.7.2 Agrokipia section (East Mitsero graben)

A similar increase in tilt down section is observed at the Agrokipia to Ayia Koroni section (figure 3.30, 3.21), which is just 3km west of the Arediou section described above, also part of the East Mitsero domain. This section starts near the Agrokipia copper mine, and transects the upper crust north to south, including the famous Klirou Bridge locatily, and then two typical Basal Group localities. Again, the topmost lavas are restored to near horizontal after uplift correction, and progressively become more tilted with increasing stratigraphic depth.

Near the top of the section at localities AGP01-04,10,11 at -96m the average tilt corrected lava orientation is 338°/09°NE, and this increases to 003°/14°E by -217m at AGP05-06. One of the few outcrops where traditional LPL-UPL contact is visible is AGP05 at the Agrokipia mine at -217m. The photograph in figure 3.31 shows the pinky-grey UPL in the centre and on the right and the LPL and stockwork are the dark brown areas on the left-hand edge. A fault trending NE-SW through the Agrokipia mine is reported by Malpas (1990) to offset the orebody. The LPL-UPL contact at the Agrokipia mine coincides closely with the boundary between the high-Ti and low-Ti lava series (figure 3.8).

The next outcrop is AK06 at Klirou Bridge (-753m) which is 4km south of Agrokipia. This outcrop is typical of the lower portion of the LPL on account of the high dyke abundance occurring as swarms (~30%) and the numerous thin sheet flows, hyaloclastite breccia and large pillows are also present. Tilting of the lavas has increased further to 013°/28°E, and the dykes have an orthogonal relationship dipping

177°/73°W, although these west-dipping dykes are cut by a younger east-dipping dyke (photo in figure 3.32).

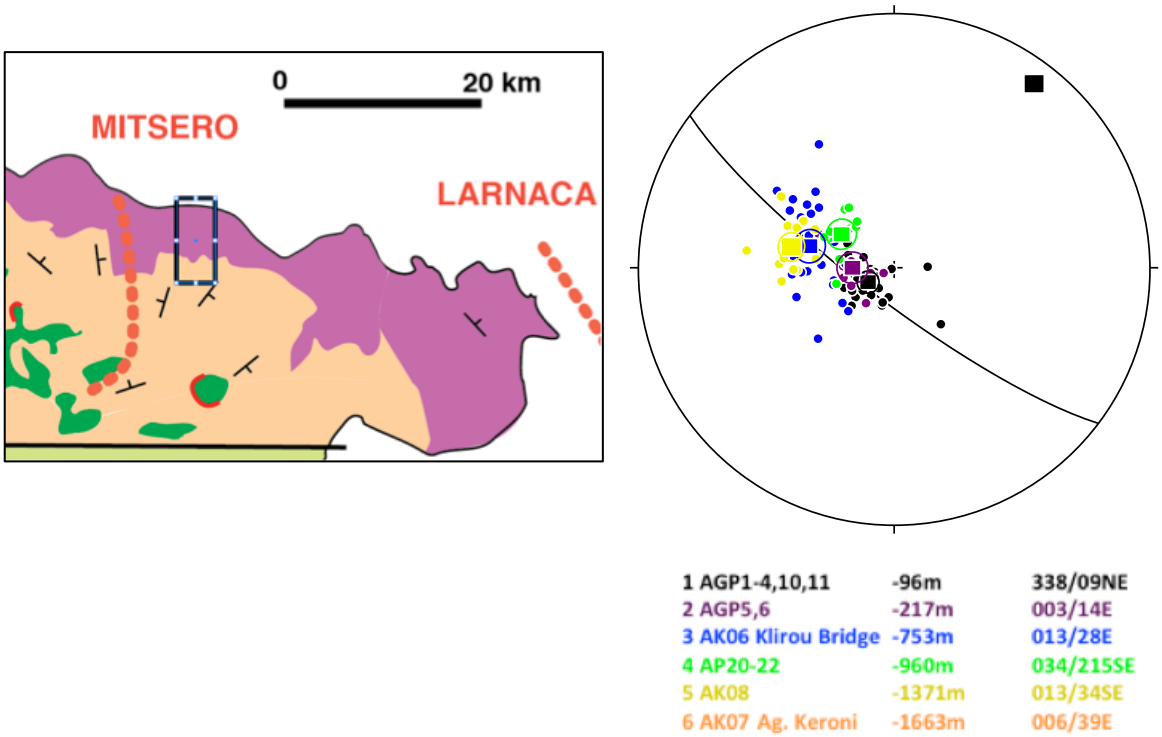

Figure 3.30 Progressive unconformity down the Agrokipia section

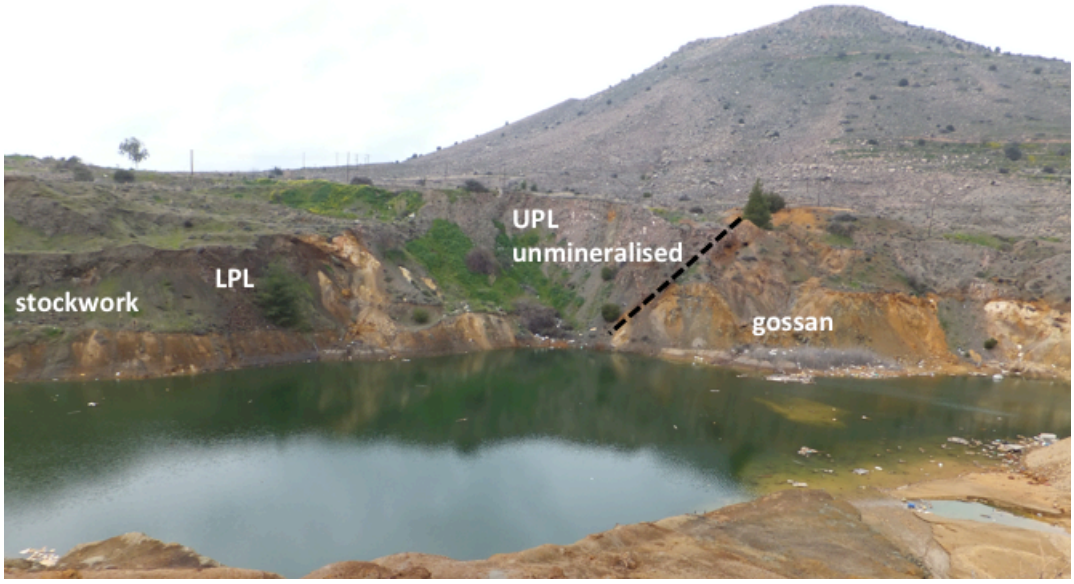

Figure 3.31 Field photo of Agrokipia mine. Mineralised stockwork occurs within the 'lower pillow lavas', the 'upper pillow lavas' are unmineralised. The orange gossan is bound by a fault (dashed line) at the contact with UPL.

Figure 3.32 Photo of Klirou Bridge – classic Lower Pillow Lava outcrop. There is an orthogonal relationship between lava and dyke tilts.

The lowermost lavas are found as narrow (<10m wide) screens of pillow lavas at locality AK07 near Agia Koroni deep within the Basal Group at -1663m. This outcrop is characteristic of the Basal Group, the large pillow lavas 1-2m are metamorphosed to greenschist facies as evidenced by abundant chlorite, epidote, pyrite present. The in situ orientations are shown in figure 3.33 (black=lava, pink=dyke), the lavas and dykes here have an orthogonal relationship which indicates they were tilted by the same rotation and of the same amount.

As with the Arediou section, the Agrokipia section shows progressively deeper dips at the deeper depths within the crust, and again the increase in tilt is systematic. All the poles to plane for the lavas of this transect are plotted in figure 3.34(g), and they fall comfortably on a best fit girdle of 111°/86°S which had a pole of 021°;04°. The inferred rotation axes based on the observed change in orientations down the Arediou and the Agrokipia sections are both shallowly plunging to the NNE. The total amount of tilting for the Agrokipia section is 31° east (compared to 43° for the Arediou section).

Figure 3.33 Basal Group out crop at Agia Koroni. Large pillow lavas (1.5m) in the lower half of photo are pale green and dipping to the right (plotted in black on stereonet). Dykes are grey-brown in upper part of photo, dipping to the left, (plotted in pink).

3.7.3 Other sections

The increase in tilt down-section recorded at Arediou and Agrokipia are not unique; there are several sections which show the same pattern (figure 3.34). The best additional examples of this tilt behaviour are from Alveka, east Kato Pyrgos, Lefke, Mitsero, Kambia, and Lythrodondas. Some of the sections do not show steeper dips for successively deeper lavas, but yet may still form a distribution of poles to plane than fit along a best fit girdle, sections such as Limnitis, Vyzakia, Xyliatos, Politiko, and Theotokos. While other sections have a uniform tilt from top to bottom, these section do not form a best fit girdle because each locality is approximately the same as the rest, e.g., Vouni, Soli, Flasiana, west Solea, east Solea, and Peristerona.

Not all of the lava tilts are progressive unconformities. At west Mitsero, for example, the lavas dip the same in the whole domain, not increasing in steepness with greater depth (figure 3.35). Similarly for the Flasiana section in the West Solea graben all of the lavas dips approximately 154°/35°W.

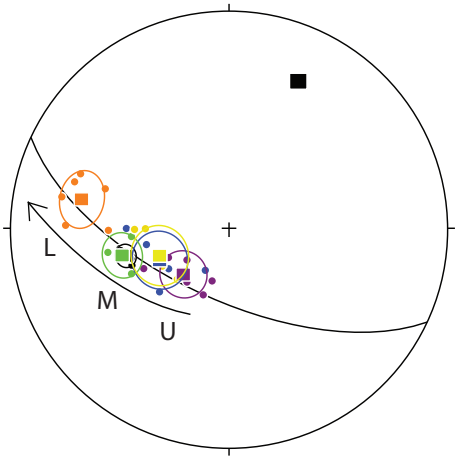

West Stavros domain
Alveka

KP10	-157m	347°/42° E
KP09	-215m	316°/24° NE
KP12	-789m	336°/28° NE
KP15	-924m	347°/42° NE
KP13	-1356m	340°/28° NE
KP14	-1414m	004°/59° E

n lava dips = 31
Best fit girdle: 116°/64° S
RA: 026°;26°
Δ tilt: 48°

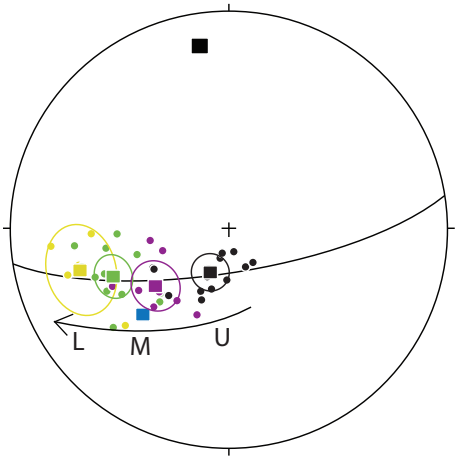

West Stavros domain
East Kato Pyrgos

VU18	-211m	294°/17° E
KP24	-574m	323°/35° NE
KP25	-664m	315°/46° NE
KP26	-716m	338°/48° NE
KP27	-915m	351°/2862° NE

n lava dips = 41
Best fit girdle: 081°/74° S
RA: 351°;16°
Δ tilt: 56°

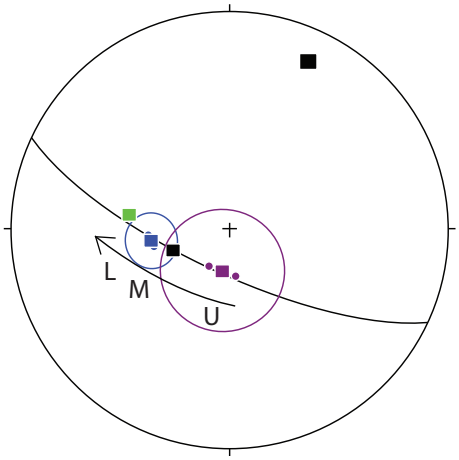

East Stavros domain
Limnitis

LI157	-20m	340°/22° E
LI158	-87m	010°/16° NE
VU12	-1065m	352°/30° NE
VU12a	-1466m	009°/38° NE

n lava dips = 6
Best fit girdle: 115°/74° S
RA: 025°;16°
Δ tilt: 40°

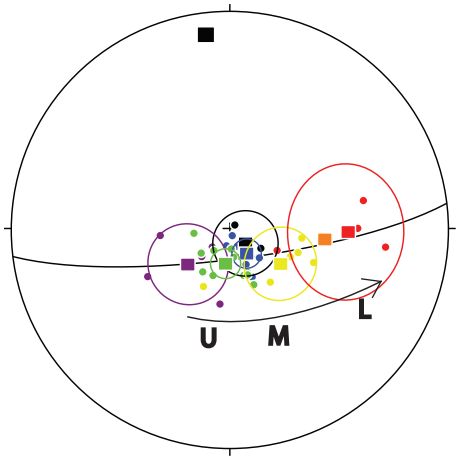

West Solea graben
Lefka

LEF12	-72m	221°/08° N
LEF10	-104m	321°/20° NE
LEF09	-124m	235°/11° N
LEF08	-197m	277°/13° N
LEF04,07	-241m	214°/23° NW
LEF22a	-537m	186°/36° W
LEF22	-838	181°/45° W

n lava dips = 38
Best fit girdle: 083°/79° S
RA: 353°;11°
Δ tilt: 45°

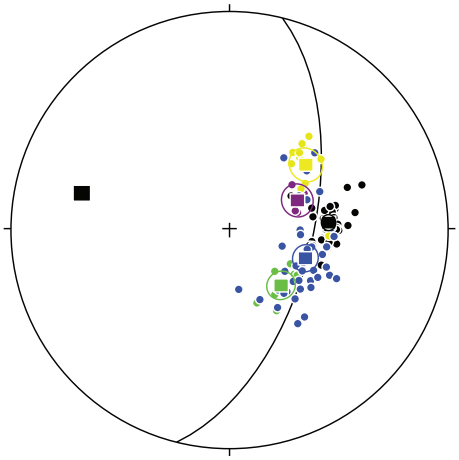

West Mitsero graben
Xyliatos

KA27,29, 02	-510m	176°/37° W
ME02	-1034m	156°/28° SW
ME03,04,XY12-20	-1250m	205°/11° W
XY09-11	-1546m	227°/28° N
XY05	-1833m	139°/38° NW
XY20	-1189m	127°/34° W

n lava dips = 93
Best fit girdle: 014°/59° E
RA: 284°;31°
Δ tilt: N/A

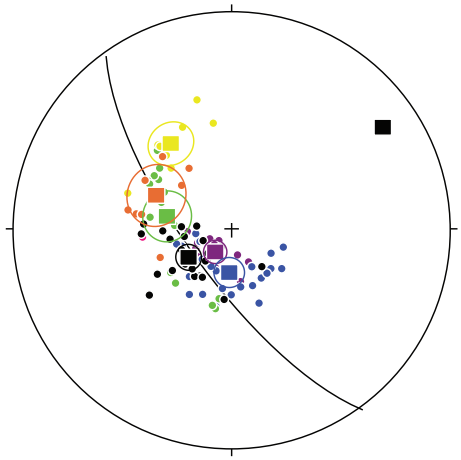

West Mitsero graben
Mitsero

MIT08,09,15,24,29	-118m	330°/18° N
MIT16,17,19	-433m	309°/10° N
MIT27,18,14,13,21	-611m	273°/16° N
MIT22,23,AP18	-867m	013°/25° E
AP15-17,19	-1137m	050°/40° SE
AP10	-1879	352°/31° E

n lava dips = 94
Best fit girdle: 139°/73° SW
RA: 049°;17°
Δ tilt: N/A

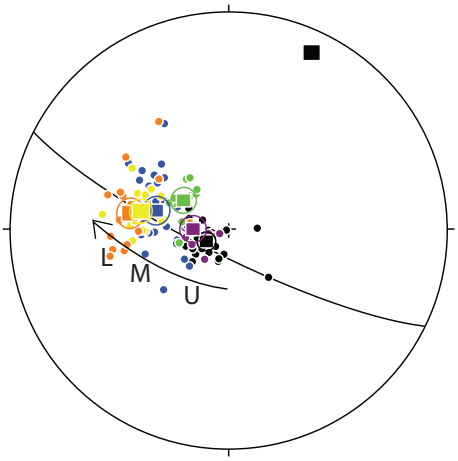

East Mitsero graben
Agrokipia

AGP01-4	-96m	338°/09° N
AGP05-6	-217m	003°/14° E
AK06	-753m	013°/28° E
AP20-22	-960m	034°/21° E
AK08	-1371m	013°/34° E
AK07,AP11,MIT04	-1663	006°/39° E

n lava dips = 106
Best fit girdle: 111°/86° S
RA: 021°;04°
Δ tilt: 31°

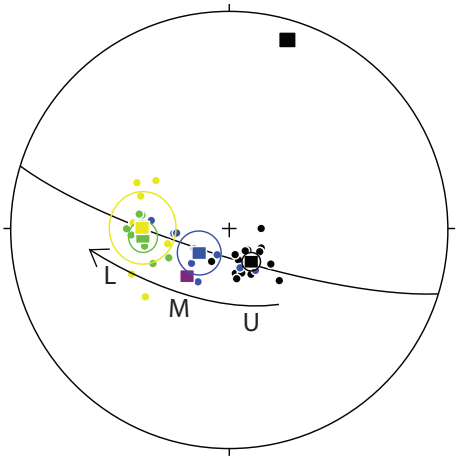

East Mitsero graben
Arediou/Akaki

AK02-4	-19m	236°/14° W
FK07	-214m	312°/23° NE
AK14,12	-292m	314°/11° NE
FK06	-411m	356°/33° E
LP08,10	-865m	002°/33° E

n lava dips = 45
Best fit girdle: 107°/80° S
RA: 017°;10°
Δ tilt: 43°

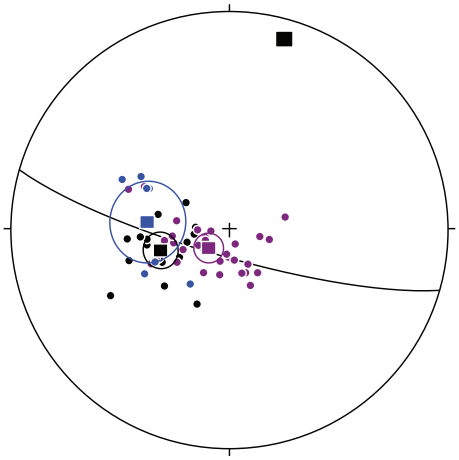

East Mitsero graben
West Politiko

LP27,28,31,34	-33m	344°/27° E
LP16-24	-205m	319°/20° NE
LP11,12	-737m	006°/31° NE

n lava dips = 54
Best fit girdle: 106°/80° S
RA: 016°;10°
Δ tilt: N/A

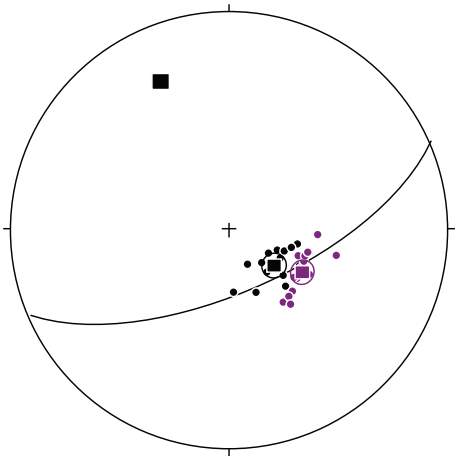

Kambia domain (Makhaeras domain)
East Politiko

LP29,30	-82m	218°/21°N W
LP15	-469m	210°/32° NE

n lava dips = 28
Best fit girdle: 062°/66° SE
RA: 332°;24°
Δ tilt: N/A

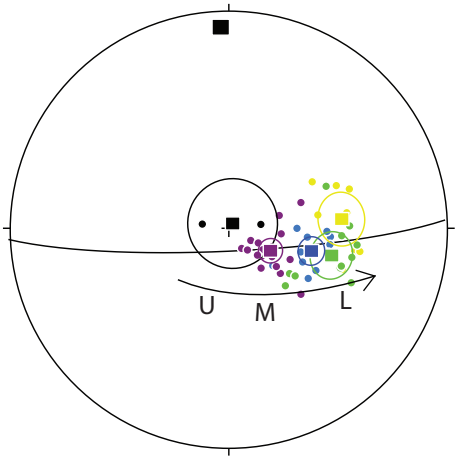

Kambia domain (Makhaeras domain)
Kambia

PDO1-3	-59m	121°/03° W
MA22,23	-170m	207°/17° NW
MA20	-166m	195°/32° W
MA17-19	-326m	194°/40° W
MA13	-629m	175°/43° W

n lava dips = 50
Best fit girdle: 087°/82° S
RA: 357°;08°
Δ tilt: 42°

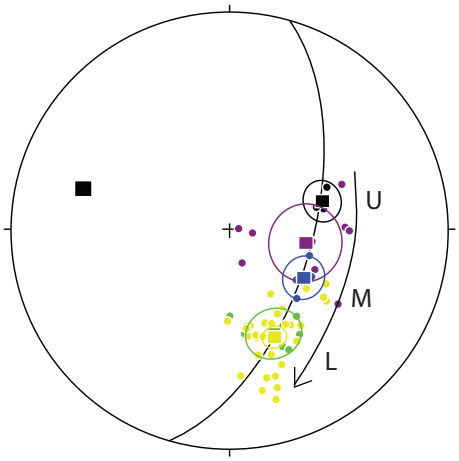

Kambia domain (Makhaeras domain)
Lythrodondas

MA26,TM04	-123m	162°/37° W
TM02,09,12,15	-494m	189°/29° W
TM20	-928m	212°/33° NW
LY15,16	-1273m	246°/43° NW
LY10,11,17	-1512m	247°/44° NW

n lava dips = 57
Best fit girdle: 016°/59° E
RA: 286°;31°
Δ tilt: 53°

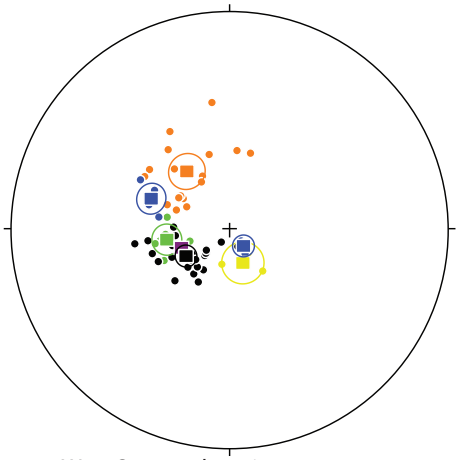

West Stavros domain
West Kato Pyrgos

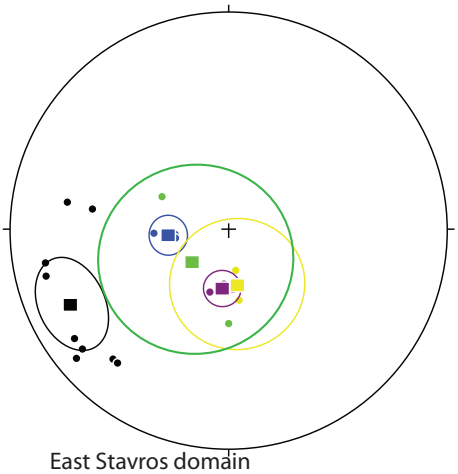

East Stavros domain
Vouni

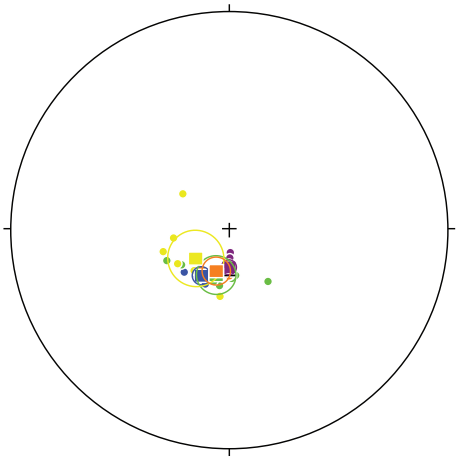

West Solea graben
Soli

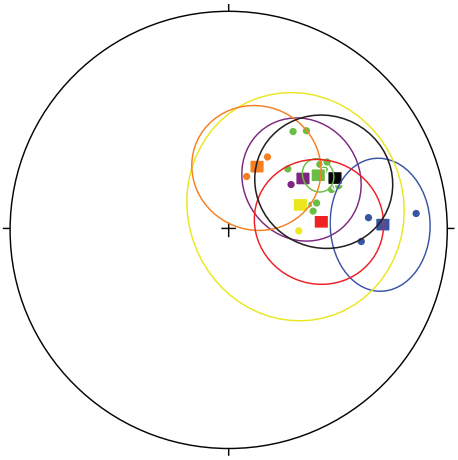

West Solea graben
Flasiana

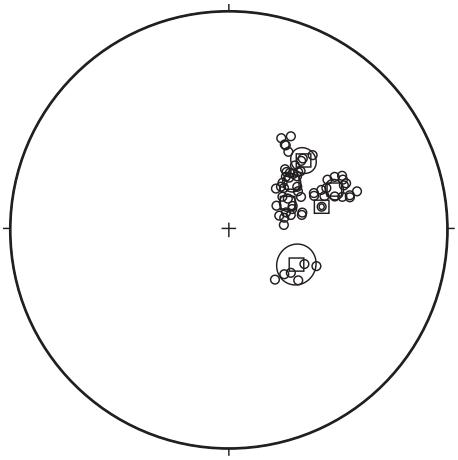

West Solea graben
Korakou

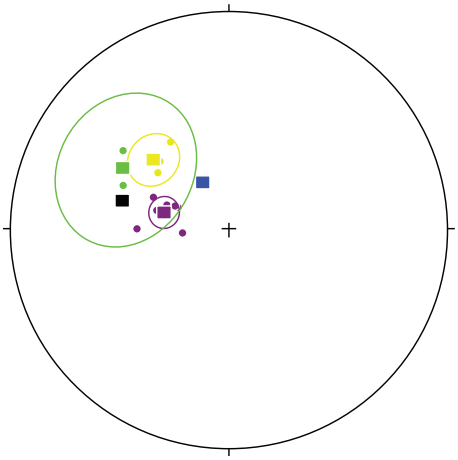

East Solea graben
Everychou

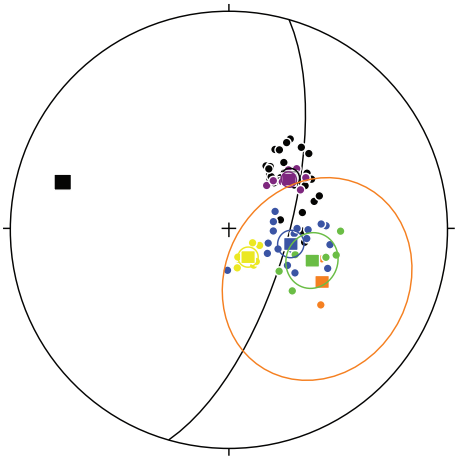

West Mitsero graben
Vyzakia

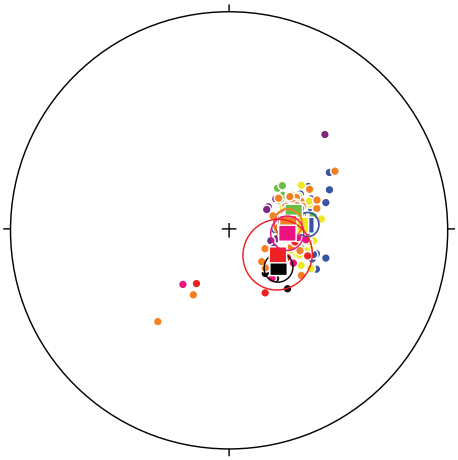

West Mitsero graben
Peristerona

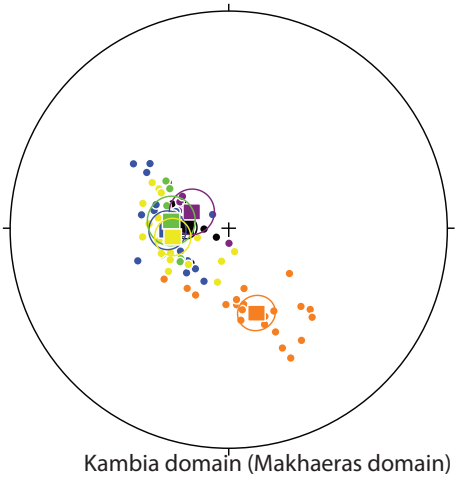

Kambia domain (Makhaeras domain)
Ayois Theotokos

In this section all the field data are presented together on a synthetic cross-sectional profile of the ophiolite. This will aid interpretation by pooling together all the structural data already discussed in this Chapter to highlight the patterns and put each observation into the context of the ophiolite.

3.1.1 Thickness variations of the upper crust

The first thing to note about the 2D profile is the great variability of the thickness of the extrusive units and Basal Group. The depth to the top of the SDC ranges from -700m to -2500m, and the thickness of the low-Ti lavas, high-Ti lavas, and Basal Group are independently variable. For example, in the western side of the Solea graben the low-Ti lavas are very thick (~850m), high-Ti lavas are only 100-300m thick, and the Basal Groups approximately the same, so the SDC is encountered at -1500m. In contrast, in the Kambia domain the low-Ti lavas are <100m thick, the high-Ti lavas are 400-800m thick, and the Basal Group are 1100-2000m thickness, giving a total thickness between 1550m to 2800m. Immediately west of the Kambia graben the thickness suddenly increases from 50-100m to ~500m at the boundary with the eastern edge of the E-Mitsero domain. Since the low-Ti lavas are apparently down thrown to the west it is probably due to a large normal fault, and this is supported by the eastward dip of the hanging wall lavas towards the fault. The same relationship is seen to 8km west at Agrokipia, the low-Ti unit increases in thickness from <300m in the footwall to nearly 1000m in the hanging wall, and again the hanging wall lavas are tilted towards the fault.

Dramatic thickness changes across the Stavros – W-Solea domain boundary are related to faulting, there is a horst block of Basal Group and high-Ti lavas capped by a thin (<100m) layer of low-Ti lavas and surrounded by thick low-Ti lavas on either side. This horst is bound to the east and west by large normal faults with displacements in the order of 800-1000m. The most abrupt changes in thickness of the extrusive rocks occur at the boundary of domains, e.g., at the Stavros – W-Solea domain boundary, at the eastern edge of E-Solea, and at the E-Mitsero – Kambia domain boundary.

The grabens were originally defined by the inward dip of the dykes and normal faults, but the new lava measurements show that the grabens are also reflected by the outward dip of lava flows. So the boundaries between the grabens can be traced further, up to the sediment contact in many places. The changes in thickness of the combined lava units are important in interpreting the mechanisms involved in accretion of the Troodos upper crust.

3.2 Other field observations

3.2.1 Characteristics of deformation

The down-section increase in dip is evidence of active growth faulting during the emplacement of lava. The faulting must have started prior to eruption so that there was fault related relief on the seafloor to pond the flows against. Possibly the faults are narrow and focused in the weak lavas units, and at the level of the SDC the strain may be less focused and dispersed across several fault zones instead of focused on one fault plane. Or even a small amount of slip could be taken up on the surface of each individual dyke, which would add up to be a large total rotation. The different deformation styles of the lavas and dykes are mainly due to the significant differences in the strength of these lithologies. Faults occurring in the lava units commonly form a fine fault gouge with a well-developed fabric. Typical shear zones of this type are 5-20cm wide with normal sense shearing as evidenced by s-shaped gouge fabric. However, in the SDC there is evidence for faulting on the surface of the dyke margins as sub-vertical slickensides. More commonly for the SDC the faults are identified by broad zones (10-30m wide) of brecciated dolerite, sometimes with quartz–epidote–sulphide assemblages indicative of hydrothermal upflow as at Moniatis (south flank of Troodos) or Apliki (~5km SSW of Ayia Koroni). With prolonged movement of the faults in the SDC, the damage zone grows wider rather than more localised and intense (which is the case for faults in the lavas).

Displacement by large normal faults is evident at depths of at least -1000m and often to -2500m as can be seen by the offsets of the units. Furthermore, they must extend to greater depths into the SDC because the dykes have been rotated by normal

faults which are parallel to the dyke margins, but it is impossible to quantify the displacements of faults within the SDC because there is a lack of stratigraphic markers with which to assess offset of horizons. Only horizontal extension by the rotation of faulted blocks can be estimated from the present dip of the dykes, which has been attempted and discussed in more detail in synthesis Chapter 6.

There are probably nine large faults of this scale across the ophiolite. They have a semi-regular spacing between 4km and 9km apart. Between these major faults there are many minor fault structures which contribute to accommodating tectonic strain. The minor faults are observable at the outcrop scale and are present in all parts of the Troodos upper crust, whereas the major structures are not directly observed- rather they are inferred by the presence of continuous brecciated damage zones, or by the intensity of hydrothermal activity, or distortion to the dips (i.e. anomalously high tilts of lava flows or dykes).

3.3 First order interpretations

Thickness variations and dip changes imply faults were active during the extrusion of lava flows, causing ponding of lava by damming flows, and causing rotation the lavas. It is a prerequisite for the fault to have formed before the lava erupted because it was the reason for the flow to be ponded, it then continued to slip because the lava dips document a down section steepening, eventually the half graben was filled in and the fault was covered/blanketed by the lavas flowing over and hiding the active tectonics beneath. The sediments were directly deposited on top of the lavas and because the seafloor topography was relatively subdued the boundary between the lavas and sediments was flat. Only the largest faults would have remained visible from the seafloor after the lavas were emplaced so the exposed faults scarps are really only the ‘tip of the iceberg’ and summing the heaves on those exposed scarps would lead to a gross underestimation of total tectonic extension.

4. Palaeomagnetic results and rotation analysis

4.1. Rationale

From the field data we can infer that the lava flows and sheeted dykes have been tilted significantly, with increasing tilts within the lavas at greater stratigraphic depths. Normal faults parallel to the dykes were active during extension of the seafloor, as can be inferred by the syntectonic nature of the volcanic units (see chapter 3 for evidence).

The goals of the palaeomagnetic investigation presented in this chapter are: (1) to quantify as much as possible these rotations in the sheeted dyke complex, and to link the dyke rotations to the seafloor spreading processes; and (2) to establish that the lavas are tectonically rotated by the same rotation axes as the SDC immediately beneath them, to support the assumption (chapter 3) that dips of flow tops are reliable tectonic markers for documenting tilting and hence extension.

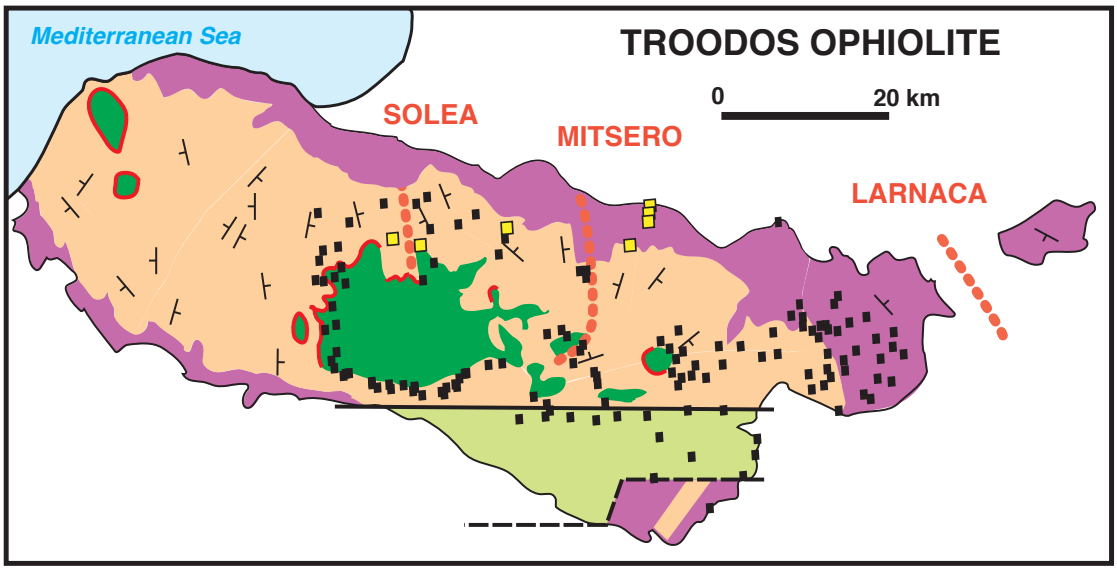

Figure 4.1 Map showing locality of new palaeomagnetic samples from lava flows (yellow) and existing dyke palaeomagnetic data taken from published sources (black dots).

There have been several palaeomagnetic studies of the Troodos SDC, particularly of the Solea graben (e.g., Allerton and Vine, 1987; Hurst et al., 1992; Varga et al., 1999) and the transform fault zone (e.g., Bonhommet et al., 1988; Morris et al., 1990). All of the palaeomagnetic and structural data from these studies of the

Troodos dykes have now been compiled into a database. In addition a small set of new palaeomagnetic samples have been collected from lava flows of the extrusive series to compare with the existing dyke samples (figure 4.1). Oriented hand-samples were collected from sheet flows and pillowed lava from seven localities across the Troodos extrusive sequence four localities from the East Mitsero graben, and three from the Solea graben. Between seven and eleven 2.5cm specimens were collected from each sampling locality, and the geological data from the outcrops were recorded (dip measurements and cross-cutting relationships). Sites with evidence of significant hydrothermal alteration were avoided.

4.2. NRM Demagnetisation experiments of lava flow samples

Natural remanent magnetization (NRM) is the permanent magnetization that is found naturally in a rock. There can be more than one component to NRM: the component that is obtained as the rock is originally formed is the primary or characteristic NRM (ChNRM), whereas any later component(s) are the secondary NRM(s) (Butler, 1992). For this study remanences were measured in the laboratory at the University of Plymouth using a Molspin fluxgate magnetometer.

4.2.1. Demagnetisation behaviour

The ChNRM has been isolated by gradually destroying the magnetization of the specimen using stepwise alternating field (AF) and thermal demagnetisation. The ChNRM were identified as the most stable component of magnetisations, on orthogonal vector diagrams (a.k.a. Zijderfeld diagrams) ChNRM is observed as the linear segment with a trajectory towards the origin (figure 4.2). Principal component analysis, or PCA (Kirschvink, 1980), is a statistical technique to identify the direction of the best-fit line through the set of demagnetisation steps based on the least squares mismatch to that line. The precision of that calculated best-fit line can be quantified using the maximum angular deviation (MAD value). Values of <10 are considered acceptable (e.g., Butler, 1992).

All specimens were found to have a stable ChNRM by the successful removal of minor secondary components. Using AF techniques most samples were found to have a stable characteristic component of magnetisation which was isolated at 15 mT. Only five specimens required further demagnetisation steps. The thermally demagnetised specimens have a stable ChNRM by 300°C (figure 4.2).

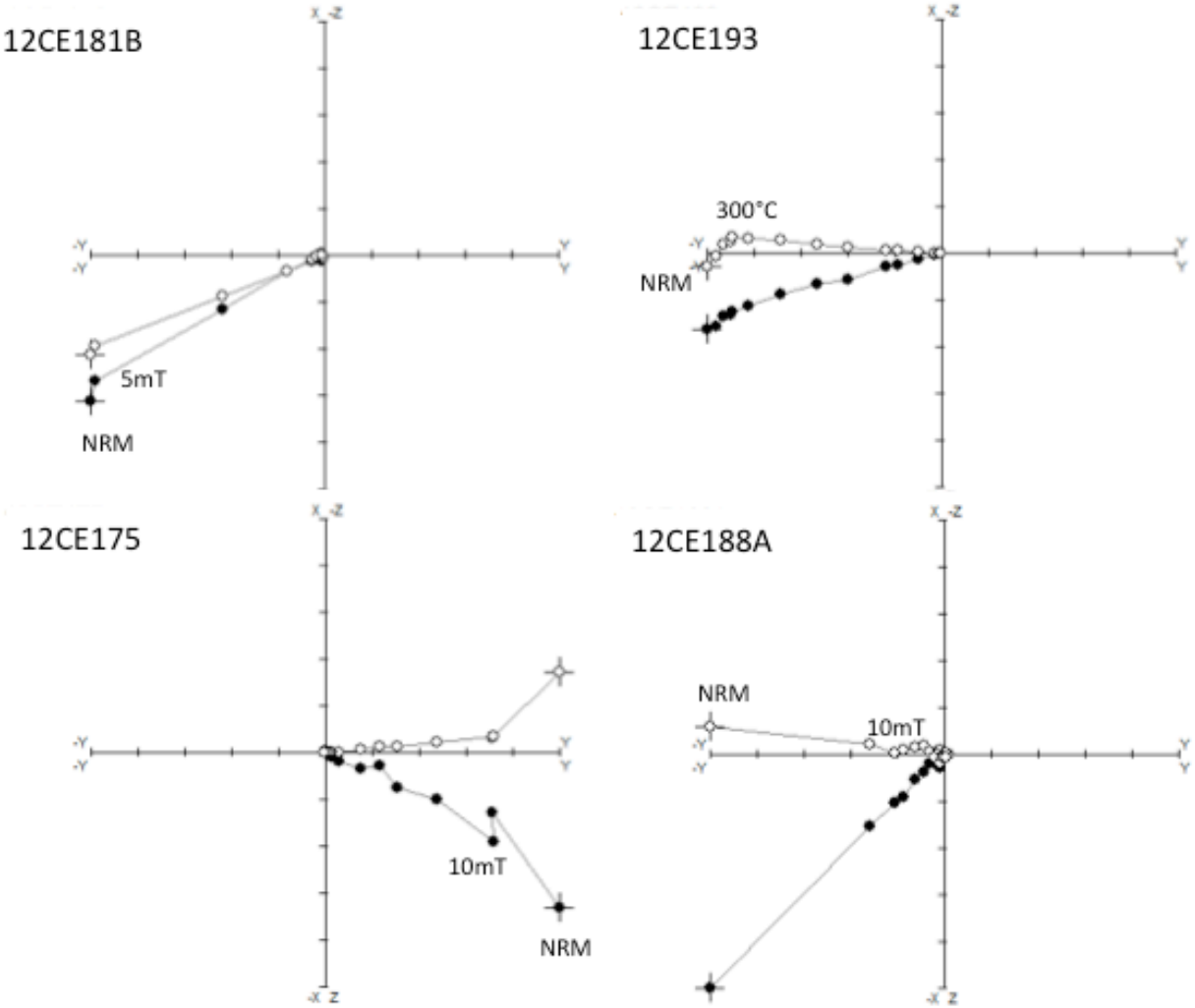

Figure 4.2 Typical examples of orthogonal vector diagrams for the Troodos lavas showing stable demagnetistion vectors showing both alternating field and thermal demagnetisation treatment.

4.2.2. Site mean directions

To determine a meaningful mean magnetisation direction for a site multiple specimens were collected at each sampled outcrop (between seven and eleven per site). The stable ChNRM identified from each individual sample have been combined to calculate the Fisher mean magnetisation direction for the site. The site mean directions were calculated using Fisherian statistics (Fisher, 1953), these are listed in table 4.1. The average direction for the locality is referred to as the site magnetic vector (SMV) and is considered to be the representative magnetisation direction for the lava flows and dykes at the outcrop (excluding cross-cutting dykes).

Table 4.1 Palaeomagnetic data from the new samples reported in this thesis.

Site	*In situ*		*K*	α_{95}	*Flow surfaces*		*Uplift tilt corrected*	
	Dec	*Inc*			*Strike*	*Dip*	*Dec*	*Inc*
Arediou	241.7	41.4	55.19	8.2	276	68	286.5	36.8
Kamaropotamos	276.3	27.3	22.10	12.0	080	25	275.7	37.9
Klirou village	284.8	31.4	42.85	10.4			287.5	44.0
Klirou Bridge	300.1	11.5	41.51	10.5			294.5	31.0
Kalo Chorio	041.7	88.8	32.22	9.9			284.3	37.0
Ayios Georgios	266.4	32.9	121.07	5.1			262.6	67.8
Evrychou	096.4	42.3	16.69	23.2			263.0	60.5
Korakou	141.5	84.4	29.29	9.7	047	28	287.5	44.0

4.2.3. Troodos Magnetic Vector

The first studies of the palaeomagnetism of the Troodos ophiolite discovered that the declinations of primary remanence vectors from samples from across the massif consistently pointed almost due west, rather than the expected north (Moores & Vine, 1971). This was interpreted as evidence for a 90° anticlockwise rotation of the entire Troodos massif. Subsequent studies confirmed and refined Moores and Vine's interpretation, leading to the definition of a Troodos-wide palaeomagnetic reference magnetic vector, the Troodos Magnetic Vector (TMV), by Clube et al. (1985). The TMV, which is based upon many hundreds of palaeomagnetic samples from extrusive rocks and metalliferous sediments of the Perapedhi Fm across the ophiolite, is taken as a measurement of the mean magnetisation direction for the Troodos microplate.

The TMV has since been updated and refined as more samples have been measured; the most recently published TMV, of 272.5°;38.4° (α_{95}=6.5; Morris et al., 2006), is used in this study.

Deviations of the site magnetisation vector (SMV) away from the TMV are taken to record post-magnetisation structural rotations. In the present study, the magnetic vectors measured in the dykes and lava flows have been corrected for uplift tilt (correction= anticlockwise rotation of 12° about axis of 279°;00°), the same correction as has been applied to the field data (see section 3.5.3 for explanation of the regional uplift tilt correction).

For cases where the SMV α_{95} ellipse overlaps with the TMV α_{95} ellipse there is no statistical evidence at the 95% confidence level to indicate any structural rotations have taken place (stereonet in figure 4.3).

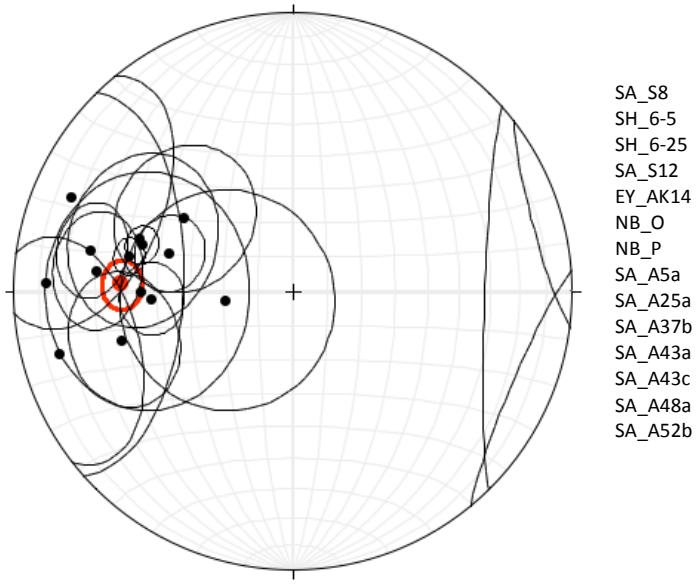

Figure 4.3 Red α_{95} ellipse = Troodos Magnetic Vector (TMV), black α_{95} ellipses = Sample Magnetic Vectors (SMV) which overlap with the TMV α_{95} ellipse. These samples were not used for net rotation analysis because there was no statistically significant deviation between TMV and SMV.

4.3. Net rotation analysis

Traditional methods of correcting for tectonic deformation require back-rotating palaeohorizontal surfaces to horizontal around horizontal axes to restore the inclination, followed by a rotation about a vertical axis to restore the declination. But this approach often leads to unrealistic rotations since rotation axes are rarely a

combination of only vertical or horizontal rotations, and leads to errors in declination (MacDonald, 1980). Except in simple, precisely known settings (as with the removal of the uplift tilt performed here: see above), a far more robust way to describe complex deformation is by a single rotation of an inclined axis, which can simultaneously restore the dykes back to vertical and restore the SMV to the reference direction. This net tectonic method of analysis was devised by Allerton & Vine (1987) and was applied to the analysis of the rotation of Troodos dykes, and also to the horizontal case (lava flows) for sites with no dyke orientation data. The technique was refined by others to include more systematic analysis of errors and uncertainties in the method (e.g., Morris et al., 1998)

4.3.1. Principles and assumptions of the net tectonic method

The algorithm of Allerton & Vine (1987) has several inherent assumptions which are considered to be reasonable, these are:

1. the reference vector (here the TMV) must be representative of the palaeo-geomagnetic field;
2. magnetisation predates the structural deformation;
3. the dykes were intruded vertically, and;
4. there has been no internal deformation within the sample.

The angle β is the angle between the dyke pole to plane and the sample magnetisation vector (SMV) of the dyke, and (assuming no internal deformation has occurred) will not change during rotation. Therefore, the original orientation of the dyke pole to plane must lie somewhere around a small circle centred on the TMV with a radius of β (figure 4.4). If β is greater than the inclination of the TMV ($\beta > 38.4°$) the small circle will intersect the primitive circle at two points and the original dyke pole to plane must be one of those two points, so there are two solutions to consider (both solutions the dyke was originally vertical). In the two solutions scenario the net rotation algorithm must be carried out twice, once for each original dyke orientation. But if β is $< 38.4°$ the small circle does not intersect the primitive circle and the original dyke orientation cannot be restored to vertical (figure 4.5). In these cases

there is only one solution for the original dyke strike and the shallowest pole to plane (steepest dyke dip) is chosen.

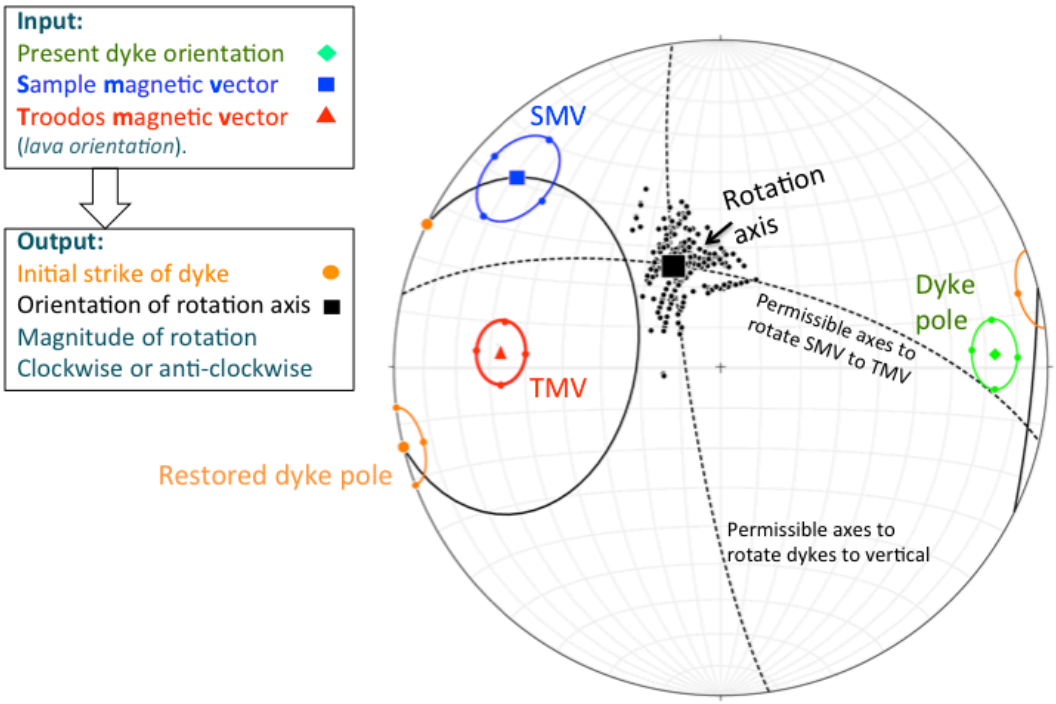

Figure 4.4 Example of the net tectonic rotation analysis using the algorithm of Allerton & Vine (1987). The black small circle centred on the TMV has an angle of $\beta > 38.4°$ and represents the possible initial dyke poles, where it intersects the primitive solution marks the two solutions for an initially vertical dyke. Dashed great circle striking N-S bisects the initial dyke pole (orange) and the present dyke pole (green). Dashed great circle striking almost E-W bisects the SMV (blue) and TMV (red). Rotation axis (black square) at the intersection of the two bisectors.

There are multiple permissible rotation axes that can rotate the original dyke pole to the present dyke pole, and these axes may lie anywhere along the great circle that bisects the original dyke pole and the present dyke pole (figure 4.4 and 4.5). Similarly, there are multiple permissible rotation axes that can rotate the TMV to the SMV and these axes must lie along a great circle bisecting the two magnetic vectors. At the point where the two great circles of permissible axes intersect is the single rotation axis that can simultaneously rotate the dyke poles and the magnetic vectors from their original orientation to their present orientation (figure 4.4).

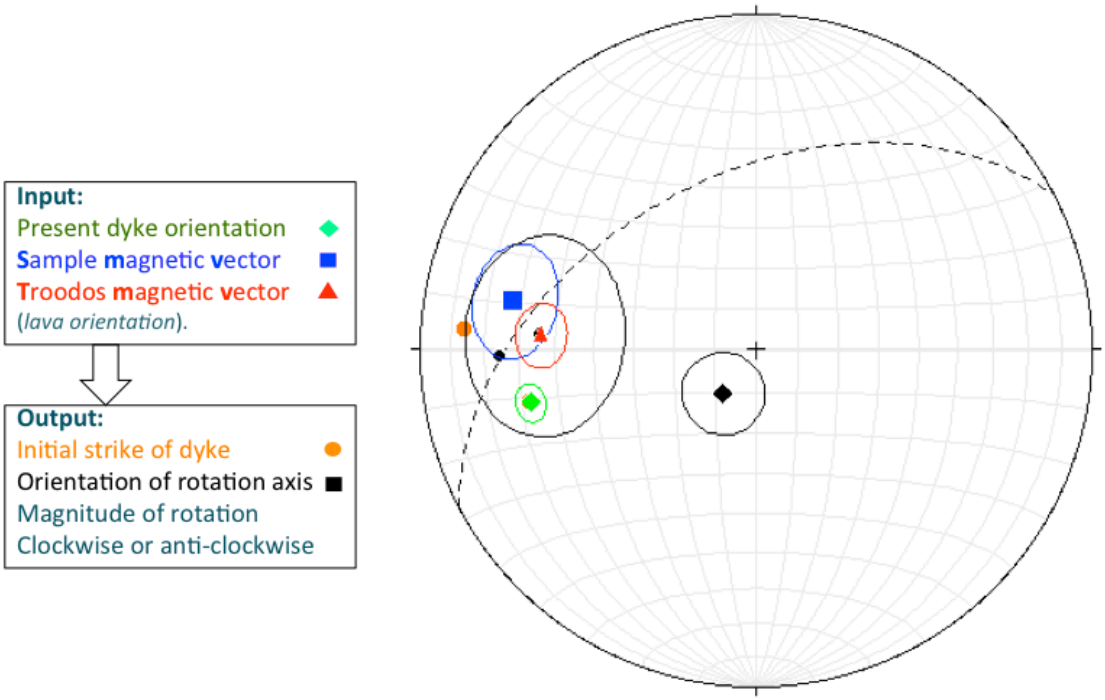

Figure 4.5 Example of the net tectonic rotation analysis using the algorithm of Allerton & Vine (1987). Symbols are the same as in figure 4.5. This is an example of a case with one solution because β is < 38.4° so the black small circle centred on the TMV is does not intersect the primitive circle. In these instances the dyke cannot be restored to vertical, so the initial dyke is assumed to be the steepest point around the black small circle.

It is reasonable to assume that dykes and lavas from a sampling site have been affected by the same post-magnetisation rotation. Therefore it is appropriate to use the SMV of a lava flow to back-rotate a dyke to its initial vertical orientation if the sample flow and measured dyke are from the same site.

In the present study all the new SMVs were collected from lava flows. These have been used in the net rotation analysis same way as the SMV of dykes. This net rotation analysis has been applied to my new lava palaeomagnetic data and field data in the same way as it is applied to the dyke palaeomagnetic data.

4.3.2. Selecting a preferred solution

For cases with two solutions for initial dyke pole, cases where $\beta > 38.4°$, the algorithm is run two times (one for each initial dyke orientation). The calculated rotations for each initial dyke solution are usually vastly different to each other. To choose between the two possible solutions the rotation calculated for each of the solutions is also applied to the lava field measurements (if lava dip data is available for that locality).

The preferred solution will restore (back-rotate) the lava flow dips to horizontal or closer to horizontal, while the alternative solution typically steepens or overturns the lava flows. Usually (though not always) the preferred solution will have a smaller magnitude of rotation, the initial dyke strike will be consistent with the local trend, and rotations will be similar to neighbouring localities from the same structural domain. Generally good inter-site consistency was found in a particular region (see below).

4.3.3. Estimating uncertainties

The cluster of permissible rotation axes are not distributed symmetrically around the rotation axis as identified from the input vectors, so an α_{95} ellipse around the rotation axis would not properly represent the uncertainties. Instead, the Allerton and Vine (1987) algorithm was modified by Morris et al. (1998) to better estimate the uncertainties of the rotation axis azimuth/plunge and the angle of rotation. The modified algorithm will take into account four points around the α_{95} ellipse of each of the input vectors (i.e. TMV, SMV, present dyke pole, and initial dyke pole), to compute 125 combinations of input vectors. All the permissible rotation axes and rotation angle are output: 125-250 estimates per analysis. The calculated rotation angles are plotted as frequency histograms (e.g., figure 4.6).

4.4. Net tectonic rotation solutions

The initial orientations of sheeted dykes calculated from previous workers' palaeomagnetic data using the Allerton & Vine (1987) method are listed in table 4.2, along with the orientation of the rotation axis and angle for the preferred rotation solution of each analysis. These data have been plotted onto miniature stereonets and overlain on the Troodos geology map (GSD, 1995) for spatial interpretation. Previous palaeomagnetic studies have focused on the Solea graben (Hurst et al., 1992; Varga et al., 1999; Allerton and Vine 1987), Larnaca graben (Allerton, 1988), and the area immediately north of the STTFZ (Bonhommet et al., 1988; MacLeod et al., 1990), and within the STTFZ/Limassol Forest Complex (Allerton, 1988; MacLeod 1988; Gass et al., 1994).

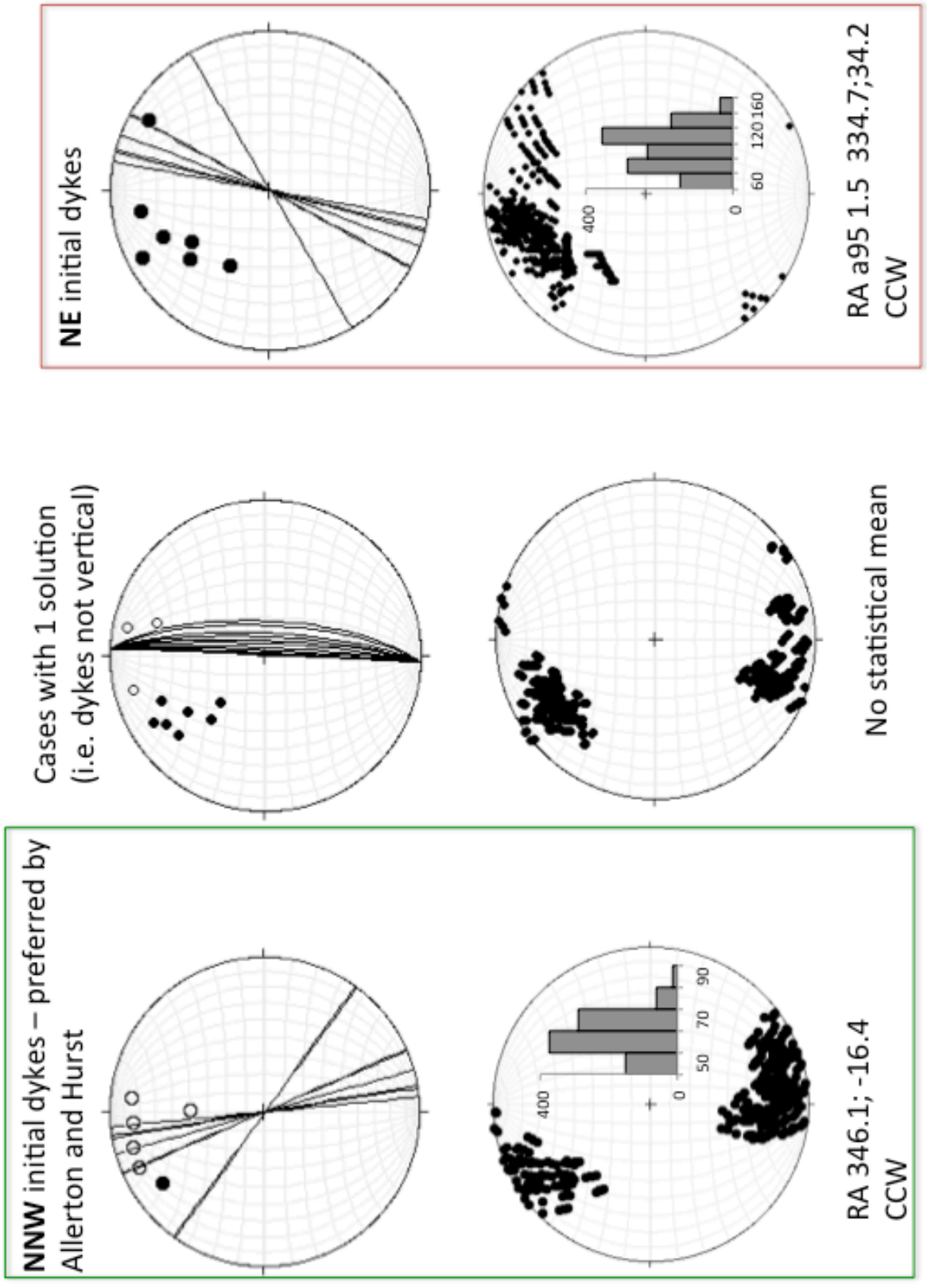

Figure 4.6 West Solea Graben. Summary of the different initial dyke strike solutions. Upper stereonets show great circle for initial dyke strike and dots for the mean rotation axis (RA). Lower stereonets show all permissible rotation axes and frequency histogram of rotation angles. CCW=counter-clockwise.

Table 4.2 Summary of all the initial orientations of sheeted dykes calculated using the Allerton & Vine (1987) method, along with the orientation of the rotation axis and angle for the preferred rotation solution of each analysis

Source	Site	Preferred solution			Initial dyke	
		Az.	Pl.	angle	Strike	dip
Solea Graben						
Young	SK16	348.1	17.9	61.6	059	90
Allerton B	S4	173.0	05.7	-64.3	003	85
Allerton B	S6	165.6	14.4	-45.0	355	90
Allerton B	S7	309.9	46.3	84.0	003	72
Hurst	5-52a-d	314.4	56.7	137.1	003	82
Hurst	5-52e,f	218.1	61.1	-91.7	003	80
Hurst	6-26a	298.9	54.5	165.1	290	90
Hurst	6-26c	169.6	16.6	-55.7	337	90
Hurst	5-78.	339.0	02.8	68.5	330	90
Hurst	6-1.	341.6	06.1	50.3	346	90
Hurst	6-2.	338.2	18.2	57.7	355	90
Hurst	6-38a	166.3	14.2	-58.4	325	90
Hurst	6-62.	158.5	02.6	-58.8	344	90
Hurst	7-86.	163.7	00.9	-49.4	322	90
Hurst	7-424	183.0	51.3	-76.6	306	90
Varga	TR209	030.7	13.7	45.5	014	90
Varga	TR214	324.1	39.8	47.5	003	74
Varga	TR221	175.7	16.5	-59.8	344	90
Varga	TR213	192.0	11.1	-30.4	003	84
Varga	TR219	329.5	18.8	58.9	003	89
Varga	TR220	333.1	22.3	55.0	003	87
Varga	TR210	325.8	21.9	45.4	336	90
Varga	TR225	325.6	24.6	47.3	003	87
Varga	TR211	197.4	28.1	-51.2	003	89
Varga	TR212	165.8	14.8	-48.7	003	86
Varga	TR215	337.1	29.0	51.7	003	78
Varga	TR216	156.5	13.8	-55.4	337	90
Varga	TR222	186.5	15.3	-60.2	350	90
Varga	TR226	318.0	26.4	61.1	003	88
Young	EV03	356.9	75.3	152.3	003	65
Allerton B	S5	019.4	16.6	-67.0	354	90
Allerton B	S8	276.4	49.8	-66.8	317	90
Hurst	6-24.	118.1	48.0	-26.5	003	74
Mitsero Graben						
Young	KA03	267.2	49.7	103.8	003	83
Allerton B	S12	265.6	14.0	36.1	324	90
Allerton B	S13	332.5	02.7	34.6	311	90
Hurst	6-66.	345.9	14.2	62.4	003	87
Hurst	6-39a	338.9	84.7	-122.8	003	89
Hurst	6-63.	355.8	07.0	67.1	330	90
Hurst	6-64.	178.9	10.2	-26.3	318	90
Hurst	7-A85	152.4	62.7	-120.1	044	90
Hurst	7-339	312.5	49.2	41.7	003	85
Hurst	6-5.	258.7	38.2	33.8	350	90
Varga	TR95-27	335.9	19.6	35.1	003	90
Varga	TR95-15	156.5	20.5	-32.6	003	87
Varga	TR95-16	257.0	53.5	-83.1	349	90
Varga	TR237	357.6	13.3	36.5	003	86
Varga	TR9-13	171.1	08.1	-62.9	342	90
Young	AK14	272.1	29.9	103.3	003	73
Young	AK06	072.5	02.7	-56.9	003	89
Young	AK08	238.6	65.3	-112.6	041	90
Larnaca Graben						
Allerton A	A3	166.7	35.1	-137.5	328	90
Allerton A	A4	203.4	40.4	-145.0	313	90
Allerton A	A5a	296.2	01.2	-41.5	335	90
Allerton A	A5b	288.4	70.2	-85.3	003	86
Allerton A	A6	167.2	09.9	-71.9	003	67

Source	Site	Preferred solution			Initial dyke	
		Az.	Pl.	angle	Strike	dip
Larnaca Graben						
Allerton A	A8	239.0	58.1	-120.5	319	90
Allerton A	A9	184.8	56.3	-130.4	330	90
Allerton A	A10	210.0	63.8	-108.6	003	84
Allerton A	A15a	220.1	72.2	-84.2	285	90
Allerton A	A15b	168.4	43.3	-62.4	003	88
Allerton A	A16	232.0	66.7	-109.4	316	90
Allerton A	A17	120.8	30.1	-56.0	047	90
Allerton A	A18	195.8	61.8	-77.4	340	90
Allerton A	A19a	260.0	64.1	-86.8	327	90
Allerton A	A20	239.4	20.3	60.4	007	90
Allerton A	A21	216.4	58.8	-78.4	003	69
Allerton A	A22	306.9	10.8	66.8	318	90
Allerton A	A23	079.5	87.6	-157.8	337	90
Allerton A	A24	199.7	37.0	-143.3	301	90
Allerton A	A25b	258.4	25.1	151.2	293	90
Allerton A	A26a	349.6	76.0	-152.3	003	61
Allerton A	A27	227.0	77.7	-99.0	333	90
Allerton A	A28	285.7	45.3	-67.4	323	90
Allerton A	A30	151.0	69.3	-61.7	323	90
Allerton A	A32	136.7	48.2	-33.7	278	90
Allerton A	A34	176.0	59.9	-71.1	354	90
Allerton A	A35	273.1	56.7	-135.1	003	64
Allerton A	A37a	353.4	54.2	-27.2	003	85
Allerton A	A37b	252.2	35.9	-36.6	311	90
Allerton A	A38	174.6	18.7	-64.8	003	81
Allerton A	A43a	265.4	54.1	-164.5	329	90
Allerton A	A43c	270.1	59.0	76.1	343	90
Allerton A	A44	168.7	49.5	-48.5	003	85
Allerton A	A45a	277.1	64.2	-125.5	003	85
Allerton A	A45b	284.4	64.7	-155.9	325	90
Allerton A	A47	223.1	74.3	-96.5	342	90
Allerton A	A48a	263.4	25.7	115.6	294	90
Allerton A	A48b	322.6	36.0	-50.4	301	90
Allerton A	A49	165.0	44.4	-148.4	327	90
Allerton A	A50	201.4	71.4	83.9	333	90
Allerton A	A51	222.3	73.5	-80.8	287	90
Allerton A	A52a	182.5	72.9	-110.7	334	90
Allerton A	A52b	046.0	23.1	-30.7	356	90
Allerton A	A53	318.2	75.3	(-+)176.5	282	90
Allerton A	A54	298.1	45.2	142.5	318	90
Allerton A	A55	194.1	60.2	-66.0	324	90
Allerton A	A56	185.1	50.0	-38.4	325	90
Allerton A	A57	305.4	17.5	120.3	309	90
Transform zone						
Bonhommet	A	180.0	62.2	-65.4	000	90
Bonhommet	B	286.5	65.1	-110.0	324	90
Bonhommet	C	245.2	69.6	-141.3	317	90
Bonhommet	D	230.3	71.6	-154.0	303	90
Bonhommet	F	293.2	68.6	-164.5	302	90
Bonhommet	H	279.1	74.5	-110.2	339	90
Bonhommet	I	293.6	70.5	-125.4	323	90
Bonhommet	K	301.9	66.5	-110.7	339	90
Bonhommet	L	126.6	69.9	-46.3	003	85
Bonhommet	N	312.5	55.7	-51.4	315	90
Bonhommet	O	258.0	69.9	-14.1	003	82
Bonhommet	P	242.6	68.8	-21.1	330	90
Bonhommet	Y	199.6	62.5	-102.0	332	90

Young = this thesis **Allerton B = Allerton 1989** **Varga = Varga et al. 1999**

Allerton A = Allerton 1988 **Hurst = Hurst et al. 1992** **Bonhommet = Bonhommet et al. 1988**

+ rotation angle = anitclockwise

- rotation angle = clockwise

4.4.1. West Solea domain

The Solea graben structure probably represents a fossil ridge axis which was deformed during seafloor spreading when the ridge was active (Varga and Moores, 1985).The preferred solution for initially NW striking dykes requires shallowly N- to NW-plunging rotation axes which are parallel to the dyke strike (figure 4.7), with an anticlockwise rotation about a shallowly N-plunging axis in the order of 60°-80° (figure 4.7b). There is very good inter-site consistency of the orientation of the rotation axes for the NW solution (figure 4.6, above), the Fisher mean rotation axis = 346.1°;-16.4°.

The alternative NE solution requires far greater angles of anticlockwise rotations (80°-140°) about shallowly to moderately inclined, non-dyke strike parallel rotation axes oriented 334.7°;34.2°. Azimuths of axes deviate from initial dyke strikes by >50°. The one-solution cases strike 002.5° with variable steep initial dyke dips and have rotation axes orientations identical to the NE solution.

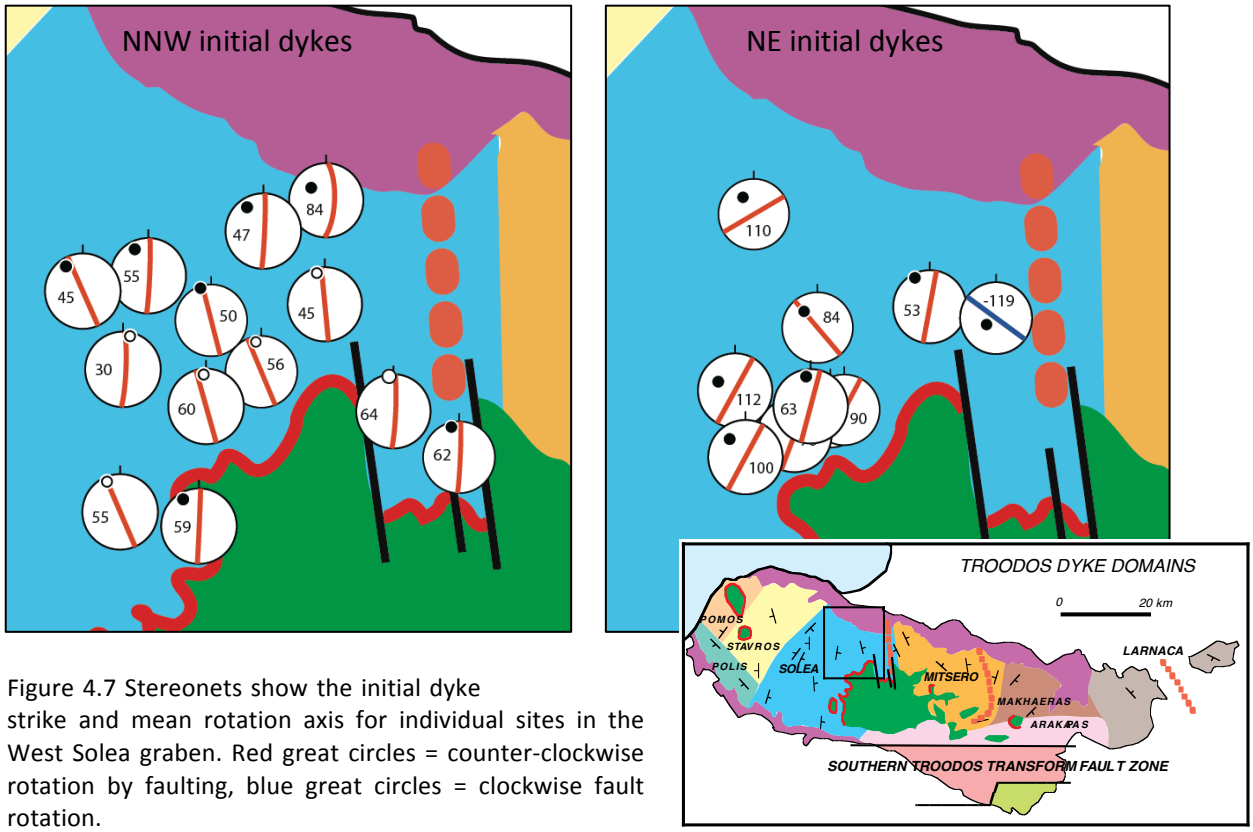

Figure 4.7 Stereonets show the initial dyke strike and mean rotation axis for individual sites in the West Solea graben. Red great circles = counter-clockwise rotation by faulting, blue great circles = clockwise fault rotation.

4.4.2. East Solea domain

The East Solea domain is only 5-6 km wide, and has fewer palaeomagnetic sites in comparison to the West Solea domain (figure 4.8). Generally the dykes are moderately to steeply dipping to the west and are mirroring the inwards facing dykes of the opposite side of the graben, although the strike of the dykes on the east side of Solea graben are notably more variable (Hurst et al., 1992).

Selecting the most appropriate solution for this domain is problematic because both the NW and NE initial dyke solutions generate huge differences in rotation axis orientations and sense and angle of rotation. Most of the rotation axes from these sites, whether from either of the two solutions cases or the one solution cases, are steeply inclined (seven of the eleven rotation axes are inclined >50°). Further palaeomagnetic data and lava flow orientation data are required from this area in order to select a preferred solution.

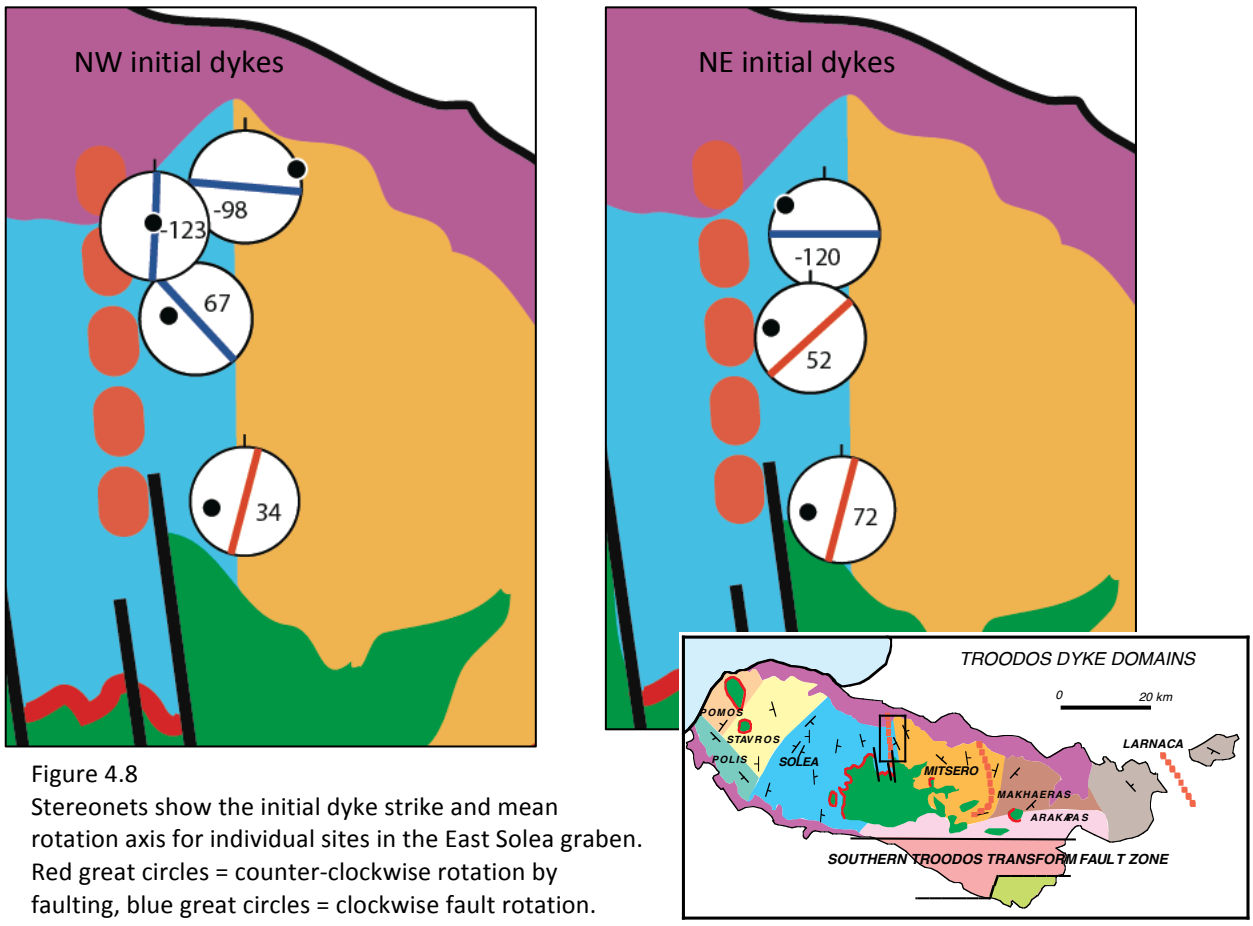

Figure 4.8
Stereonets show the initial dyke strike and mean rotation axis for individual sites in the East Solea graben. Red great circles = counter-clockwise rotation by faulting, blue great circles = clockwise fault rotation.

4.4.3. 'Inter-graben zone' SDC horst block

The 'inter-graben zone' (Eddy et al., 1998) refers to the large horst block of dykes between the Solea and Mitsero grabens where the majority of the dykes are steeply dipping towards the East, forming a horst block of SDC and Basal Group with only a thin layer of lavas covering it.

The two site S13 and KA03 with an initial NW striking dyke have small angles of rotation (35°-36°), but the orientation of the rotation axis differs greatly (figure 4.9). These two sites are ~5km apart and have been interpreted individually because they are so different. The mean rotation for site S13 is oriented 330°;04°, with magnitudes of rotation between 30°-50° and anticlockwise sense of rotation by faulting (figure 4.10). This sub-horizontal rotation is consistent extension along normal faults as would be expected for the western Mitsero graben.

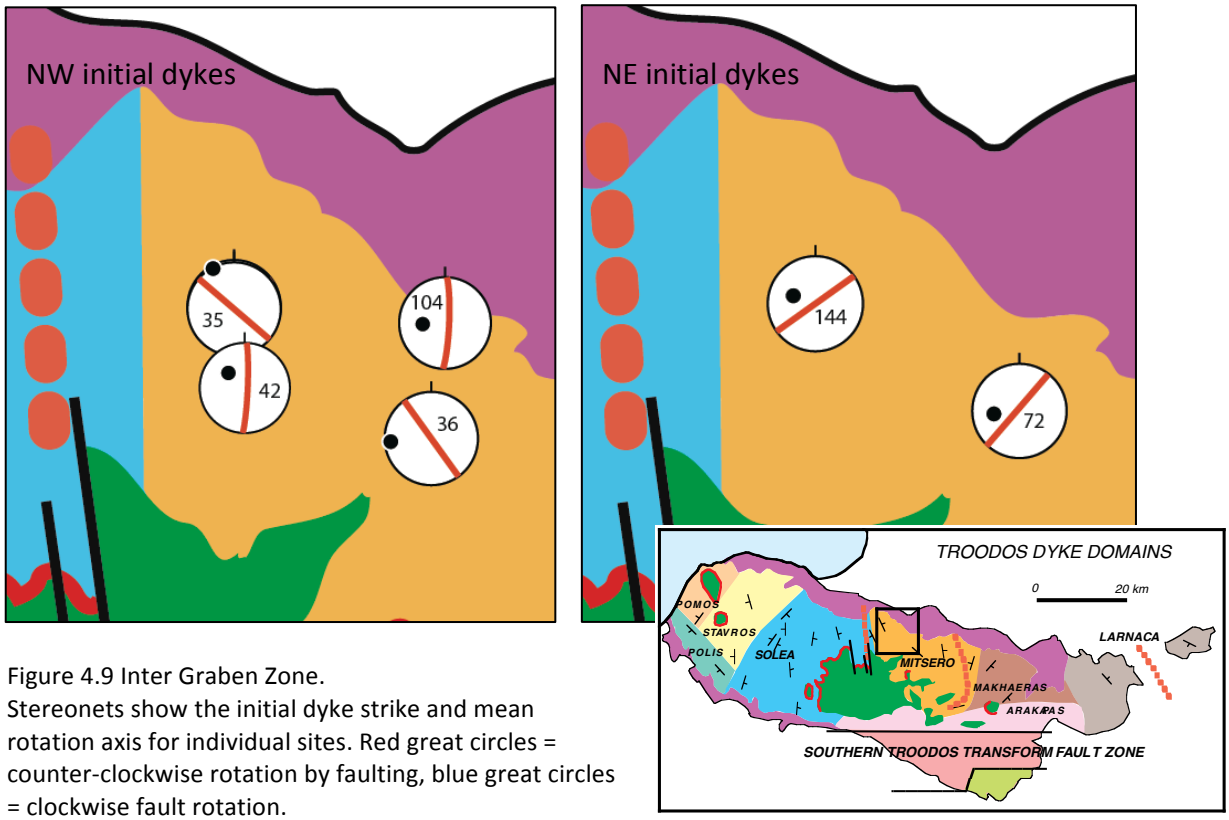

Figure 4.9 Inter Graben Zone.
Stereonets show the initial dyke strike and mean rotation axis for individual sites. Red great circles = counter-clockwise rotation by faulting, blue great circles = clockwise fault rotation.

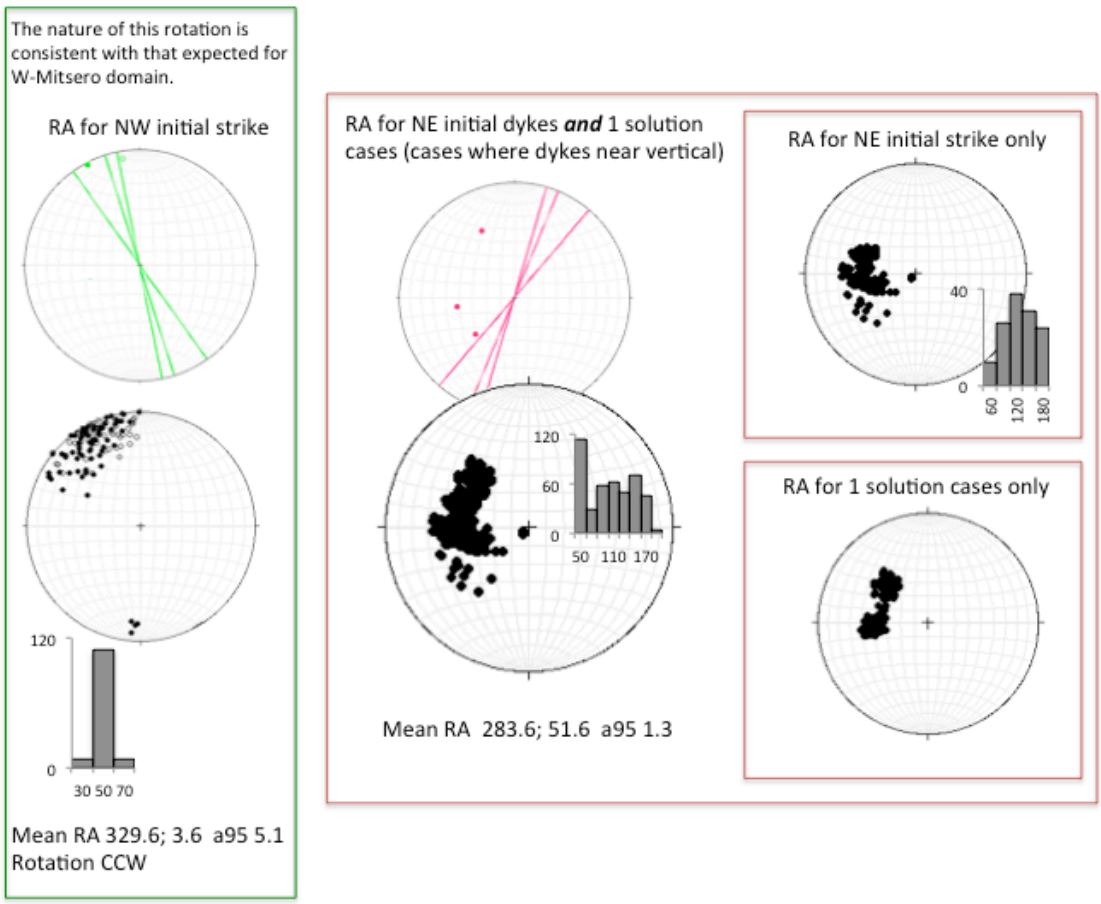

Figure 4.10 Inter Graben Zone. Summary of the different initial dyke strike solutions. Upper stereonets show great circle for initial dyke strike and dots for the mean rotation axis (RA). Lower stereonets show all permissible rotation axes and frequency histogram of rotation angles. CCW=counter-clockwise.

Site KA03 has a sub-horizontal WSW oriented rotation axis and an anticlockwise rotation of 36°. This site is at the eastern margin of this horst block from near the uppermost part of the basal group. This horst block is bound by a large east dipping normal fault named the Alestos Forest fault by Eddy et al. (1998). This is a region of intense hydrothermal alteration and mineralisation of the lavas, which Eddy et al. (1998) interpret as related to the large N-S trending Alestos Forest normal fault and associated ENE trending transfer faulting which goes right through the Memi and Alestos mines. The rotation for KA03 might be explained by their proximity to the ENE trending transfer faults.

The NE dyke strike solutions and the cases with one solution have similarly oriented rotation axes which cluster very well so they have been grouped together (figure 4.10). These cases have much steeper rotation axes, the mean is 284°;52° and the rotations angles range between 70°-180°.

4.4.4. East Mitsero domain

The three sites from this domain were collected during this study from lava flows; however the site AK02 is not used for further net rotation analysis because the SMV α_{95} ellipse overlaps with the TMV. Of the remaining sites there is no obvious solution which best describes the data (figure 4.11). The permissible rotation axes for site AK08 are plotted in figure 4.10b, which has a mean rotation of 338°;26°- this is parallel to the initial NW dyke strike.

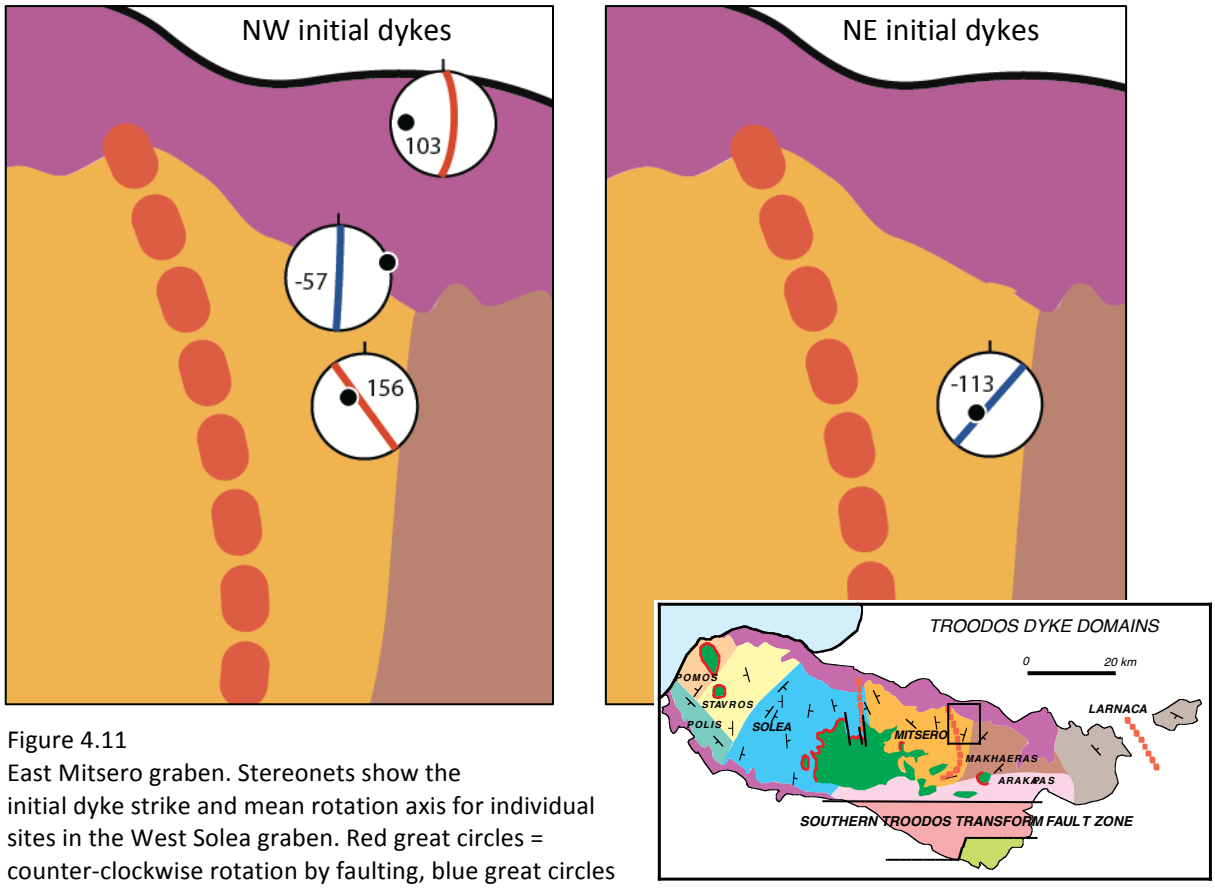

Figure 4.11
East Mitsero graben. Stereonets show the initial dyke strike and mean rotation axis for individual sites in the West Solea graben. Red great circles = counter-clockwise rotation by faulting, blue great circles = clockwise fault rotation.

4.4.5. Transform area (Bonhommet et al., 1988)

The NW solution requires steeply plunging rotation axes which are trending parallel to the NW initial dyke strikes (figure 4.12). There is good inter-site consistency as indicated by the tight clustering of axes in figure 4.13. The mean rotation is clockwise about an axis oriented 255°;71° with rotations of up to 165°. This is the preferred

solution because the rotations are remarkably consistent and this solution was preferred by Bonhommet et al. (1988) to account for the swing in dyke strikes north of the Arakapas fault belt.

The NE solution has rotation angles between 57°-110°, which is significantly lower than the NW solution, but the orientation and sense of rotation are extremely variable between the sites so this is not the preferred solution.

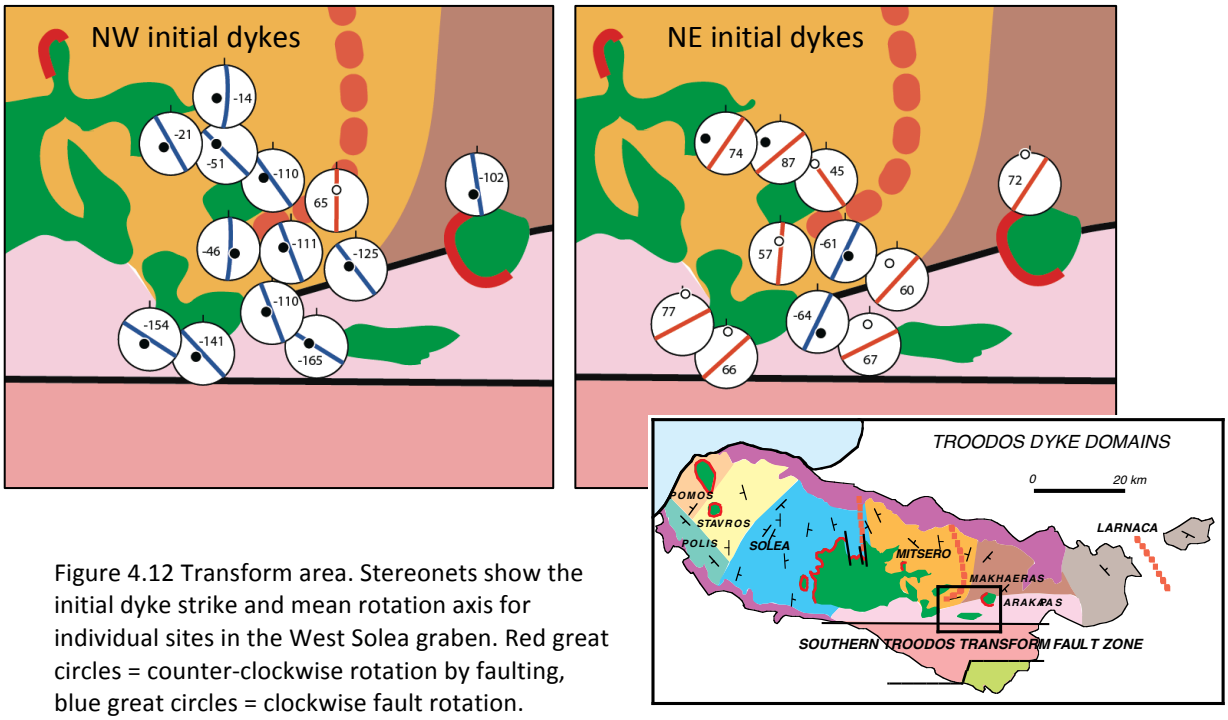

Figure 4.12 Transform area. Stereonets show the initial dyke strike and mean rotation axis for individual sites in the West Solea graben. Red great circles = counter-clockwise rotation by faulting, blue great circles = clockwise fault rotation.

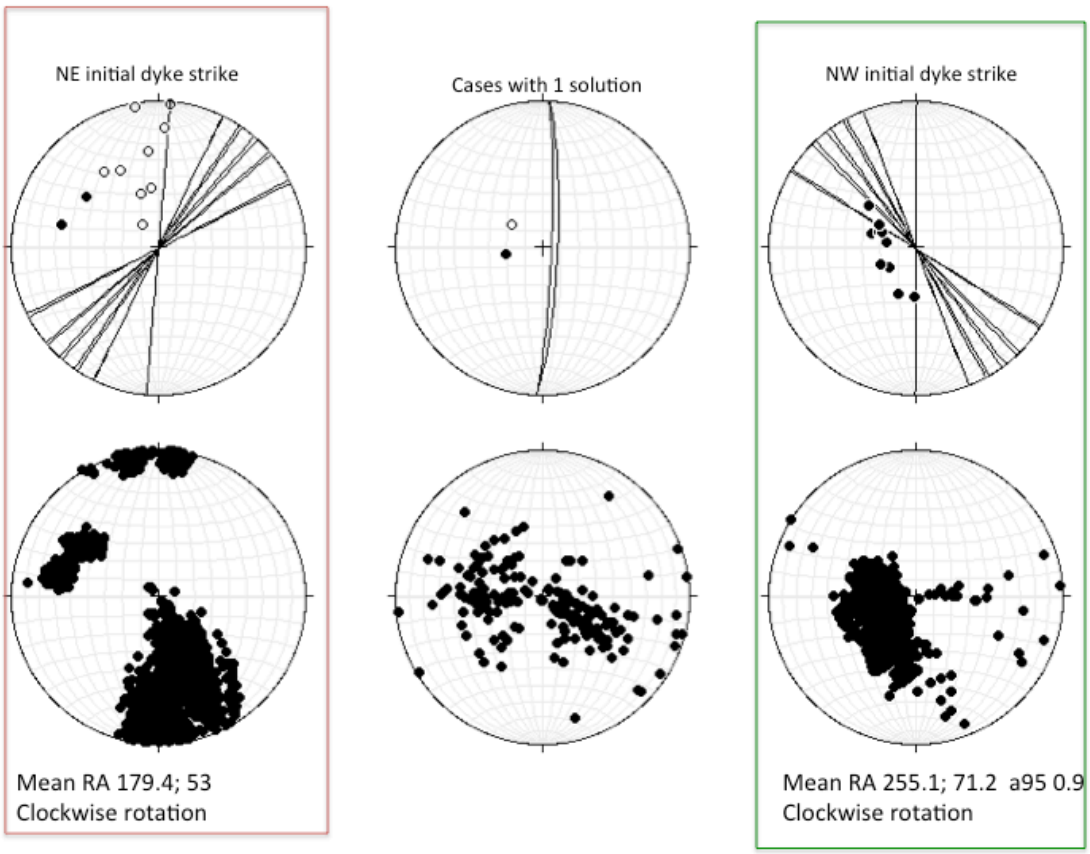

Figure 4.13 Transform area. Summary of the different initial dyke strike solutions. Upper stereonets show great circle for initial dyke strike and dots for the mean rotation axis (RA). Lower stereonets show all permissible rotation axes and frequency histogram of rotation angles. CCW=counter-clockwise.

4.4.6. West Larnaca graben domain

Rotations in the Larnaca graben are of two distinct sets each documenting different styles of rotation. One set requires large rotation about steeply plunging rotation axes. Rotations of this type are observed in the basement lavas which is part of an older and more deformed terrain. The other set requires rotations about shallowly inclined rotation axes. Rotations of the second set are restricted to the younger infill lavas which are significantly less deformed than the basement lavas.

The different phases of rotation are associated with multiple sets of faults which cross-cut each other. The earlier fault set associated with the large rotations about steep axes are related to an earlier episode of spreading (possibly at the Mitsero graben) and then later rotations have further tilted the basement. Whereas the rotation of the infill lavas are associated with the cross-cutting faulting, and the shallowly incline rotation axes indicate a spreading related tilting of the infill lavas.

Allerton interprets this area as a younger terrain which erupted infill lavas directly over the basement lavas and this newer terrain could be from a ridge propagating from the north to cross cut the older basement terrain.

4.5. First order interpretations

Using the net tectonic rotation analysis method it is possible to assess the rotation history and make inferences on the style of tectonics which was involved. As discussed in section 4.4 above there are some regions which show rotations of the SDC are typical of extensional faulting at a graben such as at a spreading centre, in this case the N-S trending Solea graben. These spreading related rotations have been documented best in the West Solea domain, also in some parts of the horst block between the Solea and Mitsero grabens, and again in the youngest portions of the Larnaca graben. Rotations of this type are characterised by shallowly plunging rotation axes trending roughly N-S, with a sense of rotation which would tilt the originally vertical dykes to their present in-ward dipping orientations on either side of the grabens. Since the rotation axes are sub-parallel with the initial dyke strikes, it is reasonable to suggest the rotation took place along dyke parallel normal faults which also dip towards the graben centre. Dyke parallel faults are frequently seen on all parts of the SDC across the ophiolite (Varga, 1991).

4.5.1. Application to lava dips

The rotations presented here have been based on palaeomagnetic data, the vast majority of them from the SDC. The dyke palaeomagnetic data for the West Solea graben show consistent rotations throughout the domain, indicating the tectonic regime is the same across this domain. Rotations from this region have been compared to the lava field data to draw comparisons with the tilting of the extrusive rocks with the rotations of the sheeted dyke complex.

In figure 4.14 the permissible rotation axes derived from the dyke palaeomagnetic data using the NW initial dyke solutions. The rotation axes have been coloured for different angles of rotation, the mean rotation axis is shown with an $\alpha 95$

ellipse, mean rotation is anticlockwise with axis of 166.1°;16.4°. In blue are the lava dip data measured in the West Solea graben showing the mean pole to plane and α95 ellipse for each locality. Dipping to the west the lava become more steeply tilted at greater depths (figure 4.14 labels 'U', 'M' and 'L' are upper, middle and lower respectively), in complement to the east dipping dykes (not plotted here). The mean lava poles lie very neatly along a best fit girdle (dashed blue great circle) and the pole to the girdle is 339°;07°, which is an approximation of the rotation axis. Using the field data alone the rotation can be loosely defined as an anticlockwise rotation of ~55° around a sub-horizontal axis trending NNW-SSE, falling well within the cluster of permissible rotation axes of the dyke data.

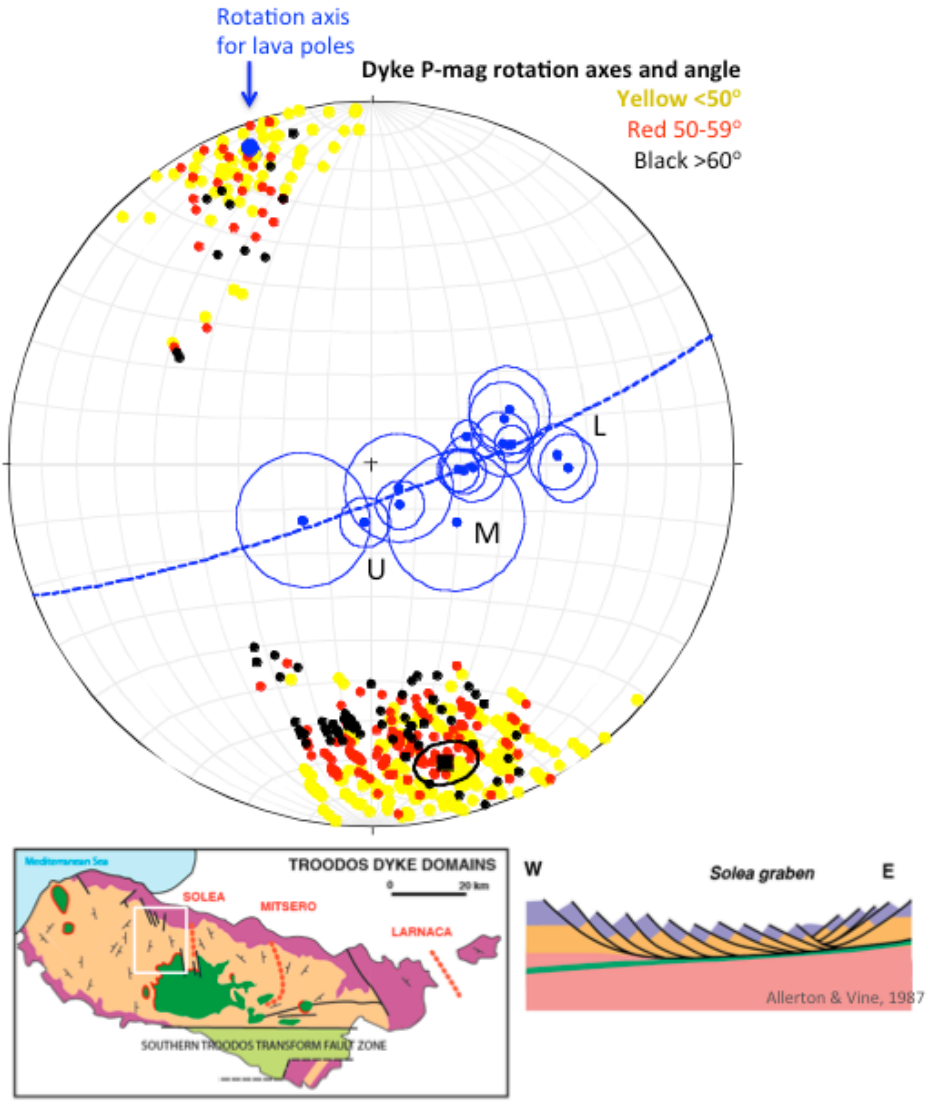

Figure 4.14 West Solea. Rotation axes calculated from dyke palaeomagnetic data are consistent with rotation axis from lava field measurements. Rotations are spreading related.

A strong similarity between the lava field measurements and the dyke rotations is also observed for the 'inter-graben' zone at the western most part of the Mitsero graben (figure 4.15). Only the rotation axes from site S13 are shown in figure 4.15, yet there is a very good fit between the mean rotation axis and the pole to the best fit girdle through the lava poles to plane. In this case the field data indicate an anticlockwise rotation about and axis oriented 334°;12° with a rotation angle of ~45°. This is remarkable similar to the results of the net rotation analysis based on dyke data which gives a mean rotation of <50° anticlockwise about an axis of 329.6°;03.6°, only a few degrees different from the rotation axis of the lava field data set.

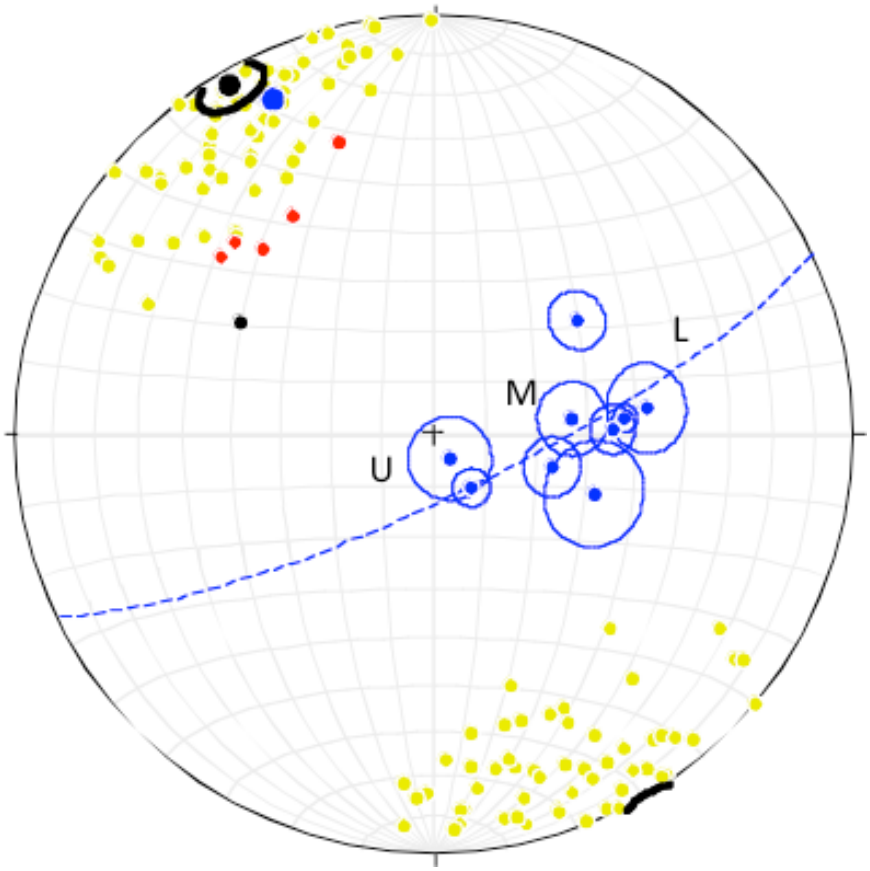

Figure 4.13 West Mitsero Rotation axes calculated from dyke palaeomagnetic data are consistent with rotation axis from lava field measurements. Rotations are spreading related.

So the observed tilts of the lava measurements are entirely consistent with rotations derived from palaeomagnetic data of the sheeted dyke complex immediately beneath. Rotations of both the SDC and extrusive sequence probably occurred at the same time because the same rotations can tilt the dykes and the lavas to their present

attitudes. Consequently the tilting of the lava is also a result of tectonic rotation via dyke-parallel faulting during spreading, and probably not related to subsidence of the lava pile. It is therefore appropriate to use the orientation lava flows as markers of tectonic tilting.

5 Geochemistry

5.1 Rationale

There have been numerous geochemical studies of the Troodos lavas over the past few decades, a great many of which are very detailed and have revealed much about the petrogenesis of the magmatic crust (e.g., Cameron, 1985; Rautenschlein et al., 1985; Taylor, 1990; Schouten & Kelemen, 2002; Pearce & Robinson, 2010). Early attempts to explore spatial variation in the geochemistry of the extrusive sequence were made by Taylor & Nesbitt (1988) and Taylor (1990). Most of the volcanological and petrogenetic studies, however, were often based on local areas with little attempt to link their conclusions to broader scale tectonic models and structural observations. The geochemical study conducted here and presented in this chapter brings together all the available data for the first time, together with 115 new analyses, with the aim of considering the data on an ophiolite-wide regional scale, reconciling geochemical variations with field observations in the context of spreading structure and upper crustal accretion mechanisms.

The lava compositions and the spatial distribution of geochemically distinct lava packets has the potential to reveal much about the processes involved in accreting the upper oceanic crust of the Troodos ophiolite; not just magmatic processes, but also volcanological and tectonic processes. The aim of this geochemical investigation was to compile and add to the database of samples to expand the coverage of data and to assess all the available geochemical data on a Troodos-wide scale. In chapter 6 the geochemical results and conclusions are interpreted in the context of the structural and stratigraphic results and inferred crustal architecture to develop a spreading history for Troodos and a model for the magma plumbing system. It is not within the scope of the project to create a new petrogenetic model, instead the most appropriate parts of existing models have been re-interpreted with new structural and stratigraphic data from this study.

5.1.1 Dataset

A database of 627 whole rock geochemical analyses has here been compiled from published sources, and includes 115 new analyses. The analyses in the database have come from various labs around the world using a number of techniques (XRF, ICP-MS, ICP-OES) to analyse for major element oxides, trace elements and rare earth elements (REE). The lavas analysed range from the topmost lavas down to the lowest lava screens in the Basal Group, and span the entire width of the ophiolite from Pomos on the west coast to Ayia Anna in the east.

The sampling strategy was to target areas that were not previously well-sampled to improve the sample density across the ophiolite, especially the north flank. Where possible, the samples were collected along N-S 'vertical' transects going systematically from the top of the extrusive section down to the lowermost lavas in the Basal Group. In the region east of Solea the sampling was less systematic; however this region was previously under-sampled and coverage is now improved overall.

To prepare samples for analysis each rock was cut, milled and dissolved, under clean conditions to avoid contamination. Major element oxides were analysed using inductively coupled plasma spectrometry (ICP-OES). The much less abundant trace elements were analysed using inductively coupled plasma mass spectrometry (ICP-MS). A detailed description of the lab procedure is found in the appendix. Data are normalised to chondrite values using the C1-average values of Anders & Grevesse (1989). All the analyses in the database have a UTM grid location, and estimate of stratigraphic depth (see section 3.1) so each analysis can be fitted into the structural framework, exactly as done for the field data. This is key in the approach to interpret both geochemical and field data together by using 2D across-axis profiles of the ophiolite (figure 3.3).

5.1.2 Previous work

The Troodos massif was first recognised as a piece of oceanic lithosphere by Gass (1968). Since then the lava geochemistry has played a role in redefining the tectonic setting. Miyashiro (1973) and Pearce (1975) suggested an extensional environment

near a subduction zone because the lavas were not like MORBs found at typical MOR. As discussed in chapter 2, Miyashiro noted that the Troodos lavas had a broad range of silica, typically 50-65 wt.% but with some up to 70 wt.%, in marked contrast to the lower and narrower range for MORB tholeiites of 45-55 wt.%. Differences in the Troodos lavas with MORB include the occurrence of highly depleted boninite-like lavas, and higher initial water contents in the Troodos system than at MOR.

The presence of two distinct lava suites, the Upper and Lower Pillow Lavas, has been noted in almost every study, however, the origin of the two suites is a matter of disagreement. The upper unit is nearly always more primitive, often containing olivine or clinopyroxene phenocrysts, whereas the lower lavas are more evolved and generally aphyric. This consistent characteristic of the lavas passing from evolved at the bottom to primitive at the top led Schouten & Kelemen (2002) to suggest the two lava suites are cogenetic and related by fractional crystallisation. Other studies, however, found that the two lava groups cannot be related by fractionation alone, because the compositional variation indicated a difference in source depletion between each suite (e.g., Cameron, 1985; Portnyagin et al., 1997; Coogan et al., 2003).

Previous workers (e.g., Rautenschlein et al., 1985; Bednarz and Schmincke, 1994) subdivided the Troodos lavas on their titanium content; however, it will be demonstrated below that, although an effective discriminant in the more primitive lavas, it does not discriminate between them for the full range of compositions. Here TiO_2 is used in conjunction with other immobile elements to establish a more robust classification. It is important first to establish the geochemical basis for a classification and to then explore the reasons for the compositional variations. The way to test the existing geochemical models is to determine whether variations in the geochemistry of Troodos lavas are due to fractionation (and volcanological) effects (as suggested by Schouten & Kelemen, 2002), whether the observed compositions are controlled by source variations as suggested by Cameron (1985), Rautenschlein et al. (1985) and Taylor (1990) among others.

5.1.3 Water

Water may be coming from the descending slab, releasing water as it dehydrates which enters the mantle source region. Even in the field there is evidence indicating the presence of water: the crystallisation order in the lower crustal plutonic wehrlites show that olivine crystallised first, followed by clinopyroxene, and the last phase is interstitial plagioclase. This contrasts with primitive cumulates found in modern MORB, which are troctolites (olivine-plagioclase-bearing; e.g., Gillis et al., 1993). Experimental studies of basalt crystallisation sequence indicate that clinopyroxene will crystallise before plagioclase if the initial water content is 2.7-3.0% H_2O (figure 5.1 from Feig et al. (2006).

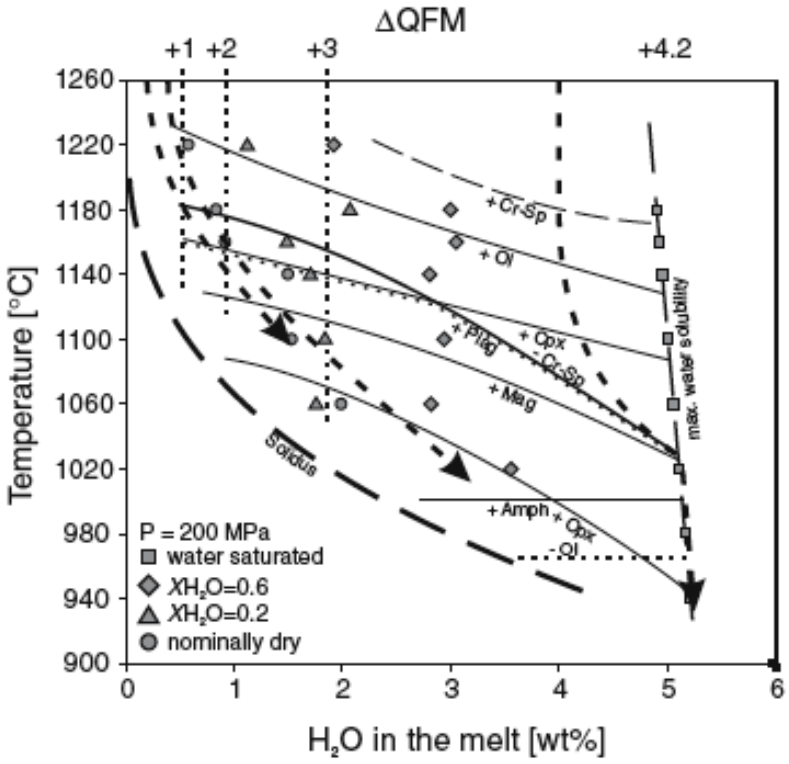

Figure 5.1 From Feig et al. (2006). Arrows show the crystallisation order of mafic minerals in hydrous and anhydrous conditions. Clinopyroxene crystallises before plagioclase if there is water in the system.

Boninite-like lavas are present in the Troodos extrusives sequence, particularly in the Limassol Forest Complex and Arakapas Fault Belt (Cameron, 1985; Murton, 1989; Rogers et al., 1989; Gass et al., 2004) and some from the northern flank of the ophiolite (Taylor & Nesbitt, 1988; this study). These high-MgO, high-SiO_2 rocks have

never been found at modern MOR; instead they are known to occur in intraoceanic forearcs in association with early stages of subduction, or forearc rifting. They require the most refractory of mantle sources to account for the degree of depletion and high degrees of partial melting at shallow levels (e.g., Falloon & Danyushevsky, 2000). The most recent boninitic eruption was recorded in 2009 by (Resing et al., 2011) near the Tonga Ridge in the NE Lau Basin.

A study by Muenow et al. (1990) analysed the volatiles (H_2O, CO_2, S, Cl, F) of fluid inclusions in glasses from the Troodos extrusives, using high temperature mass spectrometry techniques. Of the three unaltered glass samples with fluid inclusions the H_2O ranged from 2.11 to 2.30 wt.%. Water was released at temperatures of 700°-1050°C, implying that it was magmatic, as hydrous alteration typically releases water at lower temperature (starting at 250°C).

5.1.4 Alteration and element mobility

Many of the lava samples in the data compilation are highly altered, as evidenced by LOIs (loss on ignition) >5%. Typical LOI for the lava whole rock sample is between 5-10%, however there are some with significantly higher LOI: >20% in extreme cases. Loss on ignition of fresh glasses averages 3.3%, which probably approximates to the original water content of the lavas. Because the LOI of the altered lavas far exceeds 3.3% the most likely cause for this hydrous alteration is weathering and (particularly) low grade metamorphism due to hydrothermal circulation. To be able to compare like with like the major element oxides of all samples have been recast to volatile-free compositions.

The lavas have undergone various alteration styles and to different degrees, partly depending on where in the stratigraphy they are from. As previously mentioned in chapters 2 and 3, the original Geological Survey Department mapping (e.g., Wilson, 1959; Bear, 1960; Gass & Smewing, 1973) recognised an alteration front through the extrusive sequence, with the topmost lavas showing signs of seafloor weathering at zeolite facies metamorphism (100-220°C), whereas in the lower lavas celadonite is common, and some of the deepest Basal Group lavas have been altered to greenschist facies (350-500°C) .

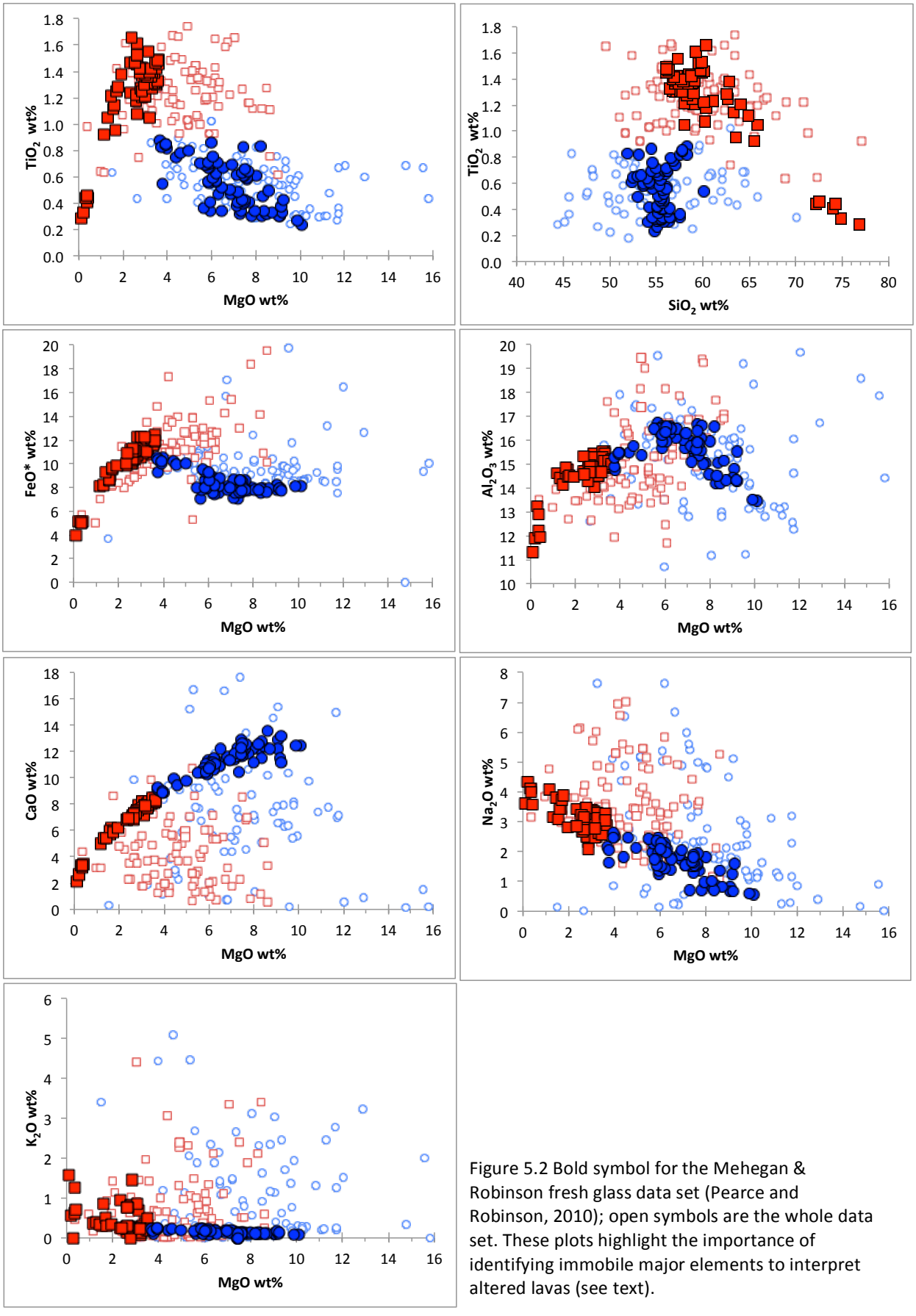

Figure 5.2 Bold symbol for the Mehegan & Robinson fresh glass data set (Pearce and Robinson, 2010); open symbols are the whole data set. These plots highlight the importance of identifying immobile major elements to interpret altered lavas (see text).

The lava database contains some 137 fresh volcanic glass analyses, which make an excellent benchmark to compare both the old and new lava analyses with. These glasses are from the Mehegan and Robinson dataset used in Pearce & Robinson (2010), which have been analysed by electron microprobe for major oxide elements. By plotting major elements of the glasses together with the lavas it is possible to identify which elements have been mobilised during weathering and hydrothermal alteration and which have remained immobile (figure 5.2).

Consistently the non-glassy lavas have lost considerable amounts of CaO through alteration, yet have been significantly enriched in Na_2O, FeO and K_2O. Fortunately there is a robust similarity in TiO_2 of the lavas and glasses, showing TiO_2 to be the most immobile of the major elements. The range in values of MgO are similar for both glasses and lavas when looking at the low-Ti lavas only, with the exception of a handful of lavas with >11 wt.% MgO (these were picritic lava samples, which are not found as glasses). It should be noted that restricted range of MgO of the glasses is largely because glass dataset does not represent the full range of compositions of the lavas, partly due to the presence of phenocrysts in the lavas. As for SiO_2 and Al_2O_3, there is clearly a difference between the glasses and the lavas, but it does not seem to be a systematic increase or decrease.

In the succeeding classification and interpretation of the lavas therefore CaO, Na_2O, or K_2O, or Al_2O_3 are not used, due to their proven mobility, and MgO and SiO_2 are used with care. It is entirely appropriate to use TiO_2 for interpreting the lavas and to classify them, as it has demonstrated to be relatively immobile by Pearce (1975). The mobility of the trace elements and REEs are not as easy to establish because the Mehegan and Robinson dataset were not analysed for trace elements. But from other studies (e.g., Michard, 1989) it is considered that Cr, Y, Zr, Ti, Sm, La, Nd, Yb, Th are all generally immobile during hydrothermal activity or under medium grade metamorphism.

5.2 Classification of lava suites

The fresh glasses of the low-Ti group are plotted in blue on the TAS (total-alkalis vs silica) classification diagram below (figure 5.3), fall mostly in the basaltic andesite field with a few andesites. The high-Ti group glasses are mostly andesites and

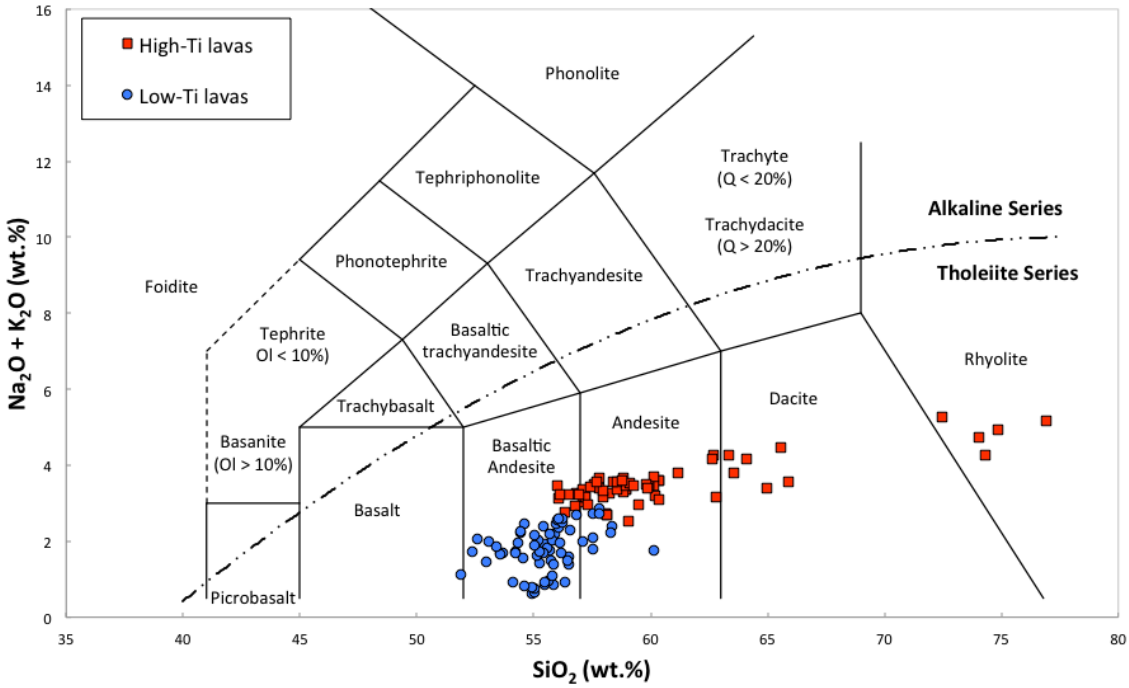

Figure 5.3 Total alkali versus silica (TAS diagram). Only glass data are plotted because they are freshest.

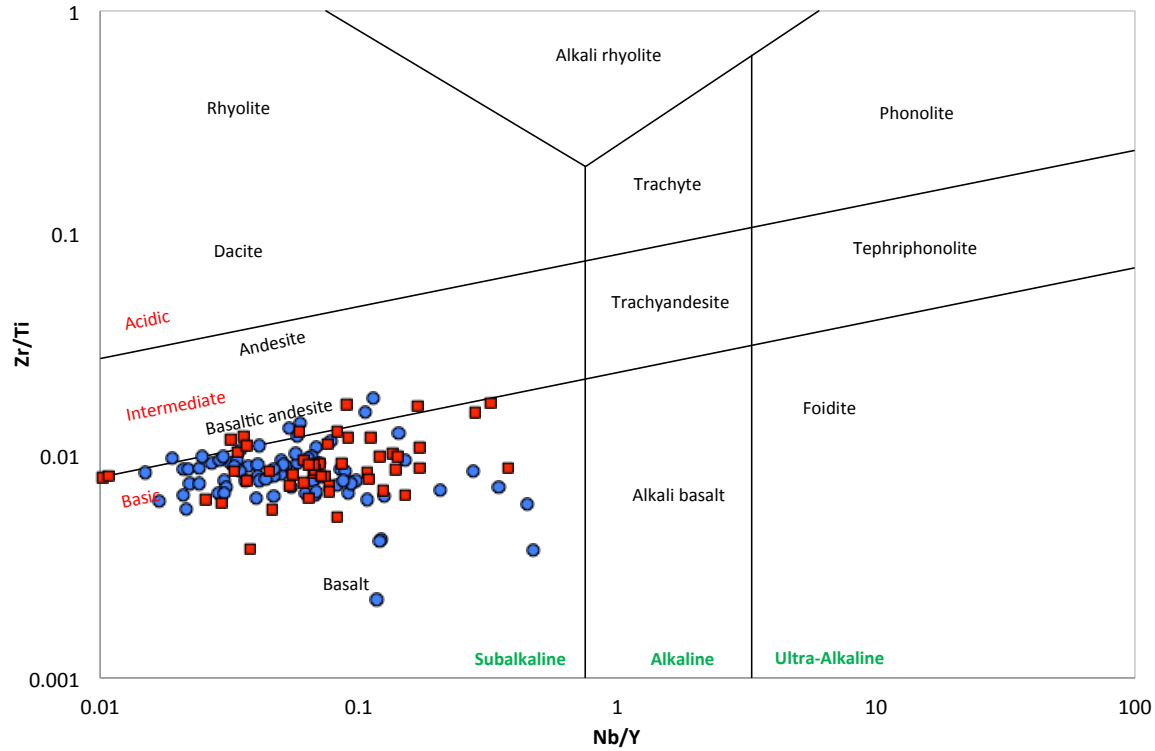

Figure 5.4 From Pearce (2014), after Floyd & Winchester (1975). TAS proxy diagram based on immobile elements. In comparison to the TAS diagram above, this proxy diagram classified the high-Ti lavas (red) and low-Ti lavas (blues) as mostly basalts.

basalitic andesites, with a few dacites and rhyolites. As a general guide the lower high-Ti lavas are more evolved than the upper low-Ti group of more primitive lavas. However, the TAS is dependent on element which have been shown to be mobile (figure 5.2). Therefore the TAS proxy diagram (figure 5.4), is more reliable because it is dependent on ratios of immobile elements. This diagram classifies almost all of the samples as basalts, and a few as basaltic andesites.

Boninites cannot be discriminated on the TAS diagram because the low TiO_2 and high SiO_2 and MgO make them different from typical andesite and basaltic andesite. To discriminate the boninites TiO_2 and SiO_2 contents of the glasses have been regressed to the expected values for 8 wt.% MgO (referred to as Ti8 and Si8, following terminology of Klein & Langmuir, 1987). Regression of TiO_2 (or SiO_2) values to Ti8 (or Si8) is done by applying the gradient of the trend-line through the whole glass data set, any measured TiO_2 value can be calculate the predicted TiO_2 value for 8% MgO. Ti8 vs Si8 plot can identify any boninites which are high MgO and high silica rocks with low TiO_2. Boninites are typical of island arcs at the early stages of subduction, they are defined by Pearce and Robinson (2010) as Si8 >52 wt.% and Ti8 <0.5 wt.% (figure 5.5). Several authors have documented the presence of boninites in the Arakapas transform zone (e.g., McCulloch & Cameron, 1983; Cameron, 1985; Rogers et al., 1989; Gass et al., 1994).

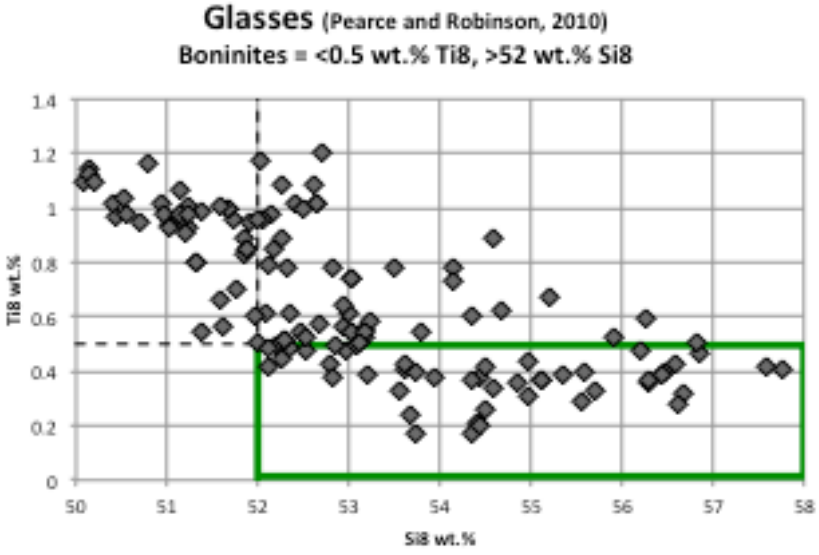

Figure 5.5 Ti8 versus Si8 of the Troodos glasses to identify the boninites using definition of Pearce & Robinson (2010). Ti8=TiO_2@ MgO 8 wt.%, Si8=SiO_2@MgO 8 wt.%. Lavas which fall within the green field are classified as boninites in accordance with the criteria of Pearce & Robinson (2010).

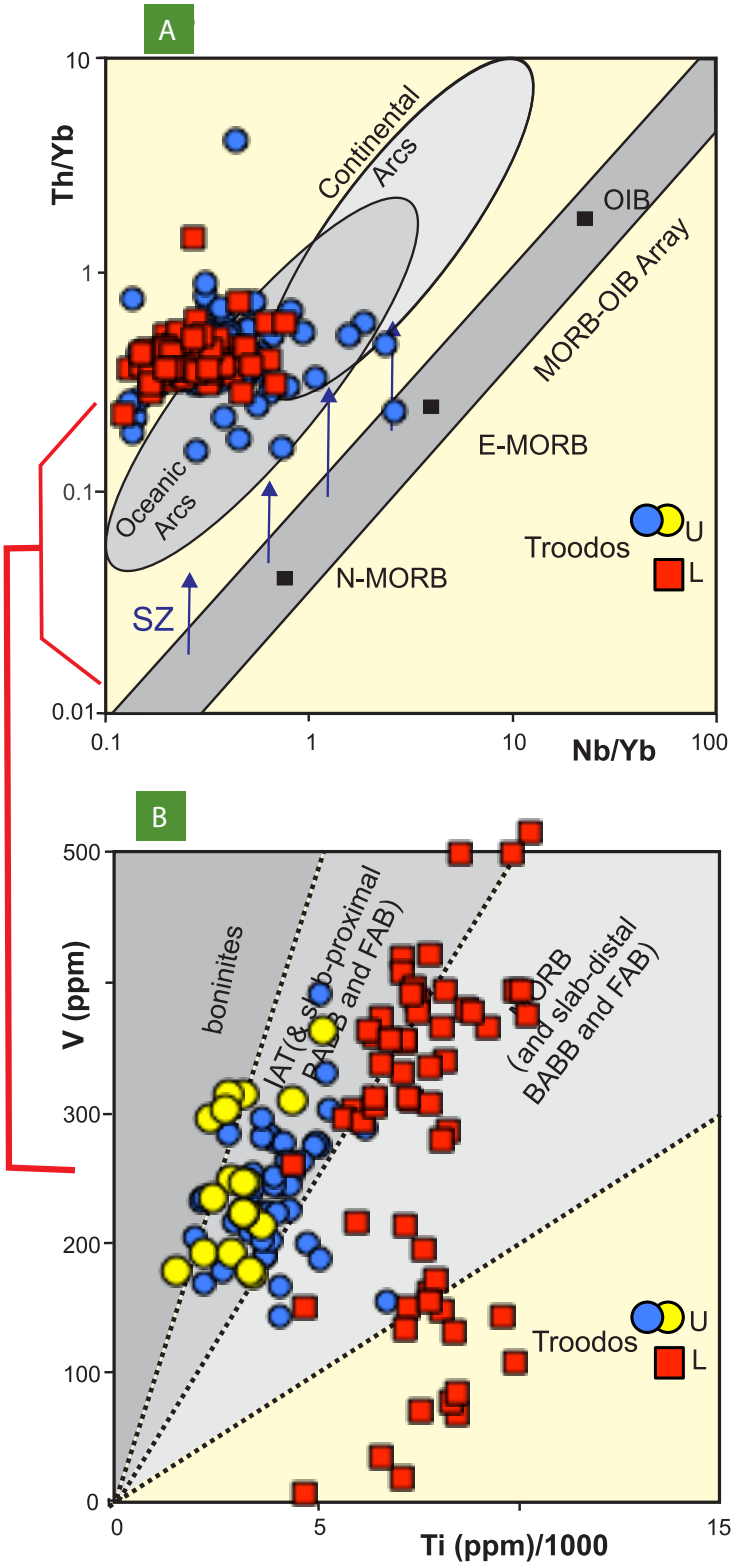

Figure 5.6 Discrimination diagrams for fingerprinting tectonic setting of lavas, adapted from Pearce (2014) with data from this study. (A) Th/Nb proxy identifies the subduction zone (SZ) signature for all Troodos lavas; (B) Ti-V subduction-melting proxy to distinguish Arc tholeiite, MORB & BAB, OIB & basalts (fields from Shervais, 1982).

To distinguish the tectonic settings Shervais (1982) developed the Ti-V diagram (figure 5.6B) which is a proxy for SSZ melting and is capable of discriminating volcanic-arc tholeiites, MORB and alkali basalts. Because Ti is incompatible it will become more depleted with increasing degrees of partial melting which is a consequence of water release during subduction. The degree of melting will approximately double to 20% with the addition of 0.2 wt.% H_2O to a mantle, and the Ti content of the melt will be reduced by about half (Kelly et al., 2006). Variability of V is a function of the oxygen activity within the magma because V has three oxidative states with differing incompatibilities, the ratio of the more incompatible states increases with oxygen fugacity. Greater oxygen fugacity at subduction zones leads to higher V in the SSZ melts (Pearce, 2014). The ratio of Ti/V is influenced either by depletion of Ti and/or by enrichment of V, but V enrichment is a subduction-specific process.

Three lava series can be distinguished using the Ti/V diagram. High-Ti lavas are dominantly in the MORB and BAB field. Low-Ti lavas mostly lie within the arc tholeiite field. And the LREE-enriched low-Ti lavas have the lowest Ti/V ratio making this group fall between the boninite and island arc tholeiite fields.

However, after oxide saturation is reached in the magma the Ti/V ratio dramatically increases. On this diagram the low-Ti lavas lie in the arc tholeiite field, and the high-Ti lavas are dominantly in the MORB and BAB field. A small number of high-Ti lavas fall within the OIB or alkali basalt field, but this is most likely a relic of oxides fractionating in the melt and increasing the ratio

In chapter 3 it was demonstrated that a systematic geochemical sub-division exists within the Troodos extrusive section, see section 3.3 for detailed geochemical stratigraphy across the north flank of the ophiolite. The justification of the subdivision of the lavas into high-TiO_2 and low-TiO_2 is largely based on step-wise changes in TiO_2 content and also Y ppm, Zr ppm, and Zr ppm content (section 3.4). In this section the nature of the chemical variation between the high-TiO_2 and low-TiO_2, will be compared between the sections.

Subdivision of the lava groups is in the first instance based upon TiO_2 wt.%, with the majority of the analyses being split into either a high-Ti group of >0.90 wt.% or a low-Ti group of <0.90 wt.%, with virtually no overlap between the two clusters of

lava on the TiO_2 vs MgO plot (figure 5.2). Only a small portion of the dataset cannot be subdivided on this basis alone; in these instances other available analyses must be used in conjunction (see below). Another small subset of the lavas and glasses cannot be divided purely on the TiO_2 content: these are the samples with <0.70 wt.% TiO_2 and very low MgO (<1 wt.%). Since MgO is compatible with olivine it will decrease in the melt during fractionation, and the TiO_2 increase in the melt because it is incompatible until the point of oxide saturation.

Although the Ti-based classification of the lava subdivisions above is relatively robust for the more primitive compositions, it becomes problematical for the more evolved liquids. The liquid line of descent for Troodos-type liquids (figure 5.7) is relatively linear between ~12 and 5 wt.% MgO because the trend is controlled by fractionation of olivine. Within this range of compositions the two lava groups are clearly distinct, following parallel vectors with different TiO_2 contents for a given degree of fractionation. The curve becomes more inclined between ~5-3.5 wt.% MgO because the fractionation of clinopyroxene and plagioclase are contributing to the composition. If fractionation continues still further the TiO_2 content will rapidly drop below ~3.5 wt.% MgO due to the partitioning of TiO_2 into oxides such as ilmenite or magnetite after the melt reaches oxide saturation. In fact, below 5 wt.% MgO when the fractionation is no longer purely controlled by olivine, the TiO_2 –MgO diagram is not as effective at discriminating between lava groups.

5.2.1 MELTS modelling

MELTs modelling of TiO_2-MgO covariation for the Troodos lavas (figure 5.7) shows the liquid lines of descent to be very dependent on the model input parameters, such as water content, oxidation state, and starting composition. This shows that modelling of major element variations alone will be insufficient to assess whether the two lava suites are related by fractionation or are of distinct parent magmas. Trace element variations are likely to be much more sensitive. These are explored in section 5.3 below.

Some of the lava and glasses have been modelled to calculate the geochemistry of the melts using the geochemical modelling algorithm MELTS

(Ghiorso & Sack, 1995). For each section through the extrusive sequence two glass or lava whole rock analysis was selected for MELTS modelling (one from the low-Ti group, one from the high-Ti group). The most primitive samples with LOI <10% were chosen, and only samples with the full set or major element analyses. Modelling was calculated at 2.18 wt.% H_2O (best estimate based on data from Muenow et al., 1990), pressure at 1000 bars, and the fO_2 constraint was assumed QFM for all.

A significant number of fractionation curves can be generated in MELTS by varying parameters such as the fO_2, H_2O content, and starting composition (including initial TiO_2 content), for which reason the resulting curves cannot be relied upon to define uniquely a specific liquid line of descent to explain the natural variation in Troodos lava geochemistry. The effect of adding just 1 wt.% H_2O lowers the level of enrichment of TiO_2 during fractionation because increasing water progressively suppresses crystallisation of plagioclase, resulting in a lower gradient in the curve between ~3-6 wt.% MgO (MacLeod et al., 2013).

In the example (figure 5.7) below TiO_2-MgO data for the section EE-Mitsero is plotted in bold symbols and the fractionation curve was calculated from a low-Ti glass sample from the section. The curve fits the low-Ti lavas from this area well for MgO >6 %, suggesting that within the (stratigraphically defined) group the low-Ti lavas may be related to each other by fractional crystallisation. However, this particular liquid line of descent does not uniquely fit the low-Ti group because with the onset of clinopyroxene crystallisation at ~6 wt.% MgO the modelled TiO_2 increases sharply, with values equal to some of what are thought to be high-Ti lavas.

The modelled fractionation trends of the L-REE enriched low-Ti lavas (yellow dots) are the same as the low-Ti lavas, as can be seen in the examples from East Stavros and West Mitsero (west) in figure 5.7.

Since the majority of lavas and glasses have intermediate MgO contents between 3-6 wt.% the TiO_2-MgO plot alone is not enough to distinguish the lava groups, and trace elements are needed to help classify the lavas. The MELTS algorithm can only calculate liquid composition from major oxide elements so there are no modelled trace element curves.

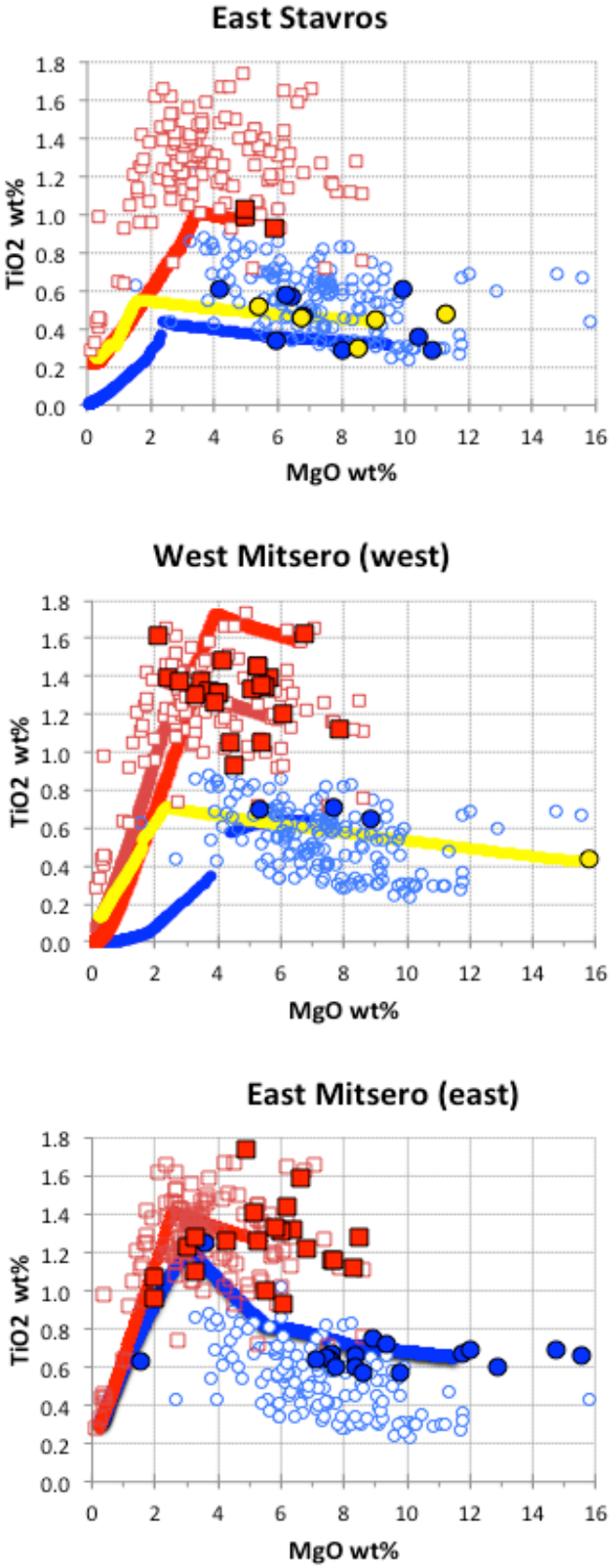

Figure 5.7 TiO_2-MgO in bold symbols (red = high-Ti, blue = low-Ti); all lava and glass samples plotted with open symbols; blue line is MELTS fractionation curve for low-Ti glass sample 343 from Rautenschlein et al. (1985).

As shown in chapter 3, the low-Ti groups are usually found in the upper part of the extrusive section; often coinciding with the upper pillow lavas, which are commonly olivine phyric. In the lower parts of the extrusive section the high-Ti lavas occur within the lower pillow lavas and Basal Group units, which are almost exclusively aphyric. It should be noted that in the overwhelming majority of instances the geochemistry of the Basal Group lavas are identical to the lower pillow lavas – the only difference being the proportion of dykes present – hence both are classed here as a single group (the high-Ti series).

5.3 Fractionation differences between the groups

Investigation of the lava and glass geochemistry has revealed a number of lines of evidence which indicate there are differences in fractionation between the two main lava groups. Major element plots of the glasses show that the low-Ti glasses are lower in SiO_2 and richer in MgO than the high-Ti glasses, which means the low-Ti glasses are less evolved. Immobile trace elements for the lavas can be sensitive to fractionation, such as Cr or Zr. The more evolved high-Ti lavas always have higher Zr (>41 ppm), and low-Ti lavas are mostly <41 ppm. Abundance of Cr also separates the two groups efficiently, majority of high-Ti lavas have Cr <40 ppm and low-Ti are mostly >40 ppm, although there is a small degree of overlap.

5.3.1 Cr-Y

The Cr-Y plot (figure 5.8) is useful to establish whether liquids that have experienced some amount of fractionation are related or unrelated because Cr ppm (y-axis) is sensitive to fractionation whereas Y ppm (x-axis) is a proxy for partial melting or depletion of the source as well as fractionation. Chromium is highly sensitive to fractionation because it is compatible with the minerals olivine, orthopyroxene, clinopyroxene and the spinels. In the Cr-Y plot there is a very wide range of Cr values from <1 to >1000 ppm, with greater Cr contents representing primitive melts and lower Cr values more fractionated and evolved melts. Because Y is incompatible in

the Troodos mantle source region (garnet is not thought to have been present; e.g., Rogers et al., 1989) it will be higher in melts that have been produced from smaller degrees of partial melting, and lower for melts derived from greater degrees of partial melting (figure 5.8). If the two lava groups were genetically related they would plot as one single cluster on a Cr-Y plot with a sub-vertical liquid line of descent. But the Y variation might instead be reflecting original variation of Y in the source, and therefore it might be an indicator of depletion in the mantle source as well or instead of being a partial melting proxy. The behaviour and partition coefficients of Ti and Y are very similar and both can be used as a proxy for the degree of partial melting.

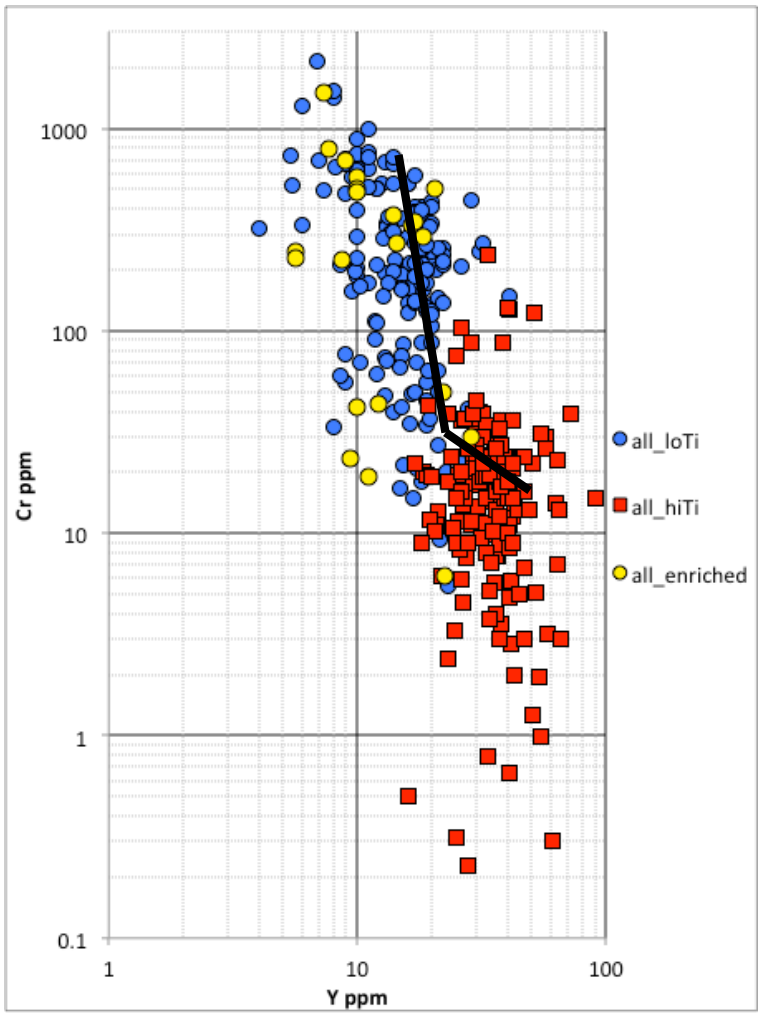

Figure 5.8 Cr-Y bivariate plot. Black line is steeply inclined vector (vector from Alabaster et al. (1982) for fractional crystallisation is the liquid line of descent. Y is controlled by source processes such as partial melting and/or depletion. Increasing degrees of partial melting would shift the vector left, as does increasing depletion of the source. The two lava suites plot as two distinct fields, the high-Ti lavas have more Y than the low-Ti lavas, yet very few samples have intermediate Y concentration.

In this case the high- and low-Ti lava groups plots as two discrete clusters, which do not lie on one single liquid line of decent, therefore they must have been derived from different parent magmas. The Cr-Y plot was reproduced for each domain across the northern flank of the ophiolite and even at a local scale most sections showed the upper low-Ti unit is unrelated to the lower high-Ti unit by fractionation. Since the low-Ti lavas have lower Y this could either suggest they derived from greater degrees of partial melting, or that they are from a more depleted mantle source, or both. The high-Ti lavas might be from a less depleted source, or from smaller degrees of partial melting, or a combination of the two.

To be more rigorous about assessing the fractionation effects, the liquid line of decent should be plotted for the Cr-Y plots by deriving an accurate fractionation vector. Liquid lines of descent can be calculated from mineral proportions, partition coefficients of the mineral phases, and the geochemistry of the melt (which can be determined by geochemical modelling); however, little experimental or theoretical data exist to constrain the relative phase relations in a system such as that of the Troodos suite.

Where the compositional variation in a section of lavas cannot be explained by the effects of fractional crystallisation of a single parent magma, the origin of the variation must be from differences in mantle source or melting conditions. In the section below the details of the source differences and reasons behind the compositional variations will be explored.

5.4 Source variation

The next aspect is to establish whether or not the parent melt for the primitive low-Ti lavas is related to the evolved high-Ti lavas by fractionation paths - i.e. if they are cogenetic suites. This can be achieved by using elements which are sensitive to subtle variations in the source, most commonly chondrite-normalised REE diagrams are plotted to assess general patterns in trace elements and identify obvious source variations.

5.4.1 REE patterns

Chondrite-normalised multi-elements REE plots are a useful tool for quickly and visually displaying the geochemical characteristics of rocks since different source processes produce distinctively shaped REE patterns. As per convention the rare earth elements have been arranged in order of increasing compatibility from left to right (figure 5.9). The patterns of most of the lavas in both groups is quite similar to MORB, highly incompatible LREE La through to Sm are slightly depleted compared to chondrite, while middle to heavy REE Sm through to Lu show sub-horizontal profiles indicating no significant depletion. Overall the profiles of most of all of the high-Ti lavas and most of the low-Ti lavas are similar, and the REE patterns broadly resemble MORB (Rollinson, 1993).

However a minority of lavas that do not this MORB-like REE pattern, but must have experienced a different or additional history of depletion/enrichment events. One group shows an enrichment of LREE from La to Nd, on the profiles an upward kick is visible at the far left (figure 5.9), though coupled with a strong depletion of Sm to Lu (the middle to heavy REE), to give a broadly U-shaped REE profile as shown by the downward sloping profile on the right and centre of the diagrams. Another group shows strongly and continuously decreasing concentrations from Yb to La. Both, therefore, must be derived from highly depleted mantle sources (to give the low middle with respect to heavy REE), though those with the U-shaped profiles require some separate process to increase the LREE.

All of the depleted samples, whether showing this LREE enrichment or not, are exclusively from the low-Ti lava unit, and are nearly always from the topmost lavas (figure 5.10). The LREE enriched samples are very similar to lavas found elsewhere have been classified as boninites (Cameron, 1985; Rogers et al., 1989; Pearce and Robinson, 2010). Although all except one of the boninites are enriched in LREE, not all the LREE enriched samples are boninites.

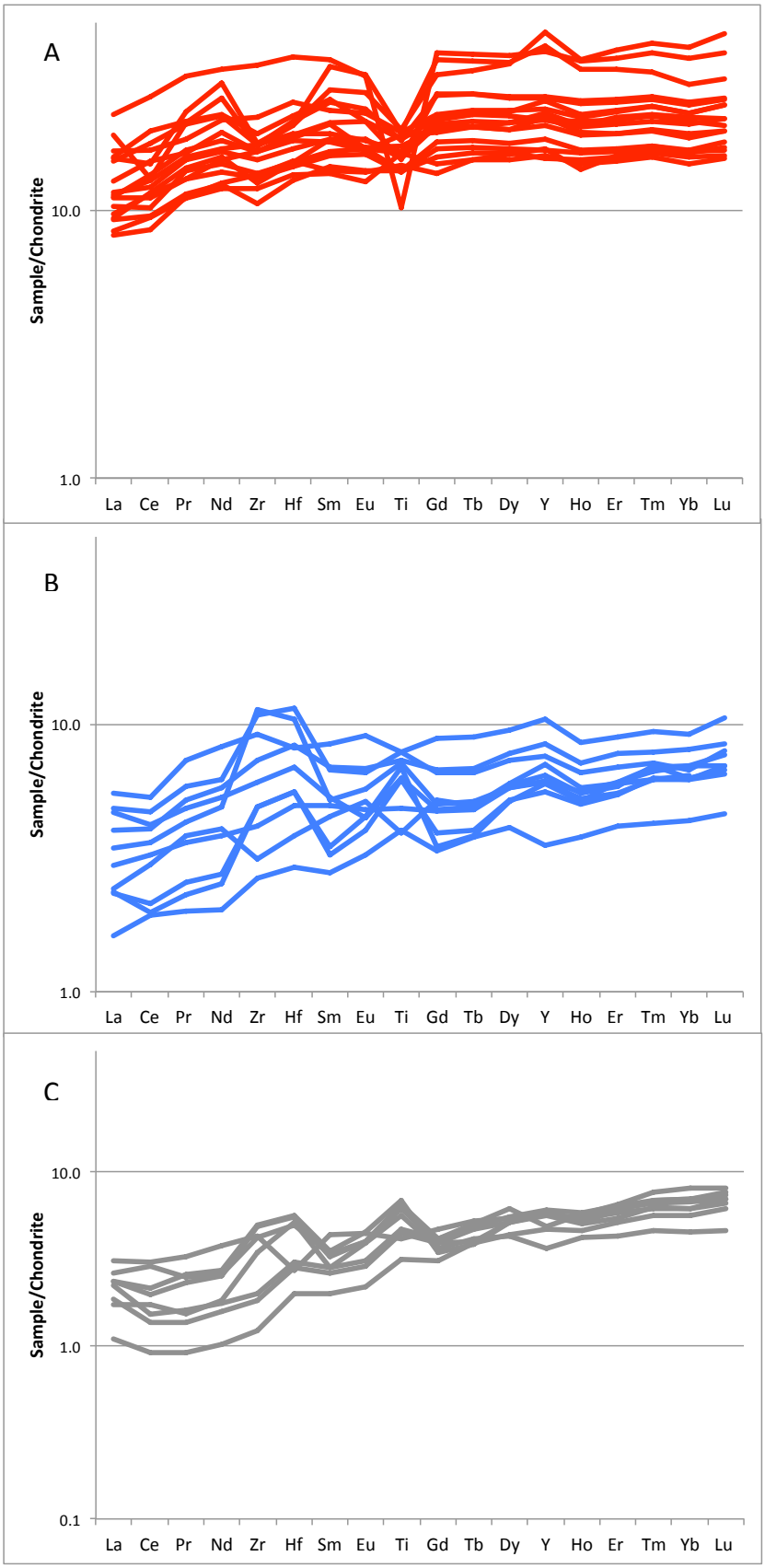

Figure 5.9 Chondrite normalised REE plot. Element are arranged in order of increasing compatibility from left to right. (A) high-Ti lavas; (B) low-Ti lavas; (C) L-REE enriched low-Ti lavas.

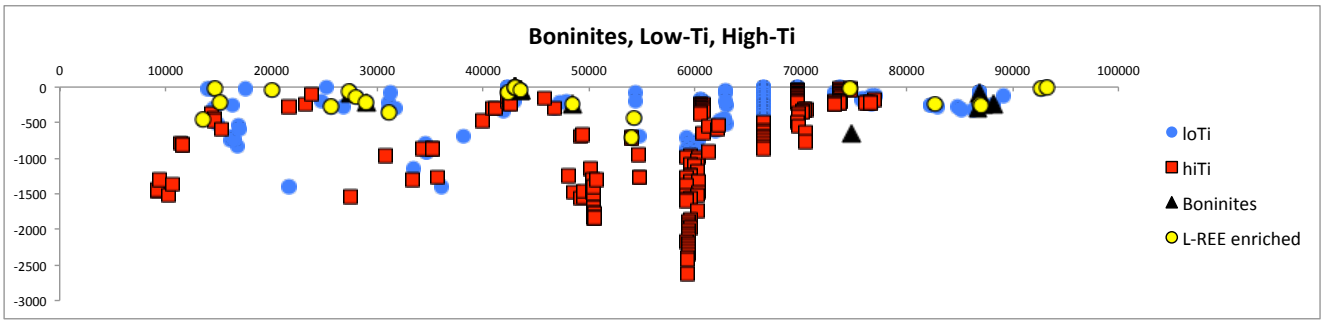

Figure 5.10 2D profile yellow=LREE enriched samples; black=boninites; blue=low-Ti, red=high-Ti.

5.4.2 Trace element ratios

A better understanding of the REE profiles can be gained from looking at the ratio of two elements from the REE diagrams as this gives more information about the slope of the line along key parts of the profile, allowing a quantitative comparison of REE patterns and assessment of the entire dataset in one step. Ratio-ratio plots are used to target specific portions of the REE patterns by selecting element ratios where the gradient of the pattern differs, and are very much more sensitive to subtle variations between samples.

To compare the middle to heavy REE the ratio $Sm/Yb_{(N)}$ is used (i.e. normalised to chondrite (Anders and Grevesse, 1989) (figure 5.11), and to compare the light REE the ratio $La/Sm_{(N)}$ is used; by plotting the two ratios against each other the subtle differences in REE shapes become clearer ($La/Sm_{(N)}$ ratio of 1=flat REE pattern, >1=enriched, <1=depleted).

The majority of the lavas, both high- and low-Ti, fall within a tight cluster representing a REE pattern depleted in LREE but flat through the M-HREE. In terms of the REE, therefore, the two lava groups are virtually indistinguishable. However, outside of the main cluster the two groups of highly depleted (low $Sm/Yb_{(N)}$) samples are readily apparent (fig. 5.11). These lavas are distinctly more depleted than the rest of the low-Ti lavas and the high-Ti lavas, probably due either to greater degrees of partial melting of the source, or to melting of an already more depleted source. The correspondingly low $La/Nd_{(N)}$ in the second sub-group supports this interpretation. This cannot however be the case for the LREE enriched lavas from the low-Ti group (yellow in figs. 5.11), which are depleted in M-HREE (low $Sm/Yb_{(N)}$) yet have elevated ratios of $La/Sm_{(N)}$. This decoupling of light vs middle-heavy REE requires

these lavas to have incorporated an additional component enriched in LREE. Investigation of the nature of this component is beyond the scope of this thesis, but could potentially be something like melted sediment (e.g., Rogers et al., 1989; Plank, 1995).

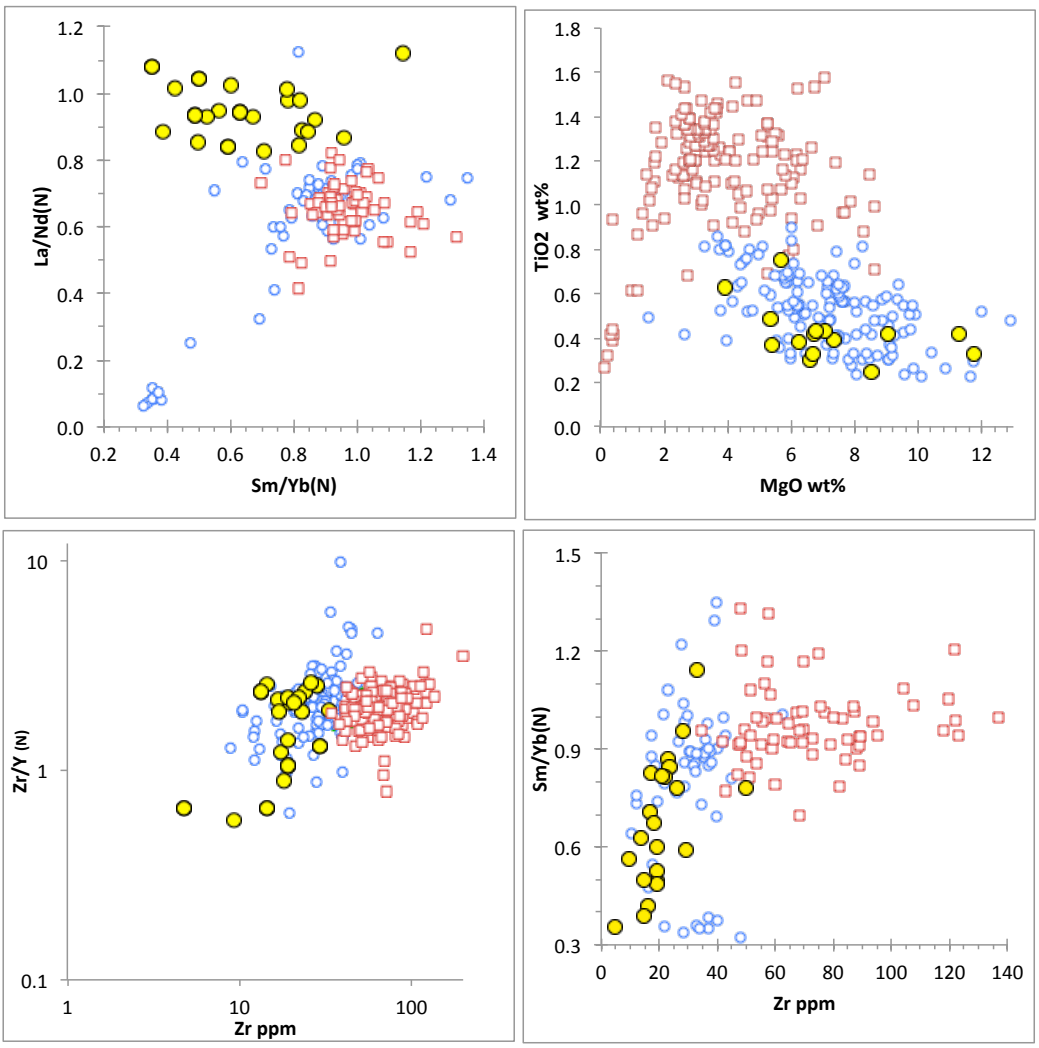

Figure 5.11 Yellow = LREE enriched depleted low-Ti lavas, blue = all low-Ti lavas, red = all high-Ti lavas. The normalised La/Nd versus Sm/Yb plots identifies the most depleted samples (low Sm/Yb) are also enriched in LREE (high La/Nd).

5.4.3 Ratio-depth plots - Ti/Zr, Zr/Y, Sm/Yb, La/Nd, Ti/V

Other commonly used elements for general source depletion signatures are TiO_2, Y, and ratios such as Zr/Y, Sm/Yb, La/Nd, Ti/V, because ratios vary as a function of source processes without being affected by fractionation. Stratigraphic plots of TiO_2 and Y shows an obvious kick at the same depth in all sections, as seen in figures 3.5 to 3.12; however, there are very few sections showing a similarly systematic and obvious

step-change in Ti/Zr, Zr/Y, $La/Nd_{(N)}$, or $Sm/Yb_{(N)}$ down section from low-To lavas to high-Ti. This suggests there is no significant source control on the lava composition, apparently in contrast to the deduction made from Cr-Y co-variation (section 5.3).

In the following sections trace element ratios are plotted on stratigraphic plots for each of the structural domains from northern Troodos, with the aim of identifying whether upper and lower lavas are cogenetic or not.

5.4.3.1 West Stavros domain (figure 5.12)

No noticeable difference exists at the boundary between the high-Ti and low-Ti lava groups for the Ti/Zr, Zr/Y or Sm/Yb ratios. The very topmost lavas, however, have highly variable $Sm/Yb_{(N)}$ ratio, because some of the low-Ti group are boninitic lavas with more marked depletion within the middle to heavy REE. The high-Ti lavas have a very narrow range of $La/Nd_{(N)}$ (0.6-0.7), yet the low-Ti lavas have a more varied ratio of $La/Nd_{(N)}$ and generally higher (0.6-1.0). Only in the Ti/V ratio is the difference between the two lava groups more noticeable, with a step-wise decrease in Ti/V up section at the boundary of the groups.

The West Stavros lava stratigraphy shows a very subtle change from less depleted source for the high-Ti lavas to a slightly more depleted, source or at least more variably depleted source, for the low-Ti lavas. The change in degree of depletion suggested that there is a source control on the geochemistry of the lavas here.

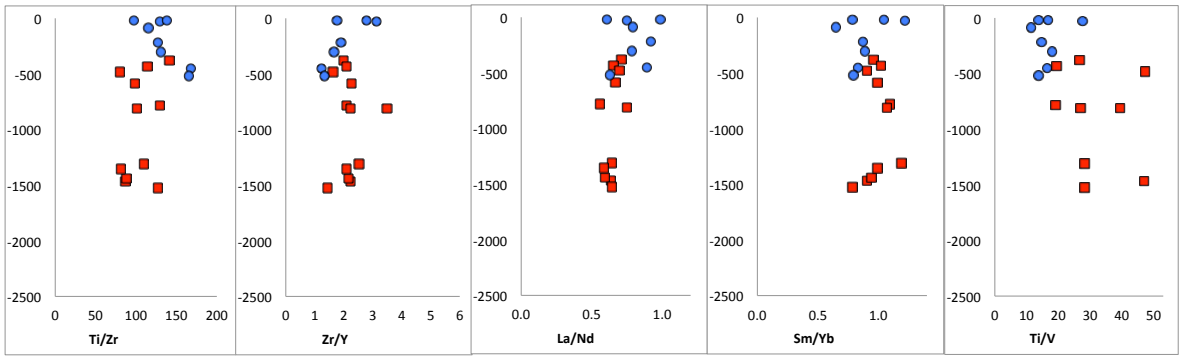

Figure 5.12. West Stavros trace element ratio plots. For the ratios Ti/Zr, Zr.Y, $La/Nd_{(N)}$ and $Sm/Yb_{(N)}$ there is little significant difference between high-Ti and low-Ti lavas. But the Ti/V ratio is lower for the low-Ti lavas- this could be a result of increased oxygen fugacity in the melt (possibly due to increased water content). The apparent interbedding of the high-Ti and low-Ti lavas here is not real but is an artefact of the inclined boundary between the lava groups because it is conformable with the dip of the lava flows (see figure 3.14).

5.4.3.2 West Solea (figure 5.13)

Only Ti/V ratio shows a difference between the lava groups; again the low-Ti lavas have lower Ti/V ratio and the high-Ti lavas have higher Ti/V ratio. The other ratios do not show any change with depth or for the different groups. West Solea is one of only two sections were the low-Ti are not above the high-Ti, instead they are interbedded and the stratigraphic relationship between the two lava groups is unclear.

Because the Ti/V ratio is lower for the low-Ti lavas this is evidence for the source conditions having a higher oxygen fugacity, probably because magma was more hydrous than the source for the high-Ti lavas; however, the mantle source difference must be a slight one because the other four ratios show little difference between units.

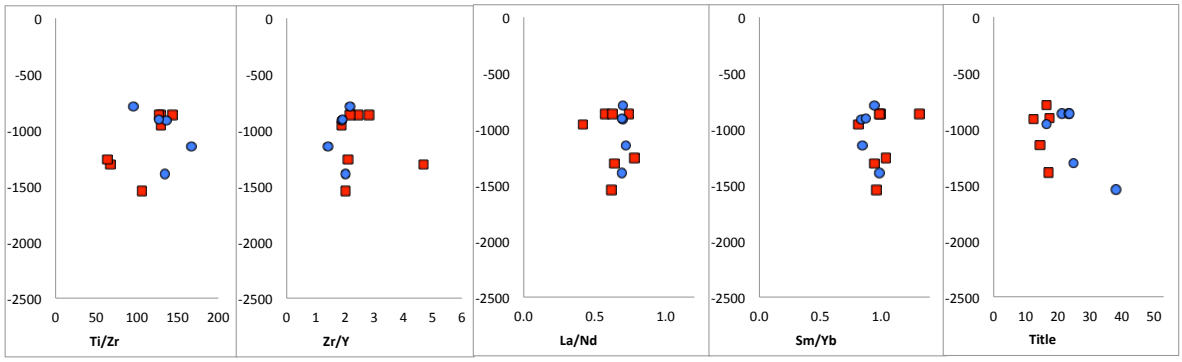

Figure 5.13 West Solea trace element plots. No difference in ratio for high-Ti and low-Ti lavas, except for the Ti/V ratio which is higher for the high-Ti lavas.

5.4.3.3 East Solea (figure 5.14)

Source depletion is more obvious at the East Solea section, with nearly all five ratios showing a step-change across the boundary of high-Ti and low-Ti lavas, always from less depleted at depth to greater depletion for the low-Ti lavas. Here, only the Zr/Y ratio does not exhibit an upward increase in source depletion, there is clearly a source control on the geochemical difference between the lava groups.

Variation in the degree of source depletion (from less to more) is likely the dominant control in composition difference between the high-Ti and low-Ti lavas for the East Solea section, because most of the ratios show a step-wise change at the boundary.

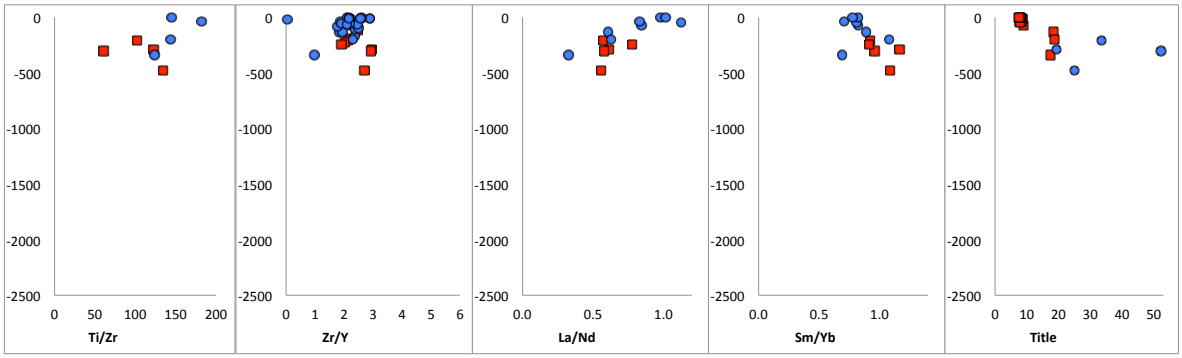

Figure 5.14 East Solea trace element ratio plots. Except for Zr/Y, all the ratios show step-wise change in ratios at the boundary between high-Ti and low-Ti lavas. The low-Ti lavas have a signature for stronger depletion of the source.

5.4.3.4 West Mitsero (west) (figure 5.15)

All five ratios for the West Mitsero (west) section show little systematic change from the high-Ti lavas to the low-Ti, with the exception of one low-Ti sample which shows the 'U-shaped' low $Sm/Yb_{(N)}$ and high $La/Nd_{(N)}$ signature, depleted (low) Zr/Y and low Ti/V. This section shows no evidence of any source variations between the lava groups, unlike the East Solea section just a few kilometres west (5.4.3.3). Therefore, apart from the one anomalous sample at the top of the section, the composition variations of the two lava suites at this section must be a result of only magma chamber processes (i.e., fractional crystallisation), so the lavas here could be cogenetic.

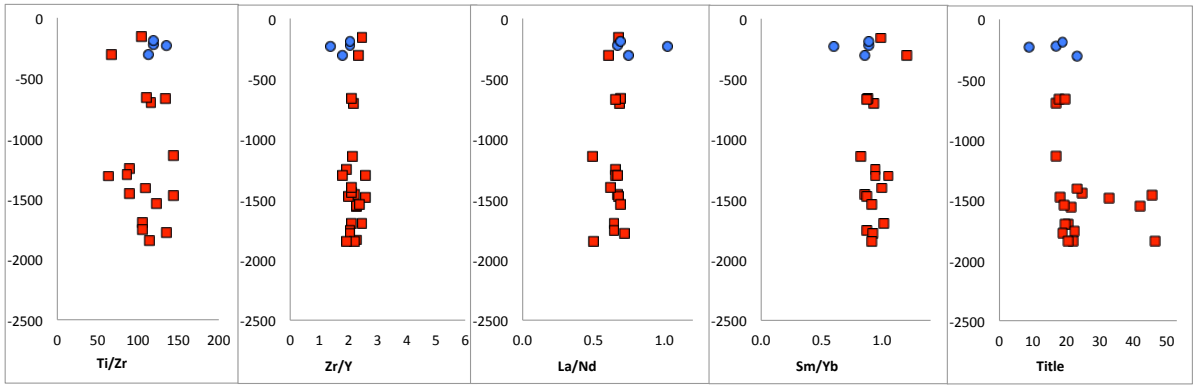

Figure 5.15 West Mitsero (west) ratio-depth plots. Apparent interbedding of high-Ti and low-Ti lavas because the top of the section crosses a large normal fault (see figures 3.1 & 3.18), the two shallow high-Ti lavas are on the footwall (on top of the horst block) and the four low-Ti lavas are <1km to the east in the down-thrown hanging wall.

5.4.3.5 West Mitsero (figure 5.16)

At the West Mitsero section the high-Ti lavas show a very narrow range for Ti/Zr, Zr/Y, $La/Nd_{(N)}$ and $Sm/Yb_{(N)}$. In contrast, the West Mitsero low-Ti lavas are more variable, and are neither consistently more or less depleted than the high-Ti lavas. This section, as with the WW-Mitsero section (5.4.3.4), has overlapping ranges for each of the ratios suggesting there is probably no source variation between the two groups and the section is probably cogenetic.

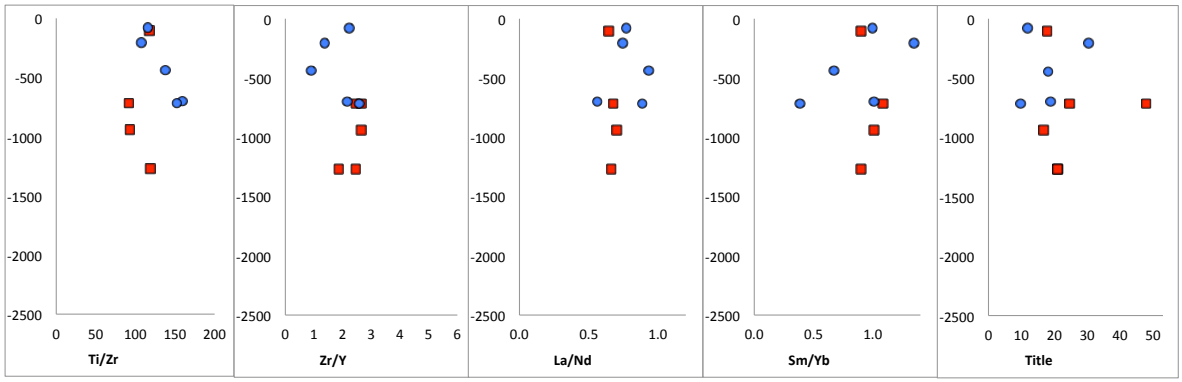

Figure 5.16 West Mitsero ratio-depth plots. This section is probably cogenetic because there are no real differences in the ratios for either lava group. The variation in composition between the high-Ti and low-Ti is probably due to fractional crystallisation.

5.4.3.6 East Mitsero (figure 5.17)

Unfortunately, there is not a complete set of element analyses for all of these samples. From the Zr/Y and Ti/V plots, where there are data for the low-Ti lavas, there appears to be little systematic change in ratio from the high-Ti to the low-Ti lavas, although the low Ti/V ratios (~10) in two of the low-Ti lavas are more similar to the depleted low Ti/V upper lavas in adjacent sections. As for the $La/Nd_{(N)}$ and $Sm/Yb_{(N)}$ ratios the high-Ti lavas from east Mitsero are consistent with high-Ti lavas from other sections. The available data from this section are insufficient to draw a firm conclusion, but could potentially be cogenetic rather than resulting from two different sources.

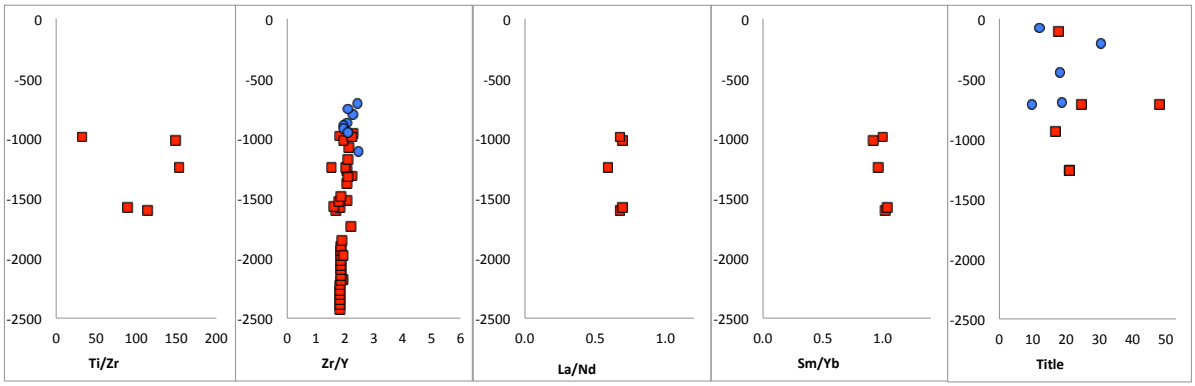

Figure 5.17 East Mitsero ratio-depth plots. Unfortunately there is not a full set of analyses for all the elements of the samples. Zr/Y and Ti/V show no systematic change down section, so the East Mitsero section is potentially cogenetic.

5.4.3.7 East Mitsero (east) (figure 5.18)

There is a lot of data for this section, because it includes the well-studied Akaki section and three boreholes from the drilling project. Because the depth of the boundary between the lava groups is at different depths in different fault blocks the area has been divided into three parts (A Agrokipia, B Arediou, C Politiko) from west to east in figure 5.18.

Part A shows no change in Ti/Zr or Zr/Y ratios for high-Ti and low-Ti lavas, although there are no data for the other ratios for part A. Part B is unusual because the Ti/Zr, Zr/Y and Ti/V show no change down the section, but the $La/Nd_{(N)}$ and $Sm/Yb_{(N)}$ show a significant step-wise decrease at the boundary. These low-Ti lavas are the most highly depleted of all from the Troodos ophiolite, showing both low $Sm/Yb_{(N)}$ and $La/Nd_{(N)}$; unlike the 'U-shaped REE' group, they do not show any LREE enrichment (see section 5.4.2). Part B, therefore, shows some evidence of a source difference for the two lava groups. Part C shows some evidence for the low-Ti lavas being more depleted because the Ti/Zr ratio is slightly lower.

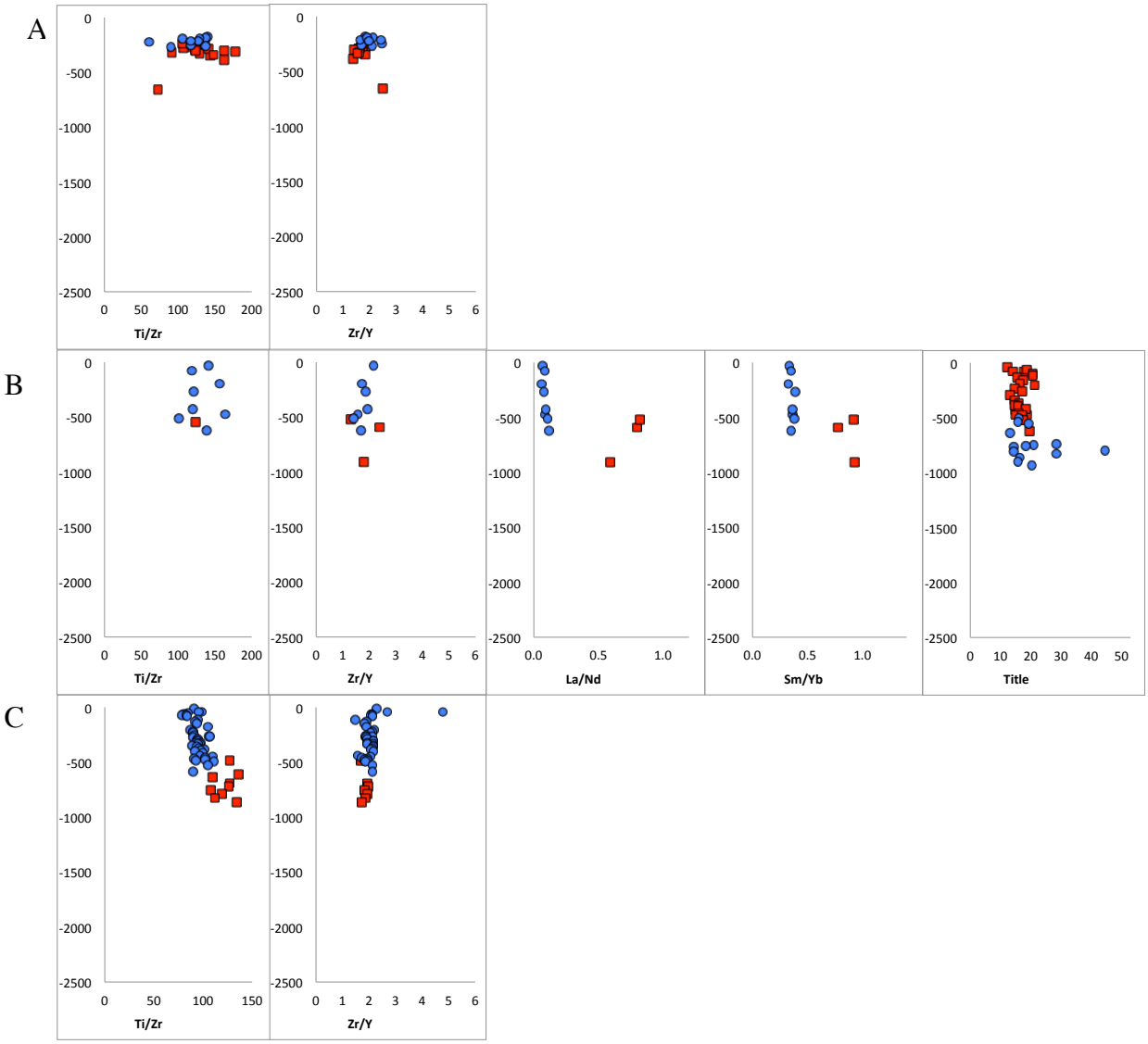

Figure 5.18 East Mitsero (east) is split into parts from west to east: A (Agrokipia), B (Arediou), and C (Politiko).

5.4.4 Kambia domain (Makhaeras domain) (figure 5.19)

In this section there is a slight difference in source signature between the two lava groups. There is a very narrow range of Ti/Zr ratio for the high-Ti, and the low-Ti lavas are more variable and slightly more depleted. A similar pattern is even more pronounced for the Zr/Y ratio- these low-Ti lavas are far more variable than the high-Ti lavas.

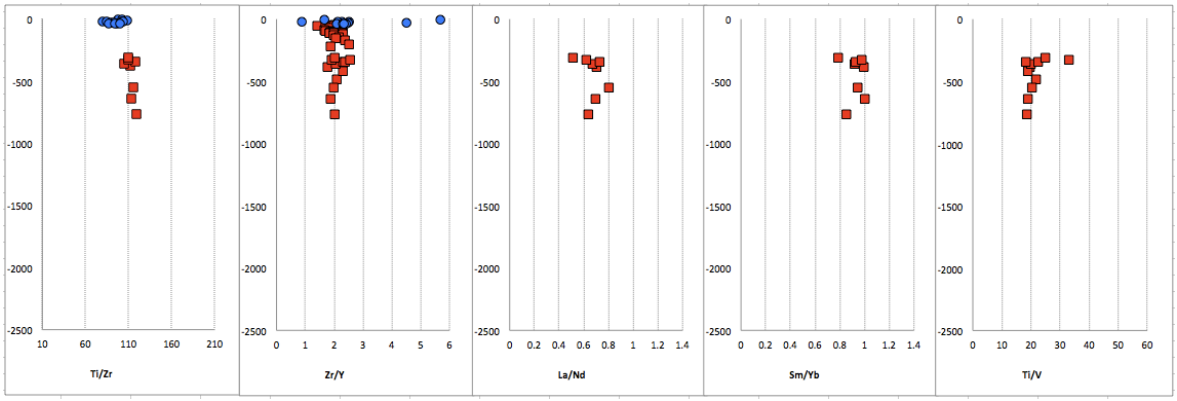

Figure 5.19 Kambia domain (aka Makhareas domain) ratio-depth plots. The low-Ti lavas are very variable, some of the low-Ti samples are more depleted than the high-Ti lavas.

Only in some of the sections is there a horizon of widely variable ratios at the topmost portion of the low-Ti lava group, where this highly variable horizon occurs there is no change in other ratios at the same depth. The highly variable horizons occur at much shallower than the boundary of the high-Ti and low-Ti lava group, correlating with the strongly depleted boninitic-like lavas which are LREE enriched. Unfortunately there are no Ti/V data for the low-Ti group here with which to compare to the lavas below and in adjacent sections.

5.4.5 Initial conclusions

Trace element ratios from the different stratigraphic sections show contrasting evidence for source variations, with no simple relationship. 'Boninitic' lavas with re-enriched, U-shaped REE profiles occur within the uppermost low-Ti lavas in a few sections, most notably in the west, and must represent a limited late-stage extrusive episode. Systematic depletions in mantle source, as represented by the REE and Zr/Y ratios, are observed at the high-Ti to low-Ti step-boundary in some sections but not others. The most systematic change, which is apparent in all sections for which sufficient data are present, is in Ti/V ratio, which generally decreases abruptly across the high-Ti to low-Ti boundary.

Ti/V ratio is sensitive to oxygen fugacity in the system because vanadium has three oxidation states, the effect of adding water increases the oxygen activity of the melting process and increases the proportion of higher oxidation states (Rollinson, 1993). This ratio was used by Shervais (1982) as a proxy to distinguish tectonic

environment. The ratio is extremely sensitive to changes in fO_2, and can detect subtle changes in the source conditions which are not detected using the typical source signature ratios. The implications of this for magma plumbing are discussed in chapter 6.

5.5 Lava Viscosity

Schouten and Kelemen (2002) propose that the difference between the evolved, high-Ti lower lava series and the more primitive, low-Ti upper lavas is simply one of viscosity: more primitive, lower viscosity lavas erupted at the axis are simply able to flow further, thus blanketing older (high-Ti) lavas that have moved off-axis.

Lava viscosity was calculated using the method of Giordano et al. (2008) from the rock compositions of the lavas. The input for the calculations are weight per cent of major elements SiO_2, TiO_2, Al_2O_3, FeO, MnO, MgO, CaO, Na_2O, K_2O, P_2O_5, and the volatiles H_2O and F_2O_{-1}, as normalised to 100%. The water content of the lavas is an area of uncertainty (see earlier in the chapter for further comments), but Muenow et al. (1990) estimate 2.18% H_2O based on fluid inclusions within the lavas. The concentration of $F_2O_{-1,}$ is unknown since it was not analysed in any of the lavas so was assumed to be 0%. Viscosity for each sample was calculated at a range of temperatures from 1400°C to 600°C at intervals of 100°C to account for a range of temperatures that exceed the likely eruptive temperatures and go beyond the lowest flow temperature of the lavas. A selection of analyses were chosen from the main geochemical database; only those with a full set of major elements could be used, of those, a broad selection from the high-Ti, low-Ti, and LREE-enriched units were chosen. In total 250 analyses were selected, including a number of analyses from the CY-1/1a drill cores, volcanic glasses from Pearce and Robinson (2010), and various other analyses.

A previous study on the viscosity of Troodos lavas by Schouten and Kelemen (2002) used analyses reported from the CY-1/1a drill cores. Schouten and Kelemen (2002) calculated viscosities at both 0 wt.% and 5 wt.% H_2O, documenting an order of magnitude increase in the viscosity downhole when calculated at eruption temperature using the Sisson and Grove (1993) method. Schouten and Kelemen (2002) concluded that the lavas were segregated on the flanks by viscosity differences, however the CY-

1/1a data do not show a stepwise decrease in viscosity at the high-Ti/low-Ti boundary from their viscosity calculations, or at any other position within the section, as might be expected if the viscosity was an efficient mechanism for lava segregation. Rather the viscosities gradually decrease from the bottom up. The conceptual model does not indicate any faults or tilting of either the lavas or the dykes, and assumes the lavas dip away from the axis due to subsidence.

5.5.1 Effects of water

To better understand the effect of water content on viscosity the 250 lavas were calculated at 0% (an underestimate), 2.18% (best estimate) and 5% H_2O (overestimate). And a small subset of 11 analyses were calculated from 0-5 wt.% H_2O at increments of 1%.

As expected, the presence of water decreases the viscosity, as a result of depolymerisation of silicate chains in the melt, the viscosity at any given temperature is highest for the anhydrous lavas (figure 5.20). Adding just 1 wt.% H_2O into the melt makes a dramatic reduction in lava viscosity: at 1000°C (e.g., sample NT-13) the viscosity is reduced by 30% from 5.24 at 0% to 3.7 at 1 wt.% H_2O. Interestingly, when the H_2O content is increased further in 1% increments the viscosity reduction is less and less, until there barely a detectable difference between 4% and 5% H_2O.

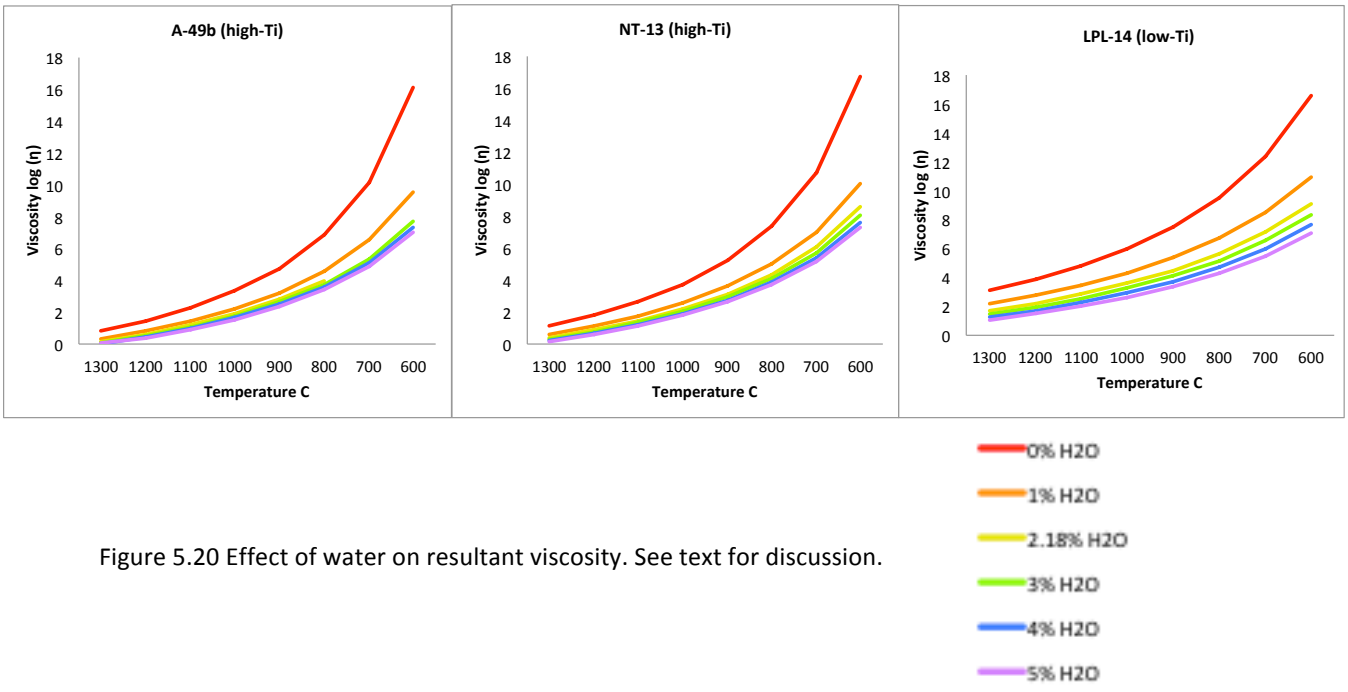

Figure 5.20 Effect of water on resultant viscosity. See text for discussion.

The effect of water on lava viscosity is far more obvious at lower temperatures, so the anhydrous lava viscosity at 600°C far exceeds that of a lava with 1% H_2O. This is represented on the plots of figure 5.20 by the coloured lines of increasing water contend becoming splayed at temperatures less than 1000°C.

5.5.2 Composition

Composition of the lava has a strong control on the viscosity of the fluid. Unsurprisingly, there is a very strong, positive correlation of SiO_2 content with viscosity, below are selected major elements of the glasses plotted against viscosity at 1000°C (figure 5.21). A similar pattern is seen in the Na_2O contents, although there is a less perfect correlation with viscosity. The CaO content forms a very strong negative correlation with viscosity, as does MgO however viscosity only increases significantly below ~5 wt.% MgO.

The combined effect of the different elements on viscosity compounds the effect of each element rather than cancelling each other out. The high-Ti lavas are more viscous because they have high SiO_2 and low CaO, low MgO and yet high Na_2O, whereas the low-Ti lavas are less viscous because they have low SiO_2, high CaO, high MgO and low Na_2O.

5.5.3 Temperature

It is necessary to model the lava viscosity at a range of permissible temperatures because cooling after eruption of lavas is rapid and would take place during flow and then continue further after emplacement until completely cooled. Cooling rates are dependent on the volume of lava erupted and on the rates of eruption, both of which are difficult to accurately estimate, the range of likely cooling rates are…As temperatures increase, the bonds of the silicate molecules in the melt weaken and the viscosity decreases as a result of shortening the chains of silica and allowing the fluid to flow more freely. In a detailed study by Philpotts & Dickson (2000) chains of plagioclase were imaged in basaltic melts using x-ray computed tomography scans,

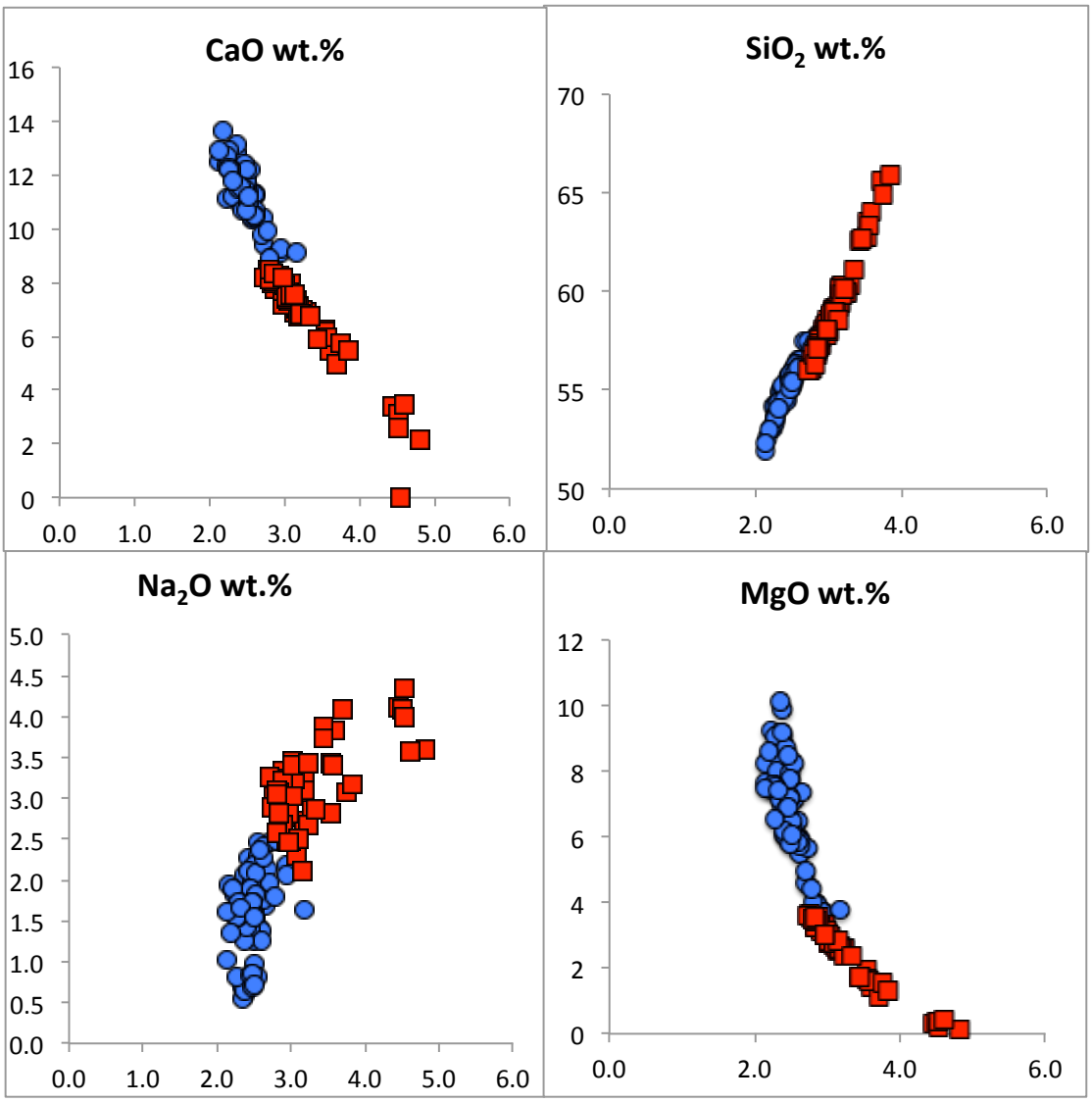

Figure 5.21 Viscosity of fresh volcanic glass. Calculated viscosities (units of log η) and the variation according to major element. See text for discussion.

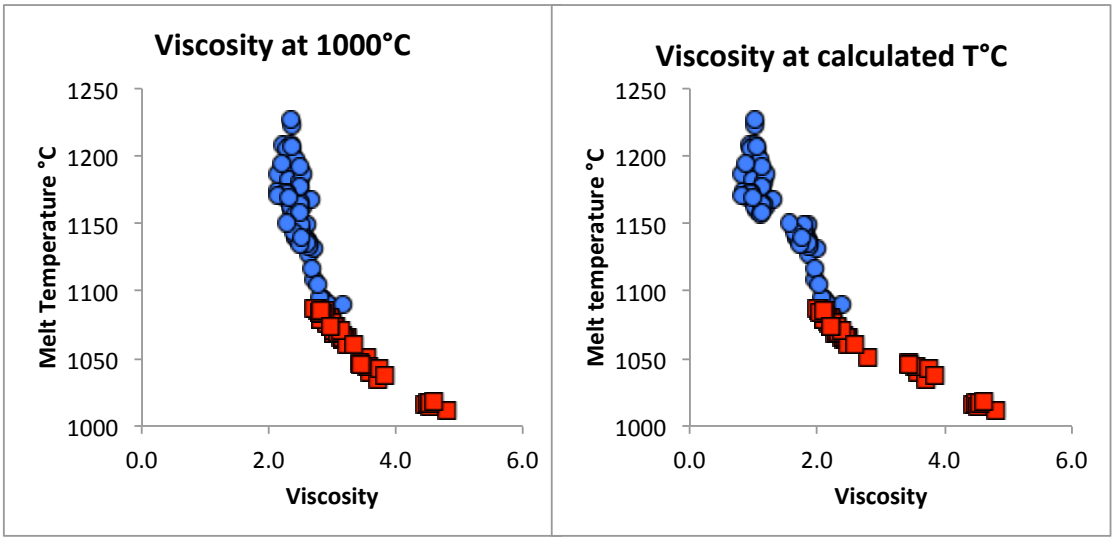

Figure 5.22 Effect of temperature on resultant viscosity (units of log η). See text for discussion.

revealing plagioclase-chain networks interconnected in three dimensions which limits melt flow by reducing porosity with greatest effect at lower temperatures.

Viscosity has been calculated for different temperatures ranging from 1300-600°C at intervals of 100°C, temperature and viscosity are plotted below for three of the fresh glasses. Predictably the viscosity increases at lower temperatures, but the relationship between temperature and viscosity is non-linear. Between 1300°C and 1000°C the viscosity increases in a linear manner, but from 1000-600°C the viscosity increases far more with every 100°C decrease in temperature.

Figure 5.22 shows the temperatures calculated for the glasses, viscosity is calculated at a constant 1000°C here, and clearly the low-Ti group would have been hotter and less viscous than the high-Ti which is also more variable in viscosity. The geothermometer method from Sano and Yamashita (2004) used MgO wt.% as a proxy for melt temperature, as expressed in the equation:

$$T\ (°C) = (21.61 * MgO\ wt.\%) + 1009$$

When the viscosity was plotted for individually calculated temperatures the viscosity difference between the two lava groups would be even more pronounced. Temperatures were calculated using the MgO proxy for the fresh glasses as shown in the plot above, with viscosity calculated to the nearest 100°C of the melt temperature. The low-Ti group would have been hotter (1223-1090°C) than the high-Ti lavas (1086-1012°C), with no overlap in temperatures between the two groups because there is no overlap in the MgO content.

The combined effect of the temperature and composition on the viscosity compounds the difference between the two lava groups. As can be seen from the trend in figure 5.22, the higher temperature and high-Mg/low-SiO_2 composition of the low-Ti lava group makes these the least viscous, ranging from 0.8-2.4 log η. Only minimal overlap occurs with the high-Ti groups, which range from 2.0-4.8 log η. The spatial pattern of the viscosities (calculated at eruption temperature) shows clear subdivision of the two lava groups, the low-Ti lavas are all at the least viscous end of the spectrum <1 log η, whereas the high-Ti lavas have a full range of viscosities.

Despite the high SiO_2 content of the boninites, they are likely to have contained more water than the rest of the lavas, so their viscosity could be even lower

than that calculated here. The water content for the viscosity calculations here is assumed the same for all lavas.

5.5.4 Stratigraphic viscosity patterns

Viscosity of the lavas are plotted on the 2D-profile to display the spatial and stratigraphic position of each viscosity analysis (figure 5.23). Viscosity was calculated for the best temperature estimate at 2.18 wt.% H_2O.

All of the low-Ti lavas are low viscosity, restricted to relatively narrow range of viscosity (< 0.50 – 1.49 log η), with one exception in the Larnaca graben. There are a mixture of highly viscous and low viscosity lavas within the high-Ti lava group Yet the high-Ti lavas viscosities are wide range from <0.50 – 4.49 log η.

The resolution of this viscosity dataset is far less than the CY-1/1a dataset used by Schouten & Keleman (2002), because for this thesis the viscosity was not modeled for each geochemical analysis. However, each lava section shows a upward trend of decreased viscosity from the high-Ti lavas to the low-Ti lavas (figure 5.23), broadly consistent with the trend Schouten & Kelemen observed in the drill core. The only difference is that this new data show the high-Ti lavas are composed of both runny and viscous but the low-Ti are nearly always runny.

The difference in viscosity of the lava groups appears to be a real feature that is observed across the whole ophiolite. However, there was probably not sufficient difference in viscosity between the high- and low-Ti lavas to be the mechanism for their segregation, as postulated by Schouten and Kelemen (2002). Though the upper lavas are almost always low viscosity, the underlying high-Ti lavas have a variety of viscosities, and can be just as fluid as the low-Ti lavas. If the two lavas were erupted from the same site and at the same time, the expected distribution would be an interleaving of high- and low-Ti lavas at the boundary between them. Instead, the division of the two suites is usually sharp which indicates there are other factors relating to the apparent segregation of lavas.

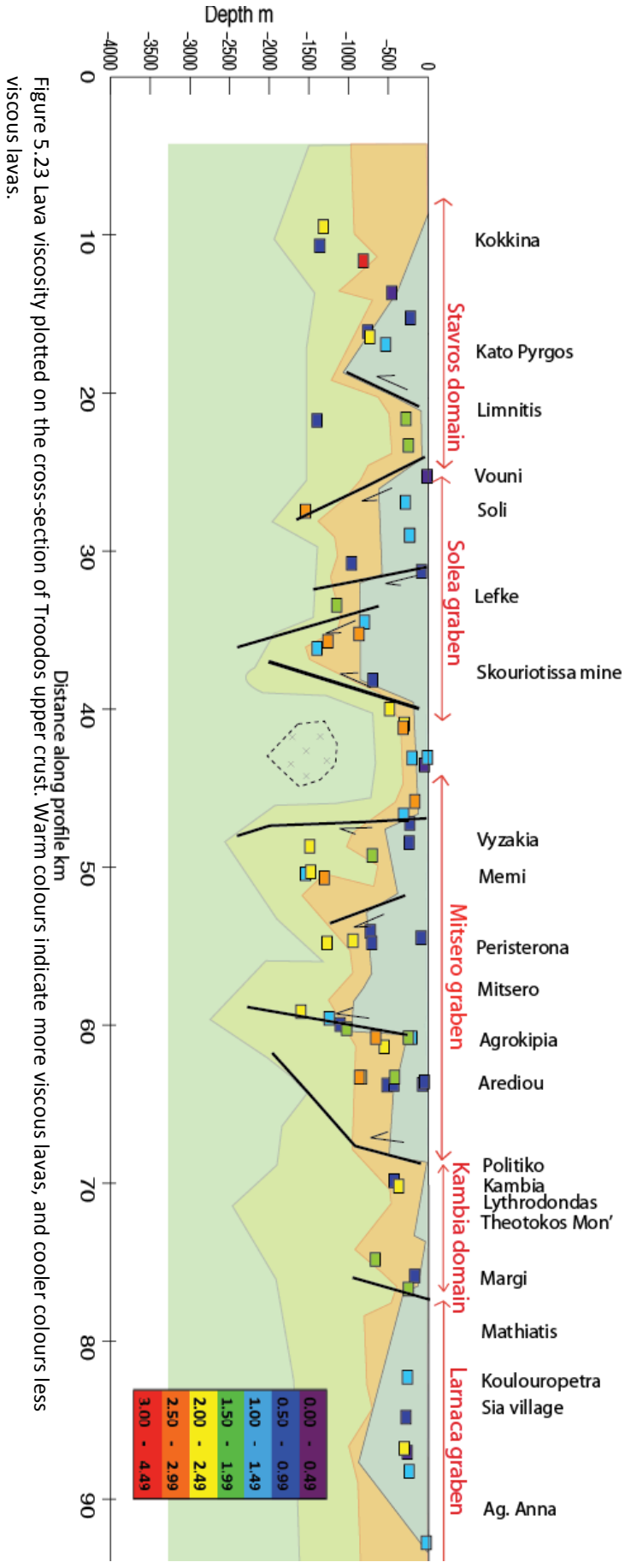

Figure 5.23 Lava viscosity plotted on the cross-section of Troodos upper crust. Warm colours indicate more viscous lavas, and cooler colours less viscous lavas.

5.6 Summary

In this chapter it has been demonstrated that there is an obvious difference in differentiation of the lava suites across the northern flank of the Troodos ophiolite. The high-Ti lavas making up the 'lower pillow lavas' and 'basal group' are more evolved than the low-Ti lavas which form the 'upper pillow lavas'. This contrast in the amount of fractionation is clearly shown in the SiO_2 wt.% and MgO wt.% on figure 5.2. However, the geochemical difference between the lavas are not purely due to crystal fractionation, as indicated by the MELTs modeling curves (figure 5.7), which show the low-Ti lavas have a separate fractionation trend from the high-Ti lavas. This suggests the lava groups originated from different parent magmas, rather than being from the same parent magma. There are subtle differences in the depletion of REE between the high-Ti lavas and low-Ti lavas. The high-Ti lavas are relatively un-depleted in M-REE and H-REE, but show some depletion of L-REE (figure 5.9). Whereas the Low-Ti lavas are depleted in middle- to heavy-REE from Nd to Yb, and also have lower total abundances of all REE in comparison to the high-Ti lavas. The low-Ti lavas are variably depleted, those lavas with the most marked depletion of middle- to heavy-REE are often slightly enriched in L-REE from La to Nd (slightly U-shaped or spoon-shaped REE profiles in figure 5.9). From investigation of the trace element ratios across the ophiolite there is a subtle hint that the low-Ti lavas have a more pronounced subduction zone fingerprint because the low-Ti lavas have lower Ti/V than the high-Ti lava in most sections with the exception of the Mitsero graben area (which does not show a difference in Ti/V in the lava sequence).

6 Synthesis Chapter

Chapter 3 documents grabens/half-grabens in the extrusive section of the ophiolite. Progressive angular unconformities within these structures are interpreted as evidence for syntectonic volcanism. Chapter 4 confirms that the tilting observed in both the SDC and the extrusive rocks is tectonic and related to fault block rotation above an active detachment. Chapter 5 explores the nature of the stratigraphic variations in lava geochemistry. In this chapter a holistic model is presented for the accretion of Troodos upper crust which incorporates all the observations from previous chapters.

6.1 Extension estimates

Central to understanding the processes operating at spreading centres is to know to what proportion of the plate separation has been accommodated by magmatic accretion of the lower and upper crust and what proportion by attenuation of the crust by extensional faulting. Tectonic extension is thought to be more important for spreading at intermediate-slow rate spreading ridges (e.g., Tucholke and Lin, 1994; Tucholke et al., 1998; Escartin et al., 1999). There are multiple methods of assessing the amount of tectonic extension of the oceanic crust, none without its problems, which are applied to the Troodos ophiolite and discussed here.

6.1.1 Strain estimates using seafloor morphology

At modern MOR the tectonic extension can only be readily estimated from the seafloor morphology. One approach has been to analyse detailed bathymetry data in conjunction with sidescan sonar imagery to identify the fault scarps exposed on the seafloor and thence sum the cumulative heaves of all the faults across a certain distance (figure 6.1a). The proportion of the sum of the fault heaves to the overall length of the study area gives a percentage of the tectonic extension. This seafloor morphology approach was first used systematically by Escartín et al. (1999) in order

to assess the extension at the Mid-Atlantic Ridge (MAR) at 29°N. Allerton et al. (2000) documented an average tectonic strain of approximately 10% and noted the tectonic strain was asymmetrical across the ridge axis, consistent with observed asymmetry in spreading rate as determined by magnetic anomalies.

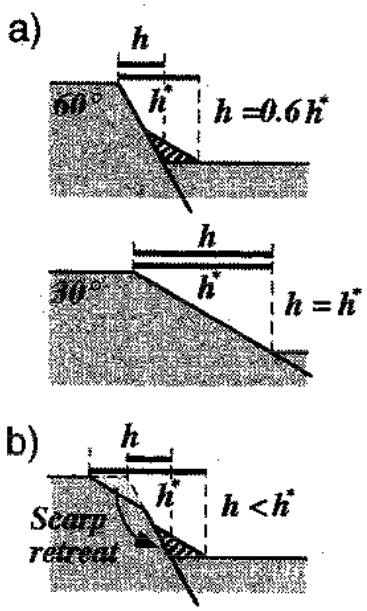

Figure 6.1 Method of calculating extension by assuming the horizontal fault heave corresponds to the amount of extension (from Escartin et al., 1999). By this method extension can theoretically be estimated from seafloor data (e.g. bathymetry, sidescan sonar) alone. However the true heave *h* may be obscured by scree slopes, degradation of the fault scarp and/or post-tectonic volcanism; it also neglects the sub-surface geometry and effects of rotational deformation, which may accommodate significantly different amounts of extensional strain.

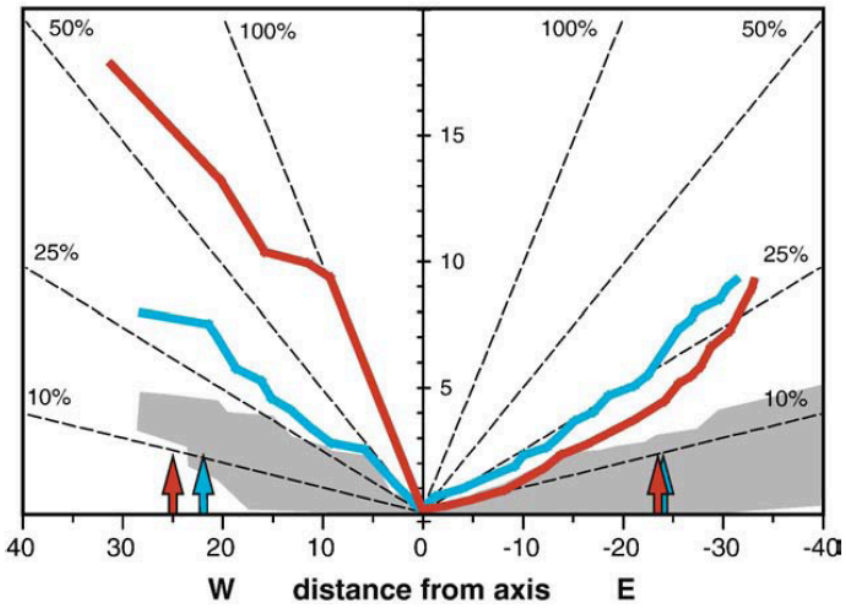

Figure 6.2 Cumulative tectonic heave versus distance from axis, from MacLeod et al. (2009). The grey area shows data from MAR 29°N (Escartin et al., 1999), blue (non-OCC section) and red (OCC section) lines are of data from MAR 13°N region.

MacLeod et al., (2009) calculated tectonic strain by the cumulative heave method for the MAR 13°N region, which is characterised by the presence of large ocean core complexes (OCC). The ridge flank containing the OCC has the highest average tectonic strain of 45-65%, and the active portions of the OCC have strains of up to 100% (see red line on West side in figure 6.2). In those areas where OCCs are not obviously present the strain is 28-35% and broadly symmetrical (blue lines in figure 6.2). The lowest tectonic strains, of 19-33% (red line on East side in figure 6.2), were found on the flanks opposite the active OCC. The marked contrast in tectonic strain across the ridge with OCC on one flank and not on the opposite conjugate flank indicates the extension is strongly asymmetrical when OCC detachment faults are active.

6.1.2 Extension estimates based on subsurface dyke geometry

An alternative method of estimating the extension was developed by Norrell and Harper (1988) for the Josephine ophiolite in California, and was applied to the Mitsero Graben in the Troodos ophiolite by Van Everdingen and Cawood (1995). This approach uses the tilting by faulting of the SDC to assess amount of horizontal extension. This method assumes the faults are planar and that the fault surface rotated, 'bookshelf' fashion, with the dyke keeping a constant angle between the two. It assumes purely dip-slip faulting parallel to dyke strike.

Applying this method to Troodos, the orientation data for the dykes have first of all been tilt-corrected to remove the uplift tilt, and then the percentage of horizontal extension calculated (%HE; following Van Everdingen and Cawood, 1995). The dip of the dykes is known, and dip of the faults is assumed to be 65° (65° is considered to be realistic, based upon the inferred initial dip of faults at the Mid-Atlantic Ridge: MacLeod et al., 2009, 2011). In order to use the lava orientations the complement to the dip must be used in place of the dyke dip. The method assumes no internal deformation within the faulted blocks; that faults are parallel; and the assumed underlying detachment surface is horizontal (figure 6.3). It is possible to calculate extension under different conditions, for example the detachment surface may be

either dipping in a synthetic or antithetic sense to the normal faults; the normal faults may be either parallel or non-parallel.

$$\%E = \left[\frac{\sin(90 + \theta)}{\sin(\alpha - \theta)} - 1 \right] \times 100\%$$

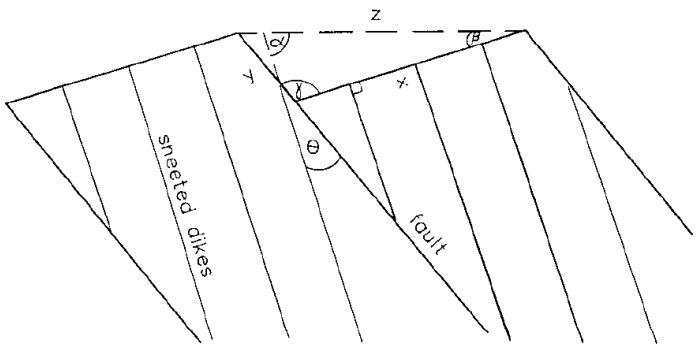

Figure 6.3 Geometric relationship of present dyke dip and horizontal extension (from Norrell & Harper, 1988). **θ** = complement to original fault dip (also angle between the fault and dyke). **α** = dip of dyke. **β** = permissible rotation on each fault set (20°-45° acceptable range, 35° used by Norrell & Harper).

For the Josephine ophiolite, Norrell and Harper (1988) document rotational deformation at the seafloor stage, concluding that the "geometrical relationship between cumulate layering, SDC, and overlying sediments indicate that a rotation of the crustal occurred at the spreading axis". Younger dykes are less rotated further supporting rotation happening at axis. Assuming the dykes were intruded vertically then they showed that the entire crustal sequence had been rotated by 50-70°.

Van Everdingen and Cawood (1995) report a subhorizontal normal fault in near SDC-gabbro boundary at Platanistasa in the Mitsero Graben which they suggest could indicate low-angle normal faulting, probably analogous to the Kakopetria detachment exposed at the Solea axis (Varga and Moores, 1985; Hurst et al., 1992, 1994).

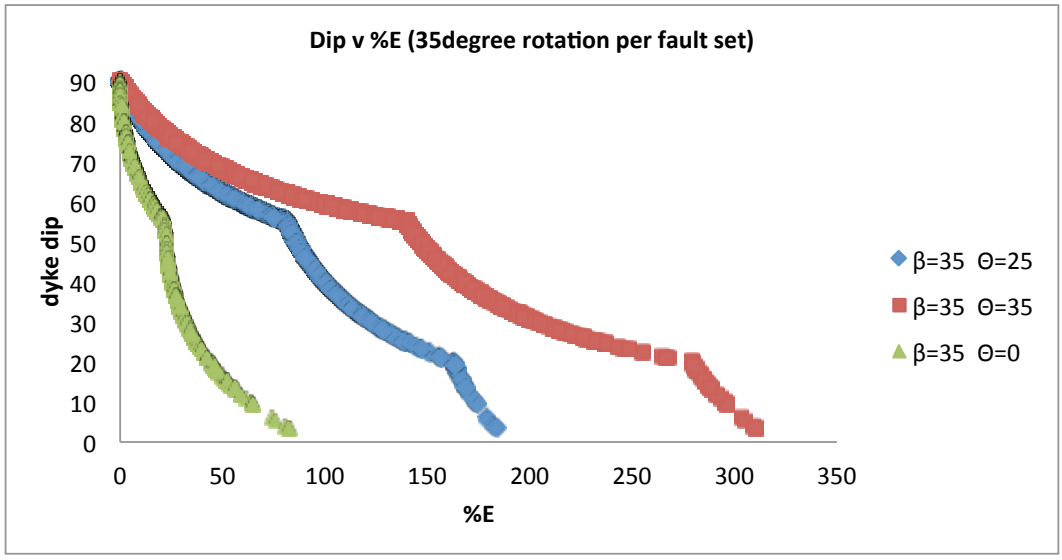

Figure 6.4 Calculated degree of extension (%E) from the Norrell and Harper (1988) and van Everdingen and Cawood (1995) method. See text for assumptions. Calculations were done using different initial fault angles; blue=fault dip 65°; red=fault dip 55°; green=fault dip 90°. All were calculated assuming 35° rotation per fault set. Θ=complement to fault dip.

6.1.3 Troodos subsurface extension estimate

Following the method of Norrell & Harper (1988) and Van Everdingen & Cawood (1995) the dyke dips were used to estimate the percentage horizontal extension. An adaptation to this method was to partition the rotation onto a second fault after 35° of rotation. Norrell & Harper (1988) consider rotation of 20°-45° on each fault set to be acceptable. The second fault sets forms at 65° and can also accommodates 35° of rotation until a third fault set forms (figure 6.4, humps form when the new fault sets are introduced). A second adaption of this method is to use the lava orientations by assuming the complement to the lava dip is equal to the dyke dip (i.e., a 20° rotation is required to tilt dykes dipping at 80° and lavas dipping at 20°). The adapted method was applied to dykes (n=2818) and lavas (n=1532), as shown in the frequency plots in figure 6.5.

The map below (figure 6.6) shows contoured data for %HE based upon the orientation of dykes and lavas across the northern flank of Troodos. Greatest extension is in the western flank of the Solea Graben (>100% extension). The Mitsero Graben has similar structural style, also exhibiting greater extension in the west side than the east side. The average degree of extension implied for northern Troodos as a whole is ~45%.

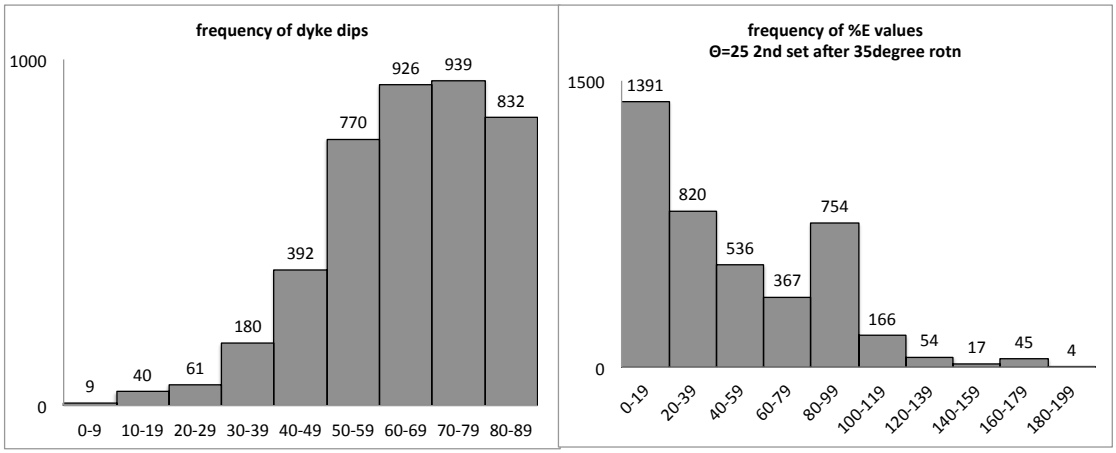

Figure 6.5. Left: Frequency of dyke dips, two peaks span dips of 60-79° which is 46% of the dykes. Mean average dip of dykes = 65°. Right: Frequency histogram of %E values, the spike at 80 %E corresponds to the appearance of the second fault set when the dyke dip <55°.

6.1.4 Troodos surface extension estimate

In chapter 3 it was shown that the Troodos lava-sediment surface is almost completely flat, with fault-related offsets of the original seafloor of no more than a few metres. It is difficult to rigorously deconvolve the effects of later faulting, but my estimate of the proportion of extension accommodated by summing the heaves of faults that were exposed on the late Cretaceous Troodos seafloor, i.e., by a method directly equivalent to that employed for the modern Mid-Atlantic Ridge (section 6.1.1 above) is much less than 1%. This contrasts markedly with the sub-surface estimate above, and demonstrates how fundamentally unsafe it is to base estimates of the component of tectonic extension upon the summation of surface fault heaves alone (e.g., Escartin et al., 1999; MacLeod et al., 2009). It may be concluded that, by analogy to the observations from Troodos in this thesis, many slow- to intermediate-spreading mid-ocean ridges may be accommodating otherwise unrecognised significant stretching – or 'hidden tectonics' – beneath the seafloor.

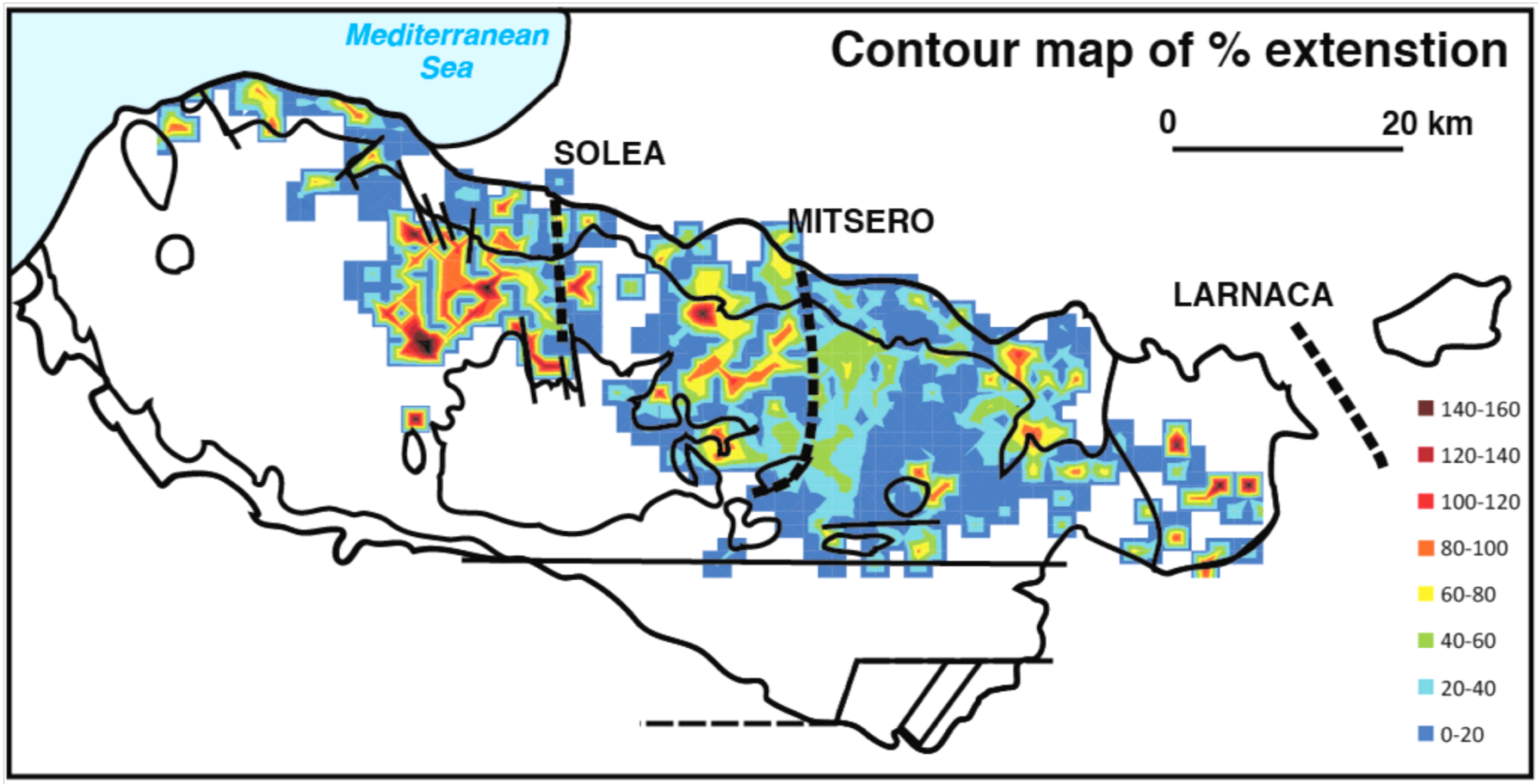

Figure 6.6 Map view of percentage extension calculated from Troodos dyke and lava dips, showing greatest extensional strains on the west sides of the Solea and Mitsero grabens.

6.2 Constraints from lava chemistry on upper crustal accretion mechanisms

6.2.1 High-Ti lavas (lower unit)

Basal group outcrops are composed of up to 90% dykes, intruding into the extrusive sequence, therefore the basal group lavas must be erupted on-axis and within the dyke injection zone. There is no geochemical distinction between the basal group lavas and the 'lower pillow lavas', therefore it follows that the entire high-Ti suite formed in an on-axis setting.

Little compositional variation is observed within the high-Ti suite: it is relatively evolved as demonstrated by high SiO_2 and low MgO, and there are no changes in the MORB-like REE profiles. These observations indicate the high-Ti melts were likely stored in a mid-crustal level melt lens, probably comparable to those present at fast-spreading mid-ocean ridges (e.g. Sinton and Detrick, 1992), which allowed the magma to both differentiate to more evolved compositions as it cooled and to thoroughly homogenise by mixing.

All the high-Ti lavas show virtually no depletion of the middle- and heavy-REE; only the light-REE are slightly depleted, in a manner similar to that observed in MORB (Rautenschlein et al., 1985). However, the Th/Yb vs Nb/Yb diagram (figure 5.6) identifies both the high- and low-Ti suites as suprasubduction lavas (Pearce, 2014).

High concentrations of Y are consistent with fractionated liquids, probably derived either from an undepleted source or one that underwent smaller degrees of partial melting. The consistently high concentrations of Zr may indicate these are early melts from the source mantle, possibly even among the first melts to come from the mantle. The melting conditions for the high-Ti lavas are likely to be dryer and/or less oxidising than the low-Ti suite because the Ti/V ratio of the high-Ti lavas is consistently >18 compared to low-Ti lavas Ti/V are constistently <18 (Shervais, 1982).

The combination of more evolved compositions, dryer melts, and cooler eruption temperatures would have made the high-Ti lavas far more viscous than the low-Ti unit. These viscous lavas would have flowed slowly from the axial setting, only travelling short distances down slope. Small syn-volcanic growth faults and mini-

grabens within the high-Ti lower lavas (Schmincke and Bednarz, 1990), similar to active summit calderas on the East Pacific Rise (e.g., Fornari et al., 1998) may also have acted to restrict the lava flow paths.

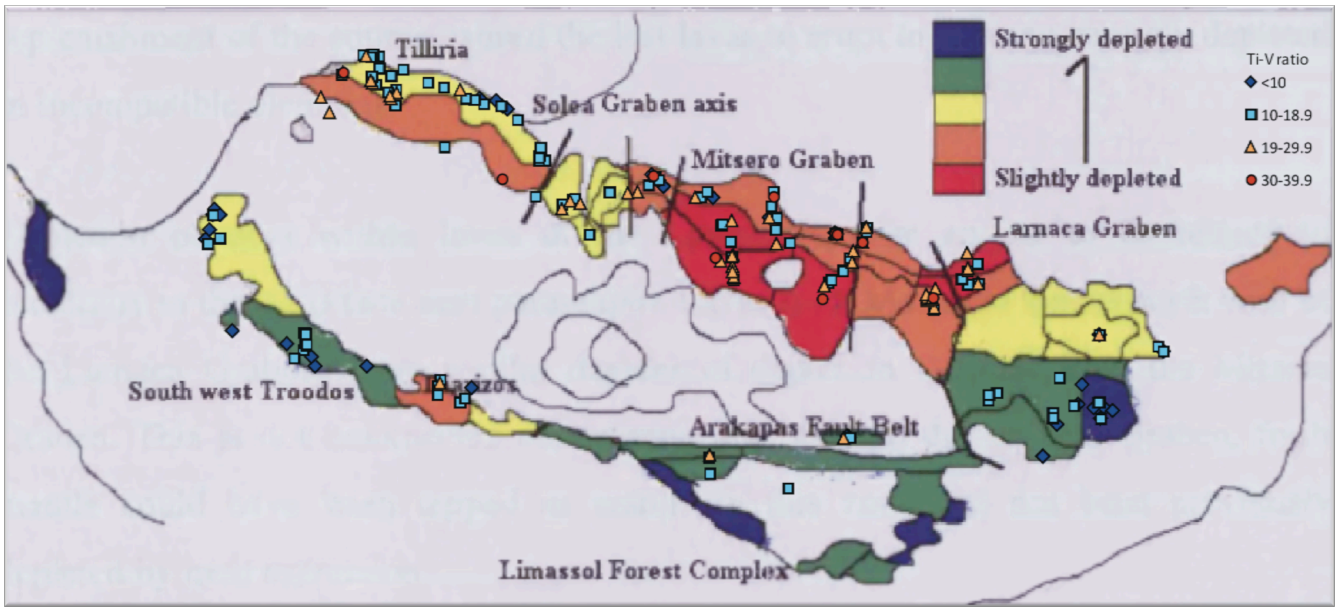

Figure 6.7 Base map from Wake (2005) shows depletion of lavas based on a combination of geochemical parameters (Gd/Yb, Nb/Yb, Ti/V, Y_{100}) overlain by Ti/V data points. Mitsero graben is the least depleted and has a greater proportion of lavas with high Ti/V ratio.

6.2.2 Low-Ti lavas (upper unit)

Upper portions of the extrusive sequence are characterised by low-Ti, higher-Mg primitive lavas, which are variably olivine- or pyroxene-phyric, and occasionally picrites occur. This lava suite is usually altered by seafloor weathering, and is in places overlain by umbers in small and discontinuous outcrops.

Compositions of the low-Ti suite are mostly more variable, particularly in terms of the depletion signatures. In many instances the REE profiles are similar to the MORB-like high-Ti suite, and yet a significant proportion of the low-Ti lavas have distinctly greater depletion of the middle- and heavy-REE (figure 5.9). Magmas forming this lava suite are more primitive and were probably much hotter on eruption (1223-1090°C for low-Ti lavas, and 1086-1012°C for high-Ti lavas), perhaps due to rapid ascent through the crust to maintain the heat.

These melts have probably bypassed the axial melt lens on ascent through the crust. By avoiding the axial melt lens the low-Ti melts were not able to efficiently mix, thus preserving their compositional variation; nor were they stored for long residence periods to differentiate to more evolved compositions before eruption. It is suggested here that the low-Ti lava unit was erupted slightly further away from the axis from deep crustal melt lenses in a 'near-axis' setting, probably directly comparable to the off-axis melt lenses recently imaged at the East Pacific Rise (Han et al., 2014). A near-axis position can account for how ascending melts may have bypassed the axial melt lens, and account for the stratigraphic relationship between the two lava units – i.e., low-Ti lavas are always overlying the high-Ti lavas. A far off-axis proper setting is rejected for the low-Ti lavas on the basis of the tectonic rotations which imply the low-Ti unit was erupted within the range of the active faulting near the ridge axis.

Most of the low-Ti lavas show evidence of derivation from a mantle source that has undergone substantial depletion: TiO_2, Y, Zr concentrations and ratios (e.g., Zr/Y) are all lower than the high-Ti lavas, and the middle- to heavy-REE (and MREE/HREE ratios) are lower. Low Y and Zr concentrations and ratios may be due to a depleted source and/or greater degrees of partial melting, and given their stratigraphic relationships probably indicate the low-Ti unit came from later (or continued) melting of the source of the high-Ti unit. However the degree to which the low-Ti magmas have been depleted varies greatly within the group, so much so that the apparent decoupling of depletion is the basis of the subdivision of the LREE-enriched depleted lavas explored in chapter 5. The LREE-enriched depleted low-Ti lavas usually correspond with the boninitic-like lavas (e.g. Rogers et al., 1989). This subgroup is often found at the top of the low-Ti lavas, forming the topmost extrusive rocks, but not always.

Melting conditions of the mantle source for the low-Ti lavas were probably hydrous and highly oxidising because the Ti/V ratio is lower than the high-Ti lavas (e.g. Shervais, 1982). The wettest lavas, those with the lowest Ti/V ratio, are of the LREE-enriched very depleted lavas. It is probable that additional water in the system has allowed further melting of already extremely depleted mantle to yield boninite-like magmas.

This depletion is, however, not uniform across the north flank of the ophiolite (figure 6.7). Sections from the Mitsero graben do not show such great depletion in the low-Ti unit. Mitsero low-Ti lavas do not have reduced Ti/V ratios, and it would appear there is a cogenetic relationship between the two lava groups. In these instances the only real difference between the lower high-Ti and upper low-Ti lava units is the degree of fractionation.

Basic viscosity estimates show the low-Ti series is mostly less viscous than the high-Ti series, and would therefore flow further distances. The low-Ti lavas as primitive, hotter, and contain more water than the high-Ti lavas, which has the combined effect to make them less viscous (Schmincke and Bednarz, 1990; Schouten and Kelemen, 2002).

6.3 Architecture of the Troodos upper crust

The geochemical stratigraphy outlined in chapter 3 has identified a sharp contact between the high-Ti lavas and the low-Ti upper lavas. This contact can be traced ~90km across the northern flank of the Troodos ophiolite with considerable vertical deviations.

A paradox is apparent in that the extrusive section changes thickness substantially (up to 800 m) across the strike of the axis and hence with time, yet the lava-sediment contact is subdued and interlava sediments and mass wasting deposits (as widely seen at modern slow-spreading mid-ocean ridges) are absent. These observations imply that there could not have been significant relief on the seafloor while the upper crust was being constructed (such sediments are characteristic of the bathymetric depression coincident with Southern Troodos transform fault zone, for example: Simonian and Gass, 1978; Gass et al., 1994). Instead the observations from northern Troodos require that there must have been a continuously subsiding and tilting relatively flat seafloor that was repeatedly repaved by successive (mostly low-Ti) lava flows, with the thickest sections of lavas accumulating in the hanging walls of the active faults.

The apparent thickness of the basal group also changes dramatically, from 200m to +1000m in phase with the variations in thickness of the lavas, although in general the basal group from the Solea graben is much thinner than other regions.

Previously the basal group thickness has been underestimated because it difficult to identify the narrow lava screens which make ≤10% of the unit and it may be misidentified as sheeted dyke complex. Estimates of the transition zone thickness of modern MORs may, too, be conservative as seismic velocities are likely to be similar to SDC proper and ocean crustal drilling would be unlikely to encounter the narrow lava screens. It has been suggested by Kidd et al. (1977) and Gillis & Coogan (2002) that the transition from SDC to lavas occurs rapidly over ~200m, which they interpret this as a narrow zone of dyke emplacement at the spreading centre. But if the basal group thickness is routinely underestimated then the widths of dyking zones may also be underestimated.

6.3.1 Growth faulting

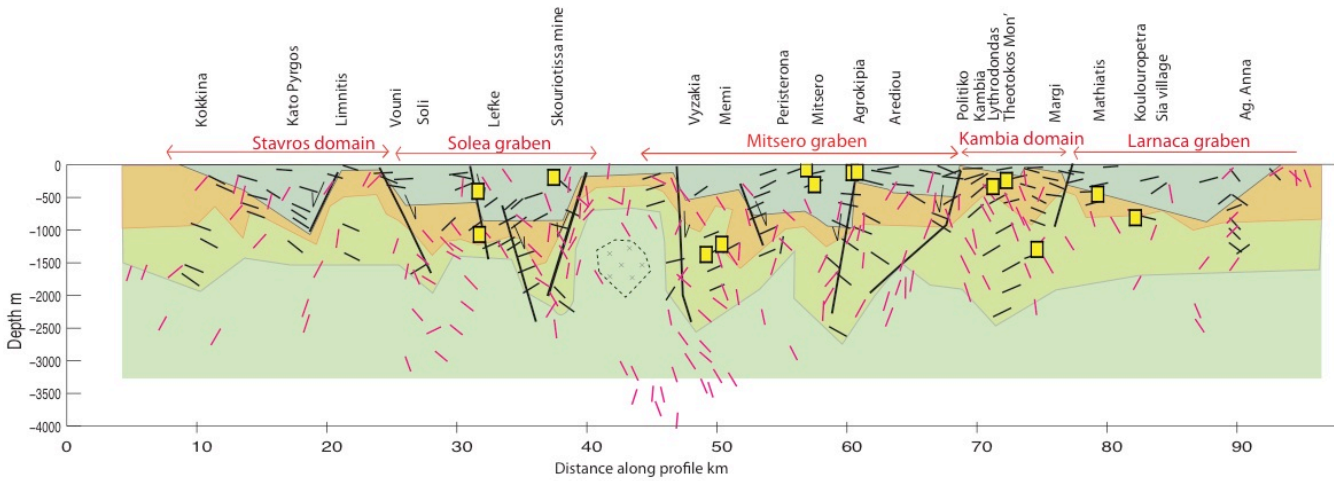

Figure 6.8. Summary of structural relationships across northern Troodos, with location of inferred or observed growth faults (thick black lines). Small black bars = actual dip of lavas; small pink bars = actual dip of dykes; yellow squares = large sulphide deposits; blue = low-Ti lavas, orange = high-Ti lavas, light green = basal group; dark green = SDC.

From the observations presented in chapter 3 the existence of large growth faults has been demonstrated and their location inferred based upon field observations, thickening/ponding of lava units, and the progressively steeper lava dips down section. In the 2D-profile above the large normal faults inferred to be responsible for the growth faulting are shown. Some are known structures on the basis of field mapping of faults, but not all. Because some of the structures will have accumulated little actual fault displacement and deformation, as a consequence of being essentially

passive dams against which lava flows have been ponded, they may have little structural expression in the field. Instead they are detectable only by the change in lava stratigraphy on either side of them. Another possible sign of their presence is the occurrence of substantial massive sulphide deposits in their vicinity. Most of the major deposits – Skouriotissa, Mavrovouni, Apliki, Memi, Agrokipia and Kambia, at least – appear to be spatially associated with the growth faults and associated rapid changes in upper lava thickness.

It can be tentatively concluded that these faults, which must have corresponded to the equivalent of near-axis valley-wall faults at modern slow- to intermediate-spreading rate ridges (albeit morphologically subdued), played an important, if not essential, role in controlling the pathway of hydrothermal discharge. This potentially explains the observation by the GSD workers that the massive sulphide deposits typically lie at the boundary between the 'lower' and 'upper' pillow lavas: exhalative deposits are localised along the valley-wall/growth faults, and buried (and hence preserved) by the blanketing of the low-viscosity low-Ti suite flowing into the active half graben.

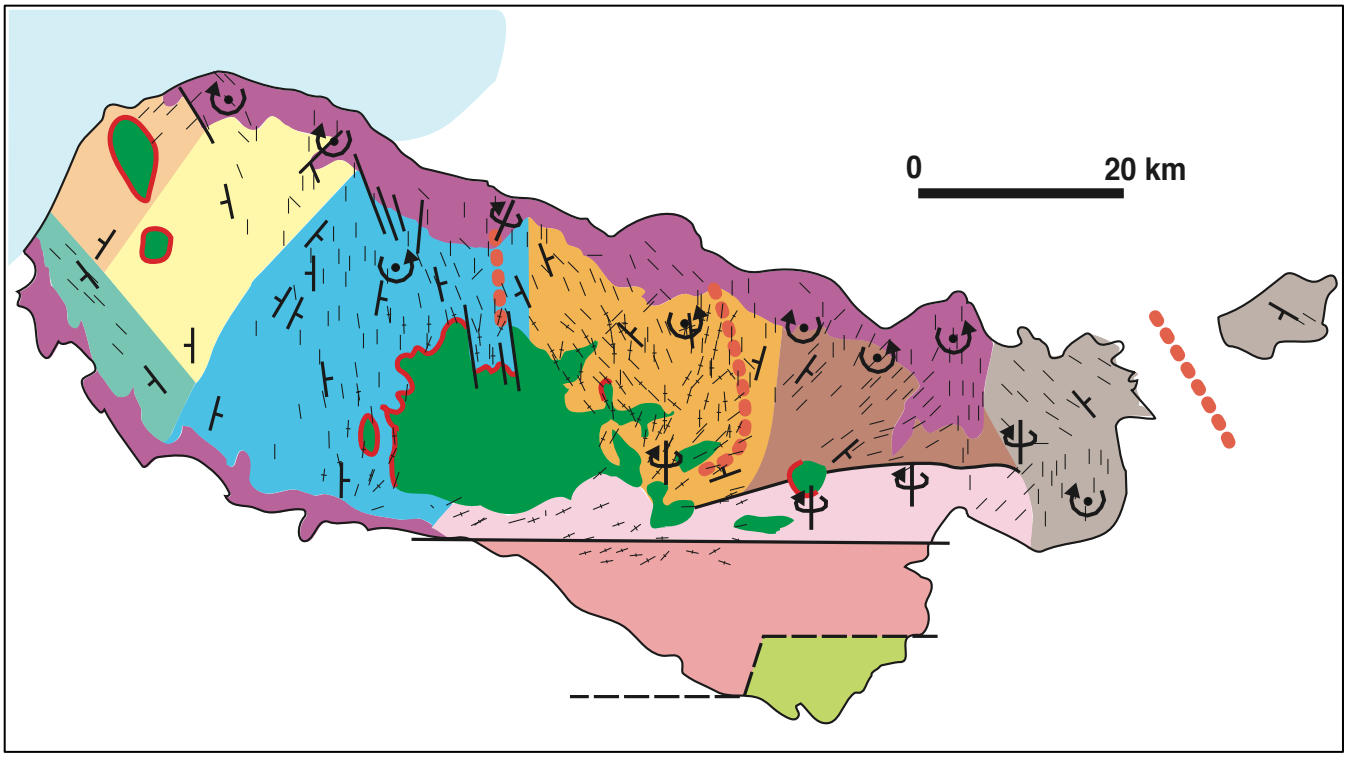

Figure 6.9 Map of tectonic spreading fabric as defined by orientations of dykes. Arrow symbols indicate the average sense of rotation of an area and the orientation of rotation axes. Upright poles represent vertical rotation axes (mostly in the transform), horizontal rotation axes are represented by dots (in the grabens).

6.3.2 Oceanic detachment fault models

Numerical modelling of oceanic detachment faults by Tucholke et al. (2008) and Buck et al. (2005) showed that a detachment fault could remain stable and long-lived if the proportion of plate separation it accommodated was approximately 50% of the total spreading budget. In this case dyking in the hanging wall of the detachment could accommodate the other 50% of plate separation, and the detachment faults roots somewhere close to the melt lens. This is potentially consistent with the situation for Troodos: the Kakopetria detachment is located at the sheeted dyke–gabbro boundary, so potentially was rooting at the (weak) melt layer. In the older Mitsero graben evidence for detachment faulting is less clear (although reported by Agar & Klitgord, 1995; and Van Everdingen & Cawood, 1995); instead Gillis (2002) shows that the base of the dykes is generally intruded by gabbros. No mylonites have been reported from the Kakopetria detachment, such as there are at the Atlantis Bank detachment (e.g., Cannat et al., 1991) which shows ductile deformation of gabbros and the melt body is found within the footwall. Instead, for the Kakopetria detachment, it is possible that magma lubricates the fault and the magma may even 'consume' the active fault as it does the base of the SDC.

More recent modelling (Smith et al., 2008; Choi and Buck, 2012), coupled with inferences from seismic data (Dannowski et al., 2010; Reston and Ranero, 2011) shows that active detachments can potentially be present at the ridge axis beneath a series of rider blocks, and that mantle rocks need not be exposed on the seafloor at oceanic core complexes (figures 6.10 & 6.11). For the case of Troodos, these rider blocks represent upper crustal blocks of sheeted dykes and lavas that were being generated in the hanging wall of the active detachment and successively rotated above the continuing (Kakopetria) detachment (figure 6.12). This scenario is comparable to the Troodos oceanic core complex model of Nuriel et al. (2009), though without the inference that the mantle was exposed on the seafloor, for which there is no evidence.

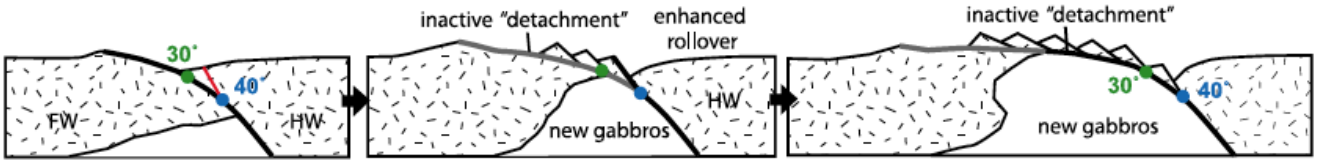

Figure 6.10. Model for the existence of a cryptic detachment fault beneath a series of surface rider blocks, showing how an active, long-lived detachment need not be exposed on the seafloor (Reston & Ranero, 2011).

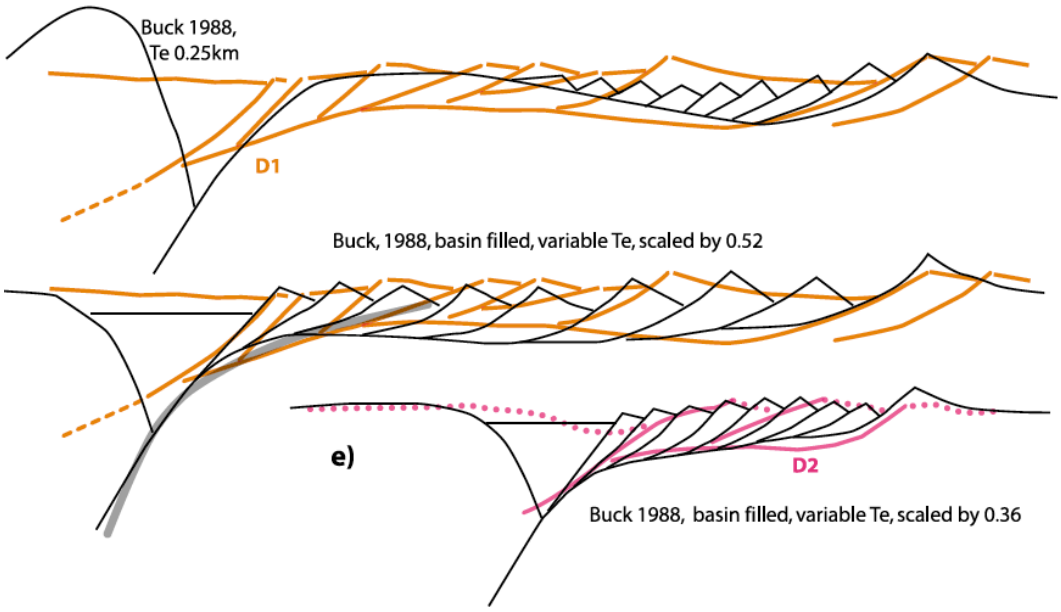

Figure 6.11. Comparison of seismic images of detachment faults from Mid-Atlantic ridge at 26°N with predicted geometries of detachments from numerical models (Reston & Ranero, 2011).

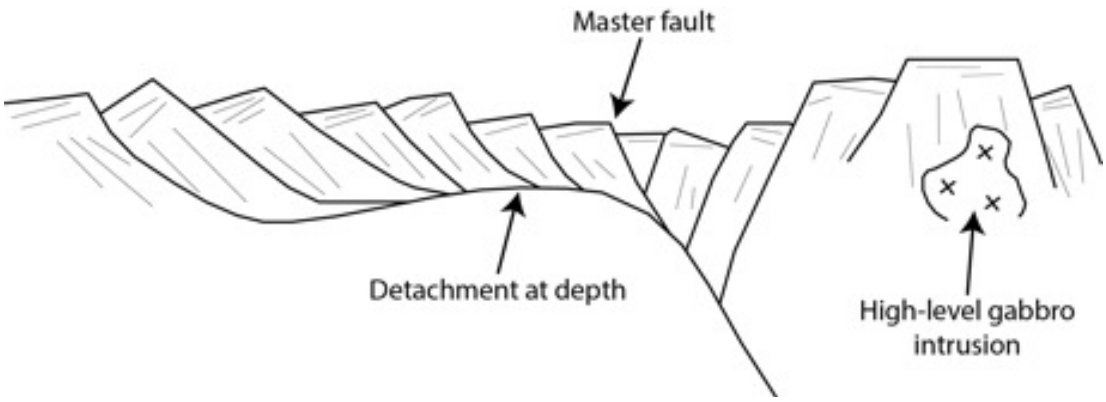

Figure 6.12. Cartoon depicting asymmetrical spreading at the Solea Graben, with tilted dykes and lavas have rotated above a detachment surface beneath.

6.3.3 Graben evolution in the Troodos Massif

Spreading is accommodated by a combination of tectonic stretching and magmatic accretion. The relative proportion of these factors may switch over time in response to changing magma supply at the ridge and spreading rate. During times of high or adequate magma supply the emplacement of gabbro sills, dykes and lavas can keep pace with plate separation. But when the magma supply is low, the accretion of new crust cannot keep pace with spreading and tectonic stretching of the crust by extensional faulting. Extension of the Troodos crust is expressed as tilting of the SDC and lavas to form the three grabens across the northern flank. Each graben represents an episode of tectonic extension during comparatively magma-poor periods, as originally suggested for the Solea graben by Varga & Moores (1990).

The grabens most likely represent fossil ridge axes rather than off-axis stretching features because the lavas were erupting at the axis (or near to it) during the formation of the grabens. In light of this factor the off-axis model proposed by Allerton & Vine (1987) can be ruled out because it does not predict the syn-tectonic eruption of lavas.

The geological evolution of the grabens is partly based on the assumption that the Mitsero graben is the earliest because the dating of plagiogranite from Ayia Vavatsinia is the oldest (C.J. MacLeod *unpubl. data*). The Solea graben probably formed later, and the cross-cutting relations at the Mitsero-Solea boundary are unclear. Clear cross cutting of dykes and structures show the Larnaca graben formed later than the Mitsero graben (e.g., Allerton & Vine, 1990).

Evolution of the grabens is summarised schematically in figure 6.13, which is an interpretation of the crustal architecture documented from the field and stratigraphy observations. The series of episodes for the graben evolution is as follows:

T1. Extensive on-axis magmatism at the Mitsero axis with little tilting. During this phase the magmatism is robust and tectonism is minor. Dykes and high-Ti lavas are emplaced to form the upper crust, and those high-Ti lavas from the western flank predate the faulting of T2.

T2. Tectonic extension increases as magmatic accretion wanes. Extension is accommodated by inward-facing faults, resulting in outward-tilting lavas and inward-tilting dykes. The crustal attenuation is asymmetric (western flank is broader and has increased extension, figure 6.6). Normal faults are probably connected at depth to a low-angle detachment fault on the western side of the axis. During this stage the low-Ti lavas were erupted despite the waning on-axis magma supply. These syntectonic lavas are notably less viscous and flow down slopes until they are dammed by inward-facing faults. The seafloor topography is relatively flat, and the topmost lava flows are sub-parallel to the sediments above, but flows are increasingly tilted with depth. Mineralisation occurs during this stage near the Mitsero axis, driven by the magmatic heat and fluids exploiting faults, to form the Agrokipia and Mitsero VMS deposits.

T3. Next event is the switch to spreading at the Solea axis. This may have happened by ridge jumping or propagation; however the exact cause cannot be determined because of the limited along-axis preservation of the ophiolite. The Kakopetria detachment fault developed early in the evolution of the Solea graben because progressive unconformities occur throughout the extrusive sequence at Solea so extrusion is entirely syn-tectonic. Blocks of upper crust are tilted by planar faults rotating above the detachment surface.

T4. Detachment faulting is still active at the Solea axis but at this time low viscosity low-Ti lavas are extruded, some possibly fed by the high-level pluton preserved at Kannavia. Ponding of lava flows occurs when flows are dammed by faults which continue to displace the lavas as they are deposited. Intense hydrothermal circulation at the Solea axis generated three large-tonnage sulphide deposits. Mavrovouni and Apliki deposits formed along a major fault near the axis, whereas Skouriotissa formed on the axis and was not buried by subsequent lavas because spreading at the Solea axis was terminated.

T5. Spreading resumes at the Larnaca axis where new Larnaca crust cross-cuts the old Mitsero terrain. The spreading fabric is at this point is NW-SE, implying NE-SW extension as opposed to the approximately E-W spreading inferred previously (see figure 6.9). It is possible this spreading centre propagated from north to south until it

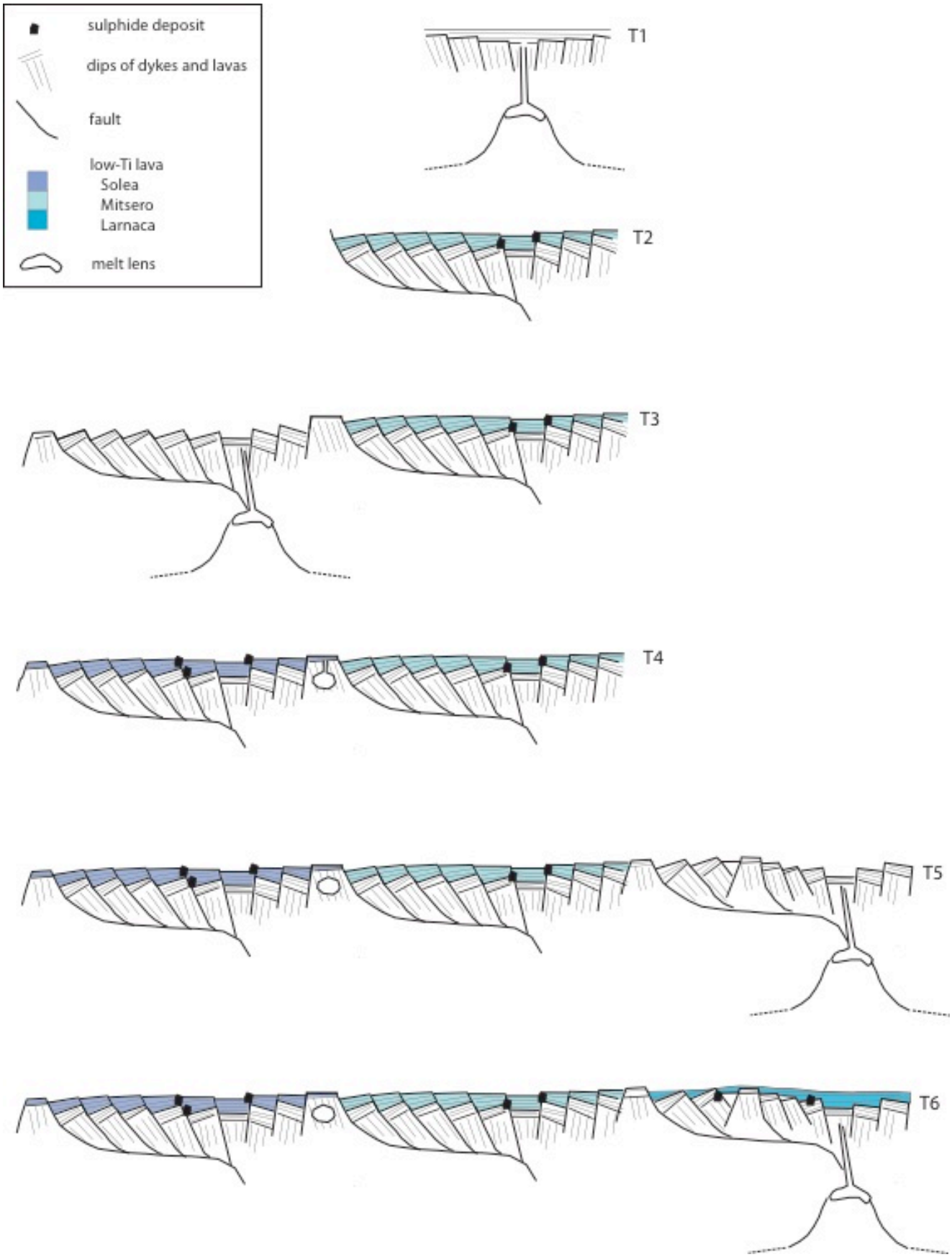

Figure 6.13. Graben evolution across the northern flank of Troodos ophiolite. Lavas were accreted one graben at a time, often at the same time as the grabens were forming due to tectonic extension.

reached the Southern Troodos transform fault zone which bounds the Larnaca graben to the south. Another detachment fault is inferred beneath the SDC because there are extensive rotations in the blocks above; however the erosion level is not sufficient to expose this structure at the surface. The Kambia domain identified on the western flank of the Larnaca graben is interpreted as a small antithetic block. This same region has N-S spreading fabric and it correlates with the Makhaeras domain previously documented in the SDC. Lavas of the high-Ti unit are steeply tilted, however there is not enough data from this area to constrain the timing of the eruptions relative to the tilting.

T6. Finally the low-Ti lavas have covered the faulted Larnaca basement, in several cases there is an angular unconformity at the contact between the significantly tilted high-Ti lavas and the less tilted low-Ti lavas, as documented by Allerton (1988; Allerton and Vine, 1990).

6.4 Accretion models – hypothesis testing

6.4.1 Models for accretion/petrogenesis must account for the following:

1. Relief at the lava-sediment contact is subdued.
2. All the lavas are tilted and therefore all bar the latest are pre- to syn-tectonic, both high- and low-Ti lavas show similar rotation axes (only the rotation magnitudes differ).
3. Rotations documented in the lavas by dip/strikes are consistent with rotations documented in the SDC by palaeomagnetics; hence the rotations are related to tectonic tilting due to spreading rather than subsidence in the lava pile (as proposed by Schouten and Denham, 2000; Schouten and Kelemen, 2002).
4. High-Ti lavas do not show pervasive seafloor weathering, nor are they overlain by sediments.
5. The only places where high-Ti lavas overlie low-Ti lavas are at the Mitsero-Larnaca graben boundary, and which are interpreted as Mitsero low-Ti ‘upper’ lavas being buried by Larnaca high-Ti ‘lower’ lavas.

6. Only in the Mitsero graben are the high- and low-Ti lava suites cogenetic. In the remaining regions of the ophiolite subtle REE and trace element variations are present between the high- and low-Ti lavas, which indicate the low-Ti melts came from more depleted source with more water and higher oxygen fugacities.
7. Some, but not all of the low-Ti lavas have slight enrichment of LREE, most of which are present in the uppermost low-Ti unit. LREE enrichment in boninitic lavas is otherwise only observed in 'transform sequence' magmas emplaced within the Southern Troodos transform fault zone (Cameron, 1985; Murton, 1986; Gass et al., 1994)
8. The thickness of the extrusive sequence varies considerably across-axis.
9. High-Ti lavas must be erupted on-axis because Basal Group lavas are intruded by many dyke swarms.
10. Depleted dykes of drill core CY-4 are not systematically younger than non-depleted dykes, according to Baragar 1990.
11. Trace elements (Cr ppm vs Y ppm) suggest two lava groups are not simply related by fractionation, but compositional variation is due to source differences (e.g., depletion/partial melting/enrichment .

6.4.2 Axial eruptions and viscosity segregation of flows

Schouten and Kelemen (2002) suggest that both groups of lava erupted from an on-axis position, but the less viscous low-Ti lavas were transported 1-2 km and deposited off-axis. In this model the melts for the two lava groups are considered to be cogenetic with a single liquid line of decent. Two spatially separate magma reservoirs are required if there are to be simultaneous eruptions of chemically distinct lavas. Or different parts of a single reservoir were tapped (i.e., top of reservoir for high-Ti lavas and base of reservoir for low-Ti lavas). This model predicts a significant amount of interbedding between the high- and low-Ti lavas because there could be flows of intermediate viscosity which can flow down slope an intermediate distance.

In Chapter 5 it was shown the viscosity difference of the two groups was not great enough to segregate the lavas, the low-Ti lavas were not so much runnier that

they were able to be completely drained from the eruption centre to the off-axis depocentre. Instead, the off-axis eruption seems a simple and feasible way to deposit lavas off-axis, and can account for the ordering (or apparent segregation) of the lavas and explain the lava geochemistry. An alternative way to account for the apparent segregation of the two lava types is that the low-Ti lavas were erupted off-axis and the high-Ti lavas erupted on-axis.

6.4.3 Simultaneous on-axis and near-axis volcanism

In this scenario the high-Ti lavas were erupted on-axis and low-Ti lavas formed at a slightly off-axis (or near-axis) setting but still within the zone of faulting. The high-Ti melts were held in a crustal level melt lens beneath the axis where they were able to fractionate, they are much more homogenised probably due to reactive porous flow during ascent through the gabbroic mush zone in the lower crust (which has been documented at the Kane megamullion by Lissenberg, 2008). Whereas the Low-Ti lavas probably bypassed the melt lens and therefore bypassed the opportunity to evolve further. Their ascent pathway may have avoided the gabbroic mush zone and so they haven't homogenised as much as the high-Ti lavas, hence the wider variety of chemistries in the upper unit. Eruptions of lava at both settings would occur during active spreading, to account for the syn-tectonic tilting found in both the axial lavas (high-Ti group) and the near-axis lavas (low-Ti group). The magma pluming could be similar to that proposed by Schouten and Kelemen (2000); a shallow melt lens for the lowers and a deeper reservoir for the uppers.

This model does not predict a hiatus in eruption of lavas between the high- and low-Ti, and this is supported by the lack of sediments found at the contact between the two lava suites. The depletion differences observed between the high-Ti and low-Ti lavas is predicted by this model, and would not be expected in the previous model (section 6.4.2)

6.4.4 'Upper pillow lavas' much later

Because the low-Ti lavas form the upper portion of the extrusive section, it has been suggested by Pearce & Robinson (2010) and Dilek et al. (2009) that the low-Ti lavas formed later than the high-Ti lavas. The observations that the low-Ti lavas have more pronounced depletion, are sometimes enriched in L-REE, and have lower Ti/V are all indicative of a marked subduction zone signature. This, in turn, is interpreted by Pearce & Robinson (2010) and Dilek et al. (2009) as a temporal change from MORB to IAT to boninitic which reflects the initiation of subduction.

This model of early, tholeiitic lavas (lower pillow lavas) followed by later, depleted lavas (upper pillow lavas) predicts that there would have been a hiatus in volcanism between the two lava groups. Further, there would be a systematic relationship of later depleted dykes cross-cutting the earlier tholeiitic dykes. However, there is no sediment horizon between the two lava suites, nor is there field evidence of seafloor wreathing within the lower pillow lavas, and Baragar et al. (1990) report no systematic cross-cutting of the dykes. The syn-tectonic tilting has been recorded in all parts of the lava section, therefore both lava suites were erupted during spreading at an active ridge.

6.5 Comparisons with modern spreading centers

6.5.1 Off-axis magmatism at the EPR

Recent studies of the fast spreading, and magmatically robust East Pacific Rise (EPR) has discovered evidence for the presence of off-axis melt lenses (OAML). A seismic study by Han et al. (2014) have imaged OAMLs at depth of 1.6-4.5 km at the base of the sheeted dyke section, they have been located beneath the ridge flanks at distances of 2-10 km off- axis. Another study of the lavas at the EPR by Canales et al. (2014) reports the presence of a network of off-axis partially molten sills at 4-8 km from the ridge. The sills are interconnected at depth via pathways which may promote the mixing of different magmas. Composition of the near-axis lavas are highly variable (Canales et al., 2014) and could be fed from the zone of mixing where the different

sills are connected. In contrast, the axial lavas were found to be typical, homogenous MORB.

Seamounts are abundant on the seafloor of fast-spreading ridges at distances of 5-15 km from axis, there are several reports of the heterogeneous composition of seamounts (e.g., Nin & Batiza (1997); Donnally, 2004). These new findings may indicate the region of the delivery of partial melts from the mantle to the crust is less focussed than previously thought. More research needs to be done to establish how much of a contribution off-axis magmatism makes to the thickening of the upper crust.

The concept of off-axis magmatism, such as at the EPR, is similar to the type of crustal accretion evoked for the Troodos ophiolite, albeit at a higher spreading rate and with greater magma supply. The variably depleted low-Ti lavas show compositional variability which and are interpreted to be erupted from a near-axis setting, which is equivalent to the heterogeneous lavas from the near-axis regions on the EPR (Canales et al., 2012). The Troodos high-Ti lavas have very similar compositions and this is comparable to the homogenous lavas found at the EPR ridge axis.

6.5.2 Discovery Transform.

The observed complexity of both the subsurface structure of the Troodos upper crust and the tectonic spreading fabric is probably related to the proximity of the spreading ridges to the transform zone. At the end of ridge segments the crustal structure becomes increasingly complex due to the interaction of extensional tectonics from the spreading centre and the transform tectonics.

The spreading fabric for Troodos (figure 6.9) shows there are domains with uniform N-S spreading fabric such as the West Solea domain (blue), however, the region of East Mitsero (orange) has a N-S fabric in the northern part and this fabric become gradually more E-W as the transform zone is approached (pink). In the eastern end of the ophiolite the spreading fabric is very variable- over distances of a few km the fabric switched suddenly from N-S at the Kambia/Makhaeras domain to NW-SE in the Larnaca graben (grey). This may be the result of a propagating ridge

from the north moving southwards towards the active transform zone, but this is very speculative.

The varied nature of the spreading fabric is seen with striking similarity, and at comparable scales, at the modern transform zones the Discovery Transform on the EPR pictured below (figure 6.14 taken from Wolfson-Schwehr et al., 2014). The bathymetric image of the seafloor highlights the spreading fabric as defined by abyssal hills and fault blocks which form perpendicular to spreading direction.

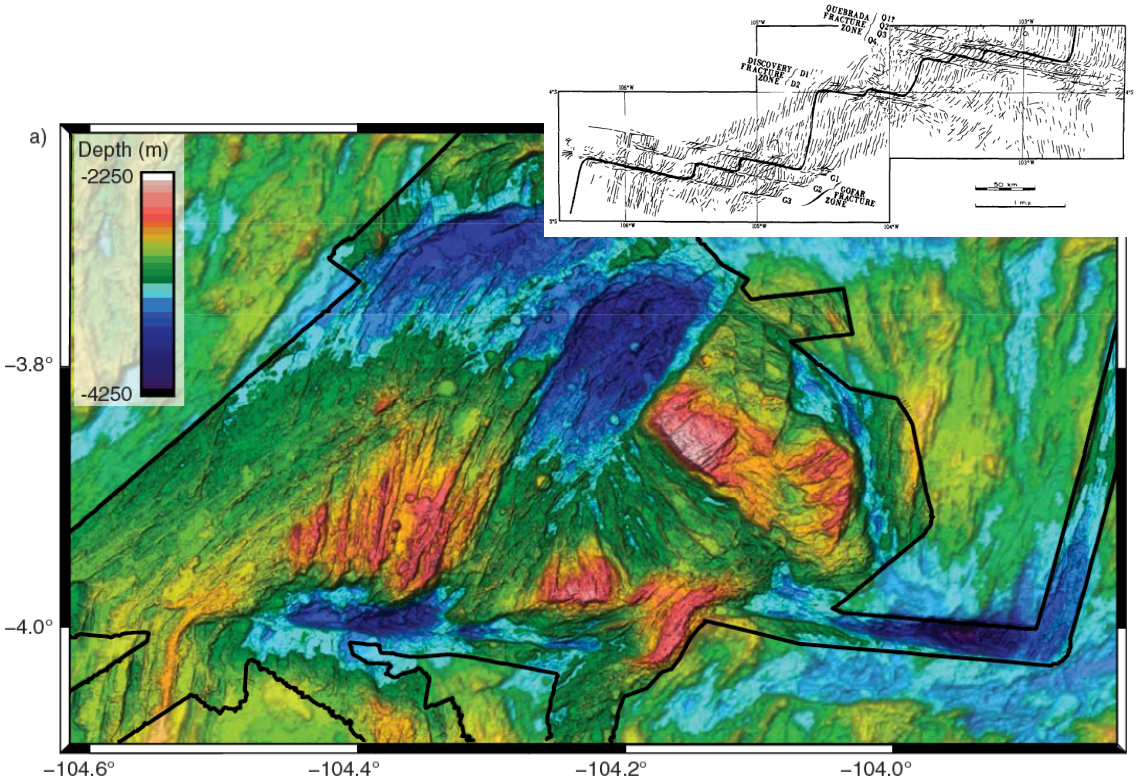

Figure 6.14 Bathymetry of the Discovery Transform zone showing tectonic spreading fabric defined by seafloor topography (from Wolfson-Schwehr et al., 2014) and inset map from Searle (1983).

Although the similarity of Troodos with these examples from the EPR are very interesting and could be a good modern-day analogue for some of the processes operating at the Troodos spreading centre, any comparisons should be made with care. The EPR is a fast spreading centre in the open ocean (MOR proper) while the Troodos ophiolite formed above a subduction zone, and probably at slower spreading rate.

7 Conclusions

This thesis has attempted to address the questions about how the upper oceanic crust is accreted at a slow to intermediate spreading ridge formed in a suprasubduction zone. The recent discovery of exposed detachment faults at ocean core complexes has highlighted the importance of tectonic extension as well as magmatic extension during seafloor spreading; however, the question of whether active detachment faults persist at depth beyond the exposed OCCs remains poorly understood.

Study of the Troodos ophiolite offers an unparalleled opportunity to examine the internal architecture of sub-surface oceanic crust formed at a slow or intermediate spreading rate ridge near a subduction zone. Original spreading structures are well preserved and exposed in two or three dimensions. The across-axis slice of oceanic crust displayed along the northern flank of the Troodos ophiolite has allowed a detailed reconstruction of the spreading history.

Structural mapping of the sheeted dyke complex and extrusive sequence has helped unravel the history of tectonic stretching and volcanism. The structural domains previously identified in the SDC define three grabens across the northern flank of the ophiolite (Varga & Moores, 1985). New lava orientation data presented here show that structural domains are also evident in the lava dips, and the graben structures are reflected in the outward dip of lava flows tectonically tilted away from the graben axes.

Further examination of the structure of N-S transects cutting through the upper crust from top to bottom reveals the presence progressive unconformities within many of the lava sections. This is expressed as flat-lying flows at the top of the section, which are sub-parallel to the undeformed overlying sediments, and a subdued lava-sediment contact. Orientation of the topmost flows are often gently dipping northwards due to the uplift of Mt. Olympus; removal of the uplift tilt restores the uppermost lavas to sub-horizontal. However, lava flow orientations become progressively more steeply tilted at great depth, documenting rotations (change in dip)

of between 31°-56° from the top to the bottom of the lava section. The distribution of poles to planes for tilted lavas along a transect typically lie along a best-fit girdle trending E-W. The pole to the best-fit girdle represents the axis of rotation. All of the rotation axes identified in this way a shallowly-inclined, and most of them are trending close to N.

In the field meso-scale normal faults are commonly found in the sheeted dyke complex. The faults are usually parallel to the dyke strike, dip towards the graben centres and effected the tilting of the SDC. These are original seafloor structures which formed near the ridge to accommodate the tectonic extension during spreading.

Rotation axes have been identified and quantified for the dykes using the net tectonic rotation analysis involving palaeomagnetic techniques (Allerton & Vine, 1987). Restoring tilted dykes to an original vertical position and restoring the dyke magnetic vector to the Troodos mean vector quantitatively constrains the orientation or rotation axis, magnitude of the rotation and sense of rotation. Rotation axes in the Solea graben SDC are sub-horizontal N-S trending, and parallel with dyke strikes – indicating the rotations are related to spreading.

The rotations identified from palaeomagnetic data of the dykes can account for the observed lava orientations immediately above the SDC, therefore confirming that tilting of the lavas is also related to spreading, rather than subsidence of the lava pile due to loading as previously supposed. The rotation axes inferred from lava field measurements are consistent with the dyke rotation axes. Such consistency between the observations implies that lava flow orientations are reliable tectonic markers, and it is appropriate to use the lava dips to assess rotations in lieu of magnetic data.

Numerous normal faults within the SDC root onto a detachment surface, which is exposed at the Kakopetria detachment; however, very little of this sub-surface tectonic activity is apparent at the seafloor because the lavas are unrotated and very few faults are exposed at the palaeo-seafloor.

The geochemical study conducted here reveals that the lavas can be divided into low-Ti and high-Ti lava groups, and these divisions broadly correspond to the traditional Upper Pillow Lavas and the Lower Pillow Lavas, respectively. At every section the boundary between the two is step-wise; always the high-Ti lavas are more evolved and less depleted, and the low-Ti lavas are always primitive, variably depleted, and nearly always contain more water.

The progressive unconformities are observed within both lava groups, demonstrating that they are both syn-tectonic units. Because the Lower Pillow Lavas are chemically identical to the Basal Group (lava-dyke transition) beneath, both of which were erupted within the dyke injection zone, we can assume the entire high-Ti lava group formed at the spreading axis itself. The lack of a sediment horizon at the boundary between the lava groups supports a near-axis setting and implies that the low-Ti lavas can only be very slightly later than the high-Ti group. The low-Ti lavas are rarely interbedded with the high-Ti lavas, which is consistent with a near-axis setting rather than on-axis proper, and this may also account to the more primitive and heterogeneous compositions, fed from later, deeper melt bodies that bypassed the melt lens.

Viscosity modelling of the lavas shows that the high-Ti lavas vary in their viscosity, but the low-Ti lavas are always low-viscosity. The low viscosity of the low-Ti lavas has implications for the filling of half grabens because these eruptions are able to flow further and are responsible for blanketing the faults beneath, thereby obscuring the evidence of tilting.

The findings from this study may have implications for modern MOR where the internal structure of the upper crust cannot be directly observed. Estimates of apparent tectonic strain based on seafloor morphology alone may significantly underestimate the true sub-surface tectonic extension. It is possible that detachment faults are active at depth even where limited evidence of faulting is seen on the seafloor, due to flat-lying lava flows blanketing the faults and obscuring the evidence of 'hidden' tectonics.

7.1 Further work

- Geochemical data from dykes and cross-cutting dykes will help establish if the younger dykes are consistently more depleted than the older dykes.
- In situ geochemistry of cumulates and better modelling of melt liquidsin order to elucidate which gabbros fed which lava suites.
- Detailed geological mapping of the Larnaca graben will help determine whether a propagating ridge has caused the different spreading fabrics.

- More precise age dates of the plagiogranites will better constrain the spreading rates, and to help understand the style of spreading i.e., asymmetrical due to detachment faulting on one side, or; to determine whether the three grabens were all spreading centres or off-axis stretching features (overall symmetry within each graben if all fossil ridges).

Reference list

Adamides, N. G. 2010. Mafic-dominated volcanogenic sulphide deposits in the Troodos ophiolite, Cyprus Part 2: A review of genetic models and guides for exploration. Applied Earth Science 119(4), pp. 193-204.

Agar, S. M. and Klitgord, K. D. 1995. A mechanism for decoupling within the oceanic lithosphere revealed in the Troodos ophiolite. Nature 374(6519), pp. 232-238.

Allerton, S. et al. 2000. Extremely asymmetric magmatic accretion of oceanic crust at the ends of slow-spreading ridge segments. Geology 28(2), pp. 179-182.

Allerton, S. and Vine, F. J. 1987. Spreading structure of the Troodos ophiolite, Cyprus: Some paleomagnetic constraints. Geology 15(7), pp. 593-597.

Allerton, S. and Vine, F. J. 1991. Spreading evolution of the Troodos ophiolite, Cyprus. Geology 19(6), pp. 637-640.

Allerton, W. S. Q. 1988. Palaeomagnetic and structural studies of the Troodos Ophiolite, Cyprus. University of East Anglia.

Anders, E. and Grevesse, N. 1989. Abundances of the elements: Meteoritic and solar. Geochimica Et Cosmochimica Acta 53(1), pp. 197-214.

Bagnall, P.S. (1960) The geology and mineral resources of the Pano Lefkara-Larnaca area. *Geol. Surv. Depart. Cyprus Mem.*, **5**, 116.

Baines, A. G. et al. 2008. The rate of oceanic detachment faulting at Atlantis Bank, SW Indian Ridge. Earth and Planetary Science Letters 273(1), pp. 105-114.

Baragar WRA, Lambert MB, Baglow N, Gibson IL (1990) The sheeted dike zone in the Troodos ophiolite. In: *Ophiolites: Oceanic Crustal Analogues* (eds Malpas J, Moores EM, Panayiotou A, Xenophontos C), pp. 37–52. Geological Survey Department, Nicosia, Cyprus.

Baragar et al., 1989 W.R. Baragar, M.B. Lambert, N. Baglow, I.L. Gibson Sheeted dikes from CY4 and surface sections: Troodos ophiolite ,in: I.L. Gibson, J. Malpas, P.T. Robinson, C. Xenophontos (Ed's.), Cyprus Crustal Study Project: Initial Report, Hole CY.

Bear, L.M., 1960. The geology and mineral resources of the Akaki-Lythrodondha area Memoir No. 3Geological Survey Department, Republic of Cyprus, Nicosia (122 pp.).

Bednarz, U. and Schmincke, H. U. 1994. Petrological and chemical evolution of the northeastern troodos extrusive series, cyprus. Journal of Petrology 35(2), pp. 489-523.

Bishopp, D. W. ed. 1952. Some new features of the geology of Cyprus. Proc. 19th Int. Geol. Congr.

Bonhommet, N. et al. 1988. Paleomagnetic arguments for block rotations along the Arakapas fault (Cyprus). Geology 16(5), pp. 422-425.

Borradaile, G. J. and Lucas, K. 2003. Tectonics of the Akamas and Mamonia ophiolites, Western Cyprus: magnetic petrofabrics and paleomagnetism. Journal of Structural Geology 25(12), pp. 2053-2076.

Buck, W. R. et al. 2005. Modes of faulting at mid-ocean ridges. Nature 434(7034), pp. 719-723.

Butler, R. F. 1992. Paleomagnetism: magnetic domains to geologic terranes. Blackwell Scientific Publications Boston.
Cameron, W. E. 1985. Petrology and origin of primitive lavas from the Troodos ophiolite, Cyprus. Contributions to Mineralogy and Petrology 89(2-3), pp. 239-255.

Canales, J. P. et al. 2012. Network of off-axis melt bodies at the East Pacific Rise. Nature Geosci 5(4), pp. 279-283.

Cann, J. R. et al. 1997. Corrugated slip surfaces formed at ridge-transform intersections on the Mid-Atlantic Ridge. Nature 385(6614), pp. 329-332.

Cannat, M. 1993. Emplacement of mantle rocks in the seafloor at mid-ocean ridges. Journal of Geophysical Research: Solid Earth 98(B3), pp. 4163-4172.

Cannat, M. et al. 1991. Stretching of the deep crust at the slow-spreading Southwest Indian Ridge. Tectonophysics 190(1), pp. 73-94.

Cannat, M. et al. 1995. Thin crust, ultramafic exposures, and rugged faulting patterns at the Mid-Atlantic Ridge (22 N). Geology 23(1), pp. 49-52

Cannat, M. et al. 2006. Modes of seafloor generation at a melt-poor ultraslow-spreading ridge. Geology 34(7), pp. 605-608.

Carr, J. M. & Bear, L. M. 1960. The geology and mineral resources of the Peristerona-Lagoudhera area. Geological Survey Department of Cyprus Memorandum #2.

Choi, E. and Buck, W. R. 2012. Constraints on the strength of faults from the geometry of rider blocks in continental and oceanic core complexes. Journal of Geophysical Research-Solid Earth 117.

Christensen, N. I. and Salisbury, M. H. 1972. Sea floor spreading, progressive alteration of layer 2 basalts, and associated changes in seismic velocities. Earth and Planetary Science Letters 15(4), pp. 367-375.

Clube, T. M. M. et al. 1985. Palaeorotation of the Troodos microplate, Cyprus. Nature 317(6037), pp. 522-525.

Clube, T. M. M. and Robertson, A. H. F. 1986. The palaeorotation of the troodos microplate, cyprus, in the late mesozoic-early cenozoic plate tectonic framework of the Eastern Mediterranean. Surveys in Geophysics 8(4), pp. 375-437.

Clube, T. M. M. and Robertson, A. H. F. 1986. The palaeorotation of the troodos microplate, cyprus, in the late mesozoic-early cenozoic plate tectonic framework of the Eastern Mediterranean. Surveys in Geophysics 8(4), pp. 375-437.

Constantinou, 1980; G. Constantinou; Metallogenesis associated with the Troodos Ophiolite. A. Panayioutou (Ed.), Ophiolites, Proceedings, International Ophiolite Symposium, Cyprus 1979, Cyprus Geol. Surv. Dep, Nicosia (1980), pp. 663–674

Coogan, L. et al. 2003. Hidden melting signatures recorded in the Troodos ophiolite plutonic suite: evidence for widespread generation of depleted melts and intra-crustal melt aggregation. Contributions to Mineralogy and Petrology 144(4), pp. 484-506.

Dannowski, A. et al. 2010. Seismic structure of an oceanic core complex at the Mid-Atlantic Ridge, 22N. J. Geophys. Res. 115(B7), p. B07106.

Donnelly, K. E. et al. 2004. Origin of enriched ocean ridge basalts and implications for mantle dynamics. Earth and Planetary Science Letters 226, pp. 347-366.

Duncan, R. A. and Green, D. H. 1980. Role of multistage melting in the formation of oceanic crust. Geology 8(1), pp. 22-26.

Eddy, C. A. et al. 1998. Seamount formation and associated caldera complex and hydrothermal mineralization in ancient oceanic crust, Troodos ophiolite (Cyprus). Tectonophysics 292(3), pp. 189-210.

Engel, A. E. J. 1963. Geologic Evolution of North America Geologic features suggest that the continent has grown and differentiated through geologic time. Science 140(3563), pp. 143-152.

Engel, A. E. J. and Engel, C. G. 1964. Continental accretion and the evolution of North America. Advancing Frontiers in Geology and Geophysics. Indian Geophysical Union, Hyderabad, India, pp. 17-37.

Engel, A. J. et al. 1965. Chemical characteristics of oceanic basalts and the upper mantle. Geological Society of America Bulletin 76(7), pp. 719-734.

Escartin, J. and Cannat, M. 1999. Ultramafic exposures and the gravity signature of the lithosphere near the Fifteen-Twenty Fracture Zone (Mid-Atlantic Ridge). Earth and Planetary Science Letters 171(3), pp. 411-424.

Escartin, J. et al. 1999. Quantifying tectonic strain and magmatic accretion at a slow spreading ridge segment, Mid-Atlantic Ridge, 29 deg N. Journal of Geophysical Research 104, p. 10.

Escartin, J. et al. 2008. Central role of detachment faults in accretion of slow-spreading oceanic lithosphere. Nature 455(7214), pp. 790-794.

Escartin, J. et al. 2007. Interplay between faults and lava flows in construction of the upper oceanic crust: The East Pacific Rise crest 9'25N-9'58N. Geochemistry, Geophysics, Geosystems 8(6).

Falloon, T. J. and Danyushevsky, L. V. 2000. Melting of refractory mantle under anhydrous and H_2O-undersaturated conditions: implications for the petrogenesis of high-Ca boninites and the influence of subduction components on mantle melting. Journal of Petrology 41(2), pp. 257-283.

Feig, S. et al. 2006. Effect of water on tholeiitic basalt phase equilibria: an experimental study under oxidizing conditions. Contributions to Mineralogy and Petrology 152(5), pp. 611-638.

Fisher, R. ed. 1953. Dispersion on a sphere. Proceedings of the Royal Society of London A: Mathematical, Physical and Engineering Sciences. The Royal Society.

Floyd, P. A. and Winchester, J. A. 1975. Magma type and tectonic setting discrimination using immobile elements. Earth and Planetary Science Letters 27(2), pp. 211-218.

Fornari, D. J. et al. 1998. Axial summit trough of the East Pacific Rice 9'10N: Geological characteristics and evolution of the axial zone on fast spreading mid-ocean ridge. Journal of Geophysical Research: Solid Earth (1978-2012) 103(B5), pp. 9827-9855

Gass, I. G., 1960, The geology and mineral resources of the Dhali area: Cyprus Geological Survey Department Memoir 4, 116 p.

Gass, I. G. 1968. Is the Troodos Massif of Cyprus a Fragment of Mesozoic Ocean Floor? Nature 220(5162), pp. 39-42.

Gass, I. G. et al. 1994. The geology of the Southern Troodos transform fault zone. Geological Survey Department, Ministry of Agriculture, Natural Resources and Environment.

Gass, I. G. et al. 1994. The geology of the Southern Troodos transform fault zone. Geological Survey Department, Ministry of Agriculture, Natural Resources and Environment.

Gass, I. G. et al. 1975. Comments on the troodos ophiolitic complex was probably formed in an island arc, by A. Miyashiro and subsequent correspondence by A. Hynes and A. Miyashiro. Earth and Planetary Science Letters 25(2), pp. 236-238.

Gass, I. G. and Smewing, J. D. 1973. Intrusion, Extrusion and Metamorphism at Constructive Margins: Evidence from the Troodos Massif, Cyprus. Nature 242(5392), pp. 26-29.

Ghiorso, M. S. and Sack, R. O. 1995. Chemical mass transfer in magmatic processes IV. A revised and internally consistent thermodynamic model for the interpolation and extrapolation of liquid-solid equilibria in magmatic systems at elevated temperatures and pressures. Contributions to Mineralogy and Petrology 119(2-3), pp. 197-212

Gibson, I. L. 1991. Cyprus Crustal Study Project: Initial Report, Holes CY-1 and 1a. Geological Survey of Canada.

Gillis, K. M. 2002. The rootzone of an ancient hydrothermal system exposed in the Troodos ophiolite, Cyprus. The Journal of geology 110(1), pp. 57-74.

Gillis, K. M. and Coogan, L. A. 2002. Anatectic migmatites from the roof of an ocean ridge magma chamber. Journal of Petrology 43(11), pp. 2075-2095.

Gillis, K. M. et al. 1992. Mobilization of REE during crustal aging in the Troodos Ophiolite, Cyprus. Chemical Geology 98(1), pp. 71-86.

Gillis, K. M. and Roberts, M. D. 1999. Cracking at the magma-hydrothermal transition: evidence from the Troodos Ophiolite, Cyprus. Earth and Planetary Science Letters 169(3), pp. 227-244.

Gillis, K. M. and Thompson, G. 1993. Metabasalts from the Mid-Atlantic Ridge: new insights into hydrothermal systems in slow-spreading crust. Contributions to Mineralogy and Petrology 113(4), pp. 502-523.

Gillis, K. M. et al. 1993. A view of the lower crustal component of hydrothermal systems at the Mid-Atlantic Ridge. Journal of Geophysical Research: Solid Earth (1978-2012) 98(B11), pp. 19597-19619.

Giordano, D. et al. 2008. Viscosity and glass transition temperature of hydrous melts in the system. Chemical Geology 256(3), pp. 203-215.

Gregg, T. K. P. and Fink, J. H. 1995. Quantification of submarine lava-flow morphology through analog experiments. Geology 23(1), pp. 73-76.

Grimes, C. B. et al. 2008. Protracted construction of gabbroic crust at a slow spreading ridge: Constraints from 206Pb/238U zircon ages from Atlantis Massif and IODP Hole U1309D (30 N, MAR). Geochemistry, Geophysics, Geosystems 9(8).

Han, S. et al. 2014. Architecture of on- and off-axis magma bodies at EPR 9¬37-40,N and implications for oceanic crustal accretion. Earth and Planetary Science Letters 390(0), pp. 31-44.

Hess, H. H. 1962. History of ocean basins. Petrologic studies 4, pp. 599-620.

Hurst, S. D. et al. 1994. Structural and geophysical expression of the Solea graben, Troodos ophiolite, Cyprus. Tectonics 13(1), pp. 139-156.

Hurst, S. D. et al. 1992. Paleomagnetic constraints on the formation of the Solea graben, Troodos ophiolite, Cyprus. Tectonophysics 208(4), pp. 431-445.

Hutchinson, R. W. and Searle, D. L. 1971. Stratabound pyrite deposits in Cyprus and relations to other sulphide ores. Soc. Min. Geol. Jpn. 3, pp. 198-205.
Kelley, K. A. et al. 2006. Mantle melting as a function of water content beneath back-arc basins. Journal of Geophysical Research: Solid Earth (1978-2012) 111(B9).

Kidd, R. G. W. and Cann, J. R. 1974. Chilling statistics indicate an ocean-floor spreading origin for the Troodos complex, Cyprus. Earth and Planetary Science Letters 24(1), pp. 151-155.

Kirschvink, J. L. 1980. The least-squares line and plane and the analysis of palaeomagnetic data. Geophysical Journal International 62(3), pp. 699-718.

Klein, E. M. and Langmuir, C. H. 1987. Global correlations of ocean ridge basalt chemistry with axial depth and crustal thickness. Journal of Geophysical Research: Solid Earth (1978-2012) 92(B8), pp. 8089-8115.

Lissenberg, C. J. and Dick, H. J. B. 2008. Melt-rock reaction in the lower oceanic crust and its implications for the genesis of mid-ocean ridge basalt. Earth and Planetary Science Letters 271(1), pp. 311-325.

Lord, A. R. et al. eds. 2000. A biochronostratigraphical framework for the Late Cretaceous-Recent circum-Troodos sedimentary sequence, Cyprus. Proceedings of the third international conference on the geology of the eastern Mediterranean. Geological Survey Department, Nicosia, Cyprus.

Macdonald, K. C. et al. 1980. Hydrothermal heat flux of the black smoker vents on the East Pacific Rise. Earth and Planetary Science Letters 48(1), pp. 1-7.

MacLeod, C. J. 1988. The tectonic evolution of the Eastern Limassol Forest Complex, Cyprus. Open University.

MacLeod, C. J. et al. 1990. Structure of a fossil ridge-transform intersection in the Troodos ophiolite. Nature 348(6303), pp. 717-720.

MacLeod, C. J. et al. 2011. Quantitative constraint on footwall rotations at the 15'45N oceanic core complex, Mid-Atlantic Ridge: Implications for oceanic detachment fault processes. Geochem. Geophys. Geosyst. 12, p. Q0AG03.

MacLeod, C. J. et al. 2002. Direct geological evidence for oceanic detachment faulting: The Mid-Atlantic Ridge, 15 45,≤ N. Geology 30(10), pp. 879-882.

MacLeod, C. J. et al. 2013. , Moist MORB, axial magmatism in the Oman ophiolite: The evidence against a mid-ocean ridge origin. Geology 41(4), pp. 459-462.

MacLeod, C. J. and Murton, B. J. 1993. Structure and tectonic evolution of the Southern Troodos transform fault zone, Cyprus. Geological Society, London, Special Publications 76(1), pp. 141-176.

MacLeod, C. J. et al. 2009. Life cycle of oceanic core complexes. Earth and Planetary Science Letters 287(3), pp. 333-344.

MacLeod, M. K. et al. 1999. The Alba Field ocean bottom cable seismic survey: Impact on development. The Leading Edge 18(11), pp. 1306-1312.

Malpas, J. 1990. Crustal accretionary processes in the Troodos ophiolite, Cyprus: Evidence from field mapping and deep crustal drilling. Ophiolites, oceanic crustal analogues: Nicosia, Cyprus, Geological Survey Department, pp. 65-74

McCulloch, M. T. and Cameron, W. E. 1983. Nd-Sr isotopic study of primitive lavas from the Troodos ophiolite, Cyprus: evidence for a subduction-related setting. Geology 11(12), pp. 727-731
Michard, A. 1989. Rare earth element systematics in hydrothermal fluids. Geochimica Et Cosmochimica Acta 53(3), pp. 745-750.

Miyashiro, A. 1973. The Troodos ophiolitic complex was probably formed in an island arc. Earth and Planetary Science Letters 19(2), pp. 218-224.

Moores, E. M. and Vine, F. J. 1971. The Troodos Massif, Cyprus and other Ophiolites as Oceanic Crust: Evaluation and Implications. Philosophical Transactions of the Royal Society of London. Series A, Mathematical and Physical Sciences 268(1192), pp. 443-467.

Morris, A. 1996. A review of palaeomagnetic research in the Troodos ophiolite, Cyprus. Geological Society, London, Special Publications 105(1), pp. 311-324.

Morris, A. et al. 2006. Palaeomagnetic insights into the evolution of Neotethyan oceanic crust in the eastern Mediterranean. Geological Society, London, Special Publications 260(1), pp. 351-372.

Morris, A. et al. 1998. Multiple tectonic rotations and transform tectonism in an intraoceanic suture zone, SW Cyprus. Tectonophysics 299(1), pp. 229-253.

Morris, A. et al. 1990. Palaeomagnetic evidence for clockwise rotations related to dextral shear along the Southern Troodos Transform Fault, Cyprus. Earth and Planetary Science Letters 99(3), pp. 250-262.

Morris, A. et al. 2009. Footwall rotation in an oceanic core complex quantified using reoriented Integrated Ocean Drilling Program core samples. Earth and Planetary Science Letters 287(1-2), pp. 217-228.

Muenow, D. W. et al. 1990. Volatiles in submarine glasses as a discriminant of tectonic origin: application to the Troodos ophiolite. Nature 343(6254), pp. 159-161.

Mukasa, S. B. and Ludden, J. N. 1987. Uranium-lead isotopic ages of plagiogranites from the Troodos ophiolite, Cyprus, and their tectonic significance. Geology 15(9), pp. 825-828.

Murton, B. J. 1989. Tectonic controls on boninite genesis. Geological Society, London, Special Publications 42(1), pp. 347-377.

Niu, Y. and Batiza, R. 1997. Trace element evidence from seamounts for recycled oceanic crust in the Eastern Pacific mantle. Earth and Planetary Science Letters 148(3), pp. 471-483.

Norrell, G. T. and Harper, G. D. 1988. Detachment faulting and amagmatic extension at mid-ocean ridges: The Josephine ophiolite as an example. Geology 16(9), pp. 827-830.

Nuriel, P. et al. 2009. Fault-related oceanic serpentinization in the Troodos ophiolite, Cyprus: Implications for a fossil oceanic core complex. Earth and Planetary Science Letters 282(1), pp. 34-46.

Pearce, J. A. 1975. Basalt geochemistry used to investigate past tectonic environments on Cyprus. Tectonophysics 25(1-2), pp. 41-67.

Pearce, J. A. ed. 1980. Geochemical evidence for the genesis and eruptive setting of lavas from Tethyan ophiolites. Proceedings of the International Ophiolite Symposium, Cyprus 1979. Ministry of Agriculture and Natural Resources, Cyprus.

Pearce, J. A. 2014. Immobile element fingerprinting of ophiolites. Elements 10(2), pp. 101-108.

Pearce, J. A. and Cann, J. R. 1973. Tectonic setting of basic volcanic rocks determined using trace element analyses. Earth and Planetary Science Letters 19(2), pp. 290-300.

Pearce, J. A. et al. 1984. Characteristics and tectonic significance of supra-subduction zone ophiolites. Geological Society, London, Special Publications 16(1), pp. 77-94

Pearce, J. A. and Robinson, P. T. 2010. The Troodos ophiolitic complex probably formed in a subduction initiation, slab edge setting. Gondwana Research 18(1), pp. 60-81.

Penrose, C. P. 1972. Penrose field conference on ophiolites. Geotimes 17, pp. 24-25.

Philpotts, A. R. and Dickson, L. D. 2000. The formation of plagioclase chains during convective transfer in basaltic magma. Nature 406(6791), pp. 59-61.

Plank, T. et al. 1995. Clarifying the mean extent of melting at ocean ridges. Journal of Geophysical Research: Solid Earth (1978-2012) 100(B8), pp. 15045-15052.

Poole, A. J. and Robertson, A. H. F. 1991. Quaternary uplift and sea-level change at an active plate boundary, Cyprus. Journal of the Geological Society 148(5), pp. 909-921.

Portnyagin, M. V. et al. 1997. Coexistence of two distinct mantle sources during formation of ophiolites: a case study of primitive pillow-lavas from the lowest part of the volcanic section of the Troodos Ophiolite, Cyprus. Contributions to Mineralogy and Petrology 128(2-3), pp. 287-301.

Rautenschlein, M. et al. 1985. Isotopic and trace element composition of volcanic glasses from the Akaki Canyon, Cyprus: implications for the origin of the Troodos ophiolite. Earth and Planetary Science Letters 75(4), pp. 369-383.

Resing, J. A. et al. 2011. Active submarine eruption of boninite in the northeastern Lau Basin. Nature Geoscience 4(11), pp. 799-806.

Reston, T. J. and Ranero, C. R. 2011. The 3-D geometry of detachment faulting at mid-ocean ridges. Geochemistry, Geophysics, Geosystems 12(7).

Richardson, C. J. et al. 1987. Metal-depleted root zones of the Troodos ore-forming hydrothermal systems, Cyprus. Earth and Planetary Science Letters 84(2-3), pp. 243-253.

Robertson, A. and Xenophontos, C. 1993. Development of concepts concerning the Troodos ophiolite and adjacent units in Cyprus. Geological Society, London, Special Publications 76(1), pp. 85-119.

Robertson, A. H. F. and Woodcock, N. H. 1986. The Role of the Kyrenia Range Lineament, Cyprus, in the Geological Evolution of the Eastern Mediterranean Area. Philosophical Transactions of the Royal Society of London. Series A, Mathematical and Physical Sciences 317(1539), pp. 141-177.

Robinson, P. T. and Malpas, J. 1990. The Troodos ophiolite of Cyprus: new perspectives on its origin and emplacement.Ophiolites, Oceanic Crustal Analogues, Proceedings of the Symposium, Troodos. pp. 13-26.

Robinson, P. T. et al. 1983. Volcanic glass compositions of the Troodos ophiolite, Cyprus. Geology 11(7), pp. 400-404.

Rogers, G. and Hawkesworth, C. J. 1989. A geochemical traverse across the North Chilean Andes: evidence for crust generation from the mantle wedge. Earth and Planetary Science Letters 91(3), pp. 271-285.

Rogers, N. W. et al. 1989. Petrogenesis of boninitic lavas from the Limassol Forest Complex, Cyprus.Boninites and related rocks. Unwin Hyman London, pp. 288-313.

Rollinson, H. R. 1993. A terrane interpretation of the Archaean Limpopo Belt. Geological Magazine 130(06), pp. 755-765.

Sano, T. and Yamashita, S. 2004. Experimental petrology of basement lavas from Ocean Drilling Program Leg 192: implications for differentiation processes in Ontong Java Plateau magmas. SPECIAL PUBLICATION-GEOLOGICAL SOCIETY OF LONDON 229, pp. 185-218.

Schiffman, P. et al. 1987. Geometry, conditions and timing of off-axis hydrothermal metamorphism and ore-deposition in the Solea graben. Nature 325(6103), pp. 423-425.

Schmincke, H. U. and Bednarz, U. 1990. Pillow, sheet flow and breccia flow volcanoes and volcano-tectonic hydrothermal cycles in the Extrusive Series of the northeastern Troodos ophiolite

(Cyprus).Ophiolites Oceanic Crustal Analogues, Proceedings of the Symposium ,Troodos. Vol. 1990. pp. 185-206.

Schmincke, H. U. et al. 1983. Troodos extrusive series of Cyprus: A comparison with oceanic crust. Geology 11(7), pp. 405-409.

Schouten, H. and Denham, C. R. 2000. Comparison of volcanic construction in the Troodos ophiolite and oceanic crust using paleomagnetic inclinations from Cyprus Crustal Study Project (CCSP) CY-1 and Ocean Drilling Program (ODP) 504B drill cores. SPECIAL PAPERS-GEOLOGICAL SOCIETY OF AMERICA, pp. 181-194.

Schouten, H. and Kelemen, P. B. 2002. Melt viscosity, temperature and transport processes, Troodos ophiolite, Cyprus. Earth and Planetary Science Letters 201(2), pp. 337-352.

Searle, R. C. 1983. Multiple, closely spaced transform faults in fast-slipping fracture zones. Geology 11(10), pp. 607-610.

Searle, R. C. et al. 2003. FUJI Dome: A large detachment fault near 64 degrees E on the very slow-spreading southwest Indian Ridge. Geochemistry Geophysics Geosystems 4.

Shervais, J. W. 1982. Ti-V plots and the petrogenesis of modern and ophiolitic lavas. Earth and Planetary Science Letters 59(1), pp. 101-118.

Sinton, J. M. and Detrick, R. S. 1992. Mid-Ocean Ridge Magma Chambers. J. Geophys. Res. 97(B1), pp. 197-216.

Sisson, T. W. and Grove, T. L. 1993. Experimental investigations of the role of H_2O in calc-alkaline differentiation and subduction zone magmatism. Contributions to Mineralogy and Petrology 113(2), pp. 143-166.

Smewing, J. D. et al. 1975. Metabasalts from the Troodos Massif, Cyprus: Genetic implication deduced from petrography and trace element geochemistry. Contributions to Mineralogy and Petrology 51(1), pp. 49-64.

Smewing, J. D. et al. 1975. Metabasalts from the Troodos Massif, Cyprus: genetic implication deduced from petrography and trace element geochemistry. Contributions to Mineralogy and Petrology 51(1), pp. 49-64.

Smith, A. J. et al. 2008. High-resolution Fourier-domain optical coherence tomography and microperimetric findings after macula-off retinal detachment repair. Ophthalmology 115(11), pp. 1923-1929. e1921.

Taylor, R. N. 1990. Geochemical stratigraphy of the Troodos extrusive sequence: temporal developments of a spreading centre magma chamber. Ophiolites, Oceanic Crustal Analogues. Proceedings of the Syposium ,Troodos 1990, pp. 173-183.

Taylor, R. N. et al. 1992. Chemical transects across intra-oceanic arcs: implications for the tectonic setting of ophiolites. Geological Society, London, Special Publications 60(1), pp. 117-132.

Taylor, R. N. and Nesbitt, R. W. 1988. Light rare-earth enrichment of supra subduction-zone mantle: evidence from the Troodos ophiolite, Cyprus. Geology 16(5), pp. 448-451.

Teagle, D. A. H. et al. the IODP Expedition 335 Scientists (2012), IODP Expedition 335: Deep sampling in ODP Hole 1256D. Sci. Drill 13, pp. 28-34.

Tominaga, M. and Umino, S. 2010. Lava deposition history in ODP Hole 1256D: Insights from log-based volcanostratigraphy. Geochemistry, Geophysics, Geosystems 11(5).

Tucholke, B. E. et al. 2008. Role of melt supply in oceanic detachment faulting and formation of megamullions. Geology 36(6), pp. 455-458.

Tucholke, B. E. and Lin, J. 1994. A geological model for the structure of ridge segments in slow spreading ocean crust. Journal of Geophysical Research: Solid Earth (1978-2012) 99(B6), pp. 11937-11958.

Tucholke, B. E. et al. 1998. Megamullions and mullion structure defining oceanic metamorphic core complexes on the Mid-Atlantic Ridge. Journal of Geophysical Research: Solid Earth (1978,Äì2012) 103(B5) pp. 9857-9866.

Urquhart, E. and Banner, F. T. 1994. Biostratigraphy of the supra-ophiolite sediments of the Troodos Massif, Cyprus: the Cretaceous Perapedhi, Kannaviou, Moni and Kathikas formations. Geological Magazine 131(04), pp. 499-518.

van Everdingen, D. A. and Cawood, P. A. 1995. Dyke domains in the Mitsero graben, Troodos ophiolite, Cyprus: an off-axis model for graben formation at a spreading centre. Journal of the Geological Society 152(6), pp. 923-932.

Varga, R. J. 1991. Modes of extension at oceanic spreading centers: evidence from the Solea graben, Troodos ophiolite, Cyprus. Journal of Structural Geology 13(5), pp. 517-537.
Varga, R. J. et al. 1999. Early establishment of seafloor hydrothermal systems during structural extension: paleomagnetic evidence from the Troodos ophiolite, Cyprus. Earth and Planetary Science Letters 171(2), pp. 221-235.

Varga, R. J. and Moores, E. M. 1985. Spreading structure of the Troodos ophiolite, Cyprus. Geology 13(12), pp. 846-850.

Varga, R. J. and Moores, E. M. 1990. Intermittent magmatic spreading and tectonic extension in the Troodos Ophiolite: Implications for exploration for black smoker-type ore deposits.Proceedings of the Symposium on Ophiolites and Oceanic Lithosphere-Troodos. Vol. 87.

Vine, F. J. and Matthews, D. 1963. Magnetic anomalies over oceanic ridges.

Wilson, R. A. M. and Ingham, F. T. 1959. The Geology of the Xeros-Troodos Area, with an Account of the Mineral Resources: Ministry of Agriculture and Natural Resources. Geological Survey Department: Memoir (1).

Wolfe, C. J. et al. 1995. Microearthquake characteristics and crustal velocity structure at 29N on the Mid-Atlantic Ridge: The architecture of a slow spreading segment. Journal of Geophysical Research: Solid Earth (1978, 2012) 100(B12), pp. 24449-24472.

Wolfson-Schwehr, M. et al. 2014. The relationship between seismicity and fault structure on the Discovery transform fault, East Pacific Rise. Geochemistry, Geophysics, Geosystems 15(9), pp. 3698-3712.